AGARD-AR-127

# AGARD

## ADVISORY GROUP FOR AEROSPACE RESEARCH & DEVELOPMENT

RUE ANCELLE 92200 NEUILLY SUR SEINE FRANCE

### AGARD ADVISORY REPORT No. 127

# Aircraft Icing

NORTH ATLANTIC TREATY ORGANIZATION

**DISTRIBUTION AND AVAILABILITY
ON BACK COVER**

AGARD-AR-127

NORTH ATLANTIC TREATY ORGANIZATION

ADVISORY GROUP FOR AEROSPACE RESEARCH AND DEVELOPMENT

(ORGANISATION DU TRAITE DE L'ATLANTIQUE NORD)

AGARD Advisory Report No.127

AIRCRAFT ICING

11 Nov 78

Advisory rept.

12 138 p.

400 043

JOB

The information in this report was presented at an AGARD Fluid Dynamics Panel
Round-table Discussion on Aircraft Icing held at the Government Conference Center,
Ottawa, Canada, on 30 September 1977.

79 01 26 083

# THE MISSION OF AGARD

The mission of AGARD is to bring together the leading personalities of the NATO nations in the fields of science and technology relating to aerospace for the following purposes:

– Exchanging of scientific and technical information;

– Continuously stimulating advances in the aerospace sciences relevant to strengthening the common defence posture;

– Improving the co-operation among member nations in aerospace research and development;

– Providing scientific and technical advice and assistance to the North Atlantic Military Committee in the field of aerospace research and development;

– Rendering scientific and technical assistance, as requested, to other NATO bodies and to member nations in connection with research and development problems in the aerospace field;

– Providing assistance to member nations for the purpose of increasing their scientific and technical potential;

– Recommending effective ways for the member nations to use their research and development capabilities for the common benefit of the NATO community.

The highest authority within AGARD is the National Delegates Board consisting of officially appointed senior representatives from each member nation. The mission of AGARD is carried out through the Panels which are composed of experts appointed by the National Delegates, the Consultant and Exchange Programme and the Aerospace Applications Studies Programme. The results of AGARD work are reported to the member nations and the NATO Authorities through the AGARD series of publications of which this is one.

Participation in AGARD activities is by invitation only and is normally limited to citizens of the NATO nations.

ii

# FOREWORD

Icing of unprotected aircraft components is one of the major problems engineers are faced with during the development phase of an aircraft. Ice accretions, as well as their shape, have to be predicted in order to investigate their effect on aerodynamic flight safety and performance, and to decide on the need for provision of anti-or de-icing systems. Typical components where hazardous accretions may occur are wings, tails, engine inlets, hubs, antennas, propellers and rotor blades.

The Fluid Dynamics Panel of AGARD held a round-table discussion of the fluid dynamic aspects of icing. This took place following the FDP Symposium on Unsteady Aerodynamics in Ottawa, Canada, on the 30th September, 1977.

Seven contributions — two from Germany, two from Canada, and one each from France, UK and USA — were presented, covering a broad spectrum of topics such as icing parameters, icing of wings, tails, inlets, helicopter blades and icing test facilities within the NATO countries of Europe, the USA and Canada. These papers have been collected in this AGARD Advisory Report. It gives an excellent state-of-the-art survey of this subject. The subject of engine and inlet icing has been treated separately in the Spring 1978 Meeting of the AGARD Propulsion and Energetics Panel, and is reported in AGARD Conference Proceedings CP-236.

It is hoped that by this report further investigations into the establishment of atmospheric icing parameters will be initiated, that the full survey of icing test facilities will allow a proper choice, and that the described procedures and data on wing icing will be helpful to predict ice accretion on future aircraft.

B.LASCHKA
Chairman, Programme Committee
(AGARD Fluid Dynamics Panel)

iii

## PROGRAMME AND MEETING OFFICIALS

CHAIRMAN: Professor Dr Ing.B.Laschka
Messerschmitt-Bolkow-Blohm
Unternehmensbereich Flugzeuge
FE 12–Postfach 80 11 60
D-8000 München 80
Germany

## MEMBERS

M. l'Ing. en Chef B.Monnerie
Chef de la Division d'Aerodynamique
Appliquée – ONERA
29 Avenue de la Division Leclerc
92320 Châtillon
France

Dr Ing.U.Sacerdote
Direttore del Settore Spazio
Aeritalia
Corso Marche 41
10146 Torino
Italy

Dr K.J.Orlik-Rückemann
National Aeronautical Establishment
National Research Council, Montreal Road
Ottawa K1A OR6
Canada

Dr B.M.Spee
NLR
P.O.Box 90502
1006 BM Amsterdam
The Netherlands

Dr G.G.Pope
Head of Group A
Royal Aircraft Establishment
Farnborough GU14 6TD
UK

Dr H.Yoshihara
The Boeing Company
Mail Stop 41-18, P.O.Box 3999
Seattle WA 98124
USA

## FLUID DYNAMICS PANEL

CHAIRMAN: Mr J.P.Hartzuiker
Chief, Compressible Aerodynamics
Dept.
NLR
P.O.Box 90502
1006 BM Amsterdam
The Netherlands

DEPUTY CHAIRMAN: Mr J.L.Jones
M.S.202.11
Chief, Planning & Analysis
Office
NASA Ames Research Center
Moffett Field, CA 94035
USA

## PANEL EXECUTIVE

M.C.Fischer

# CONTENTS

# SOME RECENT RESULTS ON ICING PARAMETERS

W. Kleuters and G. Wölfer

MESSERSCHMITT-BÖLKOW-BLOHM

2103 Hamburg 95

West Germany

## SUMMARY

Meteorological icing data on forty-seven encounters in cumulus cloud over Western and Central Europe are here analysed statistically, and compared with similar data quoted in FAR 25 Appendix C.

The data for FAR 25 Appendix were obtained by the "Rotating Cylinder" method, a measuring device with a capacity limited to relatively low liquid water content and/or low temperatures. To overcome these limitations, the liquid water content was measured in these tests by employing a liquid-nitrogen-cooled Test Rod, enabling measurements of liquid water content of up to 3 $g/m^3$.

It is thus evident that, in the temperature range above -15 $^{\circ}C$, the MBB analysis yields values of liquid water content considerably higher than quoted in FAR 25.

## 1. INTRODUCTION

The design of ice-protection equipment requires some defining of the meteorological conditions in which the system is expected to operate. The conditions are governed by liquid water content, mean effective droplet diameter, and ambient temperature.

The investigation of icing parameters began with the development of heating wings, leading by 1948 to an accumulation of some 1000 individual measurements of water content and effective droplet size, obtained in two hundred forty separate encounters with icing conditions. After review and discussion by NASA scientists, the Technical Note 1855[1] was published, providing industry with tentative standards to fill an immediate need. These recommended design conditions were adopted by the Civil Aeronautics Administration and are still in effect today, embodied in FAR 25 Appendix C.

The design envelopes for 1) stratiform or layer clouds (the continuous maximum) and 2) cumulus clouds (the intermittent maximum) are shown in Figures 1 and 2 respectively, in the form of curves drawn from combinations of liquid water content and effective droplet diameter, for selected values of temperature.

Examination of the statistical distributions of the parameters indicated that the probability of all three variables - as represented by a single point in Figure 1 and 2 - being exceeded at any one time, was of the order of $10^{-3}$ [2]. Considering the data were obtained from one hundred sixty-seven encounters in layer clouds, and seventy-three in cumulus clouds, the statistical extrapolation to a probability of $10^{-3}$ was indeed questionable.

## 2. THE ROTATING MULTI-CYLINDER METHOD

The majority of flight measurements of liquid water content and effective droplet diameter, upon which the curves in Figures 1 and 2 depend, were made using the "Rotating Cylinder" method. A set of five cylinders (Figure 3) of different diameters (0.125": 0.5": 1.25": 3.0" and 4.5") was exposed normal to the airstream while slowly rotating. Theoretical relations involving droplet size, cylinder diameter, collection efficiency, and airspeed, were used to derive average liquid water content and effective droplet diameter [3].

The measurement of liquid water content and droplet diameter by this "Rotating Cylinder" method is subject to the following sources of error: 1) blow-off, 2) run-off 3) evaporation, and 4) variation in water concentration in the vicinity of the cylinders, due to disturbing influences from the aircraft.

In a statistical analysis, however, reasonably reliable results may be obtained provided that the errors are randomly distributed and small compared with the quantity being measured. But the problem of blow-off merits some further consideration since it imposes a systematic error, as with all instruments measuring rate of icing, the "Rotating Cylinders" are absolutely limited by latent heat effects. The following equations show the heat balance at the surface of a cylinder assuming that the surface temperature $\vartheta_0$ is 0 $^{\circ}C$ and the total temperature $\vartheta_\alpha'$ is below zero.

The various contributing factors affecting the heat balance at the stagnation point are:

    a)   The density of heat flux due to convection:

$$q_1 = \alpha \left( \vartheta_o - \vartheta_\infty' \right) \text{ with } \vartheta_\infty' = \vartheta_\infty + r \frac{V_\infty^2}{2c_p} \tag{1}$$

where:   $\vartheta_\infty$ = Static air temperature

           $r$ = Recovery factor $\approx 1$

           $c_p$ = Specific heat of the air

           $\alpha$ = Heat transfer coefficient

           $V_\infty$ = Air speed

    b)   The density of heat flux due to the temperature rise of the water. Since the temperature at the surface ist $0\,^\circ C$, a fraction f of the supercooled water changes into ice, and if L' is the heat of fusion of ice, then:

$$q_2 = -m_w \left( c_w \vartheta_\infty + f L' \right) \text{ with } m_w = E \cdot W \cdot V_\infty \tag{2}$$

where:   $c_w$ = Specific heat of water

           $f$ = Freezing fraction

           $E$ = Collection efficiency

           $W$ = Liquid water content

    c)   The density of heat flux due to evaporation:

$$q_3 = 0.62 \frac{\alpha L''}{c_p} \cdot \frac{P_o - P_r}{B} \tag{3}$$

where:   $P_o$ = Vapour saturation pressure of water or ice at the surface

           $P_r$ = Partial water vapor pressure at the edge of the boundary layer

           $L''$ = Heat of vaporization of both water and ice

           $B$ = Barometric pressure

    d)   The density of heat flux due to kinetic energy of the droplets:

$$q_4 = \frac{V_\infty^2}{2} m_w \tag{4}$$

If the surface of the cylinder is neither heated nor cooled:

$$q_1 + q_2 + q_3 - q_4 = 0$$

or:

$$\frac{m_w}{\alpha} \left( -c_w \vartheta_\infty - f L' - \frac{V_\infty^2}{2} \right) - \vartheta_\infty - r \frac{V_\infty^2}{2c_p} + 0.62 \frac{L''}{c_p} \cdot \frac{P_o - P_r}{B} = 0 \tag{5}$$

For any combination $(W, V_\infty, \vartheta_\infty)$ the freezing fraction f can be calculated by the equation (5). The limit for given values of $(W_1, V_{\infty 1}, \vartheta_{\infty 1})$ corresponding to total freezing, i.e. f = 1, is called the Ludlam-limit, which is of major importance when employing devices that measure liquid water content of a cloud by means of the icing speed.

Thus the "Rotating Cylinders" cannot operate precisely when the Ludlam limit is exceeded, i.e. when f < 1, because part of the impinging water is blown off, leading to smaller measured values of liquid water content. This built-in error increases with increasing temperature, airspeed, or liquid water content. Figure 4 shows the Ludlam limits for three cylinder diameters as used in the "Rotating Cylinder" device. The results indicate quite clearly that "Rotating Cylinders" should be used only for conditions of small liquid water content and/or low temperatures.

Since the highest liquid water content occurs in cumulus clouds - about three times greater than that in layer clouds - it was expected that the largest errors would show up in the intermittent maximum curves of Figure 2. Thus efforts were concentrated on measurements in cumulus cloud.

## 3. MEASURING EQUIPMENT USED BY MBB

### a) Liquid Water Content

To overcome the limitations associated with the "Rotating Cylinders" at high liquid water content, MBB developed a special cooled Test Rod [4], [5].

This device consisted of a hollow steel cylinder 30 cm long, and only 1 cm in diameter, to ensure a rate of catch nearly independent of droplet diameter (Figure 5). The cylinder, with an internal flow of liquid nitrogen, was exposed normal to the airstream. Three thermocouples were fitted axially at the surface to provide continuous checking of the required -160 $^{\circ}$C surface temperature. Thus, the latent heat of fusion was transferred and liquid water content of up to 3 g/m$^3$ could readily be measured, except where thickness of ice at the stagnation point exceeded 5 mm. The Test Rod was extensively calibrated in the wind-tunnel at Artington (U.K.), under the test conditions given in Figure 6, before any actual flight test measurements were made.

To check the reproducibility, more than a hundred conditions of (W, $V_\infty$, $\vartheta_\infty$) were tested. It was found that maximum error was in the order of 10 % over the test range.

### b) Droplet Size Measurement

To measure droplet size, the "Oil Slide" technique was employed. A slide was prepared by smearing a strip of glass with a small amount of a special oil. The slide was next inserted into a holder and retracted into a special sampling pole. This pole was then extended into the airflow, with the slide surface vertical and facing forward. The slide was now exposed for a short time in cloud, removed, transferred to a microscope and photographed.
Figure 7 shows a typical photograph of a droplet sample.

### c) Total Temperature Measurement

The total temperature was measured with a Rosemount temperature sensor, Model 102, suitable for operation under icing conditions. The error due to de-icing was approx. $\pm$ 0,5 $^{\circ}$C, which could be considered acceptable.

### d) Data Recording and Test Procedure

Flight tests under natural icing conditions require a very high standard of coordination in all relevant data acquisition instrumentation. Therefore, airspeed, altitude, ambient air temperature, exposure time of the Test Rod, and a time code - which was also registered on all photographs - were simultaneously recorded on a tape recorder.

The aircraft used was a TRANSALL C-160, with a maximum take-off weight of some 100.000 lbs. The tests took place over Western France and Southern Germany, at altitudes ranging from 3.000 ft to 20.000 ft.

A factor which may have had an influence on the reliability of the data, was the systematic bias introduced by obtaining measurements during flights in which icing conditions were deliberately sought, instead of being accidently encountered. The net effect, however, is expected to be negligible, because results have been compared with those of NASA, obtained when faced with the same situation.

## 4. AMOUNT OF DATA AVAILABLE

Thirty-four flights under natural icing conditions have been made, during which a total of 75 icing areas were encountered. An icing encounter, the basic unit of data, consists of all measurements made during flight through a single area of icing conditions. An icing area is defined as one that is separated by at least 40 miles of ice-free conditions from the next observed area of icing, or by a least 6000 ft of altitude from another such area.

The icing clouds have been classified as either cumulus or stratiform, icing encounters having been in forty-seven of the former clouds, and twenty-eight of the latter. Because of insufficient data, results from the stratiform cloud encounters are omitted in this report.

## 5. ANALYSIS

For direct comparison with FAR 25 Appendix C, the analysis was carried out strictly in accordance with TN 2738. For convenience, the main features of this analysis are cited here:

### Exceedance Probability

The three fundamental icing variables used to define any icing condition are the liquid water content W, the mean effective droplet diameter $D_{eff}$, and the ambient temperature $\vartheta_\infty$.

Thus, any particular icing condition may be represented by selected values of these variables, i.e. $W$, $D_{eff}$, and $\mathcal{V}_\infty$. The probability of any random icing encounter of standard extent providing simultaneous values of each of the icing variables equal to, or greater than, each of the selected values (i.e. $W \geq W_1$, $D_{eff} \geq D_{eff1}$, $|\mathcal{V}_\infty| \geq |\mathcal{V}_{\infty 1}|$) will be termed exceedance probability $P_e$, related to the icing conditions $W_1$, $D_{eff1}$, and $\mathcal{V}_{\infty 1}$,

The exceedance probability represents the probability of a simultaneous occurrence of three events which are not necessarily indepedent. In order to evaluate $P_e$, use is made of the theorem of compound probability [6] which states that the probability of a simultaneous occurrence of three events A, B, and C, is equal to the probability of the occurrence "A" times the conditioned propability of the occurrence "B" under the condition that "A" will occur, times the conditioned probability of the occurrence "C" under the condition that both "A" and "B" will occur.
This theorem may be expressed symbolically as follows:

$$P_e = P_A \cdot P_B(A) \cdot P_C(A,B) \tag{6}$$

If it is considered that the probability of exceeding certain values of $W$, $D_{eff}$, and $|\mathcal{V}_\infty|$ is analogous to the probability of the occurrence of events A, B, and C, as expressed in equation (6), then the exceedance probability $P_e$ may be represented by the product of three probability factors Q, R, and S, according to the equation

$$P_e = Q.R.S \tag{7}$$

where

$Q(|\mathcal{V}_\infty|)$     is a term that defines the probability Q as a function of $\mathcal{V}_\infty$, and expresses the probability for a given value of $\mathcal{V}_\infty$ for a random icing encounter having a temperature depression below freezing, equal to or greater than $|\mathcal{V}_\infty|$.

$R(W,|\mathcal{V}_\infty|)$     is a term that defines the probability R as a function of $W$ where $\mathcal{V}_\infty$ is specified, and expresses the probability for a given value of $W$ for a random icing encounter having a liquid water content equal to or greater than $W$, under the condition that the temperature depression below freezing is equal to or greater than selected values of $|\mathcal{V}_\infty|$.

$S(D_{eff},W|\mathcal{V}_\infty|)$ is a term that defines the probability S as a function of $D_{eff}$, when $W$ and $\mathcal{V}_\infty$ are specified, and expresses the probability for a given value of $D_{eff}$ for a random icing encounter having a value of droplet diameter equal to or greater than $D_{eff}$, under the condition that the liquid water content is equal to or greater than $W$, and the temperature depression below freezing is equal to or greater than $|\mathcal{V}_\infty|$.

Figure 8 represents a graphical plot with the variables $W$, $D_{eff}$, and $|\mathcal{V}_\infty|$, as axes. Any given icing condition $W_1$, $D_{eff1}$, $|\mathcal{V}_\infty|_1$, defined by selected values of these variables, appears as a single point $O_1$ on the plot.

Corresponding to the point $O_1$, there is an exceedance probability that a random icing encounter will provide simultaneous values of each of the icing variables, equal to or greater than each of the selected values $W_1$, $D_{eff1}$, and $\mathcal{V}_{\infty 1}$. Referring to equation (7), the value $P_{e1}$ would be given by the equation:

$$P_{e1} = Q_1 R_1 S_1$$

Thus, when $P_e$ regarded as a constant, $P_{e1}$, equation (7) defines a surface passing through $O_1$, represented by all the combinations of $W$, $D_{eff}$, and $\mathcal{V}_\infty$, which have the same probability of being simultaneously equalled or exceeded.

The preceeding theory was slightly modified by the authors of TN 2378, for that portion of the equiprobability surface that represents low values of liquid water content and large values of droplet diameter, resulting in two portions of the equiprobability surface. No reason was found to modify the theory in such a manner in this report.

## 6. STATISTICAL CALCULATIONS AND RESULTS

$Q = Q(|\mathcal{V}_\infty|)$

The "N" maximum values of $|\mathcal{V}_\infty|$ measured within N icing areas were arranged in a decreasing sequence of values of $|\mathcal{V}_\infty|$, beginning with the largest values of $|\mathcal{V}_\infty|$ and the ordinal number $m = 1$. If a certain <u>temperature</u> occured p times in p icing encounters, then only one value $\bar{m}$ was used with $\bar{m} = \sqrt{m(m+p-1)}$, where m is the first and m+p-1 the last ordinal number.

From these m values, $Q = Q(|\mathcal{V}_\infty|)$ was determined by the equation

$$Q = \frac{3m - 1}{3N + 1} \tag{8}$$

where m is the ordinal number and N the number of icing encounters.

$R = R(W, |\mathcal{V}_\infty|)$

Based on the preceeding theory, twelve temperatures $\mathcal{V}_{\infty n}$ between $-7\,^\circ C$ and $-17,5\,^\circ C$ were selected. For each temperature, the maximum liquid water contents were arranged with decreasing $W$ and $R(W,|\mathcal{V}_\infty|)$ determined by equation (8) above as follows:

$$R(W,|\mathcal{V}_\infty|) = \frac{3m - 1}{3N_n + 1}$$

where $N_n$ is the number of icing encounters with $|\mathcal{V}_\infty| \geq |\mathcal{V}_\infty|_n$.

$$S = S(D_{eff}, W, |\mathcal{V}_\infty|)$$

For selected values of W and $|\mathcal{V}_\infty|$, the function $S(D_{eff}, W, |\mathcal{V}_\infty|)$ was determined in the same way as $Q(|\mathcal{V}_\infty|)$ and $R(W, |\mathcal{V}_\infty|)$. However, it could be demonstrated that S was independent of R and Q. With these three functions - Q, R, S - the equiprobability surface for selected exceedance probabilities $P_e$ could be calculated by the formula

$$P_e = Q\ R\ S$$

## Results

Figure 9 shows the function $Q(|\mathcal{V}_\infty|)$ on normal probability paper. The curve intersects the $|\mathcal{V}_\infty|$ axis at approx. -6 °C, due to aerodynamic heating at velocities between 100 m/s and 130 m/s of the test aircraft. For purposes of design of ice protection systems in modern aircraft, however, temperatures above -6 °C are generally of no importance, because this aerodynamic heating, even during holding and descent, is greater than 6 °C.

The functions $R(W, |\mathcal{V}_\infty|)$ for $|\mathcal{V}_\infty| \geq 7$ °C, $\geq 10$ °C, and $\geq 17$ °C are shown in Figures 10, 11, and 12 respectively. The function S, which as already mentioned, is independent of W and $\mathcal{V}_\infty$, is shown in Figure 13.

For direct comparison with the plots used in FAR 25 Appendix C, a graphical representation was chosen, with liquid water content and mean effective droplet diameter for different temperatures, for three values of exceedance probability - viz. $P_e = 10^{-1}, 10^{-2}$, and $10^{-3}$ (Ref.: Figures 14, 15, and 16).

The limitations noted above for "Rotating Cylinders" show up very clearly at high liquid water contents and high temperatures. From Figure 15 it appears evident that, for temperatures higher than -15 °C, the anticipated exceedance probability of $10^{-3}$ -according to the data -15 °C from TN 1855 and TN 2738 - seems to be in fact considerably greater. Figures 14 and 15 indicate that an exceedance probability of between $10^{-2}$ and $10^{-1}$ may be assumed. Thus the results obtained from these tests tend to be in general agreement with the Ludlam theory.

For low temperatures and small liquid water content, where the "Rotating Cylinders" were expected to measure more satisfactorily, test values obtained were even lower than those of FAR 25 Appendix C. There may be several reasons for this:

a) Statistical error, due to extrapolating from limited sampling of icing encounters

b) Regional differences in meteorological conditions between US West Coast and Europe

c) Variations in liquid water content in the vicinity of the test aircraft fuselage

The statistical errors for a confidence limit of 68 % have been estimated and are shown in Figure 16 for $\mathcal{V}_\infty = -7$ °C (dotted lines). However, the upper limits thereof should be regarded with considerable caution, because statistics are no respecters of cloud physics.

Variations in liquid water content in the vicinity of the aircraft fuselage have been calculated, and account for an increase in the measured liquid water content of approx. 20%. This value has been taken into consideration in Figures 14, 15, and 16.

Finally, it may be noted that all the values of liquid water content have been corrected to 2.6 nautical miles to agree with the distance factor in FAR 25 Appendix C.

## 7. CONCLUSIONS

In conclusion, when considering criteria from - say - the last twenty years, in relation to the design and certification of any ice protection equipment for transport aircraft, it is recommended that all available current criteria on conditions of higher liquid water content, and temperatures above -15 °C, be taken into consideration in future projects.

Further worldwide observation and measurement of these meteorological conditions should be urgently initiated, employing instrumentation and technique which are not limited to measuring small liquid water content.

This would result in more solid foundations for future statistical analysis of the phenomena.

## References

1. Jones, Alun R., and Lewis, William: Recommended Values of Meteorological Factors to be Considered in the Design of Aircraft Ice Prevention Equipment. NACA TN 1855, 1949.

2. Lewis, William, and Bergrun, Norman R.: A Probability Analysis of the Meteorological Factors Conducive to Aircraft Icing. NACA TN 2738, 1952.

3. Brun, B.R., Lewis, William, Perkins, P.J. and Serafini, J.S.: Impingment of Cloud Droplets on a Cylinder and Procedure for Measuring Liquid Water Content and Droplet Sizes in Supercooled Clouds by Rotating Multicylinder Method. NACA TN 215, 1955.

4. Kleuters, W. and Wölfer, G.: Ermittlung der für die Auslegung von Enteisungssystemen erforderlichen meteorologischen Vereisungsparameter. MBB-Bericht, 1970.

5. Kleuters, W.: Neuere Untersuchungen auf dem Gebiet der meteorologischen Vereisungs- parameter, Vortrag auf der 5. Jahrestagung der DGLR in Berlin, 1972.

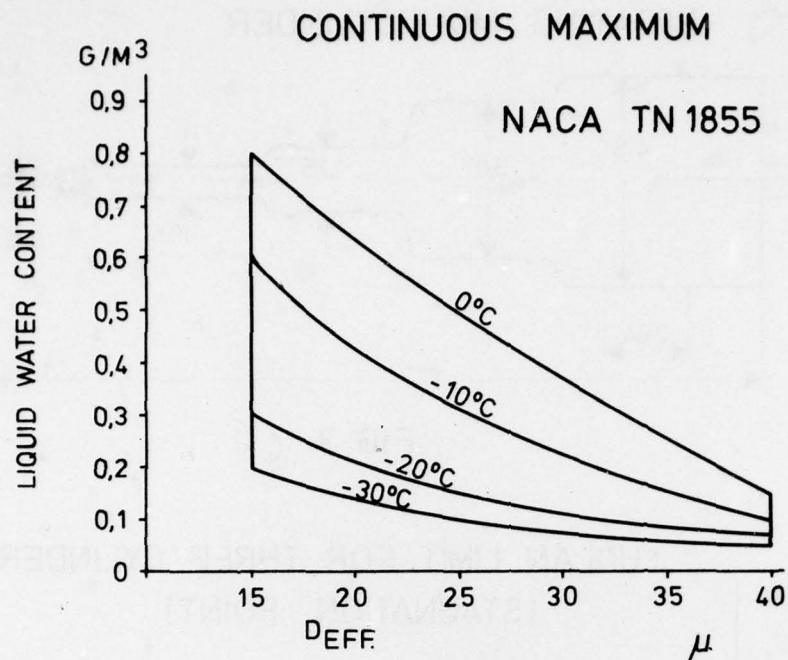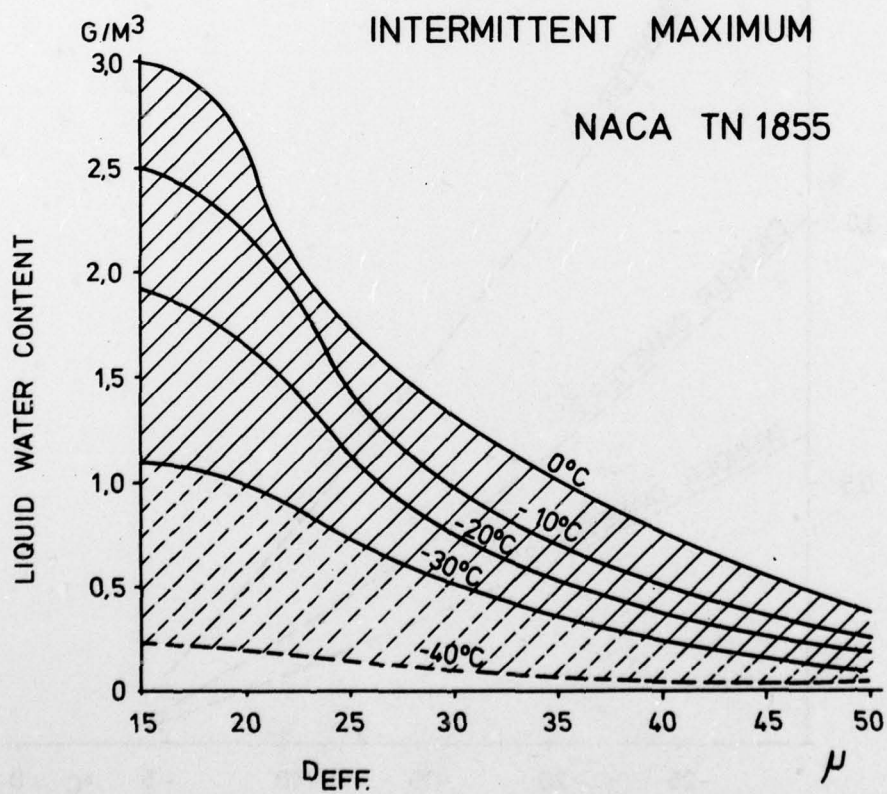6. Uspensky, J.V.: Introduction to Mathematical Probability. McGraw, Hill Book Co. Inc. N.Y. 1937, p.31.

# CONTINUOUS MAXIMUM

## NACA TN 1855
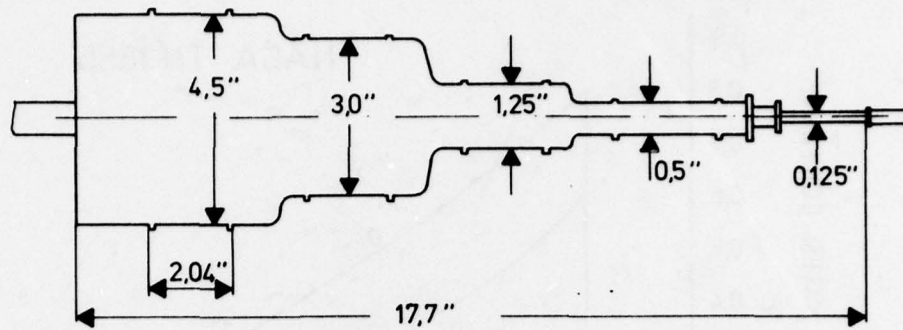


FIG. 1

# INTERMITTENT MAXIMUM

## NACA TN 1855



FIG. 2

# ROTATING MULTICYLINDER



FIG. 3

# LUDLAM LIMIT FOR THREE CYLINDERS
## (STAGNATION POINT)



$$\text{AIRSPEED} = 100\,m/s\,;D_{eff}=20\mu\,;H=0m\,;$$

$$\frac{m_w}{\alpha}(-c_w\vartheta_\infty-L'-\frac{V_\infty^2}{2c_w})-\vartheta_\infty-\frac{V_\infty^2}{2c_p}+0.62\frac{L''}{c_p}\frac{P_0-P_f}{B}=0$$

FIG. 4

# TEST ROD

HOT AIR

FUSELAGE WALL

DIRECTION OF AIRSPEED

1cm

THERMOCOUPLES

L.N. COOLING

TO THERMOCOUPLES

ca. 30 cm

STORAGE CON-
TAINER FOR L.N.

PRESSURE
CONTAINER
FOR L.N.

VALVES

FIG. 5
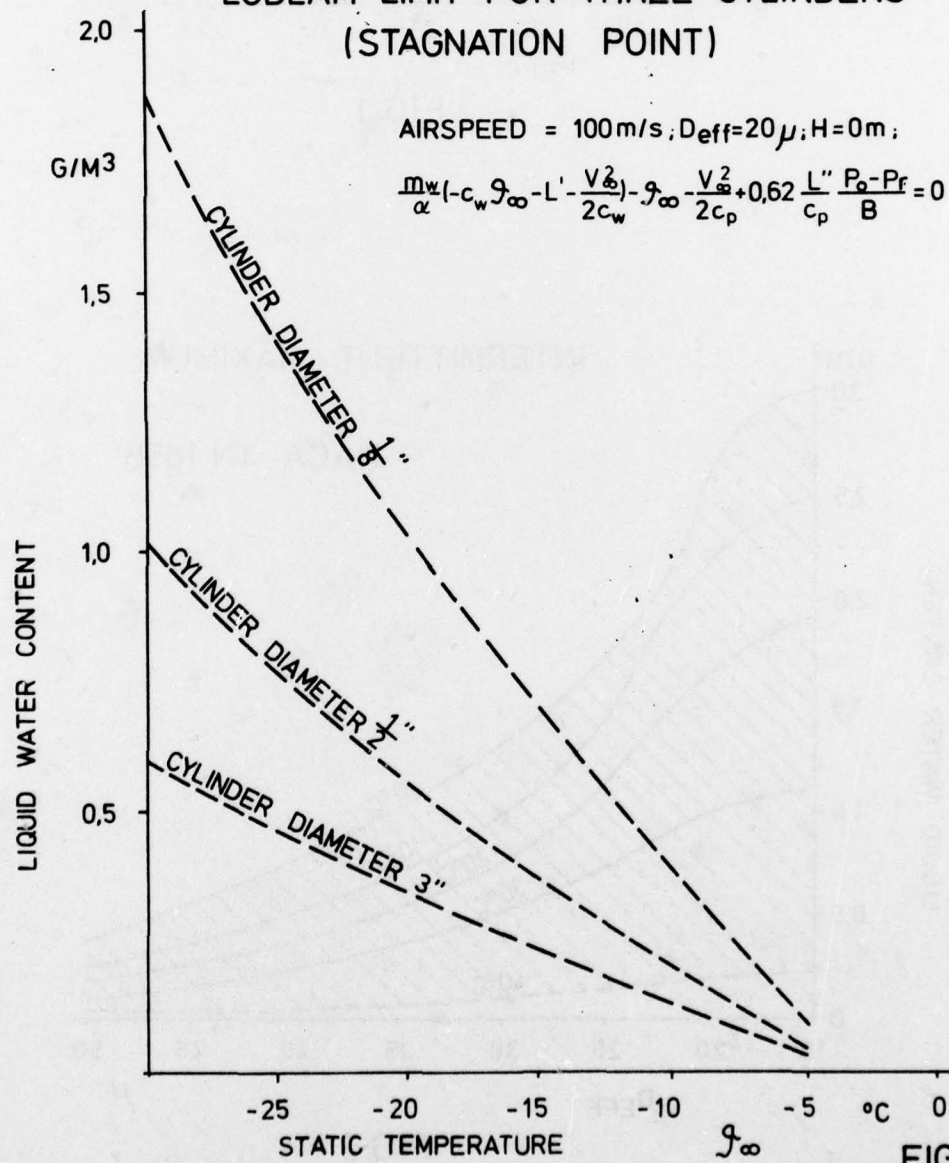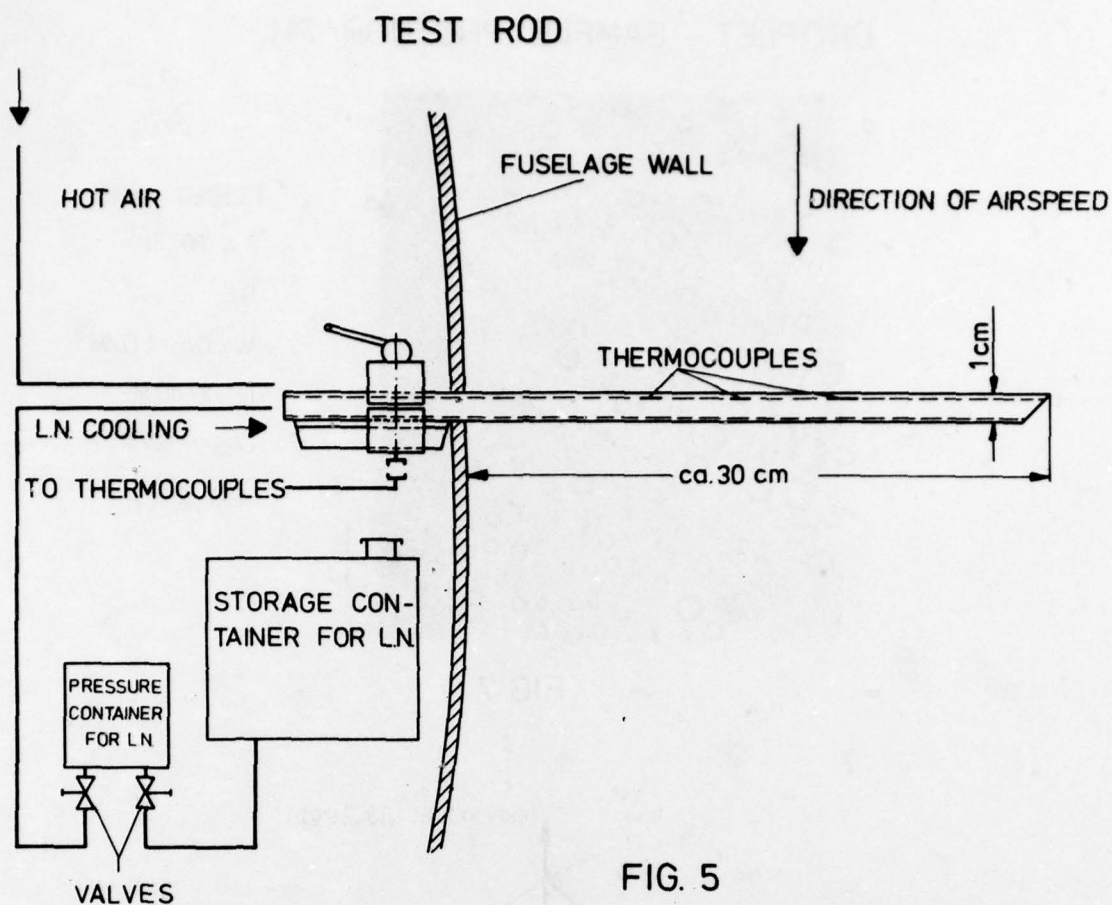
## CALIBRATION OF THE TEST ROD

TEMPERATURE RANGE : -5°C TO -30°C

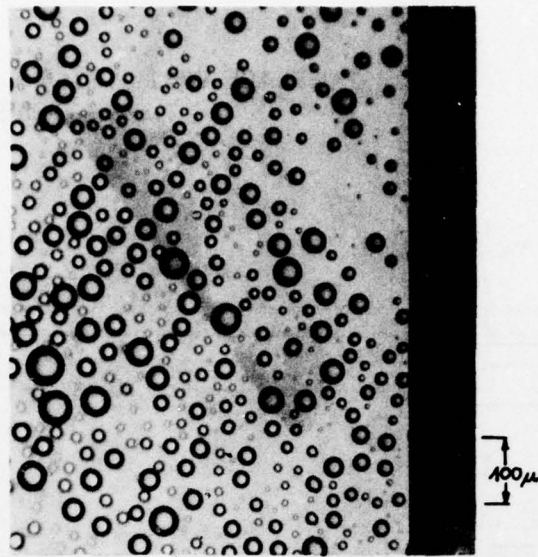AIRSPEED RANGE : $90^m/s$ TO $130^m/s$

LIQUID WATER CONTENT

RANGE : $0.2 \frac{g}{m^3}$ TO $3.0 \frac{g}{m^3}$

MEAN EFFECTIVE

DROPLET DIAMETER: $20 \mu$

FIG. 6
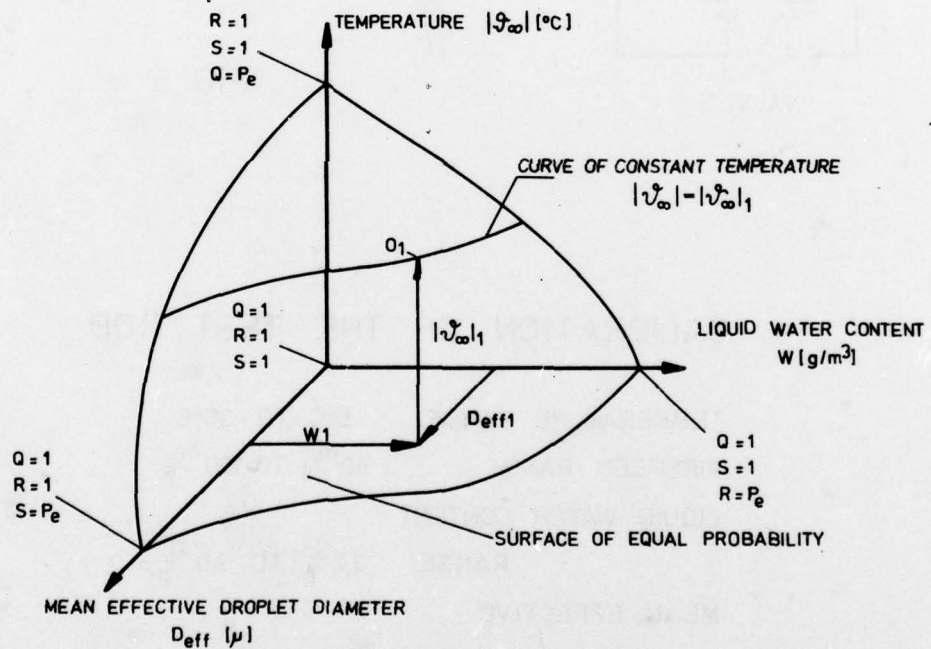
# DROPLET - SAMPLE PHOTOGRAPH



FLIGHT   M10

8.4.70 , $9^{16}$

S C

W= CA. 1 G/M$^3$

H = 1700 M

$\vartheta_\infty$ = -6,5°C

$D_{EFF}$ = 29 $\mu$

100$\mu$

## FIG. 7



R = 1
S = 1
Q = P$_e$

TEMPERATURE  $|\vartheta_\infty|$ [°C]

CURVE OF CONSTANT TEMPERATURE
$|\vartheta_\infty| = |\vartheta_\infty|_1$

O$_1$

Q = 1
R = 1
S = 1

$|\vartheta_\infty|_1$

LIQUID WATER CONTENT
W [g/m$^3$]

D$_{eff1}$

Q = 1
R = 1
S = P$_e$

W1

Q = 1
S = 1
R = P$_e$

SURFACE OF EQUAL PROBABILITY

MEAN EFFECTIVE DROPLET DIAMETER
D$_{eff}$ [$\mu$]

THE EXCEEDANCE PROBABILITY Pe$_1$ FOR O$_1$ PRESENTS THE PROBABILITY THAT THE THREE VARIABLES
$|\vartheta_\infty|$, D$_{eff}$, W  ARE EXCEEDED SIMULTANEOUSLY IN ANY ICING ENCOUNTER [2]

## FIG. 8

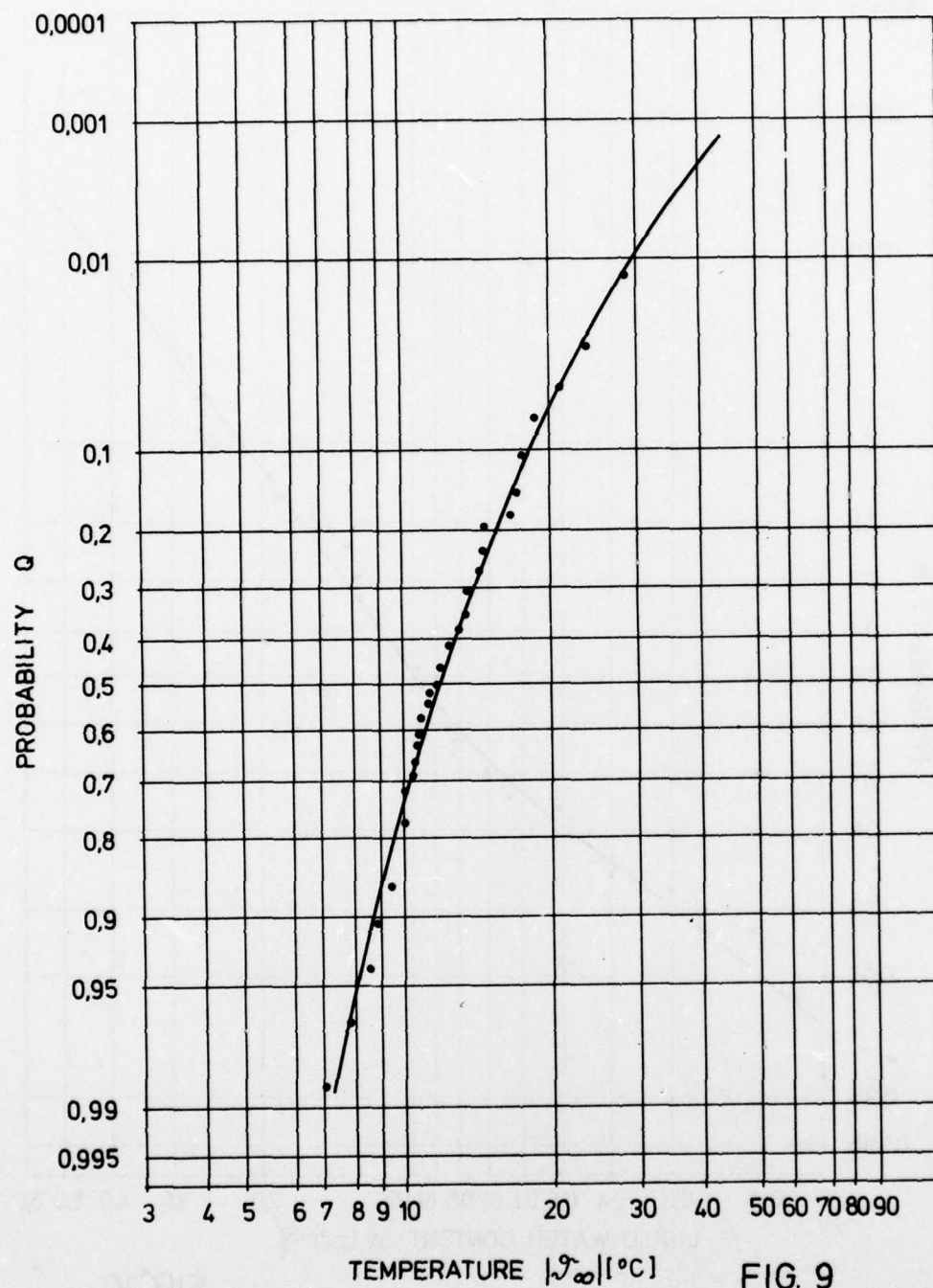PROBABILITY FUNCTION  $Q(|\vartheta_\infty|)$
CUMULUS-CLOUD

TEMPERATURE  $|\vartheta_\infty|[^\circ C]$       FIG. 9

PROBABILITY FUNCTION  R(W, $|\vartheta_\infty|$)
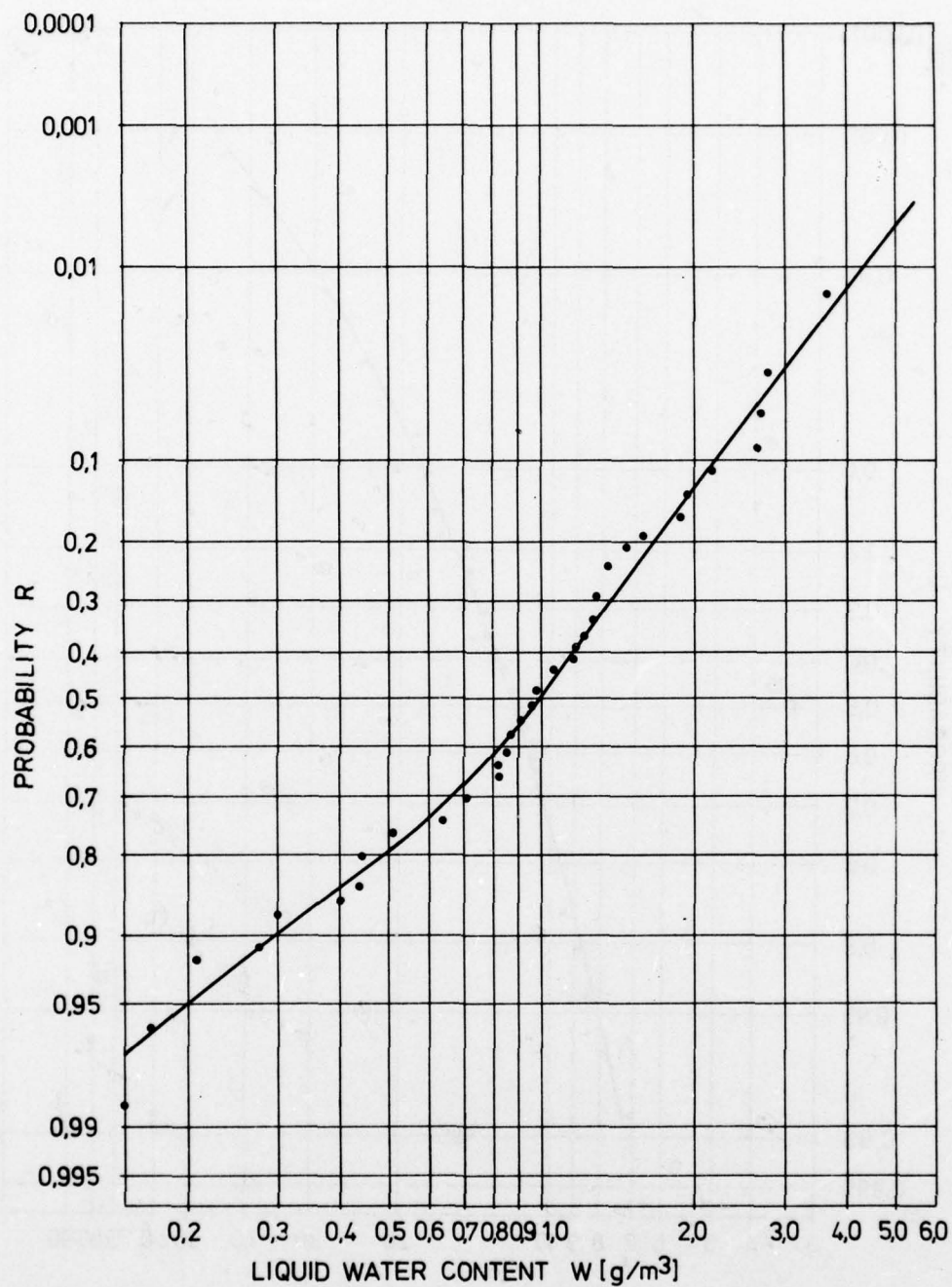$|\vartheta_\infty| \geq 7°C$ , CUMULUS–CLOUD

FIG. 10

PROBABILITY FUNCTION $R(W,|\vartheta_\infty|)$
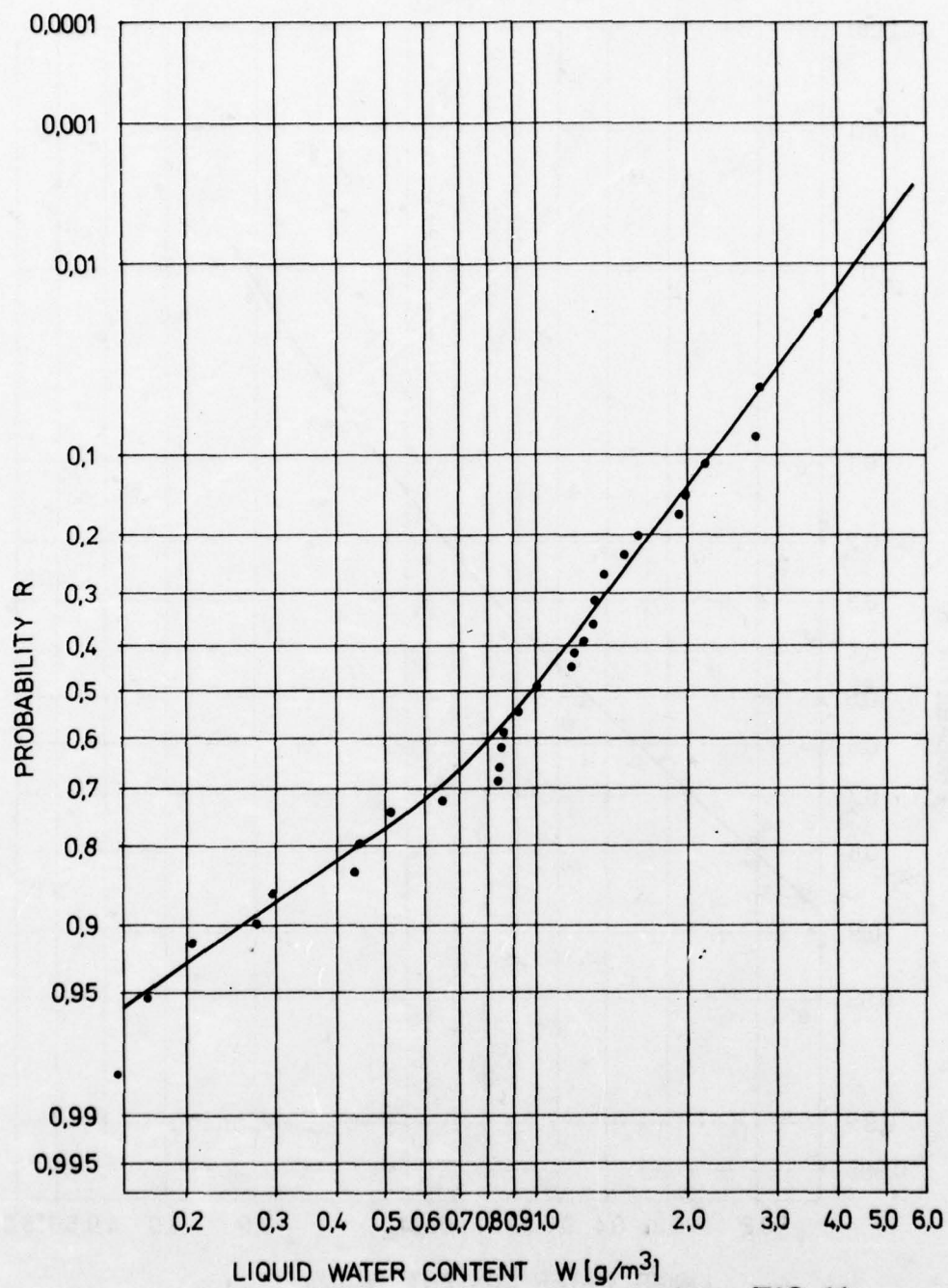$|\vartheta_\infty| \geq 10°C$, CUMULUS−CLOUD

FIG. 11

PROBABILITY FUNCTION $R(W,|\vartheta_\infty|)$
$|\vartheta_\infty| \geq 17°C$, CUMULUS−CLOUD
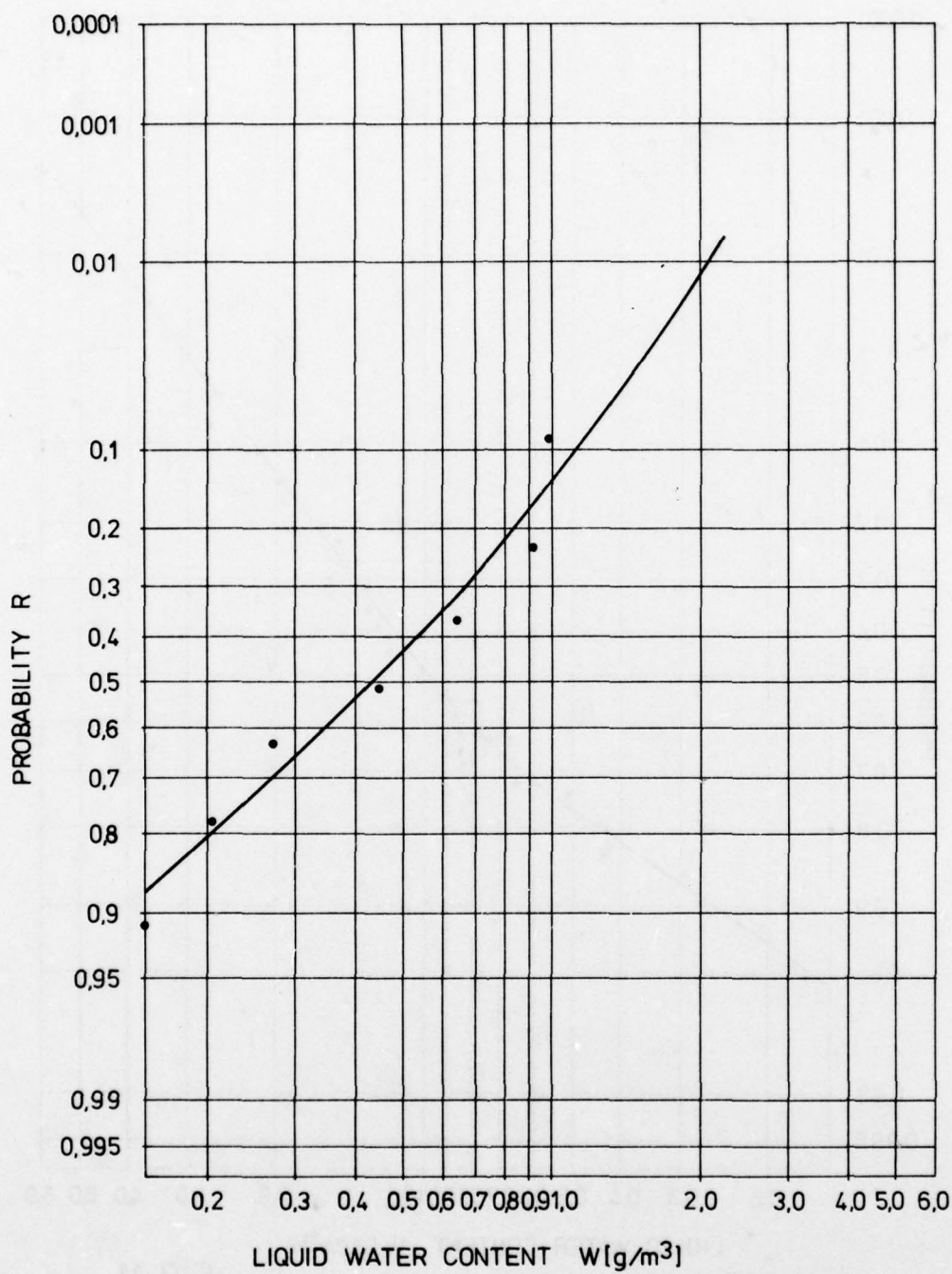
FIG. 12

PROBABILITY FUNCTION $S(D_{eff}, W, |\vartheta_\infty|)$
$|\vartheta_\infty| \geq 0°C; W \geq 0,15 g/m$ ; CUMULUS−CLOUD
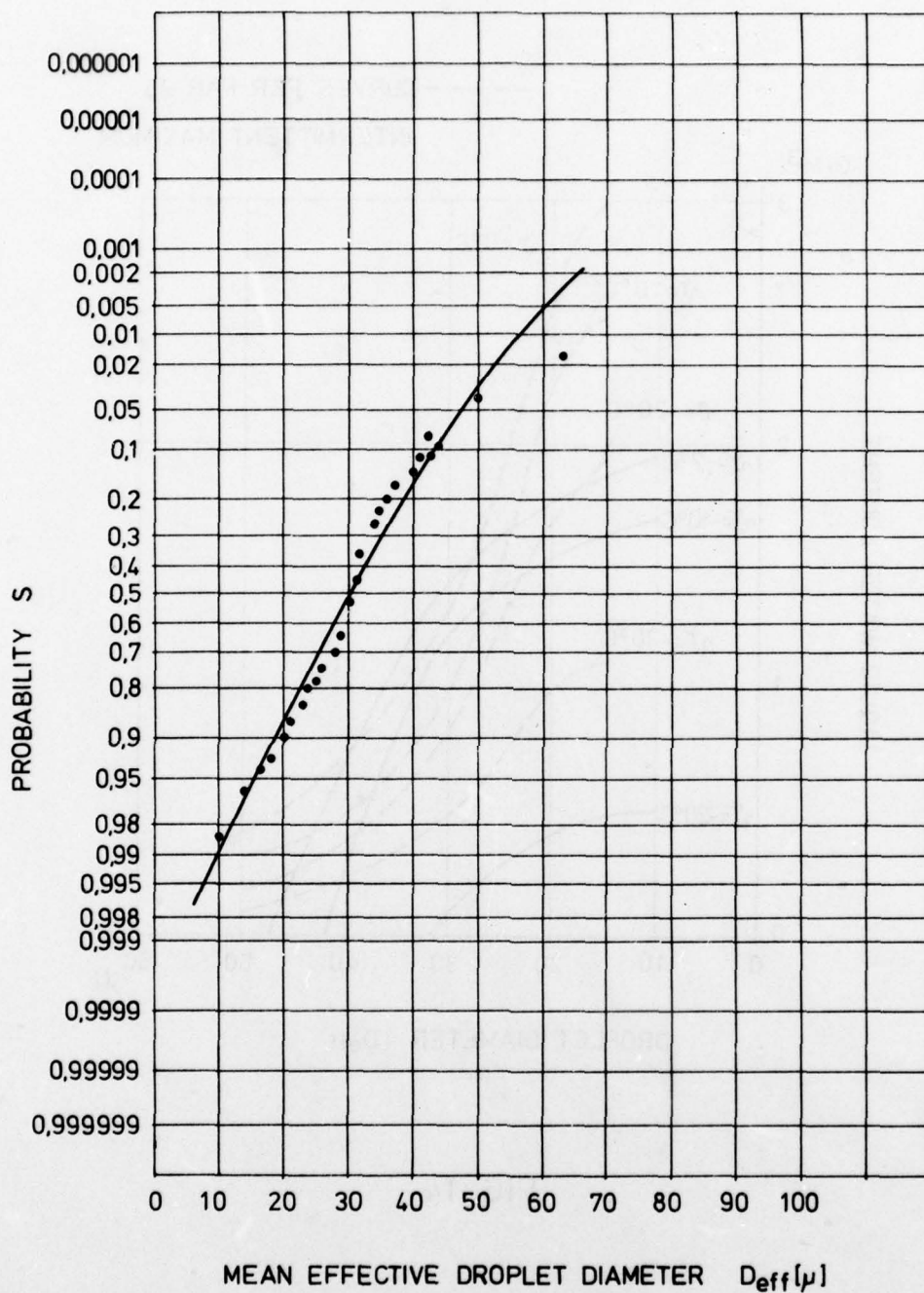
MEAN EFFECTIVE DROPLET DIAMETER $D_{eff}[\mu]$
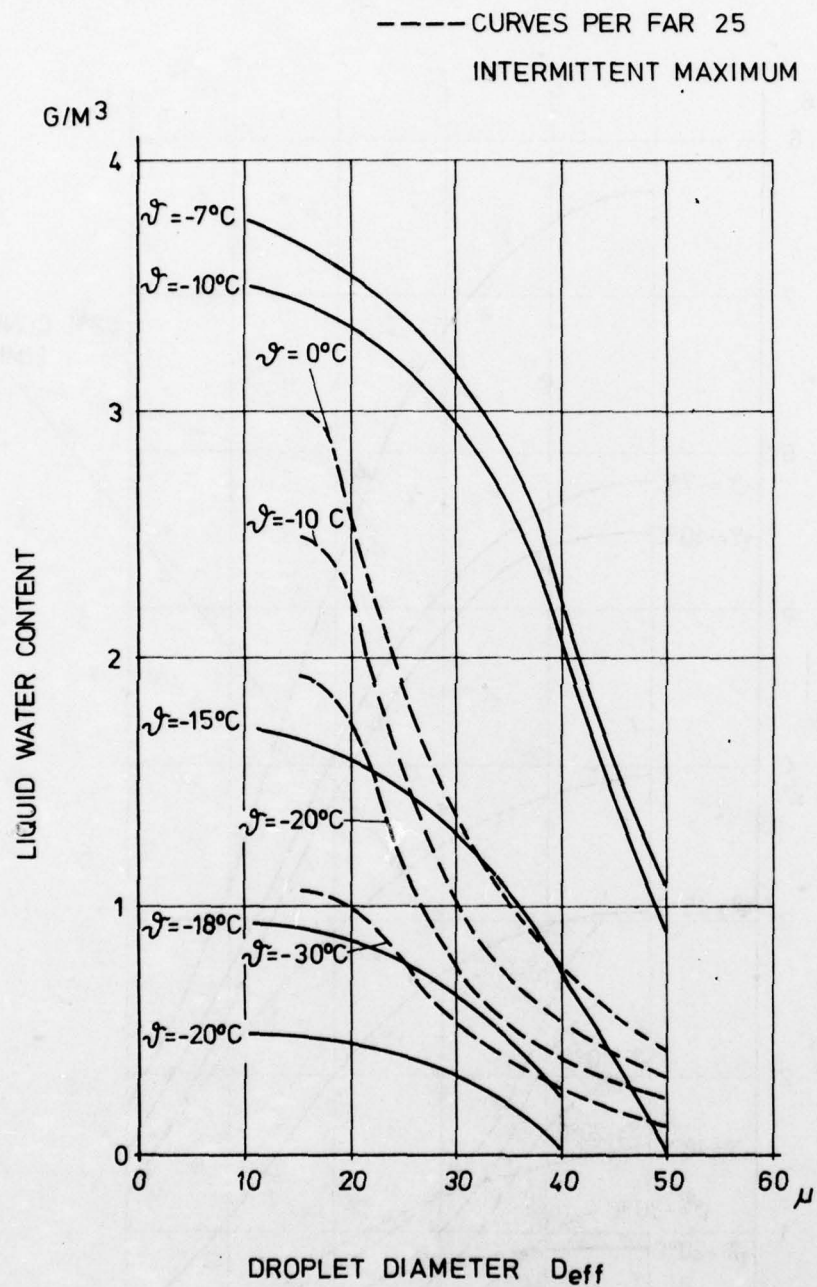
FIG. 13

# CURVES OF EQUAL PROBABILITY
## $P_e = 10^{-1}$   CUMULUS-CLOUDS
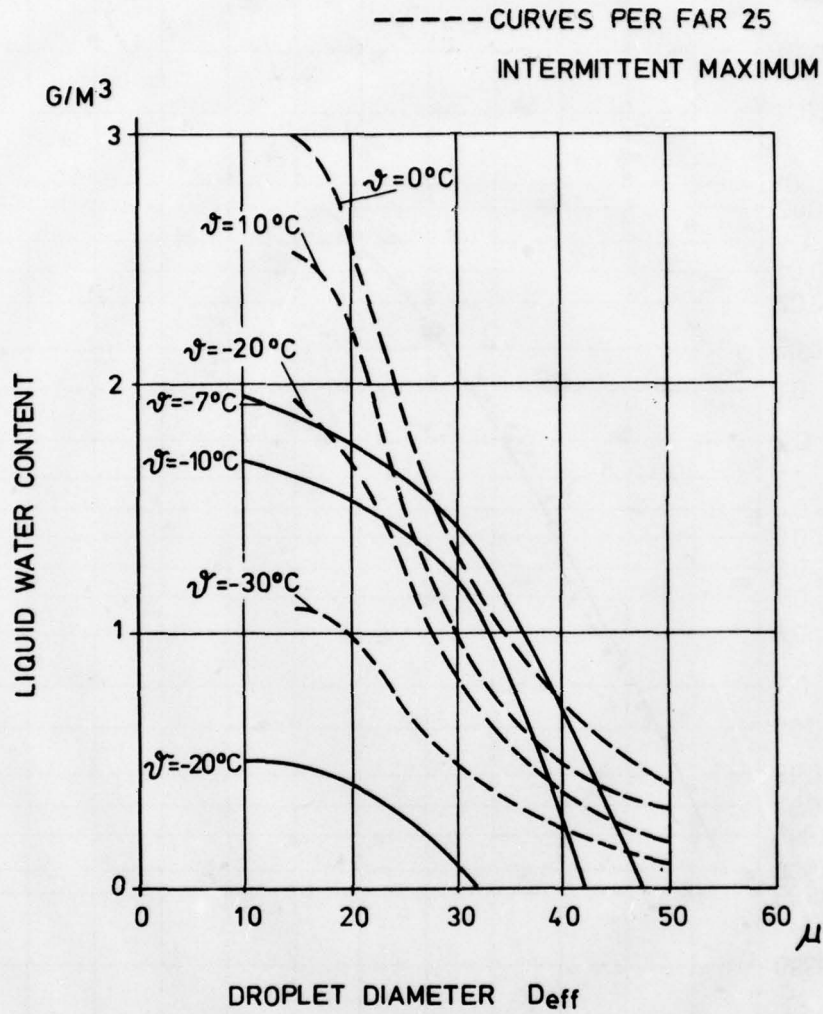


FIG. 14

# CURVES OF EQUAL PROBABILITY
## $P_e = 10^{-2}$   CUMULUS - CLOUDS

----- CURVES PER FAR 25
INTERMITTENT MAXIMUM



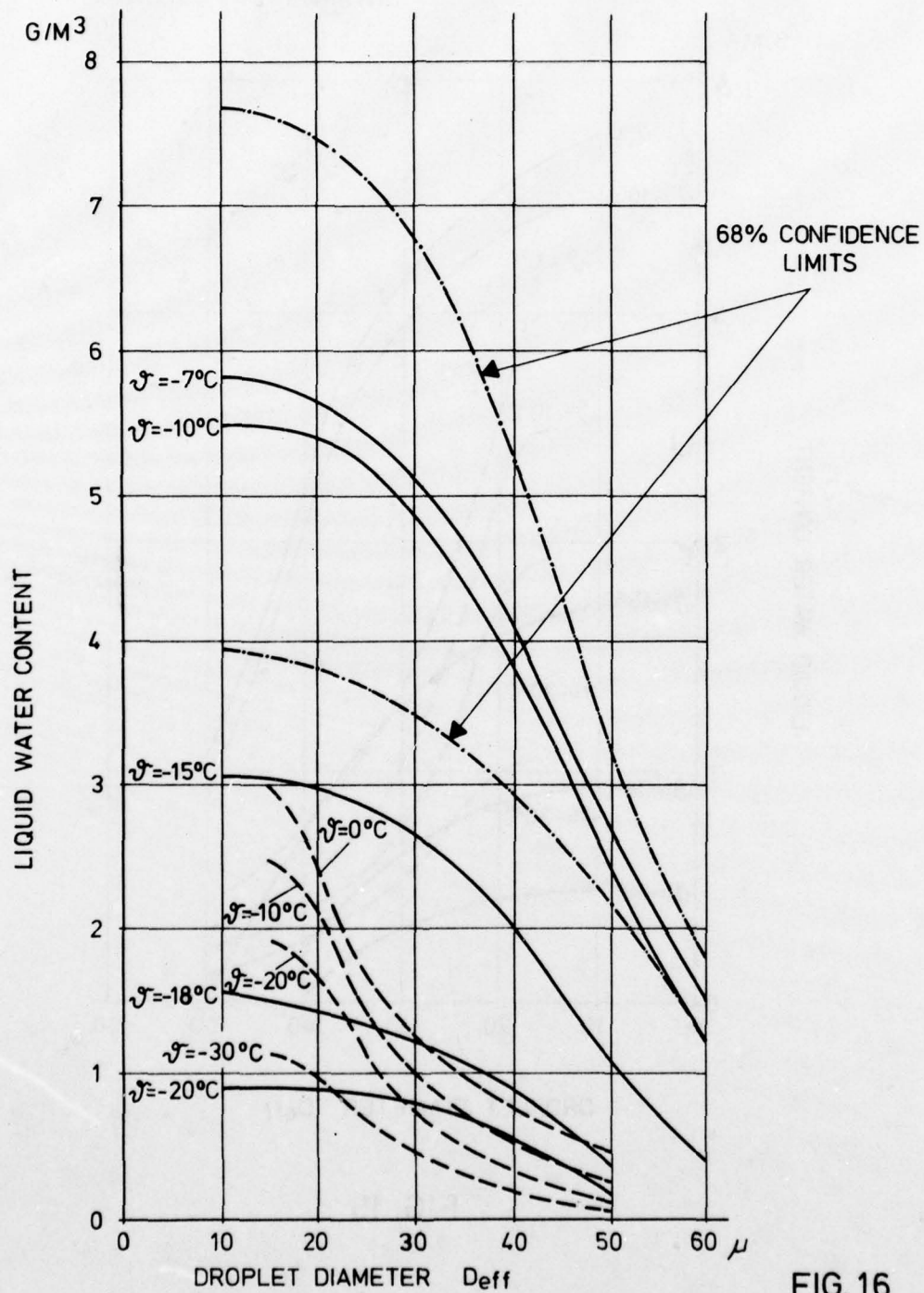FIG. 15

# CURVES OF EQUAL PROBABILITY
## $P_e = 10^{-3}$ CUMULUS - CLOUDS

---- CURVES PER FAR 25
INTERMITTENT MAXIMUM



FIG. 16

# HELICOPTER ICE DETECTION, ICING SEVERITY
# AND LIQUID WATER CONTENT MEASUREMENTS

J. R. Stallabrass
Senior Research Officer
Division of Mechanical Engineering
National Research Council of Canada
Ottawa, Canada
K1A OR6

## SUMMARY

Icing detection on a helicopter presents difficulties because of the wide relative speed range from hover to maximum cruise. High detection sensitivity is necessary at any flight speed because of the high susceptibility of the rotor blades to the effects of even quite small ice accretions. An icing detector is described that largely overcomes the problem of speed dependence and thus permits the determination of icing rate and cloud liquid water content with reasonable accuracy.

## INTRODUCTION

The susceptibility of fixed wing aircraft to cloud icing is well known, but perhaps it is not generally appreciated to what degree the flight safety of some helicopters is affected in very short time periods. This is particularly true for light helicopters (Ref. 1), but Bradley in a recent paper (Ref. 2) has shown that this can be true for larger helicopters as well, and he documents a case where intolerable rotor icing conditions were reached within a minute of the onset of icing. If helicopters are to fly IFR, and that implies flying in icing conditions, then instrumentation capable not only of quantifying the icing environment but also of providing an almost instantaneous indication of having encountered an icing condition is essential. The quantitative information provided by such instrumentation (i.e. the icing severity) is essential not only to inform the pilot so that he may take the appropriate action, but also for the proper control of any icing protection systems that may be fitted to the helicopter.

What sort of information should such instrumentation provide? The critical components on the helicopter are the engines and the rotor blades. The icing qualification requirements of the engine should ensure that no icing problems will be encountered there -- other than the danger that could result from the ingestion of shed ice or slush. Hopefully the more robust engines used in the new generation of helicopters will largely obviate this danger. That leaves the rotor blades, and clearly the information that is required in regard to them is the rate at which the ice is building up at some representative radius. The shape of the ice is also important, but this is a function largely of air temperature, which is readily measurable, as well as of the liquid water content. The presence of snow or ice crystals in the supercooled icing cloud also affects the icing rate and the shape of the ice accretion, the implications of which have not been fully appreciated until recently. It seems probable that the rapid rate of performance deterioration at high air temperatures as reported by Bradley (Ref. 2) is the result of such mixed icing conditions. The measurement of such mixed conditions is a formidable task for which at present no means exists.

## ICE DETECTION SYSTEM

An instrument has been developed to provide data on the supercooled droplet cloud conditions which represent by far the most common type of icing conditions. Because of the wide relative operating speed range of a helicopter compared to that of a fixed wing aircraft, the detection of icing conditions has presented special problems. The droplet catch rate and hence the icing rate are a function of velocity, and thus the response of an ice detector probe mounted on the fuselage of a hovering helicopter is essentially nil, while at the same time the essential components for sustaining flight (i.e. the engines and the rotor blades) are experiencing substantially the same icing rate as in cruising flight. To maintain a constant response to a given set of icing conditions regardless of flight velocity, some means of establishing a constant relative velocity between the ice sensing element and the droplet laden atmosphere is needed.

In the instrument which is referred to as the Dynamic Ice Detector, the relative velocity is obtained by moving the droplet laden air over a stationary ice sensor, rather than moving the sensing means through the ambient air. This is achieved by placing an ice collecting probe in the secondary induced flow of an air ejector. The air ejector forms the body of the instrument (Fig. 1) and comprises a smooth entry for the induced ambient air and within this entry is the primary air nozzle in the form of an annular wall jet. A short cylindrical mixing length behind the annular jet accommodates the ice collecting probe and the sensing means. The primary and secondary air flows are exhausted to the atmosphere through a diffuser.

The air required for operation of the ejector nozzle is normally delivered from the engine compressor bleed at an operating pressure of about 50 psig (345 kPa), with an air mass flow of about 0.5 lb/min. (0.23 kg/min.). By ducting the hot bleed air up the leading edge of the strut and into the plenum in the nose of the detector body, anti-icing of the strut and body is accomplished.

The induced secondary velocity experienced by the ice collecting probe is a function of airspeed and is of the form shown in Fig. 2. At low airspeed the effect of the ejector predominates and the induced velocity is essentially constant, while the ram effect predominates at high airspeeds, and the induced velocity approaches proportionality with the airspeed. The maximum operating airspeed of a helicopter normally corresponds to a point just above the knee of the curve.

For sensing the ice building up on the probe, a beam of near infrared (IR) radiation from a miniature emitter mounted in the duct wall is directed across the leading edge of the probe to a sensor in the opposite wall. As ice is accreted on the probe the IR beam is gradually occluded and once a given thickness is accumulated, logic circuits within the unit turn on electric current to de-ice the probe. The cycle can then repeat. The probe consists of a thin-wall metal tube 2.8 mm in diameter that has sufficient electrical resistance to serve as its own heater, thus no delicate internal filament is required. An ice warning signal is provided at the initiation of de-icing and its duration may be preset to any desired value.

Figure 3 shows the manner in which the voltage output of the infrared sensor varies during the ice/de-ice cycle of the detector. As ice begins to form on the probe the signal output level begins to rise at (a) from its quiescent level. When the output voltage reaches a reference value $V_{ref}$ at (b) as a result of between 0.25 and 0.4 mm of ice having accreted on the probe, the probe heater and signal lamp are activated. The probe is heated for a period, t, sufficient to ensure de-icing, and after a short cooling period ice again begins to form on it.

## MEASUREMENT OF ICING SEVERITY

Of particular significance is the linearity of the voltage ramp between points d and b in Fig. 3, because this implies that the slope in this region may be used as a measure of the rate of icing, or, more significantly, since the velocity remains essentially constant within the operating airspeed range, this slope can be used to determine the liquid water content of the icing cloud. Advantage was taken of this to develop two types of icing severity indicators. In both, the time required for the sensor voltage to rise from a level corresponding to point d to the level $V_{ref}$ corresponding to point b was measured and used to determine the average concentration between points d and b. The value determined was displayed until updated at the completion of the next icing cycle, or until a certain "time-out" period had elapsed after which the display reverted to zero if no further updates had been received.

The first type of severity indicator was a simple 3-level device in which one of the three lights, corresponding to Light, Moderate or Heavy icing severity, was lit. If the measured rise time was less than a given time, $t_1$, then the Heavy light was switched on; if the rise time was greater than $t_1$, but less than a second value $t_2$, the Moderate light was lit; and if the rise time exceeded $t_2$, then the indication was of Light icing. The reference times $t_1$ and $t_2$ could be adjusted to permit the desired severity levels to be set, for instance, the transition from Light to Moderate might be set at 0.25 g m$^{-3}$ and from Moderate to Heavy at 0.5 g m$^{-3}$.

The second type of indicator or Icing Severity Meter takes the rise time, t, and by means of a calculator chip performs the operation:

$$LWC = k/t$$

where k is a constant that characterizes the slope of the voltage ramp. The resultant value of liquid water content is displayed digitally by a LED display. The Icing Severity Meter together with the Ice Detector unit are shown in Fig. 4. As with the 3-light display, the digital LWC indication is displayed until updated or until a time-out period is exceeded.

It was thought that the 3-level system might be more acceptable as a visual icing severity indication to the pilot and flight crew where regular military or commercial operations were concerned, while the digital Icing Severity Meter was considered more applicable to test, qualification and research applications. For control of a rotor blade icing protection system it was originally thought that the 3-level system would suffice, but the digital system is so attractive and versatile that it has recently been adapted to provide this control function, as will be described later.

## PROBLEMS ENCOUNTERED

It would not be fair to give the impression that no problems were encountered in the development of this ice detector, for indeed there were problems.

The major problem that had to be overcome was that due to contamination of the optical components of the sensing system by dirt. Contamination was present in the ambient air and in the compressor bleed air. Often particles in the air, i.e. smoke, etc., would have no effect in dry air conditions, but would be a serious source of contamination when water droplets were also present in the air.

Many modifications were made to the detector to try to solve this problem, and although it may not be possible to completely eliminate it, the rate of dirtying has been reduced to what is considered an acceptable level by ventilating the optical surfaces with filtered air. The venturi suction effect in the detector duct is used to draw this air over the windows.

It was pointed out earlier that the induced velocity was essentially constant over a range of airspeeds from the hover up. It was found that the rate of icing on the probe is not constant as might be expected, but that at low airspeeds when the entry conditions are less than isokinetic, droplet concentration enhancement occurs on the centre line of the duct where the ice is sensed, with the result that the indicated liquid water content takes on the sort of characteristics shown in Fig. 5. If the induced velocity is too great, the concentration enhancement is excessive, while if the duct velocity is too low, the indicated liquid water content is too airspeed-dependent. The optimum induced velocity is that which provides an indication of liquid water content that lies within a reasonable tolerance range of the true value over the widest possible airspeed range.

Variability in the bleed air supply temperature in different helicopter installations, and the possibility of inadequate heat to maintain the detector body anti-iced under all icing conditions, resulted in a small electrical in-line air heater being installed in the detector strut. The power to the heater is modulated by a temperature controller using a sensor in the detector body to maintain the body at about +10 °C.

## PRACTICAL APPLICATIONS

Prototype ice detectors and associated liquid water content systems have been used in a number of practical applications.

One installation was made on a fixed wing aircraft and not a helicopter. This was for the natural icing flight stage of the qualification of the DeHavilland Dash 7 STOL aircraft. In this case the available bleed air pressure was low, only 18 psig, but because the flight speeds of interest were in the range 150 knots to 200 knots the low air pressure was not a serious drawback. Before installation on the aircraft, the detector was calibrated for this air pressure and at the airspeeds of prime interest, i.e. 150 and 180 knots, and correction factors were determined for temperatures near zero where Ludlum effects occur.

Fig. 6 shows a portion of the recorded data for an icing flight on 18 March 1976. It shows the detector output voltage and the air temperature. The detector voltage is seen to climb as the probe ices, to drop sharply when de-icing occurs, and then to remain low for about a 6-second probe cooling period before starting to rise again. (The grid lines are spaced at 20 seconds). The cloud variability may be judged by the varying slope of the voltage ramps. The mean shope of each ramp between the appropriate voltage levels was (in this case) measured manually and the liquid water content computed and written on the record. This value was further corrected for the air temperature of about $-3.5°C$ and the corrected LWC also noted. A vernier hot rod was also installed on this aircraft and the thickness of ice on it is noted on the record (i.e. 19 mm at time 13:10:11 and 20 mm 4 minutes later). This icing rate on the hot rod implies a liquid water content of $0.054$ $g$ $m^{-3}$, whereas the ice detector records give an average value of $0.18$ $g$ $m^{-3}$ over the same period.

A 3-level icing severity indicator was installed, and its indication is shown at the top of the recording. Light icing was indicated until the uncorrected LWC value of $0.31$ $g$ $m^{-3}$, at which time a Moderate indication was given until updated to a Light indication at the end of the ensuing icing ramp.

For the continuation of these trials in the following winter (1976-77) an Icing Severity Meter was installed in place of the 3-level system, so that a direct read-out of liquid water content was obtained.

A plot of the relevant data for a 1-hour, 26-minute icing encounter is shown in Fig. 7. Air temperature was about $-6°C$ at an altitude of 5,200 feet. Aircraft speed was about 180 knots. The liquid water content as given by the Ice Detector/Icing Severity Meter system is seen to average about 0.2 or 0.25 $g$ $m^{-3}$ for the encounter with peak values between 0.4 and 0.5 $g$ $m^{-3}$. A climb to about 6000 feet to look for more severe conditions resulted instead in less severe conditions, so the aircraft returned to its original altitude. The less severe conditions at increased altitude are also seen during the climb out at the end of the encounter.

The next and final example is that of the ice detector installation on a UH-1H helicopter equipped with an experimental rotor blade de-icing system. In this installation the ice detector output ramp voltage is fed into an Integrating Rate Unit (IRU). This unit computes the liquid water content from the ramp rise time and displays it digitally as in the Icing Severity Meter. In addition it computes from this and the detector cycle time the equivalent ice accretion increment scaled to represent that at some location on the rotor blades (usually 50% radius). These increments are accumulated until a pre-set thickness is reached or exceeded, at which point the blade de-icing cycle is initiated and the accumulator is reset to zero.

Figs. 8a and 8b, traced from the flight recorder film, show two portions of the same blade icing cycle. Fig. 8a shows the 5th, 6th and 7th ice detector cycles after initiation; the liquid water content value displayed has been entered beside each. The trace below the detector output trace represents the incremented blade ice thickness as computed by the Integrating Rate Unit; the thickness value stored in the IRU has been added beside each increment. Fig. 8b shows the 43rd, 44th and 45th ice detector cycles. After the 44th cycle the blade ice integrator has incremented to 0.403 inch; the pre-set ice thickness for blade de-icing was 0.415 inch, so on receipt of the next increment (0.017 inch) the integrator increments momentarily to 0.420 inch and then resets to zero, at the same time providing an initiating pulse to the rotor blade de-icing controller.

It may be wondered why one does not simply sum the number of ice detector cycles and initiate de-icing after, say, 45 cycles. Figs. 8a and 8b demonstrate why this procedure is not always desirable. It may be noted that ice detector cycle number 6 (Fig. 8a) gave an increment of 0.012 inch for a liquid water content of 0.34 $g$ $m^3$, while cycle number 44 (Fig. 8b) gave an increment of 0.015 inch for a LWC of 0.33 $g$ $m^3$, the reason being that although the LWC was almost the same, the cycle time had increased by 5 seconds (a 28% increase) because of the longer probe cooling time at $-2.5°C$ than at $-4°C$.

## CONCLUDING REMARKS

This paper has attempted to demonstrate the latest advances in helicopter ice detection and liquid water content measurements. It may be expected that, with the advent of micro-processors, greater advances will be seen in the not-too-distant future, particularly in the area of processing the information provided by the primary sensors to correct the final outputs for such variables as ambient temperature, airspeed, bleed air pressure and so forth.

Where mixed icing conditions are concerned, a vast amount of development work will be necessary to evolve a relatively simple system to measure such conditions on a routine basis.

REFERENCES

1. J. R. Stallabrass, National Research Council of Canada, Icing Flight Trials of a Bell HTL-4 Helicopter, 1957, NAE Laboratory Report LR-197.

2. H. B. Lake and J. Bradley, The Problem of Certifying Helicopters for Flight in Icing Conditions, Aeronautical Journal, Vol. 80, 1976, 419-433.
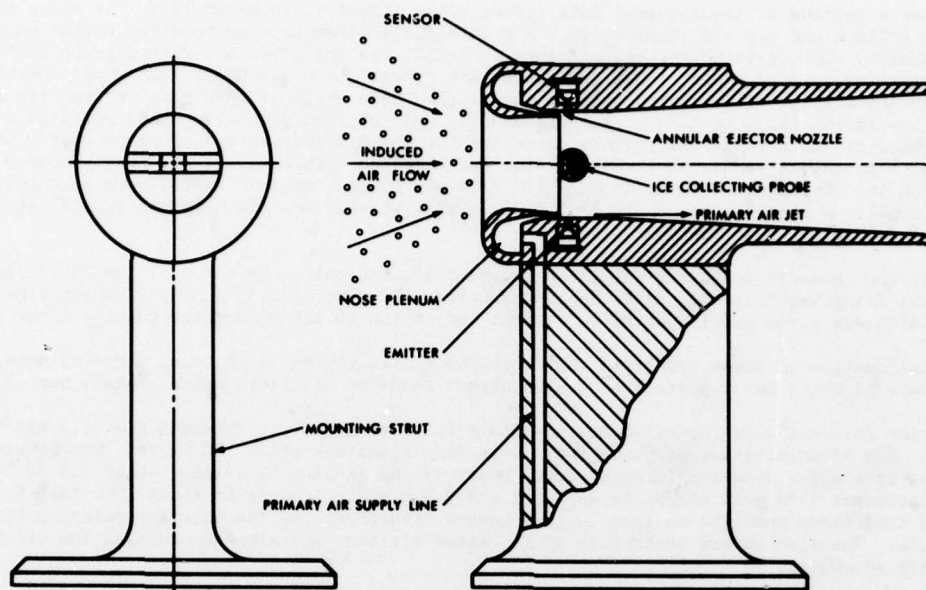
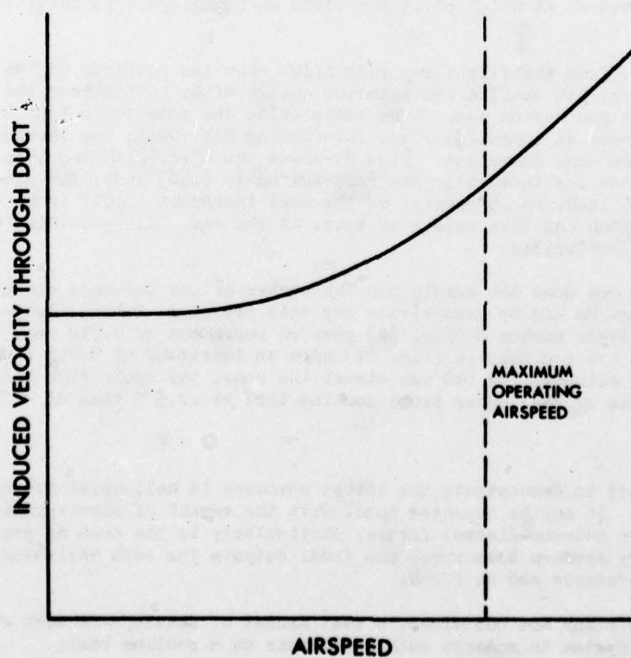FIG. 1: SIMPLIFIED OUTLINE OF DYNAMIC ICE DETECTOR



FIG. 2: INDUCED VELOCITY THROUGH THE ICE DETECTOR
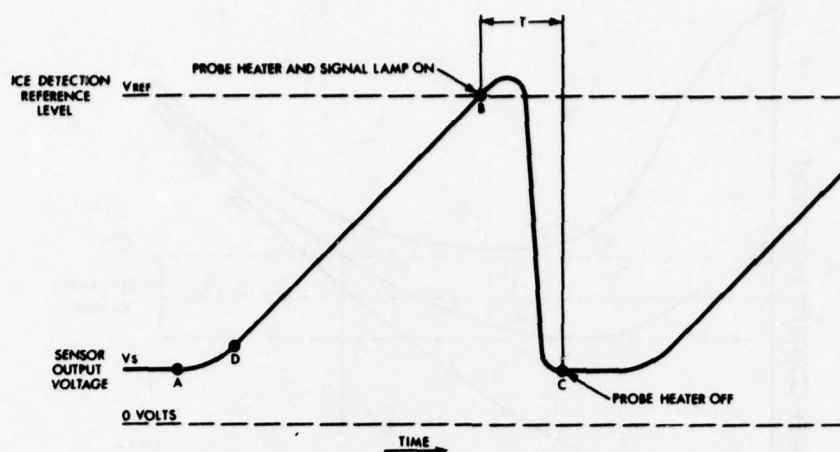AS A FUNCTION OF AIRSPEED

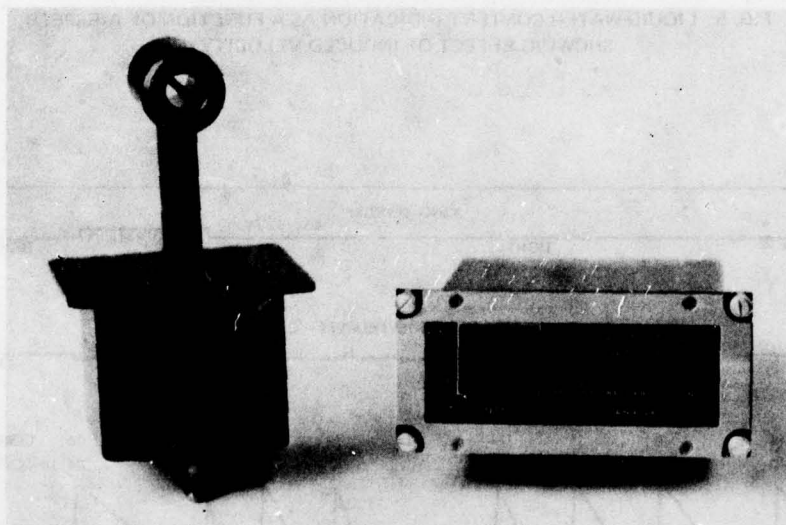FIG. 3: SENSOR OUTPUT VOLTAGE VARIATION DURING A TYPICAL ICE/DE-ICE CYCLE



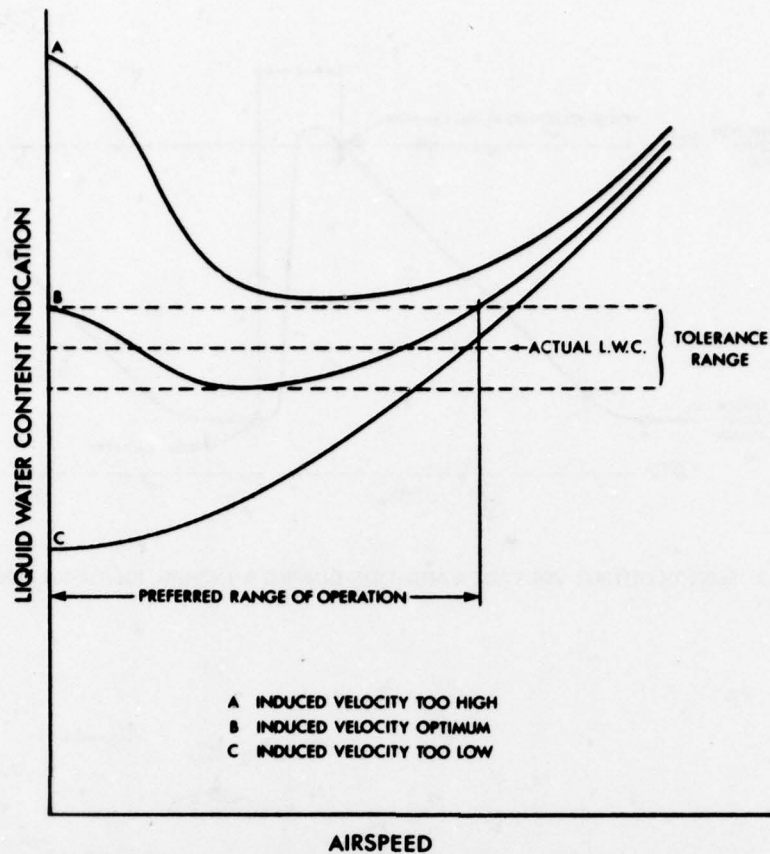FIG. 4: ICE DETECTOR UNIT AND ICING SEVERITY METER

FIG. 5: LIQUID WATER CONTENT INDICATION AS A FUNCTION OF AIRSPEED,
SHOWING EFFECT OF INDUCED VELOCITY
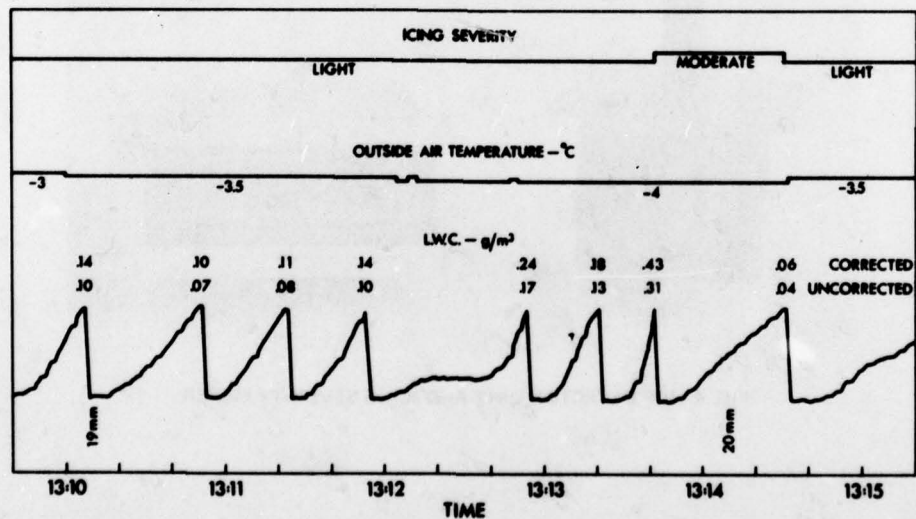


FIG. 6: PORTION OF RECORDED DATA FROM DHC-7 ICING QUALIFICATION FLIGHT
ON 18 MARCH 1976, SHOWING VOLTAGE OUTPUT FROM ICE DETECTOR AND
DERIVED LIQUID WATER CONTENTS

FIG. 7: PLOT OF DATA FROM DHC-7 ICING QUALIFICATION FLIGHT ON 25 FEBRUARY 1977,
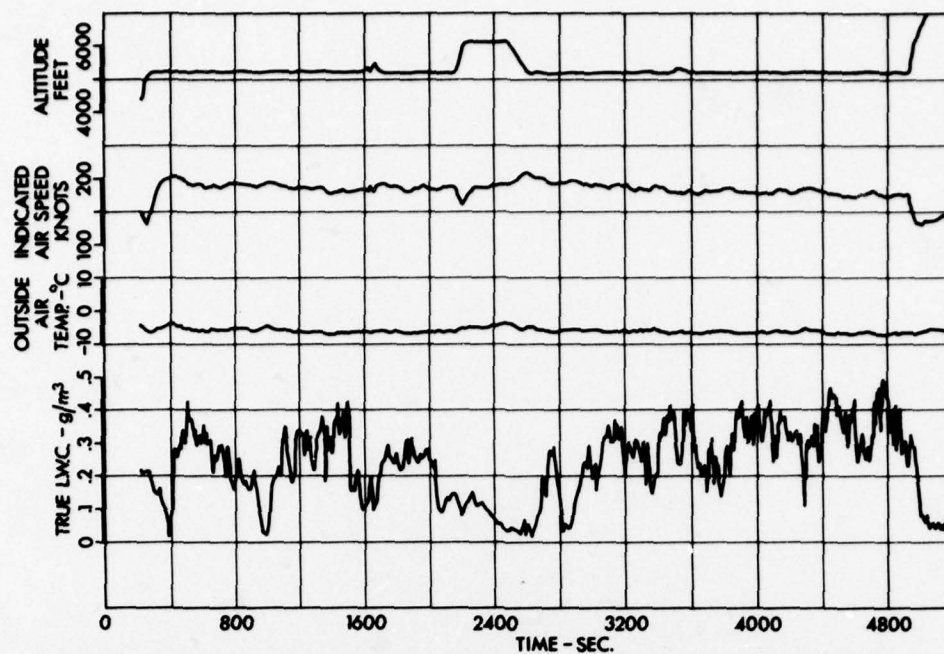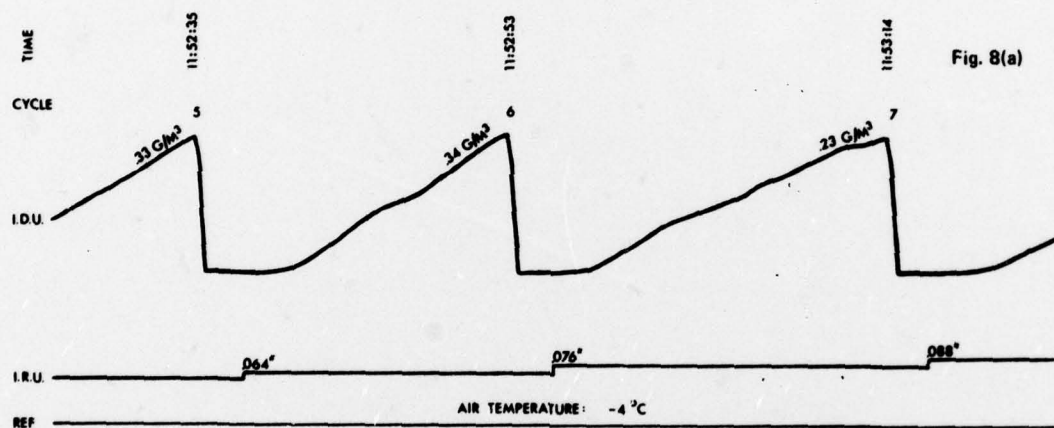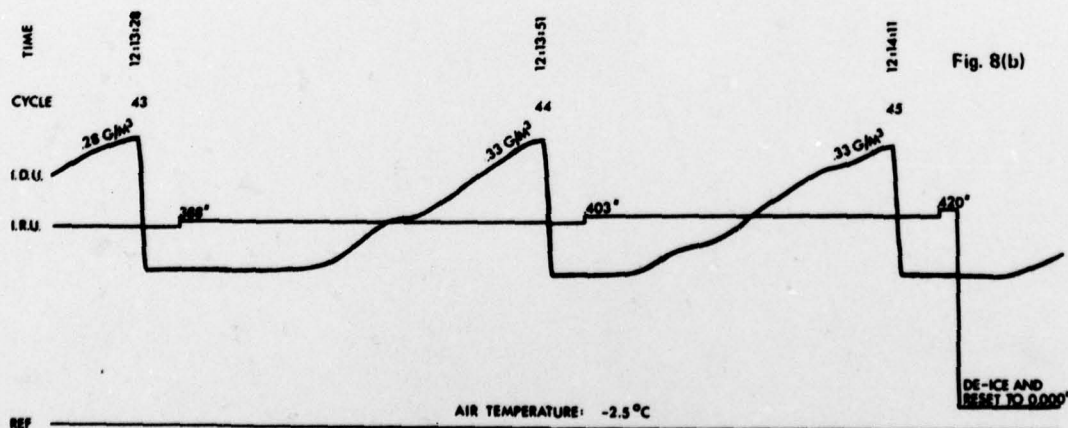SHOWING LIQUID WATER CONTENT READINGS OF ICING SEVERITY METER



FIG. 8: TWO PORTIONS OF RECORDED DATA FROM UH-1H NATURAL ICING TEST FLIGHT ON 31 MARCH 1977,
SHOWING ICE DETECTOR OUTPUT RAMP AND ACCUMULATED VALUE IN INTEGRATING RATE UNIT

ICING TRIALS ON THE FRONT FUSELAGE AND ENGINE INTAKES OF
HELICOPTERS AT CONDITIONS SIMULATING FORWARD FLIGHT

by

P. F. Ashwood
Head, Engine Test Department

R. D. Swift
Principal Scientific Officer

National Gas Turbine Establishment
Pyestock, Farnborough, Hants.
UK

SUMMARY

One of the large test chambers of the Altitude Test Facility at the NGTE has been successfully used for full-scale trials on the front fuselage and engine intakes of the Westland Sea King and the Westland/ Aerospatiale Lynx helicopters under simulated wet icing conditions.

The paper describes tests made to examine the effects of air temperature, air speed, water concentration and aircraft attitude on the extent of ice accretion. The possibility of ice ingestion by the engines during melt-off has also been studied using high-speed videotape recordings.

Data are also presented from non-rotating tests on full-scale sections of main rotor blade made to examine the effects on accretion of blade speed, pitch angle, air temperature and water concentration. The effects of cyclic pitch change have also been examined and typical results are presented.

The paper includes general comments on the use of an altitude cell for helicopter icing investigations and the accumulation of data leading to clearance for flight in icing conditions.

1.   INTRODUCTION

Clearing a helicopter for flight in icing conditions requires the assessment of data from a variety of sources ranging from small test rigs to full-scale flight trials. The final judgement on the limits of safe operation naturally leans heavily on the flight trial results, but a considerable degree of confidence can be gained and much time and expense saved by carefully designed experiments using ground-based test rigs and facilities. These enable icing to be studied under closely controlled conditions and the influence of each major variable examined separately. Ground facilities can also be used for development testing, for example the optimisation of the power input distribution to thermal anti-ice or de-ice systems, and results obtained more quickly and precisely than is possible in flight.

This paper describes the work done by the National Gas Turbine Establishment (NGTE) at Pyestock to study at full-scale ice build up on the forward fuselage and engine air intakes of Sea King and Lynx helicopters and the possibility that ice shed during melt-off may be ingested by the engines. Ways in which this problem was overcome are described. Tests to examine ice accretion on rotor blade specimens are also covered.

2.   TEST FACILITIES

NGTE has undertaken icing trials on aero-engines for the past 15 years. With the remarkable growth of engine power that has taken place during this time and the corresponding increase in the size of the supporting test facilities, in particular the increase of compressor/exhauster plant capacity and cold air supply, the Establishment has acquired a unique capability for investigating helicopter icing problems.

Figure 1 shows the largest of the altitude test chambers at NGTE, Cell 3 West. The test chamber, which has a diameter of 25 ft, can be seen on the left of the picture; the air cooler, refrigeration plant and cold store are on the right. A detailed description of this Facility is given in Reference 1.

The Cell can easily accommodate the fuselage of a Sea King or Lynx helicopter and by correctly positioning it in a free-jet air stream a large part of the forward-facing fuselage surfaces including the windscreen, cabin roof and engine intakes can be subjected to icing conditions. Figure 2 shows the test arrangement. Air drawn from atmosphere passes through the cooler, the inlet pressure control valve and into the test chamber through the blowing nozzle. This produces a jet of air some 8 ft in diameter which simulates the flight velocity. The icing cloud is generated by injecting water from an array of 242 air-assisted atomisers which can be seen in Figure 3.

No attempt is made to simulate the effects of rotor downwash. Tests made using a one-twentieth scale model of the cell installation showed that the pressure distribution over the fuselage upper surface was virtually identical to that measured in a conventional wind-tunnel. It was therefore concluded that the free-jet test arrangement gives a close representation of conditions encountered in forward flight.

The test conditions most commonly used represent flight at speeds from 90 to 160 kt with air temperatures in the range -2 to -24°C. The liquid water content is set to meet the requirements of AvP 970 (Reference 2) for either maximum continuous or periodic maximum conditions.

To avoid possible damage by ingested ice most tests are run without engines fitted, air being drawn into the intakes by an ejector system operated by the plant pressure air supply. Correct thermal

simulation of the heat inputs from the engine front frame and the gearboxes is obtained by electric heating. Some tests are run with an engine and for these the power turbine is locked to obviate the need for a dynamometer.

After completing an icing test the water sprays are turned off and the air temperature slowly increased to above freezing point to establish whether ice ingestion occurs during melt-off. To do this it is necessary to examine high speed videotape records frame by frame since the lumps of ice move too fast to be followed by direct viewing of the TV monitors.

## 3.   INTAKE ICING

Figure 4 shows typical results of icing tests after 16 and 30 minutes at temperatures of -5 and -10°C on a Sea King fitted with pitot intakes. The forward speed was 120 knots and the liquid water content was as specified in AvP 970, see Reference 2 for continuous maximum conditions. The engine and intake flare anti-icing systems prevented dangerous ice accretion on the intakes but with this type of intake the engines are vulnerable to the ingestion of ice shed from the front fuselage.

In an attempt to overcome this problem the so called "mushroom" intakes were fitted and Figure 5 shows these after icing tests at four temperatures. The front face of the port "mushroom" was unheated while that of the starboard had 1.2 kW of electrical heating. It can be seen that ice formed on the unheated "mushroom" at -4°C and on the heated "mushroom" at -15°C. Although in forward flight these intakes prevented ingestion of ice from the front fuselage, sometimes ice from the "mushroom" front face was ingested. Large ice deposits formed on the unheated area behind the intake cowls caused by water run-back from the heater mats and some of this ice was also ingested.

Tests with a Sikorsky Foreign Object Deflector (FOD) fitted to the cabin roof in front of the pitot intakes, Figure 6, indicated that with light ice deposits no ice ingestion occurred. However considerable ice accretion particularly around the edges occurred after 30 minutes icing, Figure 7A, and during melt-off some of this ice was ingested through the cut aways at the top rear edges of the deflector. With a de-icing fluid exuded from porous strips inserted flush in the front face of the FOD a marked reduction in ice accretion was achieved, Figure 7C. Some of the fluid was carried over in the air stream into and around the engine intakes reducing ice accretion in these areas and obviating the need for the auxiliary heater mats.

Sideways facing intakes, Figure 8, with electrically heated mats for anti-icing have given encouraging results at temperatures below -15°C. The mats were divided into a number of separate sections each with its own heating intensity control thus enabling the optimum heat distribution to be determined. Figure 9 shows the port intake after 30 minutes icing at -16°C. Run back ice built forward from the unheated area behind the intake but this shed clear during melt-off and did not constitute an ingestion problem. Ice shedding from the front of the fuselage also passed clear of the intakes.

Icing tests were also made on the smaller Lynx helicopter fuselage which has the engines and intakes mounted on top of the fuselage behind the rotor gearbox, Figure 10. Ice accretion along the top of the rotor gearbox cowling on the original design, Figure 11A, resulted in a number of instances of engine ice ingestion and one example can be seen in the high speed videotape recording reproduced in Figure 12. Streamlining the gearbox cowling and smoothing the windscreen "eyebrows" reduced very considerably the chance of ice ingestion from these areas.

Auxiliary air intakes, such as those required for oil cooling, are at risk in icing conditions as well as the main engine intakes. Figure 13 shows the extent to which an auxiliary intake can become blocked with ice.

## 4.   ROTOR BLADE ICING

Cell 3 West is not large enough to accommodate a complete main rotor, but full-scale tests on complete tail rotors are feasible. No such tests have yet been made but some are planned to examine the effects of inertia loading on ice accretion. It is thought that the rig could be used to clear specific designs for operation in icing conditions.

NGTE has made non-rotating tests on sections of full-scale main rotor blade to determine the effects on accretion of water concentration, droplet size, air temperature and velocity; the influence of pitch angle and aerofoil shape have also been investigated. The test rig is shown in Figure 14. The blade specimen is mounted in a gymbal-type suspension so that the pitch and yaw angles can be varied cyclically. The airspeed can be adjusted to represent conditions at selected spanwise stations.

The photograph shown at the top of Figure 15 shows the extensive ice accretion observed after a 7½ minute test at -8°C with a water content of 0.65 g/m$^3$. The picture is of a chordwise section through the ice.

Natural icing conditions are more complex than those represented by an air stream containing only supercooled water droplets and NGTE has therefore examined ice deposition in a mixed environment, that is one containing solid ice particles and supercooled water droplets. Figure 15 compares the build up after two 10 minute tests, the first at the mixed condition and the second with the same water content but with no ice particles. A comparison of results from the two tests indicated that the presence of the solid ice reduces the thickness of the accretion and produces a deposit having a much smoother contour.

## 5.   CONCLUDING REMARKS

This paper has presented a brief outline of work done at NGTE to investigate several aspects of the helicopter icing problem. The test facilities available at the Establishment allow experiments to be made at full scale. This has proved to be far more effective for development testing than either flight tests or open air facilities which rely on prevailing weather conditions to provide the icing environment.

However whilst a test facility can provide a considerable degree of confidence in the ability of a helicopter to operate in icing, the final judgement on the limits of safe operation must be based on flight trials.

REFERENCES

1.    P. F. Ashwood        An altitude test facility for large turbofan engines.
                          Journal Aircraft Vol 10 No 8,   August 1973

2.                        Design requirements for service aircraft.
                          UK Ministry of Defence Publication No AvP 970
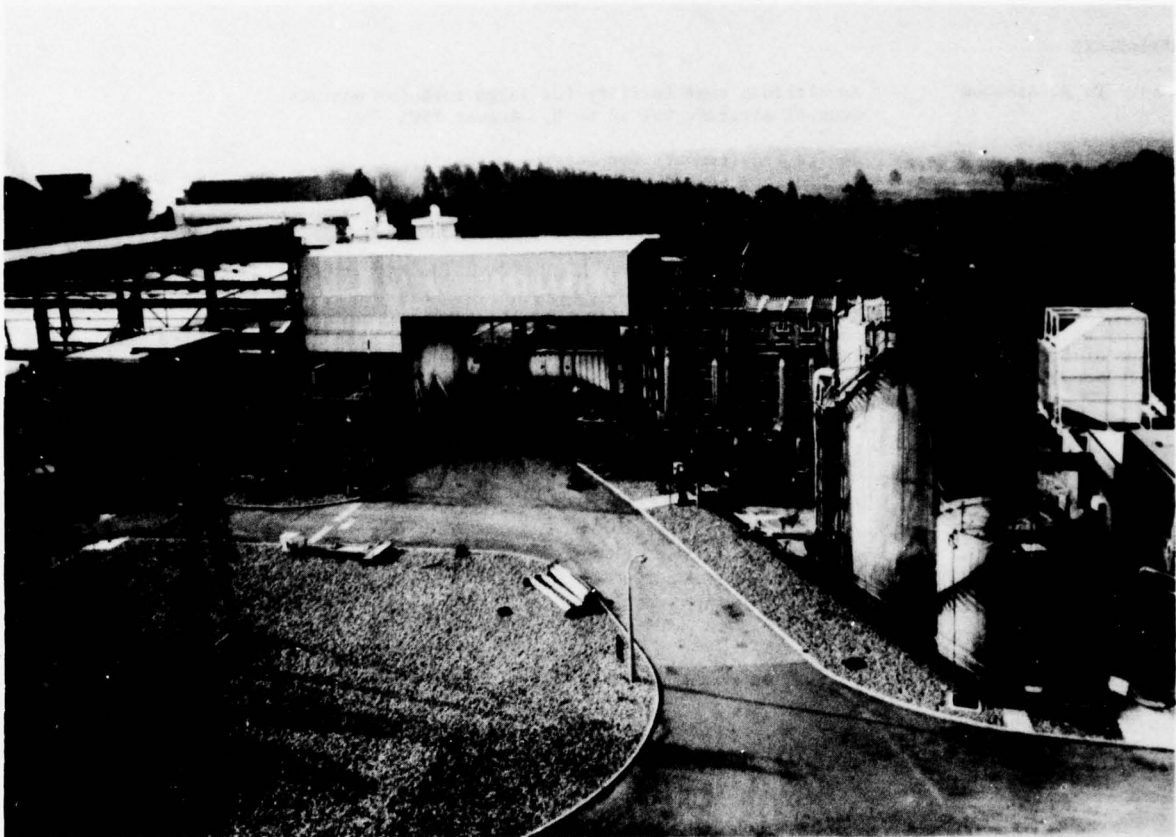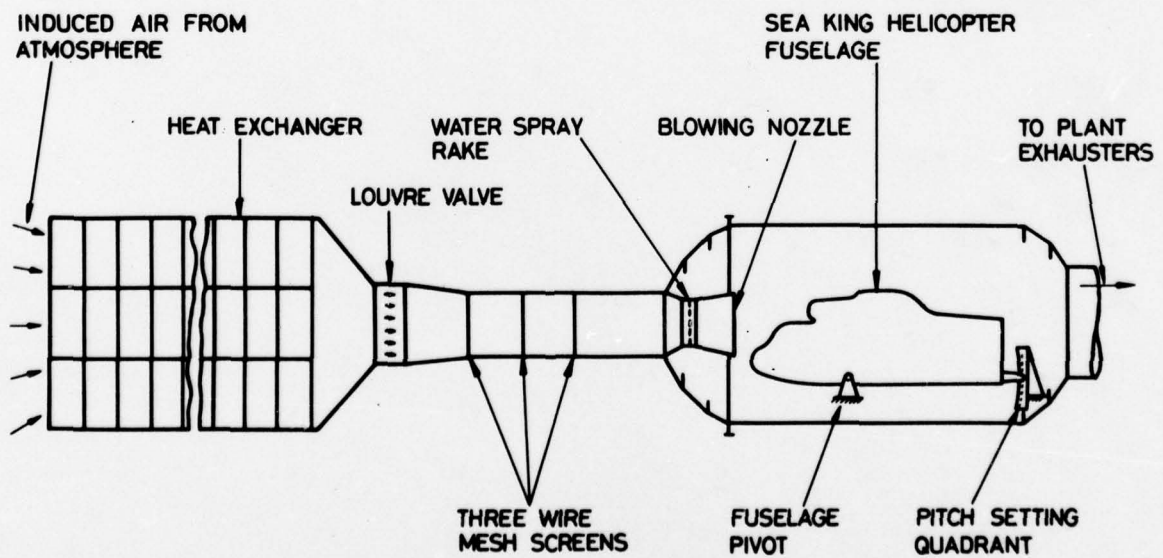
Fig.1   Cell 3 west



Fig.2   Arrangement of Sea King helicopter fuselage in cell 3 west
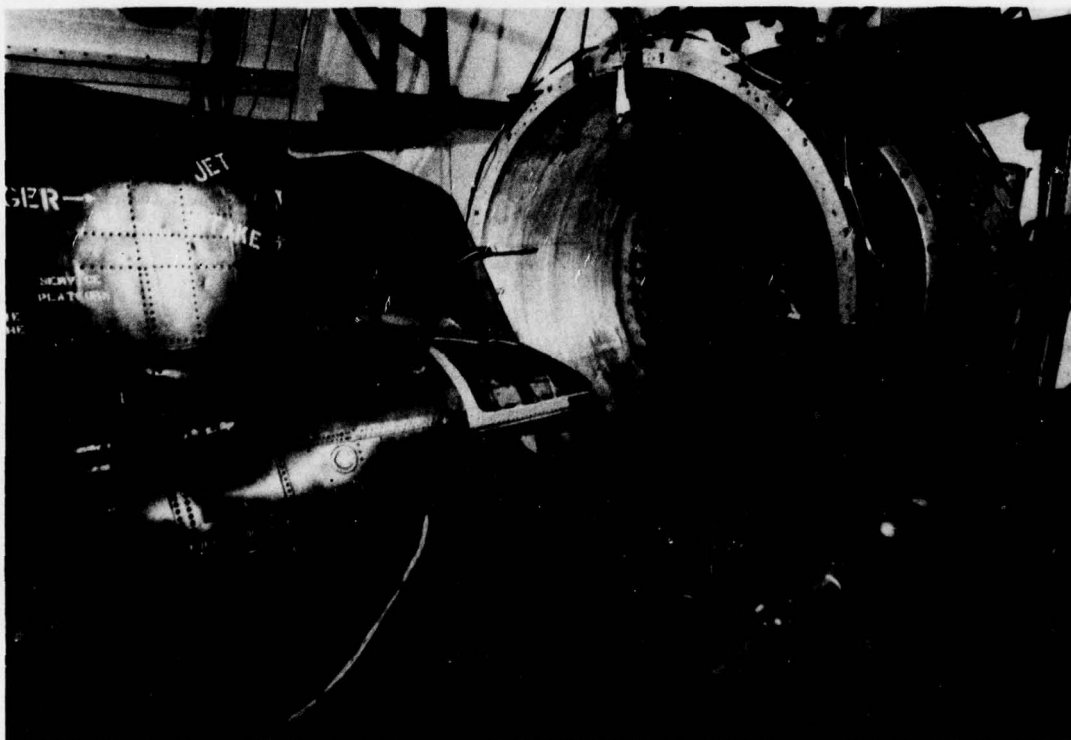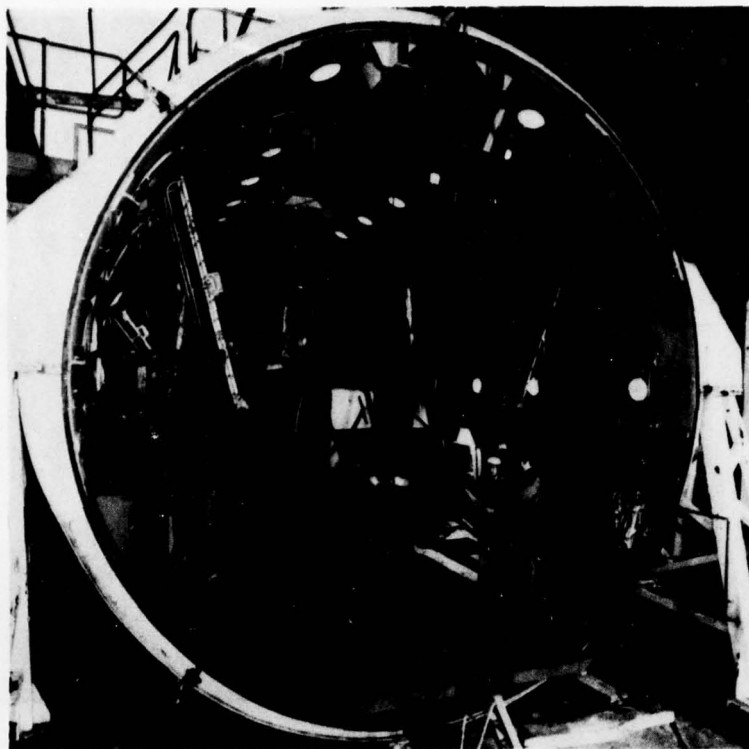
Fig.3 Installation of Sea King in cell 3 west

16 mins AT 0.7g/m³
-5°C AND 120kt
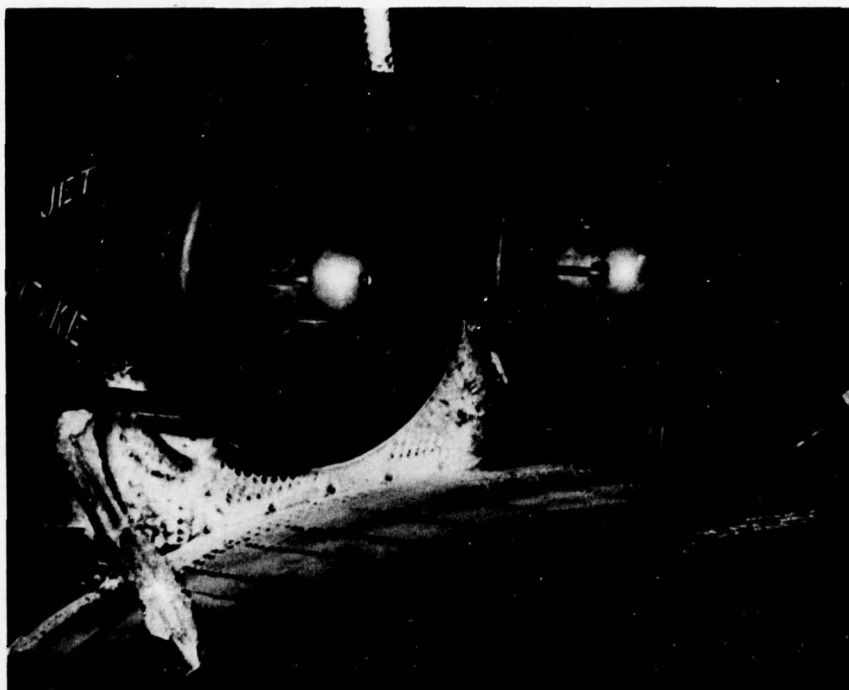
30 mins AT 0.6g/m³
-10°C AND 120kt

STBD NACELLE         PORT NACELLE
EJECTOR SIMULATOR      GNOME H1400 ENGINE

Fig.4   Sea King with pitot intakes
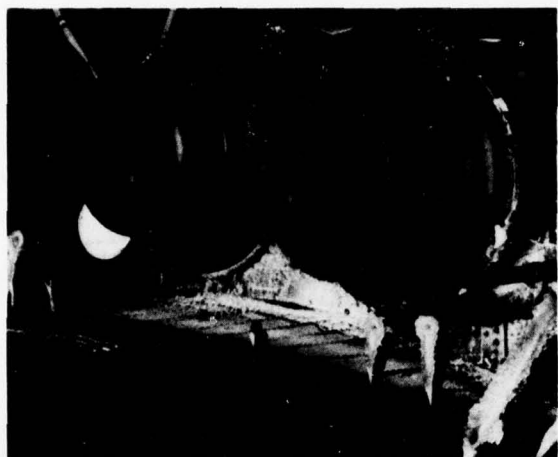
15 mins AT 0.77g/m³
-3°C AND 120kt

15 mins AT 0.77g/m³
-4°C AND 120kt

30 mins AT 0.7g/m³
-5 AND 120kt

25 mins AT 0.45g/m³
-15°C AND 120kt

Fig.5   Sea King with mushroom intakes

ENGINE BAY DOOR HEATER MAT

AUXILIARY HEATER MAT

ENGINE INTAKE HEATER MAT

AIR DRIVEN EJECTOR
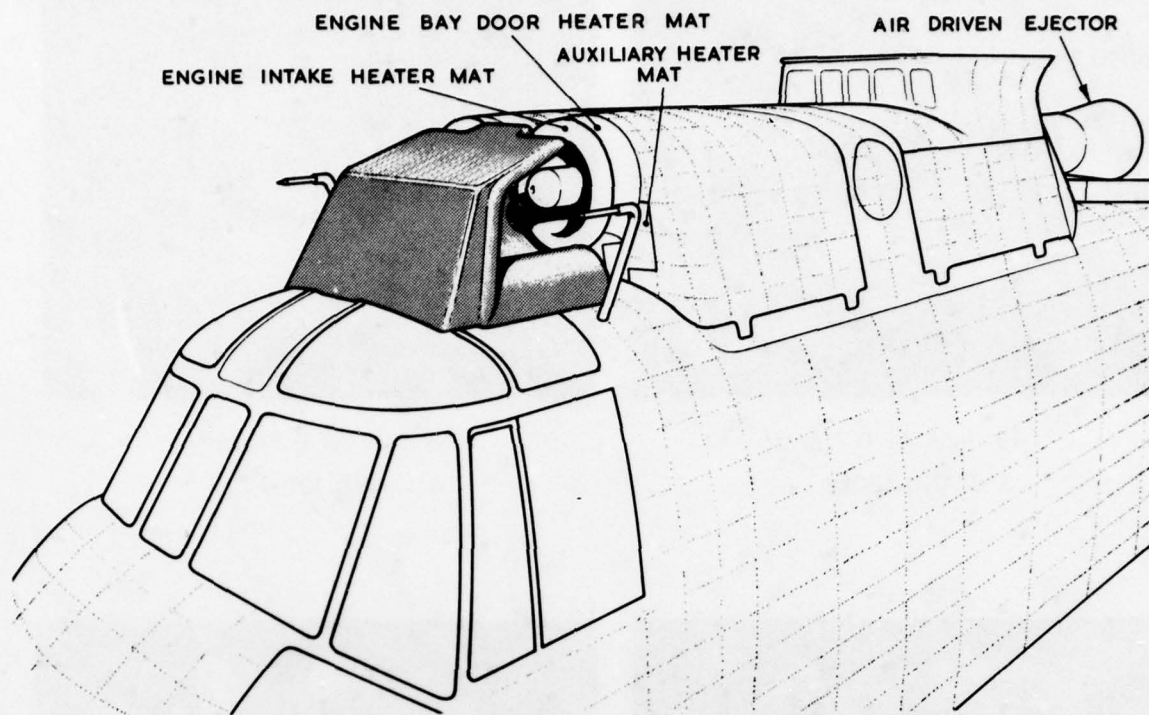
Fig.6   Sea King with Sikorsky foreign object deflector (FOD)

27 mins AT 0.75g/m³

3 mins AT 1.5g/m³

-4°C AND 90kt

27 mins AT 0.6g/m³

3 mins AT 1.2g/m³

-10°C AND 90kt

UNTREATED FOD FRONT FACE



27 mins AT 0.6g/m³

3 mins AT 1.2g/m³

-10°C AND 90kt

FOD FRONT FACE TREATED WITH DE ICING FLUID

Fig.7    Sea King with Sikorsky foreign
object deflector (FOD)

3-10

ENGINE BAY VENTILATION
AIR INTAKE

INTAKE HEATER MATS

AIR DRIVEN EJECTOR
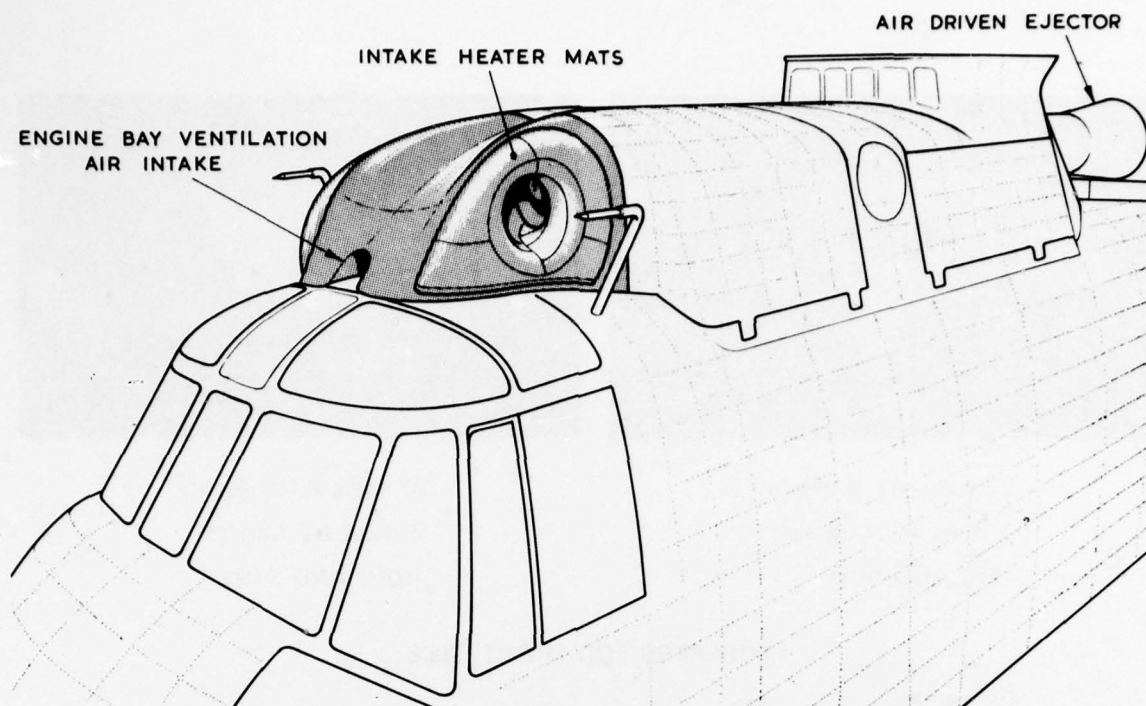
Fig.8    Sea King with sideways facing engine intakes

27 mins AT 0.4g/m$^3$

3 mins AT 0.8g/m$^3$

-16°C AND 90kt

Fig.9    Sea King with sideways facing intakes
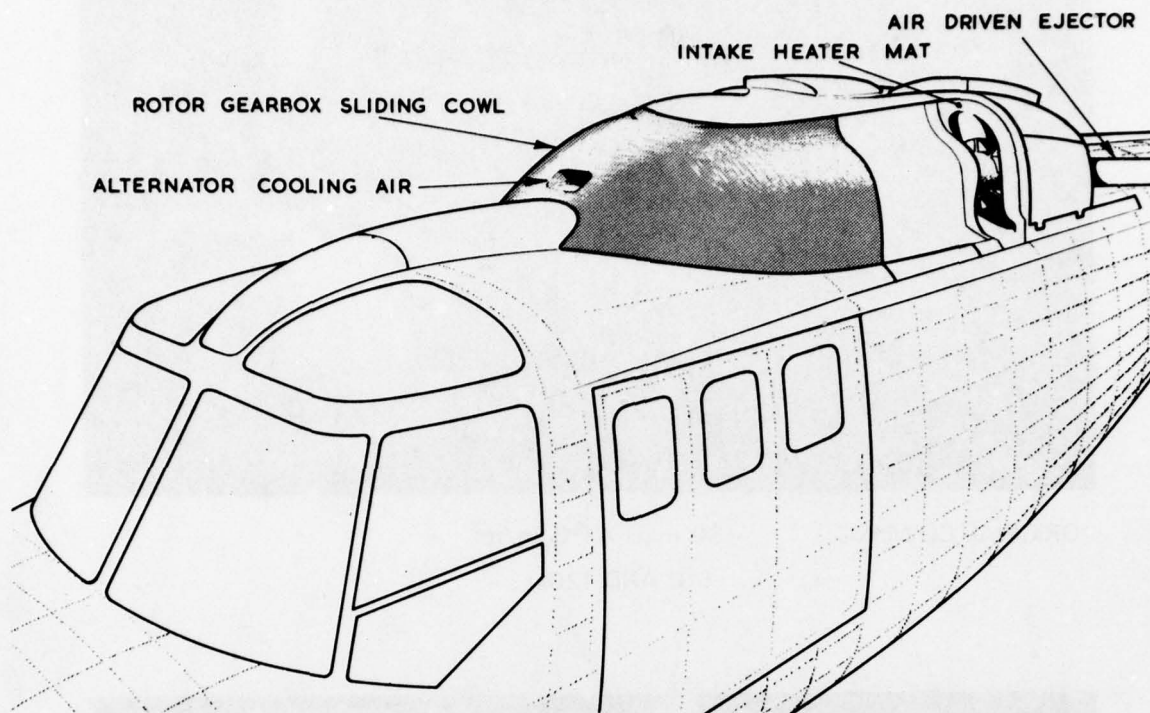
Fig.10    Lynx showing modification to the rotor gearbox cowling
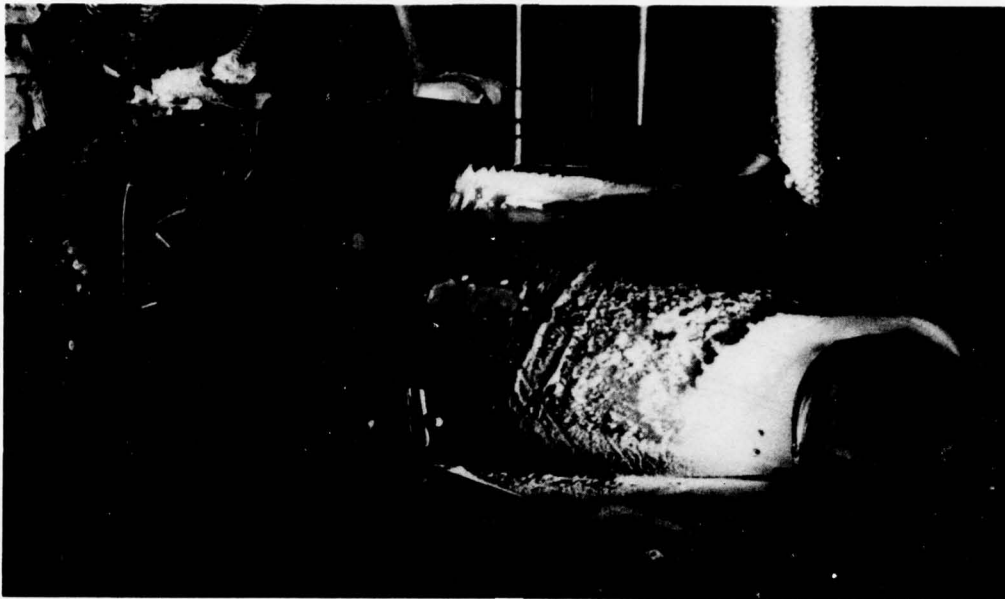
ORIGINAL COWLING          30 mins AT 0.7g/m$^3$
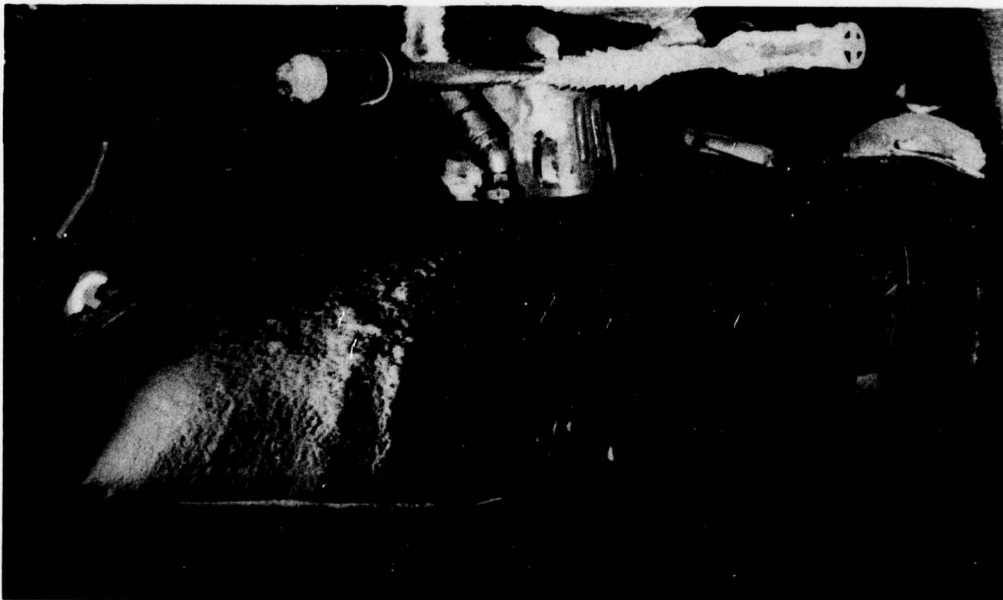
                         -5°C AND 120kt



MODIFIED COWLING          30 mins AT 0.7g/m$^3$

                         -5°C AND 120kt

Fig.11   Lynx — pre and post modification
to the rotor gearbox cowling
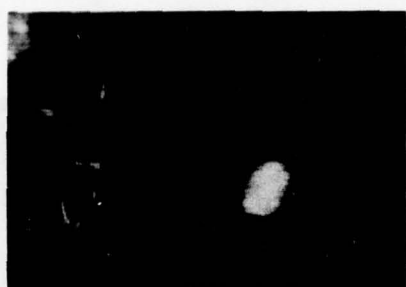
START OF EVENTS

0s
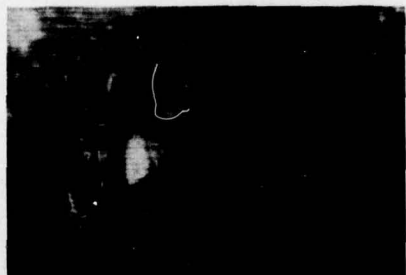
+0.08s

ICE INGESTION FROM
STARBOARD SIDE OF LOWER
LEADING EDGE OF GEARBOX
COWLING AFTER 14mins 50sec
OF MELT OFF AT $T_s$ = -5° C
AND WATER CONCENTRATION
= 0.70g/m³

+0.10s

+0.12s

+0.13s

Fig.12   Lynx — high speed television sequences ice ingestion

30 mins AT 0.7g/m³

-5°C AND 120kt

Fig.13    Lynx – ice accretion on oil cooler air intake
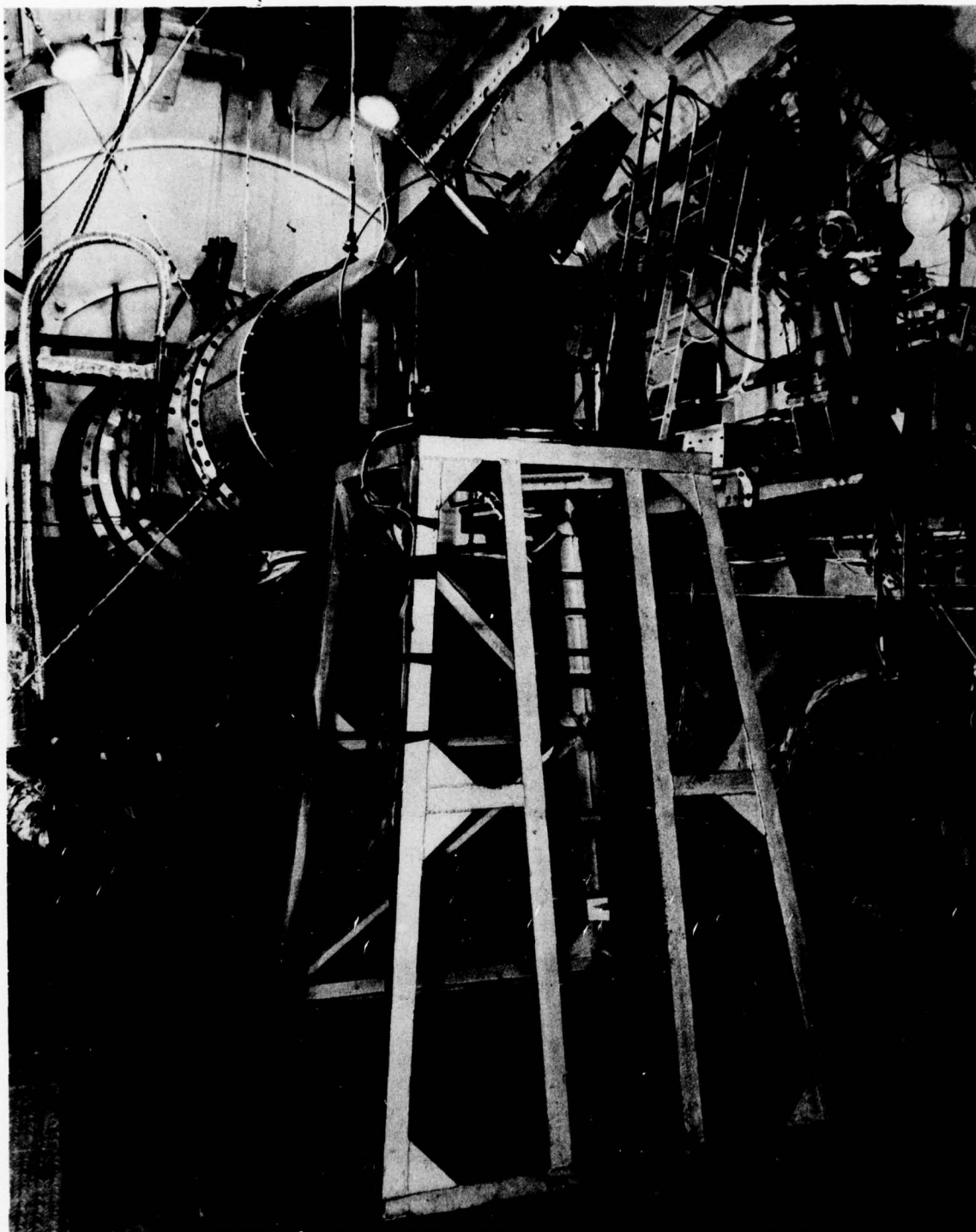
Fig.14    Arrangement of rotor blade icing test rig
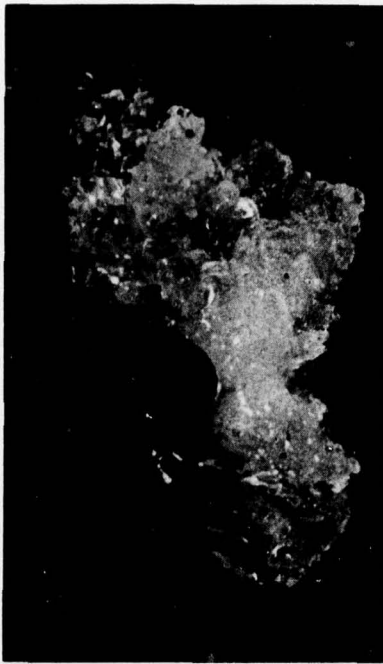
SECTION OF ICE ON JETRANGER ROTOR BLADE

AFTER 7½ mins AT 0.65g/m³ WATER

-8°C AND 339 ft/s



10 mins AT 0.2g/m³ WATER ONLY

-8°C AND 350 ft/sec
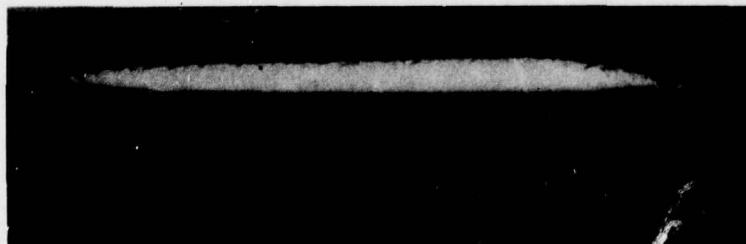


10 mins AT 0.2g/m³ WATER PLUS

0.8g/m³ ICE CRYSTALS

-8°C AND 350 ft/s

WESSEX ROTOR BLADE

Fig.15    Ice deposition on rotor blade test sections

# ICE ACCRETION AND ITS EFFECTS ON AERODYNAMICS OF UNPROTECTED AIRCRAFT COMPONENTS

by

Boris Laschka and Rudolf E. Jesse
Messerschmitt-Bölkow-Blohm GmbH
Ottobrunn / Munich, Germany

## SUMMARY

This paper gives a survey on theoretical and experimental methods applied to determine the ice accretion and its effects on the respective aerodynamics on unprotected components of a modern jet transport aircraft.
Together with an introductory outline of the mechanism and the basic mathematical equations and correlations ruling ice generation, the experience obtained for the European Airbus A300 is used to describe these methods.
In addition, an example for the prediction of trajectories of shedding ice particles as applied for the German jet transport aircraft VFW 614 is given herein.

## INTRODUCTION

Early in the development phase of the A300, it was decided not to protect the tail surfaces and the air intake system of the Auxiliary Power Unit (APU) by a de-icing or anti-icing system in order to save weight at the rear of the aircraft, electric and hydraulic power, and to simplify system design (see fig. 1). * In order to ensure airworthiness under all possible extreme icing conditions, thorough investigation, to guarantee full flight safety, sufficient flying qualities and controllability and APU system function have been performed. These studies covered the theoretical and experimental determination of the amount of ice, ice build up, and shape and the resulting aerodynamic implications, completed by flight tests under natural icing conditions [1],[2].

## 1. UNPROTECTED TAIL OF THE A300

Icing mechanism: looking into the flow field around an airfoil, as shown in fig. 2, one may find, that the supercooled water droplets due to their inertial forces deviate from the curvature of the streamlines in the vicinity of the leading edge. The larger droplets tend to deviate more from the streamlines having less curved trajectories and then impinging on the airfoil. So, the water caption problem consists in determining the droplet trajectories and, more particulary, the tangent, or limit trajectories as a function of droplet size (d).

Basic equations ruling droplet trajectories: the governing differential equation may easily be derived by the Newton law

$$\vec{K} = m \cdot \frac{d\vec{V}}{dt} \qquad (1)$$

with m as mass of the droplet

$$m = \varrho_{water} \frac{4}{3} \pi \left(\frac{d}{2}\right)^3 \qquad (2)$$

and the only force acting on the droplet given by its drag $\vec{D}$

$$\vec{D} = c_D \cdot \pi \cdot \left(\frac{d}{2}\right)^2 \frac{\varrho_{air}}{2} (\vec{V}-\vec{U})|\vec{V}-\vec{U}| \qquad (3)$$

From

$$\vec{K} + \vec{D} = 0 \qquad (4)$$

equation (1) can be transferred to

$$\frac{d\vec{V}}{dt} = \frac{3}{4} \frac{\varrho_{air}}{\varrho_{water}} \cdot c_D \cdot \frac{(\vec{U}-\vec{V})|\vec{U}-\vec{V}|}{2} \qquad (5)$$

Vector diagramm for droplet and air velocity
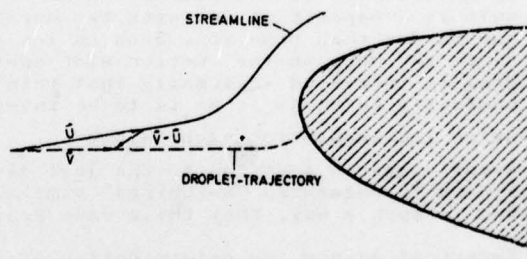
Since the droplet Reynolds Numbers are very small, the STOKE's law ($c_D = 24/Re$) for drag can be used with good approximation. The droplet Reynolds Number itself is determined from the relative velocity $|\vec{V}-\vec{U}|$ of the droplet with respect to the air.

$$Re_{droplet} = \frac{d}{\nu_{air}} |\vec{V} - \vec{U}| \qquad (6)$$

Generally, the differential equation is solved by classical difference methods in combination with a panel flow field calculation.

---

* Note:
The decision not to protect the wing slat area between the fuselage and the engine pylon was not made at this time, this was decided later according to experimental results.

Flight regime of maximum icing: for most transport aircraft, the severest icing within the flight envelope will be encountered during holding where usually the airplane by traffic control reasons is not allowed to change altitude or location arbitrarily to avoid icing regimes and where appreciable flight times have to be expected. This applies also to the A300 for which the severe special requirement of 45 minutes flight under maximum continuous icing conditions had to be fulfilled. Using the statistical metereological data as given in FAR 25 and taking into account, that the average water captions per time unit is proportional to liquid water content LWC, the true flight speed V and a caption factor K (depending on droplet diameter and tail flow)

$$\frac{dm_{water}}{dt} = K \cdot V \cdot LWC \tag{7}$$

and that the ambient temperature in the stagnation region of the tail surfaces has to be increased by $\Delta T = 0,2\ T_\infty \cdot M^2 \cdot \cos^2 \varphi$ ($\varphi$ being tail l.e. sweep), one may conclude that, for the A300 tail, biggest ice accretion occurs for ambient temperature from $-5^oC$ to $-10^oC$ and altitudes around 14 000 ft, as shown in fig. 3 for a droplet size of $d = 20\ \mu$ (demonstration case!). Though cruise velocities are higher than at holding, no severe icing is to be expected, as because of the dynamic temperature increase only at very low temperatures at which LWC is small icing occurs.

Influence of droplet size on water caption: for different airfoil geometries, one will obtain different droplet sizes for which maximum ice accretion occurs. Consequently, the influence of droplet size on total water caption of the Airbus tail surfaces was established by impingement analysis. Analysis [3],[4] shows, see fig. 4, that the biggest water caption will be with droplets diameter between $20\ \mu$ and $28\ \mu$ both for the vertical as well as for the horizontal tail. Furthermore, the calculations give evidence that ice accretion will be more severe for the horizontal tail. This is due to the fact that the horizontal tail has an absolute smaller leading edge radius than the vertical tail. It is interesting to note that for the Boeing 747 also the horizontal tail showed to be the surface with the biggest water caption, but that the critical droplet size around $28\ \mu$ was somewhat bigger than at the Airbus.

Types of ice shapes: of utmost importance for the alternation of the aerodynamic qualities is not only the amount of ice accretion but rather its shape, see fig. 5.

Chordwise ice shapes

Generally, two types of ice shapes may be observed on airfoils.

- Rime ice results from low surface temperatures and low LWC. The water droplets freeze immediately after impinging on the leading edge of the airfoil and form a soft milkywhite smooth and streamline ice shape around the leading edge. It does not occur when surface temperatures surpass $-12^oC$. From the aerodynamic point of view, these forms are not too bad, as they do not adversely effect lift- and drag characteristics of the airfoil and, sometimes, even result in an increase of lift (enlargement of airfoil-chord).

- Glaze ice (mushroom ice, double horn) forms at temperatures just below freezing point and high LWC. Glaze ice is normally formed at temperatures between $0^oC$ and $-8^oC$. At these temperatures, water droplets do not freeze immediately after impingement but run first on the profile upward or downward from the stagnation point before freezing. In this case, the temperature at the stagnation point is about $0^oC$ or above, i.e. the so-called Ludlam limit is exceeded (freezing factor < 1). The result is a deposit of ice with two horns like protrusions and normally is transparent and harder than rime ice. Such an ice shape is aerodynamically very unfavourable since the horn on the suction side spoils the flow and reduces the lift whereas the drag is increased. Naturally that mainly glaze ice need to be considered if aerodynamically critical icing is to be investigated.

Spanwise ice shapes for swept wings

On swept wings, in addition to the just discussed chordwise ice shapes accretions with considerable segmented "notchings" similar to a "lobster tail" occur. The segments are curved in such a way, that their ends are bowed towards the wing tip.

Emperical method for determination of ice height: computations assuming that
- all droplets impinging the contour freeze immediately
- breaking-off of ice deposits is neglected
do not show the mushroom shape, but a shape similar to rime ice. Such a calculation always predict ice heights considerable in excess of the real ones. This is a real gap in knowledge! Nevertheless, empirical methods are available, from which mushroom ice shapes may be derived. This method, see fig. 6, makes extensively use of measured upper horn lengths $h_{US}$, lower horn length $h_{LS}$ and thickness at the stagnation point $h_{ST}$ for different yet similar profiles, which were plotted versus a quantity I with $E_M$ is the total droplet collection efficiency and $h^*/c$ is the ratio of profile thickness [3],[5]. A thus determined ice height at the horizontal tail of the A300 is plotted versus span in the figure for a selected case and then compared with B 747. In principle, ice height decreases with increasing profile thickness or - what is tantamount - for constant thickness ratio with increasing profile chord. Almost the same ice height is found at the tip for both horizontal tails yet a different decrease of height towards the fuselage due to differences in airfoil thickness.

Experimental determination of ice shapes: it is obvious that the highly three-dimensional structure of the ice deposites as given by the mushroom and lobster-tail shape is not theoretically predictable with sufficient reliability whereas prediction of the

total captured ice can well be done, as shown before. Therefore, for the Airbus, the calculation procedure was complemented by experiments in the icing tunnel of NASA, Lewis Center, Cleveland, Ohio. Two horizontal tail-models of the A300 (model 1 with constant profile thickness, model 2 was a portion of the horizontal tail in the original design configuration) were investigated [6]. Ice accretions have been determined by making plaster casts and photographs. In order to gain an insight into the significance of the icing parameters ambient temperature $T_\infty$, flow speed V, droplet diameter d, liquid water content LWC, icing duration t and airfoil incidence , have been varied during the tests [6], [7]. Results show (see fig. 7):

   ① When varying LWC and time, while droplet diameter, velocity and temperature are kept constant, one obtains the same ice shapes for all LWC·t = const.

   ② If time varied with the same conditions, ice height will be approximately proportinal to the time period of icing, while impingement limits are independent of time. A slight nonlinear increase with time could be observed for already big ice accretions, which may be contributed to the increase of capture area with time.

   ③ If velocity and time are simultaneously varied at constant LWC, almost identical ice heights, yet different impingement limits and different horn configurations will be obtained on the condition V·t = const.

   ④ If angle of attack is varied, different ice shapes will be obtained; this condition implies migration of the stagnation point.

From steps 1 through 3 it follows:

$$ice\ height \sim LWC \cdot t \cdot V \approx const.$$
$$ice\ shape \sim LWC \cdot t \approx const.$$

Conversion of icing test results to real flight conditions: conformity with actual flight conditions could not be achieved completely during icing tests for some parameters like LWC and velocity. Moreover, since three-dimensional flow effects could not be exactly simulated, results had to be converted to actual flight conditions. Therefore, a special procedure [7], [8] has been developed for the Airbus to deduce the ice accretion making use of both calculation and test results.

- First maximum ice accretion has been calculated and substantiated by experiment. The result was that the highest ice deposit occur near the tip of horizontal and vertical tail, the higher one on the horizontal tail. Its overall height was slightly below 3 inches. Therefore, this value has been adapted as a maximum. This is in accordance with observation of Boeing Company [5] that within 26 million flight hours on different airplanes no bigger accretions have occured.
- Spanwise variation of the amount of ice has been assumed to be according to impingement analysis (see fig. 8). This has been substantiated for several tail surface sections by experimental results.
- Chordwise and spanwise ice shapes have been fully taken according to the experimental shapes. Slight adjustments from test to flight conditions have been made using similarity laws [9].

With this procedure, the most objectionable ice shapes for the A300 tail have been evaluated and selected in order to be further investigated in wind tunnel and flight test. Fig. 9 depicts these ice shapes over the span for the horizontal tail. The corresponding notches are the same as shown before.

Aerodynamic investigations: extensive wind tunnel testing with artificial ice accretions of the just described shape was performed in order to establish its influence on the most important aerodynamic data. These tests were done with complete models as well as pure tail models. The investigations included the determination of the influence of ice shapes, ice size, and notchings.

Results: In fig. 10a, the horizontal tail lift ($c_L$) versus angle of attack as determined with a tail model in the low speed wind tunnel of Braunschweig [10] shows that the deterioration effect of ice accretion sensitively depends on elevator angle. For high nose down moment elevator angles, the loss in tail power at high negative angles of attack - what is equivalent to high negative settings - has shown to be not too serious. Maneouvers of interest in that range, such as stall recovery or go around where the pilot wants or has to increase the nose down moment remain nearly uneffected. On the other hand, for high nose up moment elevator deflections, a loss in maximum negative tail lift can be observed which reduces the trimming and pulling capability at low speeds. Lift slope was associated only by minor changes. This was different to results on the vertical tail where an increase in lift slope according to the increase of fin area by the accretion was found. Ice accretions with notchings showed to have a favourable effect on stall onset as compared to results received without notchings. This is due to the effect that through the slots, high energy flow is transported into the boundary layer or into the reattached bubbles, respectively, which exist immediately behind the ice protrusions. This may also be concluded from fig. 10b, where lift versus drag for the tail model has been plotted. Generally, the $c_{DO}$-value is not effected very much by the ice but rather the drag due to high tail lift as occurs at operation with flaps and slats out.

Results of further aerodynamic invertigations:
- no influence of ice accretions on flutter characteristics of the tail surfaces
- neglectible C.G.-shift ($\approx 0,5$ percent $l\ \mu$) due to the additional weight of ice amount ($G_{ice} \approx 1.50$ kN) at the tail.

Flight test with simulated ice: simulator studies with aerodynamic data taking account for ice accretion showed that no degrading effects of any importance should be expected in flight. Nevertheless, before flight testing under natural icing conditions was released, it was decided to have a flight program with simulated ice. The shapes were chosen according to to fig. 9, but because of the aerodynamic results of the wind

tunnel tests it was decided not to incorporate the lobster tail cutting (see fig. 11).
Consequently, these flight tests have been performed under more severe conditions than
would be expected under natural icing.
The scope of investigation comprised
- forward and aft C.G. locations
- low speed tests in the clean, take-off and landing configuration, the latter inclu-
  ding one engine failure, down to $V = V_S + 5-6$ kts
- high speed tests up to $V_{MO}$ and $M = 0,835$
At all these tests, no instability or loss in control has occured, no sensible degrada-
tion of flying qualities was observed.

Flight test under natural icing conditions: between March 26 and April 9, 1973 alto-
gether 9 flights (36 flight hours) under natural icing conditions (5 flight hours) were
performed with the prototype D02 of the A300. One part of the tests was carried out over
the Mediterranean Sea between the Northcoast of Tunesia, Sardinia and Southern Italy, the
other part over the North Sea and the North-West of Germany [11]. The mean flight alti-
tude was $8.000 \leq H \leq 15.000$ ft at ambient temperatures of $-3^{\circ}C \geq T_{\infty} \geq -16^{\circ}C$ and flight
speeds of $140$ kts $\leq V_{CAS} \leq 270$ kts. The liquid water content as determined during the
flights, fluctuated between $0.4$ g/m$^3$ $\leq$ LWC $\leq 1.0$ g/m$^3$, the time periods of icing were
10 min., droplet diameter has not been recorded. Fig. 12 shows a photo of a specific
deposit on the vertical tail found during flight tests. In all cases, the maximum
assumed ice accretion was below three inches. Flight qualities of the aircraft during
ice accretion were rated as very satisfactory by the pilots.

## 2. UNPROTECTED APU-AIR-INTAKE SYSTEM OF THE A300

The demonstration of the operational ability of the APU-air-intake system under icing
conditions, postulating a save APU function and no hazardous performance degradation,
also required thorough theoretical and experimental investigations [2], [12], since the
APU was installed to cover various supply cases not only on ground but also in flight.

Critical intake components: as shown in fig. 13, the APU-air-intake system consists of
two separate intakes, the main intake supplying the APU and the second intake supplying
the pneumatic APU-cooling system equipped with a fan cooling the APU-oil cooler, -gene-
rator, compartments and -engine shroud. The components for which icing was expected are
the intake lip, guide vane, plenum splitters and spherical protection grid for the main
intake and the flat protection grid for the cooling fan intake.

Theoretical prediction of ice accretion during flight: the ice built-up during flight
operation of the APU was obtained on the basis of impingement analysis calculating the
trajectories of the droplets reaching the APU-intakes. This was examined for the same
flight cases and icing conditions used for the tail surfaces. Fig. 14 shows, how a
"LANGMUIR"-D-droplet distribution assumed in the flow infront of the A300 is changed by
the local curvature of the air flow on the fuselage, i.e. on the forebody and the tail
sweep. The average water contend in the air ingested by the APU-intakes is three times
lower as for the free stream condition.
The resulting ice accretions, here shown in fig. 15 for the critical components of the
APU main intake, are negligible in amount and height, causing no aerodynamic implica-
tions. This has been substantiated by the flight tests under natural icing conditions
[11] mentioned before, where the essential intake component (spheric protection grid)
was controlled by a movie camera. No ice accretion was found at all.

Experimental determination of ice accretion during ground operation: the demonstra-
tion of the save function of the APU-air-intakes under natural icing conditions on
ground (icing conditions: LWC = 0,66 g/m$^3$, d = 30 µm and $T_{\infty}$ = -3$^{\circ}$C) was performed by
experiment, determing the ice accretion and its influence on intake characteristics.
For this, two icing tests series have been carried out at the icing facilities of
Bundesforschungsanstalt Arsenal at Vienna using full scale air intakes in the original
design configuration [13], [14]. Correct intake mass flows simulated by fans and exact
simulation of the intake flow field were guaranteed. The ice depositions for the main
intake after 40 minutes are shown in fig. 16. The most interesting ice accretion
was generated at the spheric grid, with a compact lump of glaze ice on the side facing
the intake hole, and with ice depositions on the rest of the sphere growing on the grid
wires up to maximum height of 20 mm without blocking the grid meshes and giving an in-
sight in the flow field infront of the grid.
For the cooling fan intake ice accretion was only found on the flat protection grid, i.e.
nearly all the water was captured by the grid. The photo series in fig. 17 shows the
temporal ice built-up on the grid. The grid center was completely closed within a time
of 15 minutes leaving an open ring of 30 percent of the grid area which then remained
constant until the end of icing period. The final glaze ice block reached a height of
about 70 mm with a deep excavation at the stagnation point.

Effects of ice accretion on intake- and system-performance: the influence of the just
described ice accretions on the two most important intake parameters as ram recovery and
flow distortion has been measured during the icing tests after each icing phase using
invertable pitot-rakes. Fig. 18 shows a comparison of ram recovery $\eta_R$ and distortion
index DI without and with ice after 60 minutes ground icing for the main intake for
three APU supply cases. It is demonstrated that the loss in ram recovery and the increase
of distortion index due to icing is not critical, since for all cases the limits $\eta_{R\,MIN}$
and DI $\leq 5$ % as required by the APU manufacturer are not exceeded, i.e. the minimum
allowable intake performance is guaranteed [2].

Analysis for the cooling fan intake [2] shows (see fig. 19), that, after 15 minutes icing, the intake pressure loss due to ice accretion is stabilizing around 10 percent without reaching the maximum allowable value of 15 percent. This additional pressure losses cause only neglectible mass flow reductions without any influence on the cooling capacity of the system. The increase of distortion index is unimportant.

Ground icing tests under natural icing conditions: the demonstrations for the APU intakes have been completed by extensive ground icing tests with the second prototype of the A300 at Helsinki in Finland [15]. The ambient temperature found was between $-1^{\circ}C \geq T_\infty \geq -15^{\circ}C$ and the time period of icing was several hours. Liquid water content LWC and droplet diameter have not been measured. The fig. 20 shows two photos of ice accretions found on the main intake and the cooling fan intake. No influence on APU- and cooling system function have been ascertained during the tests. According to the demonstration procedure, the APU system of the A300 was certified for one hour ground operation under natural icing conditions and for a following in-flight operation with iced intake components.

## 3. VFW 614 ICE SHEDDING INVESTIGATIONS

Investigations of effects of ice accretion on aircraft components are not complete without looking into the "post icing phase". This is the phase where the ice-material bond is melting due to heating effects (for example dynamic temperature rise) and ice shedding starts. The possibility that larger ice particles which shed from an unprotected aircraft component could be a hazard for the aircraft or any other components has to be fully analysed, i.e. determination of shape and size of the particles and its corresponding trajectories. Such investigations have been performed for the German transport aircraft VFW 614 for which, due to the exceptional cruise engine installation, as shown in the fig. 21, ice particles breaking-off from the unprotected radome have been expected to be hazardous for the engine. The trajectories of the ice particles * have been determined in a low speed wind tunnel at Bremen with a 1:16 scale model ejecting the particles from the radome (dynamic similarity was present - "Froude-No."- Scaling) [16]. The results, matched by theory, show that, for all flight attitudes, the ice particles do not meet the engine intakes; an example is given on the photo in fig. 21.

## 4. REFERENCES

[1] B. Laschka  R.E. Jesse — Determination of ice shapes and their effect on the aerodynamic characteristics for the unprotected tail of the A300  ICAS paper No. 74-42, August 1974, Haifa, Israel

[2] R.E. Jesse  G. Thome — Funktionstüchtigkeit der APU-Einläufe unter Bodenvereisungsbedingungen  Messerschmitt-Bölkow-Blohm Report UFE 1031 and UFE 1083, 14 Apr. 74

[3] W. Kraus — Untersuchungen zur Leitwerksvereisung der A300-B, Teil 2: Theoretische Bestimmung der Eisformen und Eisverteilung  Messerschmitt-Bölkow-Blohm Report UFE 874-72, 6 June 1972

[4] W. Kraus — Weiterentwicklung des Panelverfahrens  Messerschmitt-Bölkow-Blohm Report UFE 1017, March 1973

[5] E.D. Dodson — Determination of ice shapes for unprotected B 747 flight surface leading edge  Boeing Document No. D6-30-576, 1969

[6] H. Lück — Vereisungsversuche am Höhenleitwerk der A300-B im Eiskanal der NASA LRC in Cleveland, Ohio  Deutsche Airbus Report TB-EFW-6/71, 28 May 1971

[7] N. Kiesewetter — Untersuchungen zur Leitwerksvereisung der A300-B, Teil 1: Empirische Ermittlung der Eisformen  Messerschmitt-Bölkow-Blohm Report UFE 855-72, 28 February 1972

[8] R.E. Jesse — Eisformen für die ungeschützten Leitwerke der A300-B  Messerschmitt-Bölkow-Blohm Report UFE 865-72, 20 April 1972

[9] E.D. Dodson — Scale model analogy for icing tunnel testing  Boeing Document No. D6-7976, 1962

[10] P. Giese — Windkanlmessungen am Airbus-Leitwerksmodell 108, 3 Teil VII  Deutsche Forschungsanstalt für Luft- und Raumfahrt e.V. Report No. IB-157-73 C3, 4 May 1973

[11] — Airbus Industrie, Rapport d'Essais en Vol de Certification: Justification de l'Avion en Atmosphère Givrante - Essais en Vol en Givrante Natural Mésure  Airbus Industrie Document PC/LG/MS  AI/V n° 566/73, 17 Septembre 1973

* Note:
Shape and size of the ice particles released during the tests have been defined by a special full scale icing test with the radome using the Blower Tunnel facility at Boscombe Down in England.

[12] H. Wölfer      Theoretische Bestimmung der Vereisung des APU-Luftansaugschachtes
für Boden- und Flugbetrieb
Messerschmitt-Bölkow-Blom Report UH-VB No. 1838, 29 June 1972

[13] H. Wölfer      Bodenvereisungsversuche mit dem A300-APU-Luftansaugschacht
Messerschmitt-Bölkow-Blohm Report UH-VB No. 1922, 15 August 1973

[14] H. Wölfer      Bodenvereisungsversuche mit dem A300-APU-Kühlgebläseeinlauf
Messerschmitt-Bölkow-Blohm Report UH-VB No. 1977, 9 April 1974

[15] G. Scherer      Campagne des Essais par Temps Froid
Airbus Industrie Document AI/V n° 95/74, 28 January 1974

[16] G. Anders      Aerodynamische Untersuchungen zur Feststellung möglicher Eis-
flugbahnen
Vereinigte Flugtechnische Werke - Fokker Report
Ef-586 part 1-3, 18 January 1977

EQUIPPED WITH A
DE- OR ANTI-ICING SYSTEM
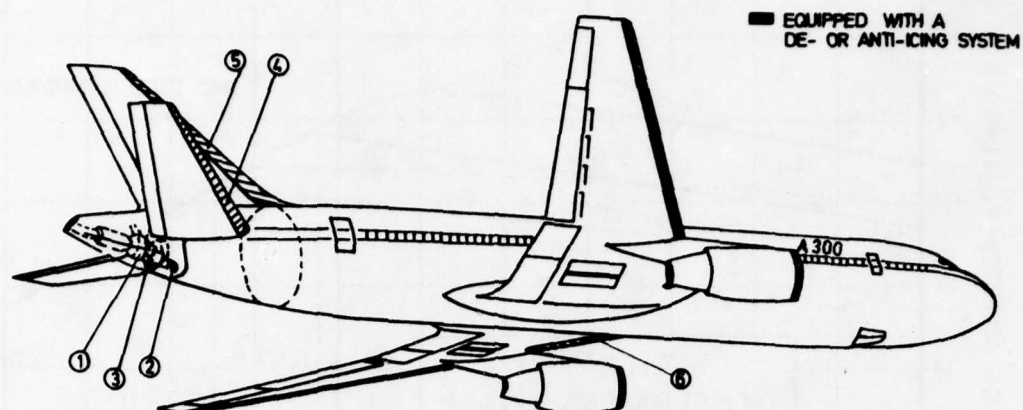
① APU
② APU MAIN AIR INTAKE
③ APU COOLING FAN INTAKE

④,⑤ LEADING EDGES OF HORIZONTAL
AND VERTICAL TAIL
⑥ SLATS BETWEEN FUSELAGE AND
ENGINE PYLON

Fig. 1    CRITICAL AIRCRAFT COMPONENTS NOT PROTECTED BY A DE-ICING OR
ANTI-ICING SYSTEM



STREAMLINE

TRAJECTORY OF SMALL DROPLETS
TRAJECTORY OF LARGE DROPLETS
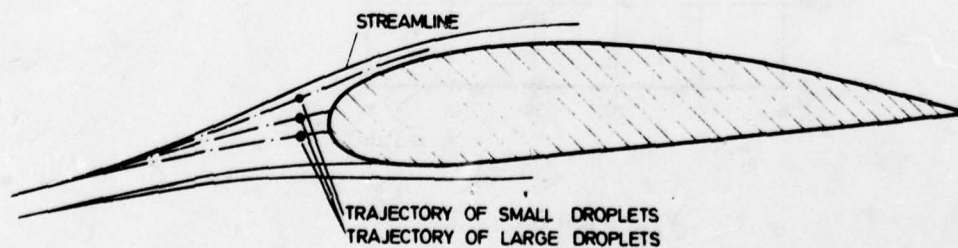
Fig. 2    DEVIATION OF DROPLET TRAJECTORIES FROM STREAMLINE DUE TO
DROPLET DIAMETER
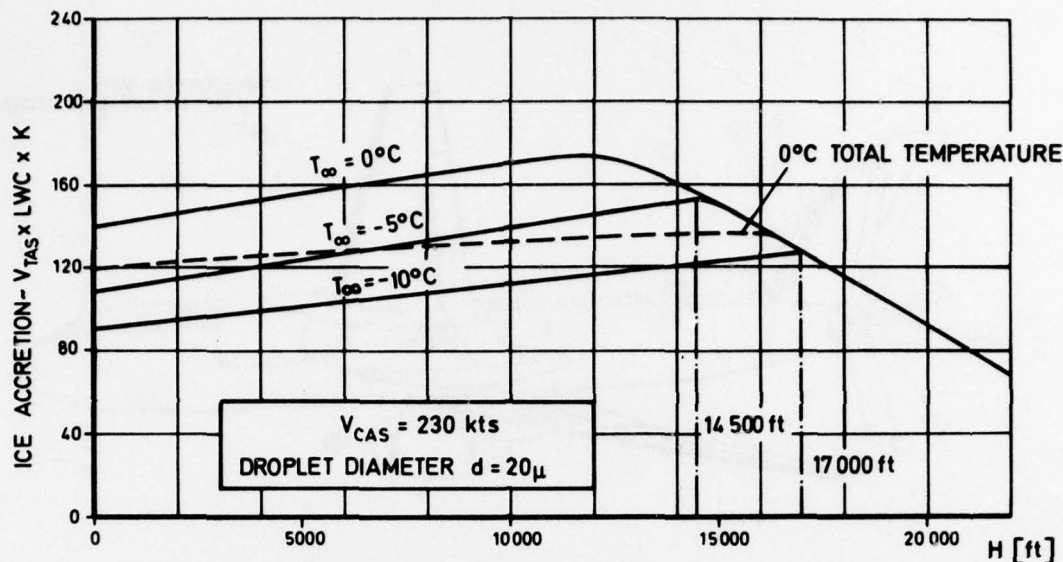
Fig. 3    AVERAGE AMOUNT OF ICE ACCRETION DUE TO FLIGHT ALTITUDE AND
AIR TEMPERATURE
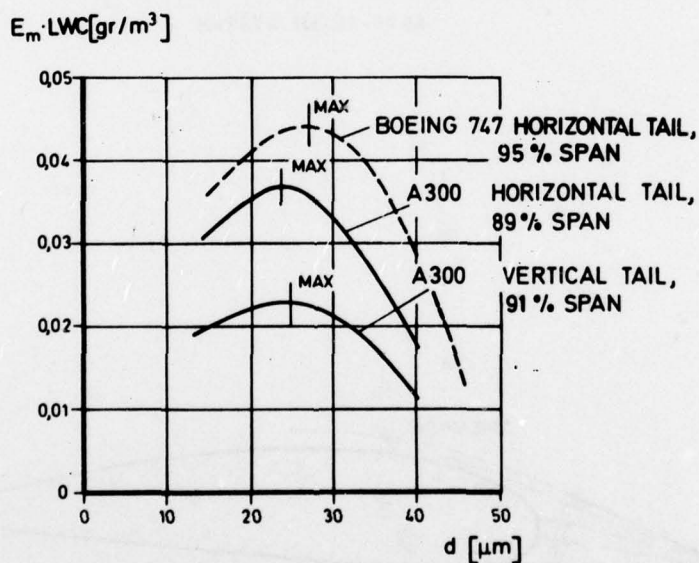


Fig. 4    WATER CAPTION FACTOR ($E_m \cdot$ LWC) OF HORIZONTAL AND VERTICAL TAIL
VERSUS DROPLET DIAMETER

RIME ICE

RUNBACK
OF
DROPLETS

STAGNATION POINT

GLAZE ICE
(MUSHROOM - DOUBLE - HORN)

Lobstertail cutting of a typical A 300 ice shape
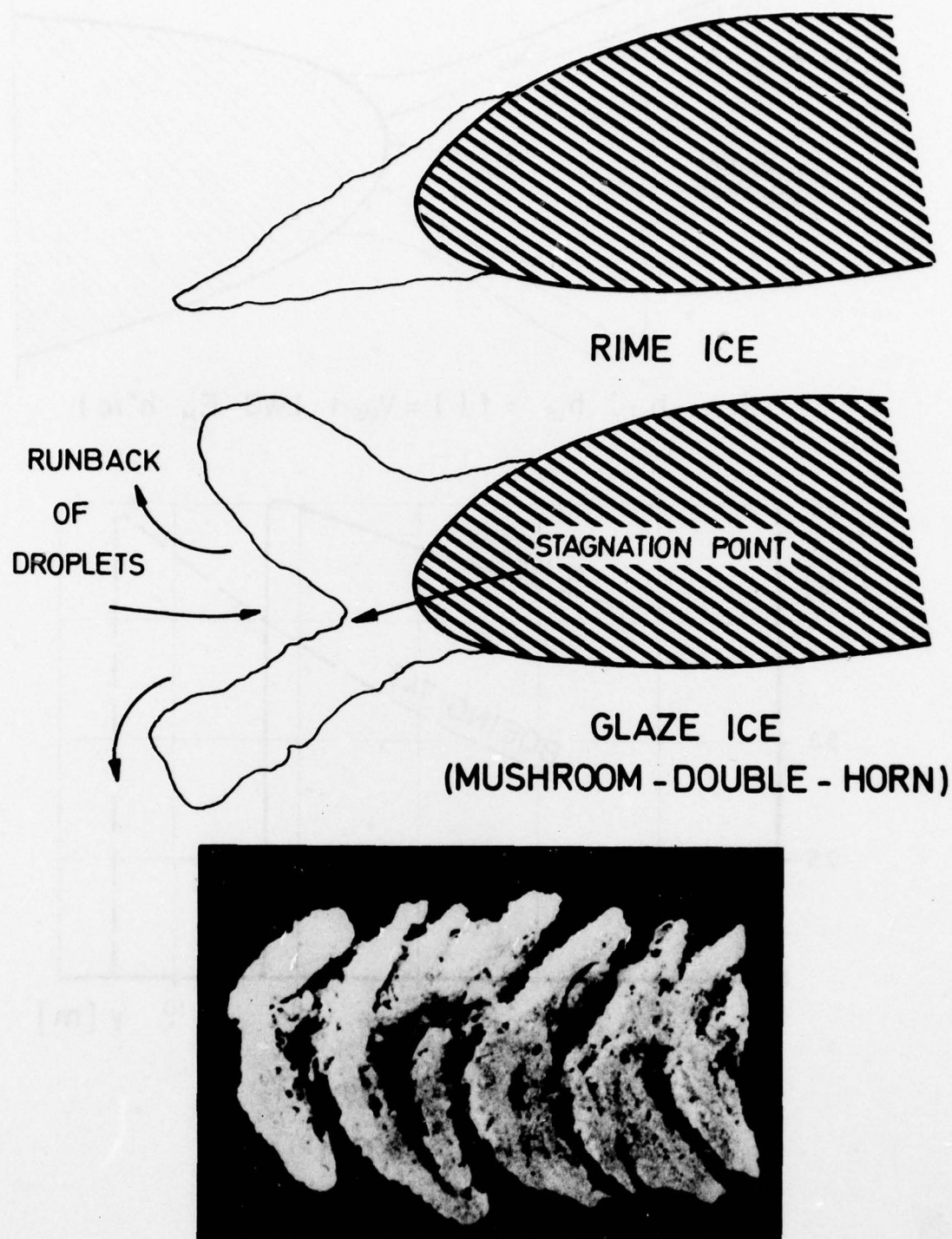
Fig. 5    CHORD- AND SPANWISE ICE SHAPES ON SWEPT WINGS
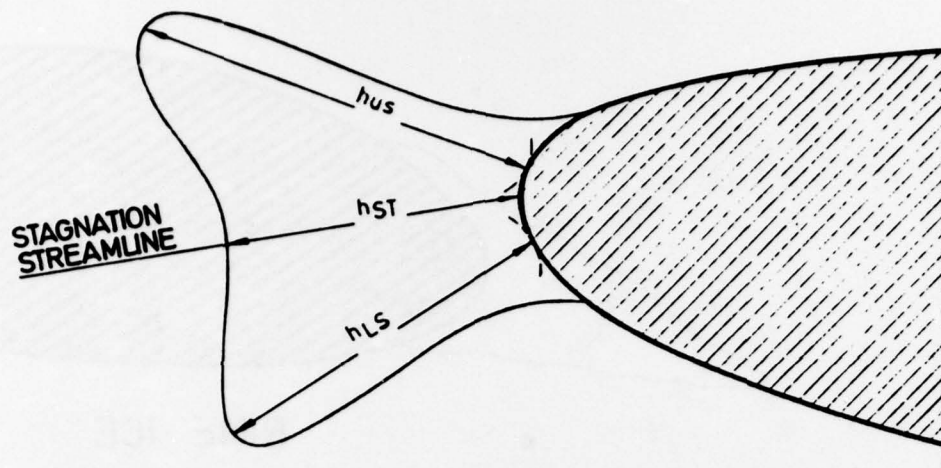
$$h_{US}, \; h_{ST}, \; h_{LS} = f \left( I = V_{TAS} \cdot t \cdot LWC \cdot E_M \cdot h^*/c \right)$$
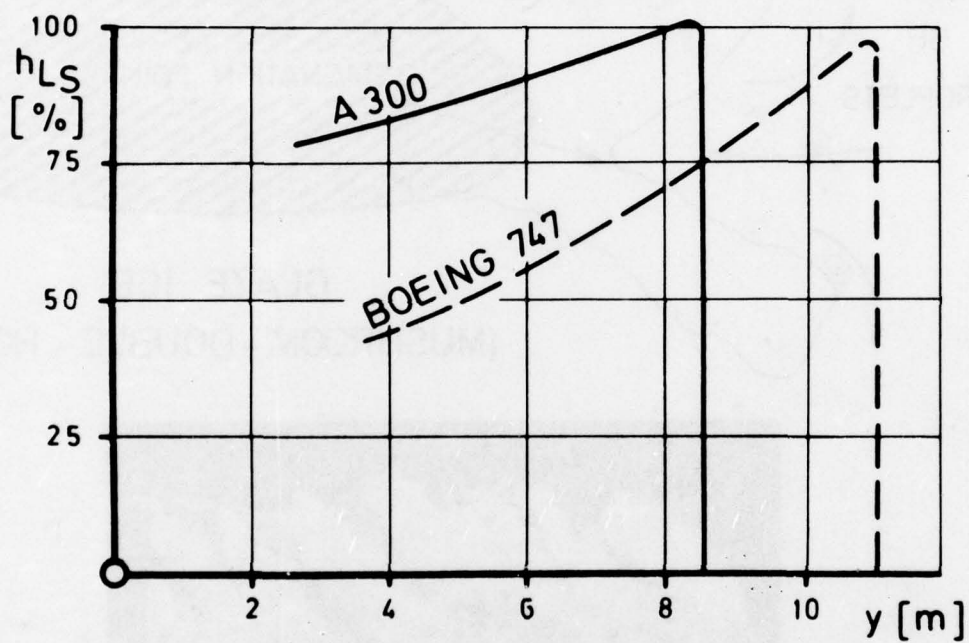
t = 30 min

H = 15 000 ft

d = 15 μ

Fig. 6    SPANWISE ICE HEIGHTS FOR HORIZONTAL TAIL

| α [°] | d [μ] | LWC [gr/m³] | T [°C] | CAS [mph] | t [min] |
|---|---|---|---|---|---|
| 0 | 16 | 1 40 | -5 | 184 | 14 2 |
| 0 | 16 | 1 30 | -5 | 184 | 15 4 |
| 0 | 16 | 1 10 | -5 | 184 | 18 2 |
| 0 | 16 | 0 90 | -5 | 184 | 22 2 |

① EFFECT OF LWC · t = const.

| α [°] | d [μ] | LWC [gr/m³] | T [°C] | CAS [mph] | t [min] |
|---|---|---|---|---|---|
| 0 | 16 | 1 15 | -5 | 192 | 10 |
| 0 | 16 | 1 15 | -5 | 192 | 20 |
| 0 | 16 | 1 15 | -5 | 192 | 25 |
| 0 | 16 | 1 15 | -5 | 192 | 30 |

② EFFECT OF ICING-DURATION

| α [°] | d [μ] | LWC [gr/m³] | T [°C] | CAS [mph] | t [min] |
|---|---|---|---|---|---|
| 0 | 20 | 1 20 | -5 | 264 7 | 13 |
| 0 | 20 | 1 20 | -5 | 242 | 14 3 |
| 0 | 20 | 1 20 | -5 | 207 | 15 7 |
| 0 | 20 | 1 20 | -5 | 172 5 | 20 |

③ EFFECT OF V · t = const.

| α [°] | d [μ] | LWC [gr/m³] | T [°C] | CAS [mph] | t [min] |
|---|---|---|---|---|---|
| 2 | 19 | 0.975 | -5 | 230 | 21.6 |
| 0 | 19 | 0.975 | -5 | 230 | 21.6 |
| -2 | 19 | 0.975 | -5 | 230 | 21.6 |
| -4 | 19 | 0.975 | -5 | 230 | 21.6 |

④ EFFECT OF ANGLE OF ATTACK

FROM STEPS 1. THROUGH 3. IT FOLLOWS
ICE HEIGHT ~ LWC · t · V = CONST.
ICE SHAPE ~ LWC · t = CONST.

Fig. 7    EXPERIMENTAL ICING PARAMETER STUDY FOR THE HORIZONTAL TAIL

$h_{MAX}$ [inch]

VERTICAL TAIL: 2,75 INCH AT
THE TIP, DECREASE OF ICE
HEIGHT DUE TO CALCULATION

HORIZONTAL TAIL: 3 INCH AT THE
TIP, DECREASE OF ICE HEIGHT
DUE TO CALCULATION

y/s [%]
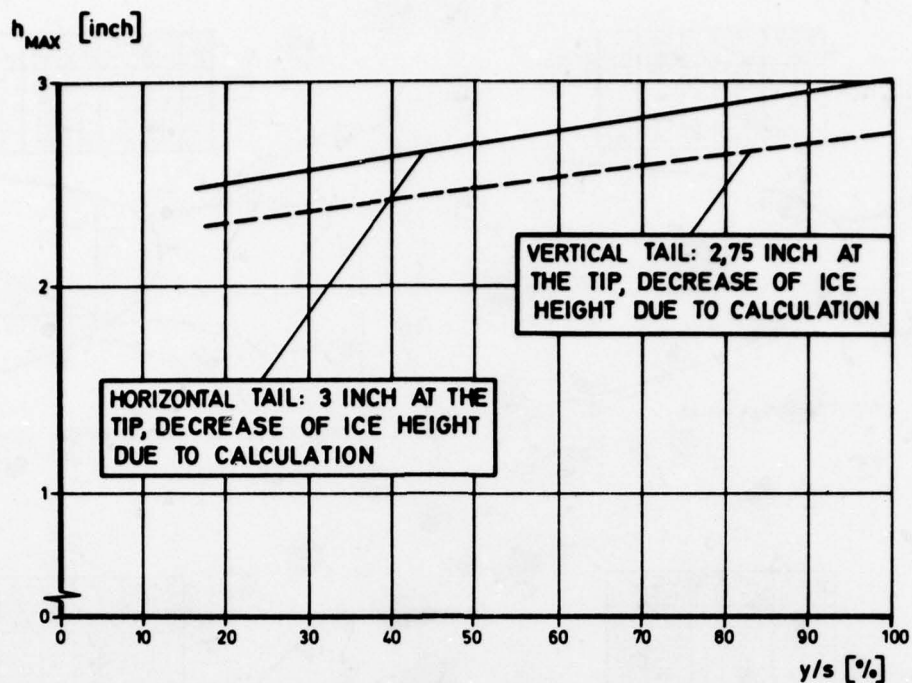
Fig. 8     MAXIMUM ICE HEIGHTS FOR HORIZONTAL- AND VERTICAL STABILIZER
(SPANWISE)

FUSELAGE CENTER LINE

y/s
25 %
40 %
68,5 %
88 %
100 %

FLIGHT ALTITUDE        H = 17 000 ft
FLIGHT VELOCITY        $V_{CAS}$ = 230 kts
HOLDING                t = 45 min
WEIGHT                 G = 100 Mp
C. G.                  = 31 % $l_\mu$
AMBIENT TEMP.          $T_\infty$ = -10 °C

y/s $_{H.ST.}$   25 %      40 %              68,5 %        88 %      100 %
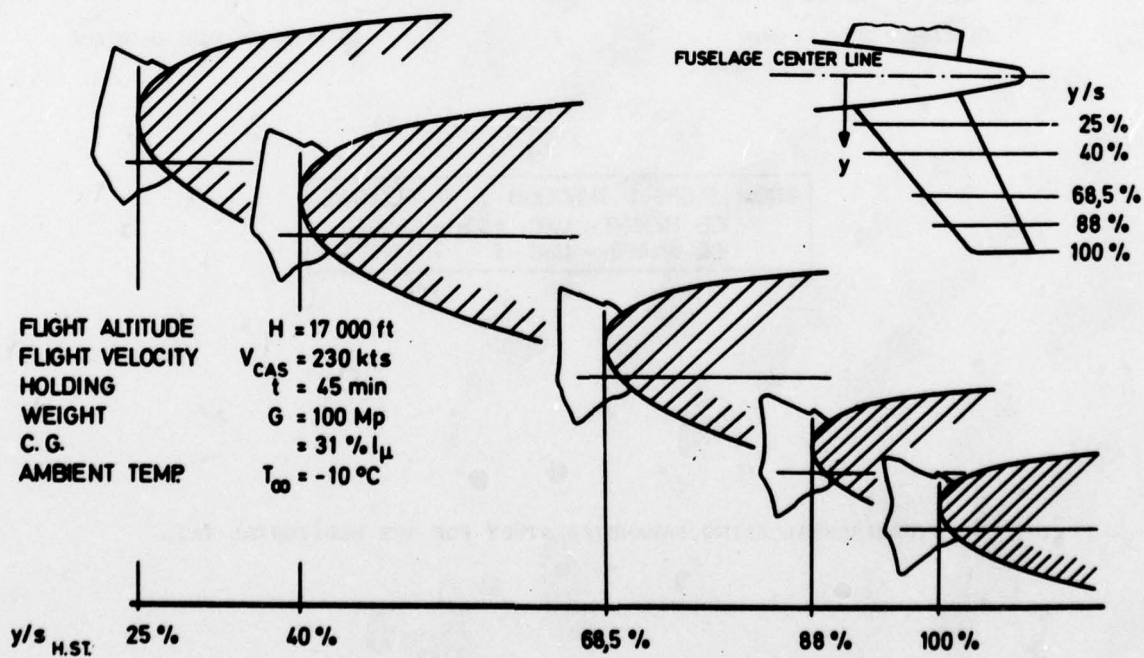
Fig. 9     MOST OBJECTIONABLE ICE SHAPES FOR THE HORIZONTAL TAIL
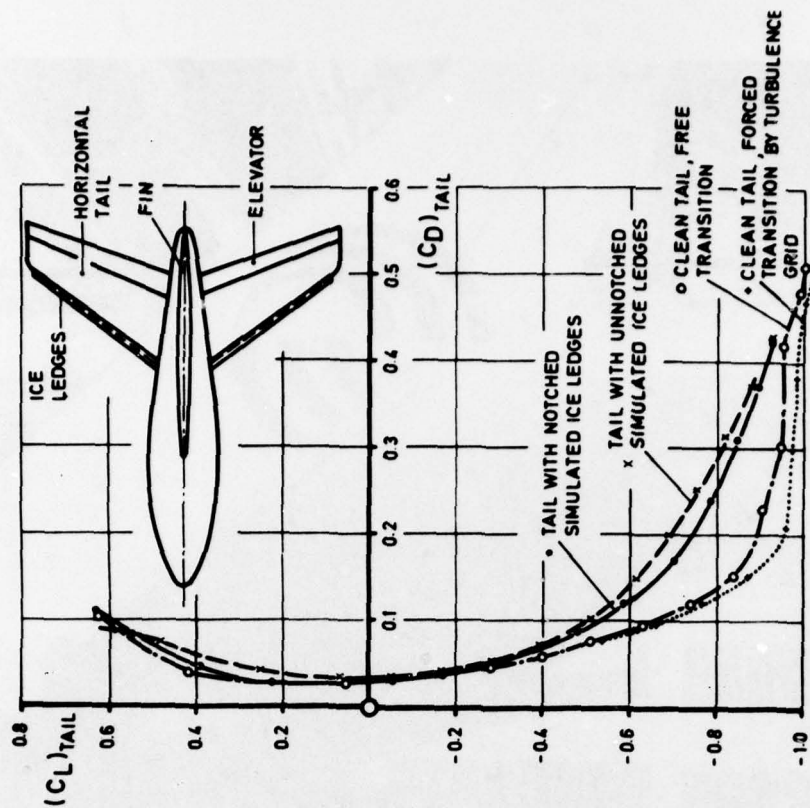
Fig. 10b  EFFECT ON TAIL DRAG
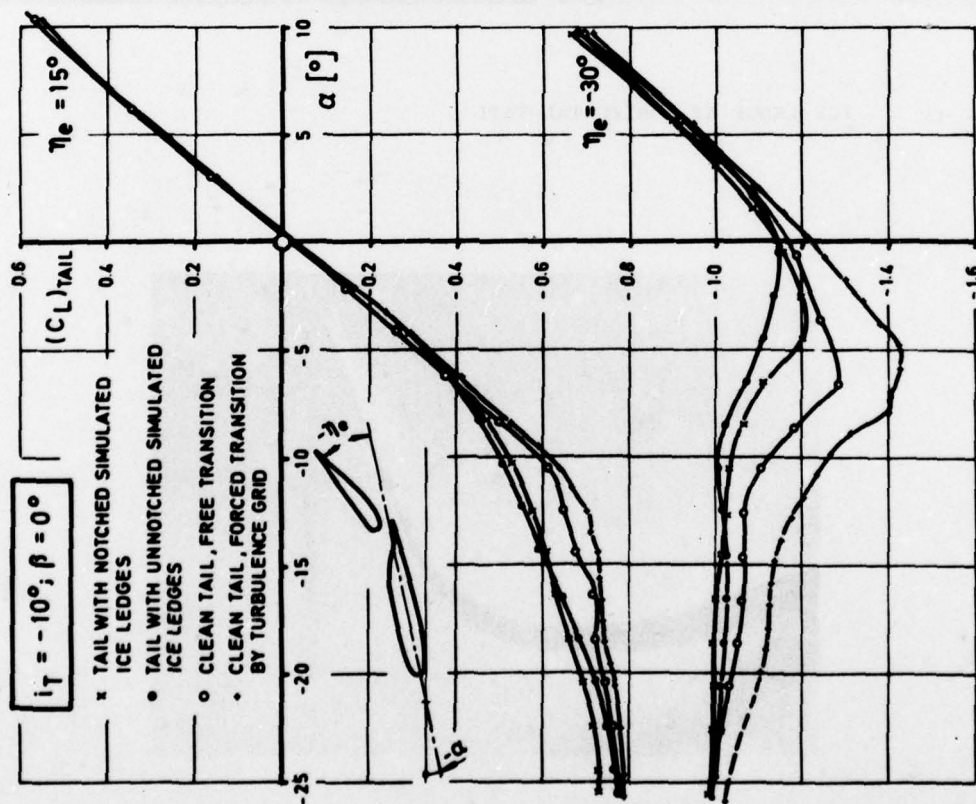
Fig. 10a  EFFECT ON TAIL LIFT

Fig. 10  EFFECTS OF ICE LEDGES ON TAIL CHARACTERISTICS

Fig. 11    ICE LEDGE AT HORIZONTAL TAIL
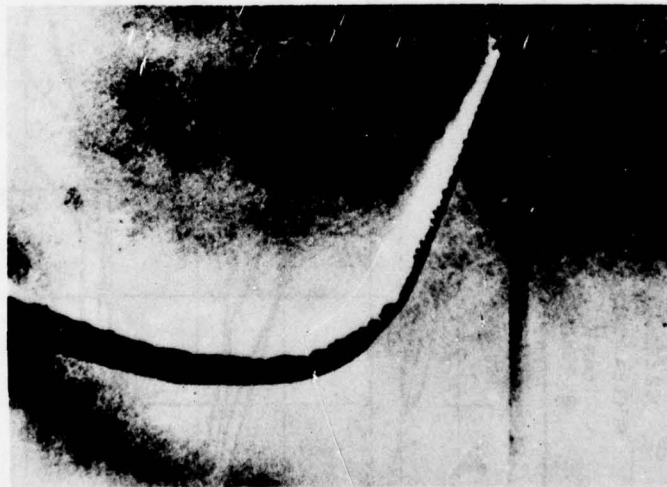


Fig. 12    ICE ACCRETION AT VERTICAL TAIL FOUND DURING FLIGHT TEST

COOLING FAN INTAKE

Konus

FANBLADES

SPLITTER-
PLATE

⑤ FLAT PROTECTION GRID

AIR FLOW

MAIN INTAKE

APU

① ② ③ ④ ⑤ CRITICAL COMPONENTS

④ SPHERICAL PROTECTION GRID

③ SPLITTERPLATE

BYPASS- DOOR

AIR FLOW

① GUIDE VANE

② INTAKE LIP
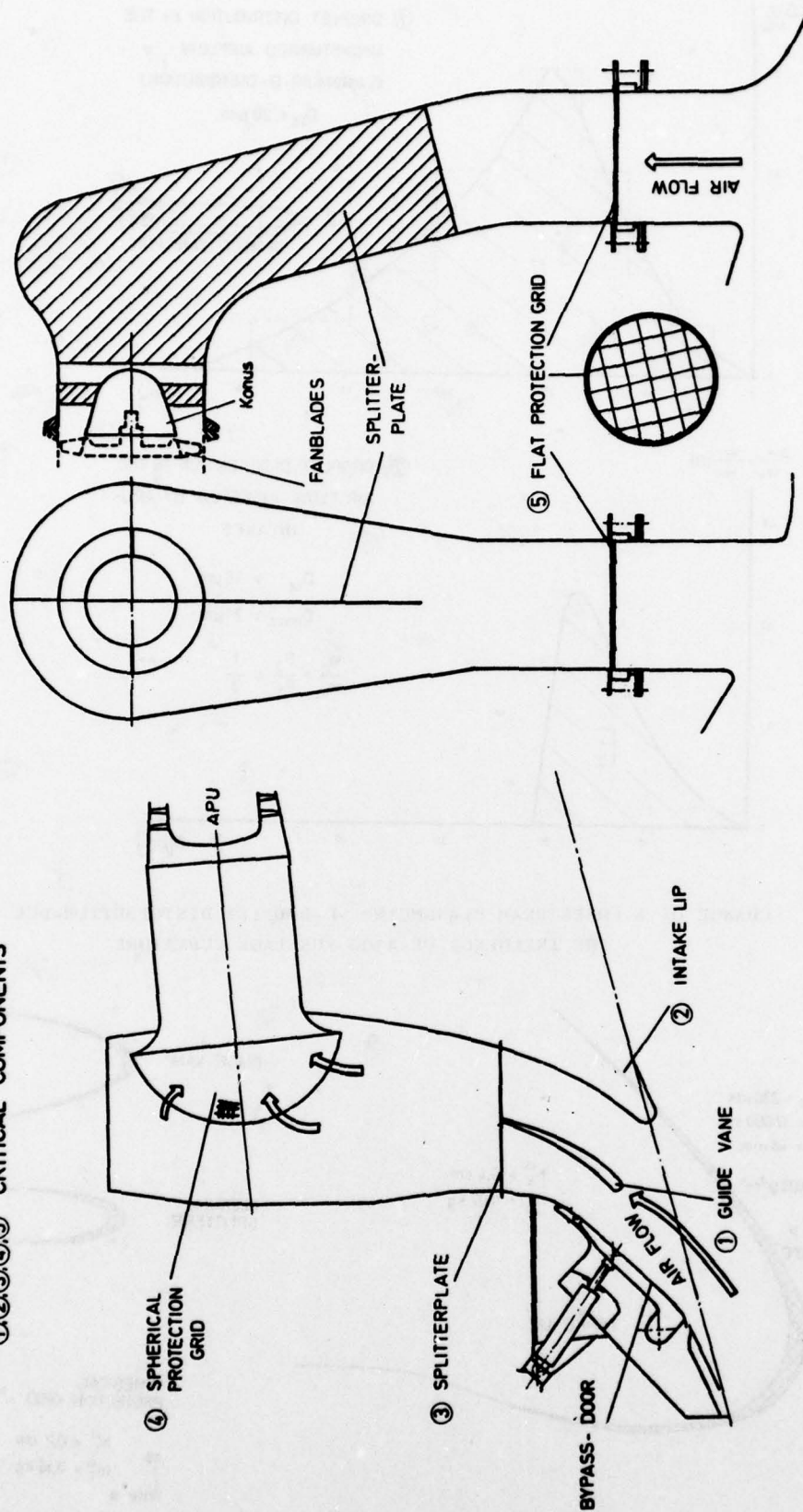
Fig. 13    DETAILS OF THE APU - AIR - INTAKE SYSTEM

① DROPLET DISTRIBUTION IN THE
UNDISTURBED AIRFLOW
(LANGMUIR-D-DISTRIBUTION)

$D_M \approx 20 \mu m$

DROPLET TRAJECTORY

② DROPLET DISTRIBUTION IN THE
AIR FLOW INGESTED BY APU-
INTAKES

$D_M = 15 \mu m$

$D_{max.} = 21 \mu m$

$\dfrac{w_a}{w_\infty} = \dfrac{F_2}{F_1} \approx \dfrac{1}{3}$
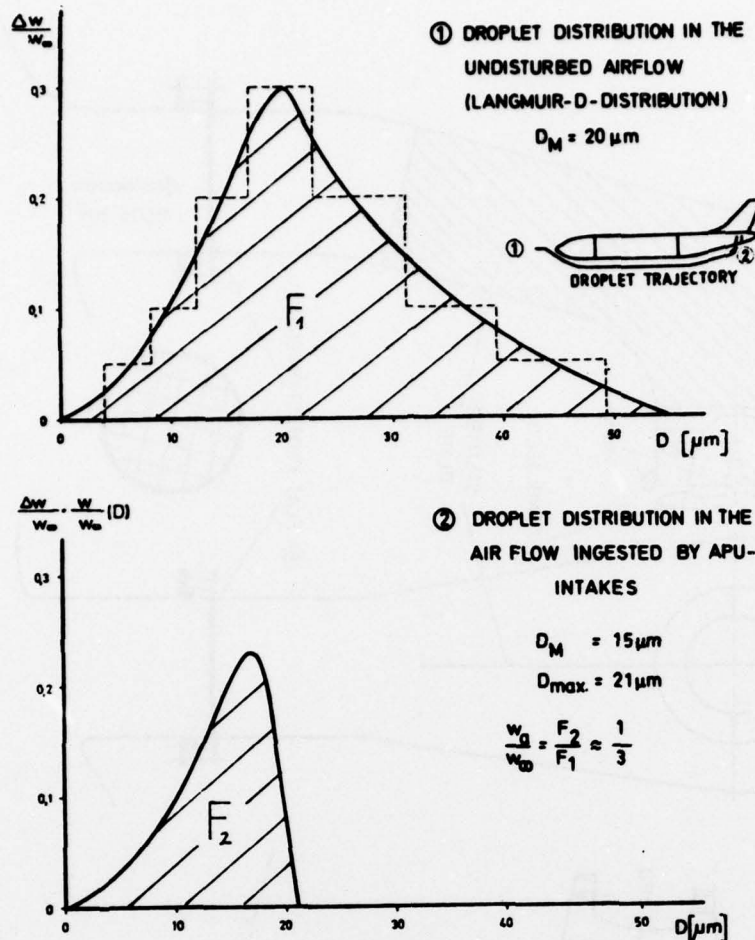
**Fig. 14  CHANGE OF A FREESTREAM "LANGMUIR" -D-DROPLET DISTRIBUTION DUE TO THE INFLUENCE OF A300 FUSELAGE CURVATURE**

**FLIGHT CASE**

Flight velocity : $V_{CAS} = 230$ kts
Flight altitude: $H = 17\,000$ ft
Holding: $t = 45$ min.
Liquid water contend.: $LWC = 0.13\,gr/m^3$
Eff. droplet diameter: $d = 20\,\mu$
Ambient Temp.: $T_\infty = -10°C$

GUIDE VANE
$h_E^{45} = 0.2$ cm
$m_E^{45} = 9$ g

$h_E^{45} = 0.4$ cm
$m_E^{45} = 0.07$ kg

PLENUM
SPLITTERS
$h_E^{45} = 0.4$ cm
$m_E^{45} = 24$ g

INTAKE LIP

SPHERICAL
PROTECTION GRID
$h_E^{45} = 0.2$ cm
$m_E^{45} = 0.16$ kg

Wire ø
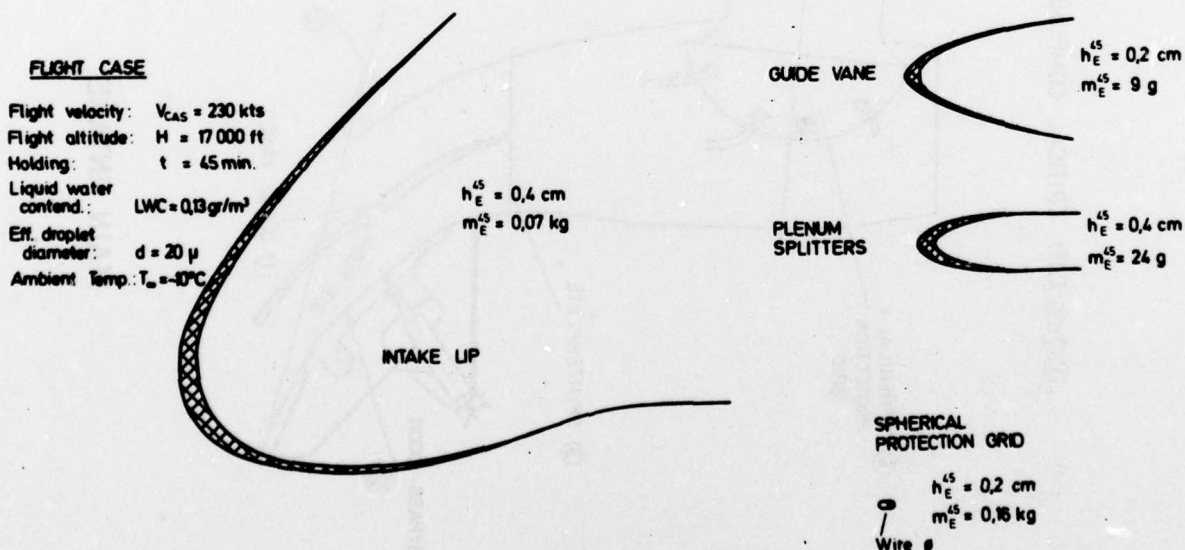
**Fig. 15  THEORETICAL PREDICTED ICE ACCRETION AT THE CRITICAL COMPONENTS OF THE MAIN INTAKE DURING FLIGHT**

ICING CONDITION; LWC = 0,66 gr/m$^3$, d = 30 μm, T$_\infty$ = -3°C
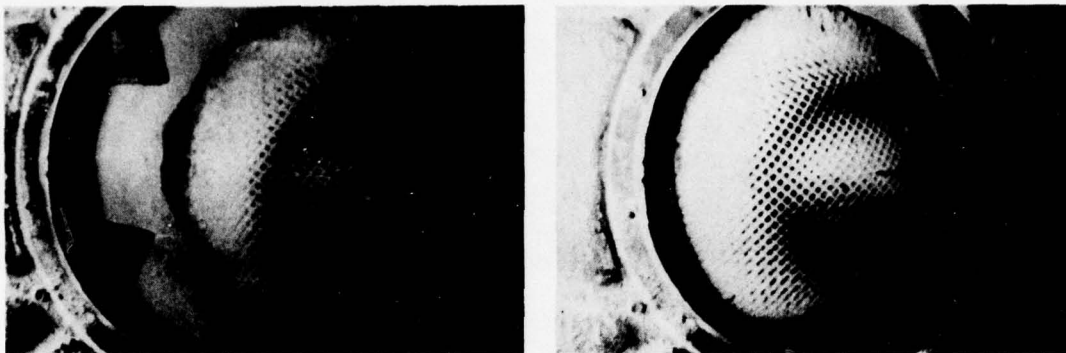


SPHERICAL PROTECTION GRID



INTAKE GUIDE VANE AND PLENUM CHAMBER
SPLITTER PLATES

Fig. 16     ICE ACCRETION AT APU-MAIN-INTAKE COMPONENTS AFTER 40 MINUTES
ICING DURATION

ICING CONDITION; $LWC = 0.66 \, gr/m^3$, $d = 30 \, \mu m$, $T_\infty = -3° C$
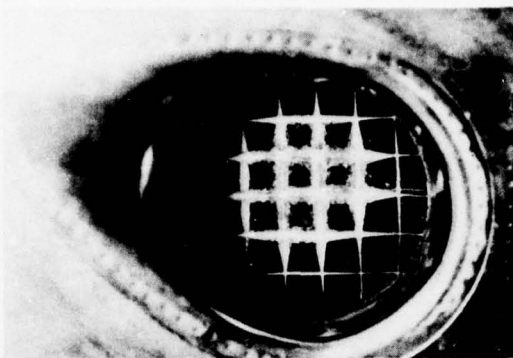


ICING DURATION  t = 5 minutes
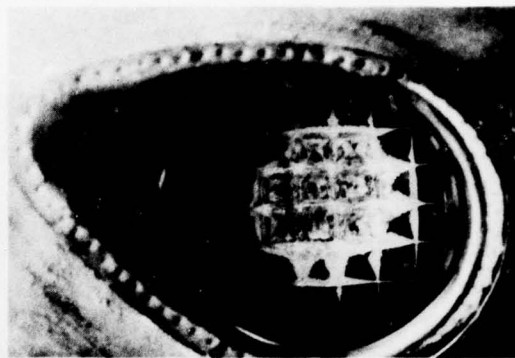
t = 10 minutes
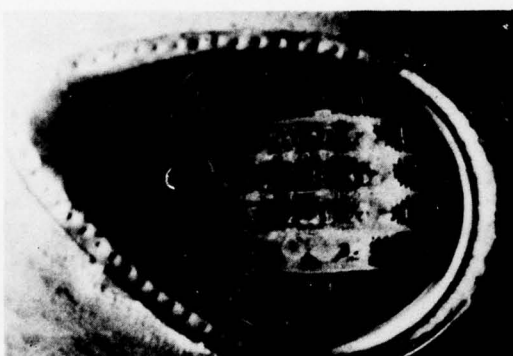
t = 15 minutes
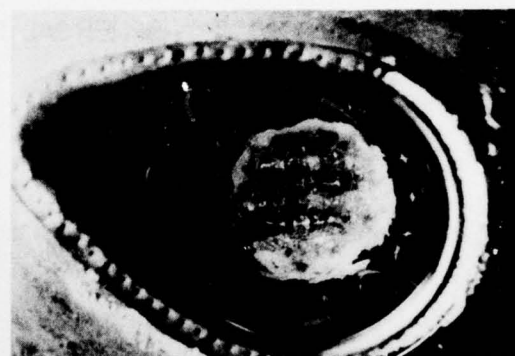
t = 25 minutes
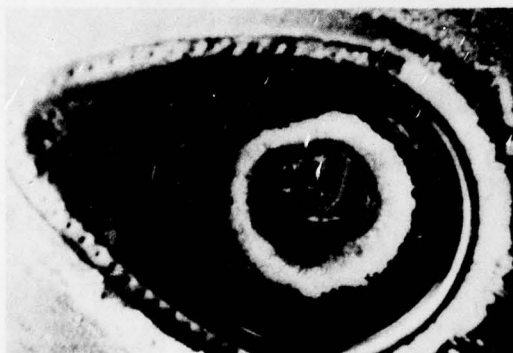
t = 60 minutes

Final excavated ice-block (t = 90 minutes)

Fig. 17    TEMPORAL ICE-BUILD-UP AT THE FLAT PROTECTION GRID OF THE
APU-COOLING FAN INTAKE

| RAM RECOVERY | APU - SUPPLY CASE | FLOW DISTORTION INDEX |
|---|---|---|

1. ECS + GENERATOR SUPPLY
$N_1 = 92,4 \%$

◄ $\eta R_{min.}$
(H = 6000ft, $T_\infty$ 30°C; G = 360lb/min.; N = 115PS)

INCREASE IN DISTORTION
INDEX DUE TO ICING

PRESSURE RECOVERY
LOSS DUE TO ICING

$LWC = 0,66 \ (gr/m^3)$;

$T_\infty = -3 \ (°C)$;

$d = 30 \ (\mu m)$;

REQUIRED
DI ≩ 5%

2. CRUISE ENGINE STARTING
(MES) ON GROUND
$N_1 = 100 \%$

◄ $\eta R_{min.} = 0,866$
(H = 8000ft; $T_\infty$ ≥ -1°C; N = 115PS)

PRESSURE RECOVERY
LOSS DUE TO ICING

$LWC = 0,66 \ (gr/m^3)$;

$T_\infty = -3 \ (°C)$;

$d = 30 \ (\mu m)$;

$\eta R$

0,98   0,96   0,94   0,92   0,90   0

3. "ESSENTIAL UNIT" - OPERATION
(BY-PASS-DOOR IN FLIGHT POSITION)
$N_1 = 89 \%$
( $M_\infty = 0,86$; H = 30000 ft; $T_\infty$ ≥ ISA + 10°C; N = $N_{min.} = 86PS$ )

PRESSURE RECOVERY
LOSS DUE TO ICING

$LWC = 0,66 \ (gr/m^3)$;

$T_\infty = -3 \ (°C)$;

$d = 30 \ (\mu m)$;

$\eta R_{min.} = 0,575$ ►

$\eta R$                                                         DI(%)

0,64   0,62   0,60   0,58   0           0   1   2   3   4   5   6

--- VALUES WITHOUT ICE ACCRETION

Fig. 18    MAIN INTAKE RAM RECOVERY AND DISTORTION INDEX AFTER 60 MINUTES
GROUND ICING FOR DIFFERENT APU SUPPLY CASES
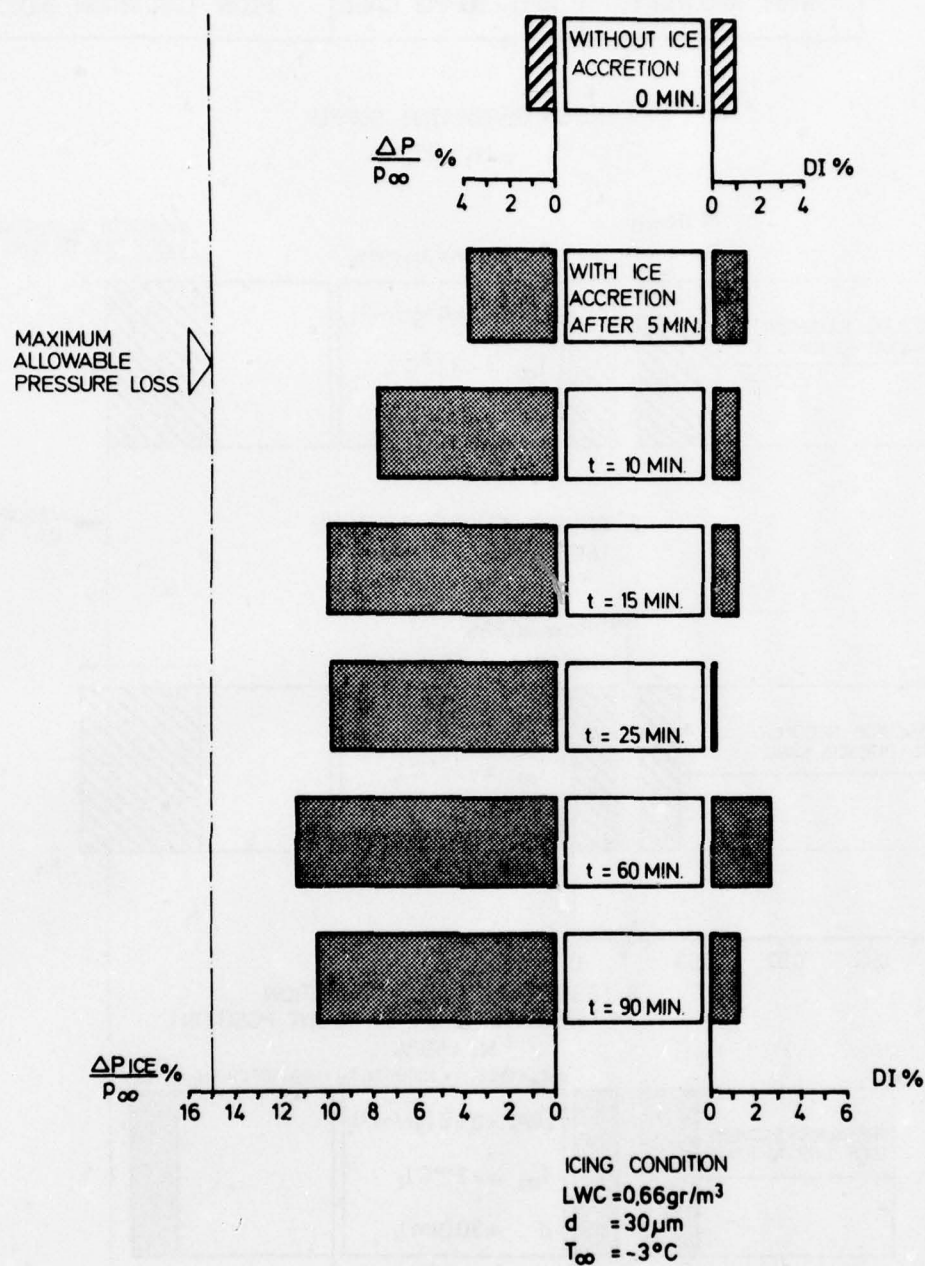
Fig. 19   ADDITIONAL PRESSURE LOSSES AND DISTORTION INDEX DUE TO ICE ACCRETION
ON THE PROTECTION GRID OF THE APU COOLING FAN INTAKE DURING 90
MINUTES GROUND ICING CONDITIONS

ICING CONDITIONS: -1° ≤ T∞ ≤ -10°C , LWC ,d unknown, t several hours
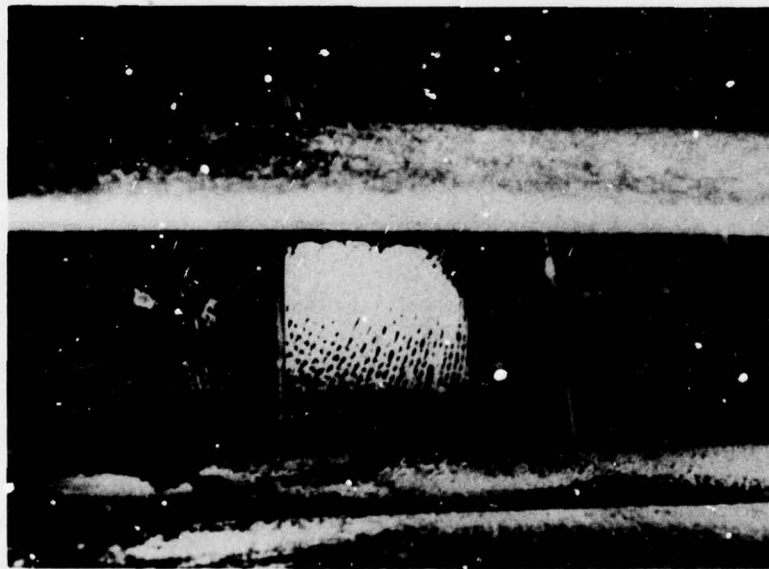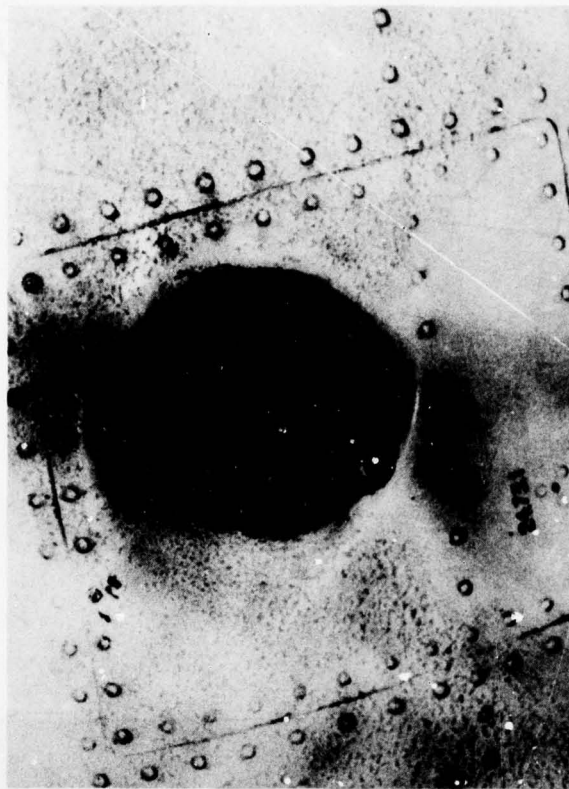
COOLING FAN AIR INTAKE
(ICE DEPOSITION WAS BREAKING-OFF AFTER
SHUT-DOWN OF THE APU)

MAIN AIR INTAKE

Fig. 20   ICE ACCRETION FOUND ON APU-AIR-INTAKES DURING GROUND ICING TESTS
IN HELSINKI WITH AN A300 PROTOTYPE

ICE DEPOSIT ON
UNPROTECTED RADOME

HAZARDOUS PATH OF A
ICE PARTICLE BREAKING-OFF
FROM RADOME

VFW 614

$\alpha_{A/C} = 0°$

$\beta_{A/C} = 0°$

$Q = 0,83 \text{ KN/m}^2$

Fig. 21    EXPERIMENTAL DETERMINATION OF TRAJECTORIES OF ICE PARTICLES
BREAKING-OFF FROM THE RADOME ICE DEPOSIT OF THE VFW 614

# A THEORETICAL AND EXPERIMENTAL MEANS TO PREDICT ICE ACCRETION SHAPES FOR EVALUATING AIRCRAFT HANDLING AND PERFORMANCE CHARACTERISTICS

By
Ramon W. Wilder

The Boeing Company
Seattle, Washington

## SUMMARY

To determine the need for airfoil ice protection systems and the effects of large ice shapes on airplane performance, Boeing initiated a research program to obtain basic ice accretion and ice shedding data on typical jet transport swept airfoils. This program, sponsored by the Federal Aviation Agency, was conducted in the NASA 6-foot by 9-foot icing tunnel at Cleveland, Ohio.

An empirical relationship derived from basic airfoil water catch parameters was used to correlate measured ice accretion rates with theoretical water impingement parameters. This correlation used glaze ice heights and angles measured from the plaster casts of the actual ice shapes as taken from the two swept airfoil test models. Results of this correlation show that ice accretion characteristics are dependent on airfoil shape, particularly leading edge radius, camber and angle of attack.

Complex trends of the data obtained in this test program precluded a general ice accretion relationship with other airfoils. Additional testing of other airfoil shapes and angle of attack would provide for broader application of the ice cap calculation procedures developed herein.

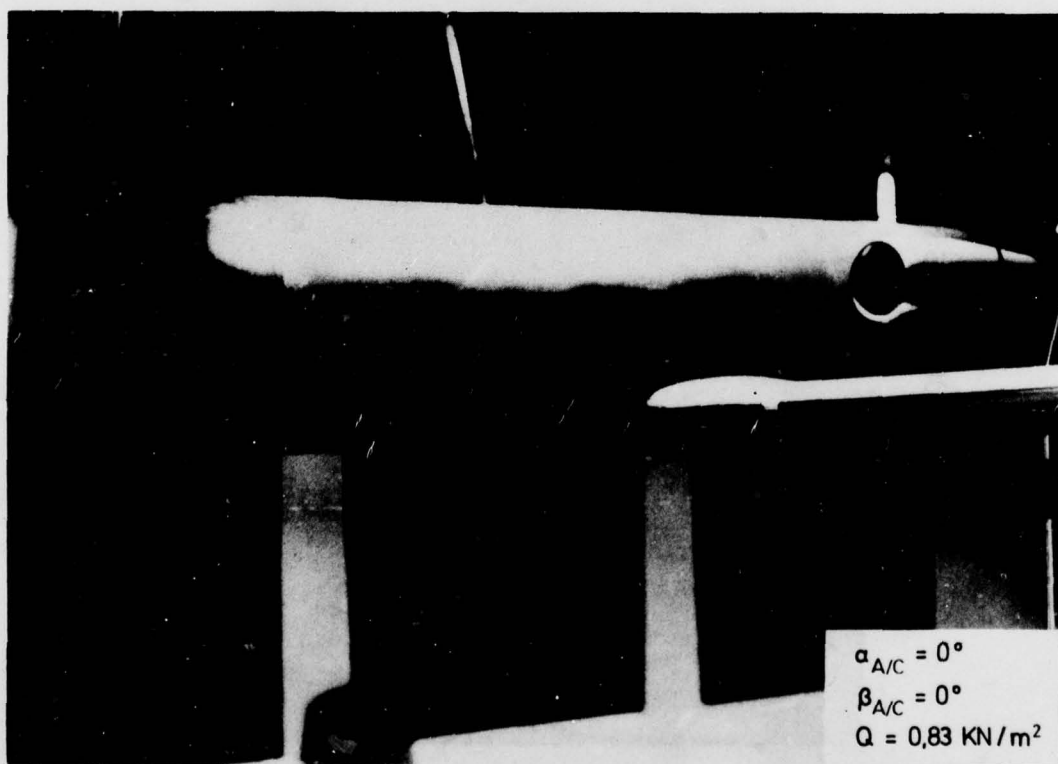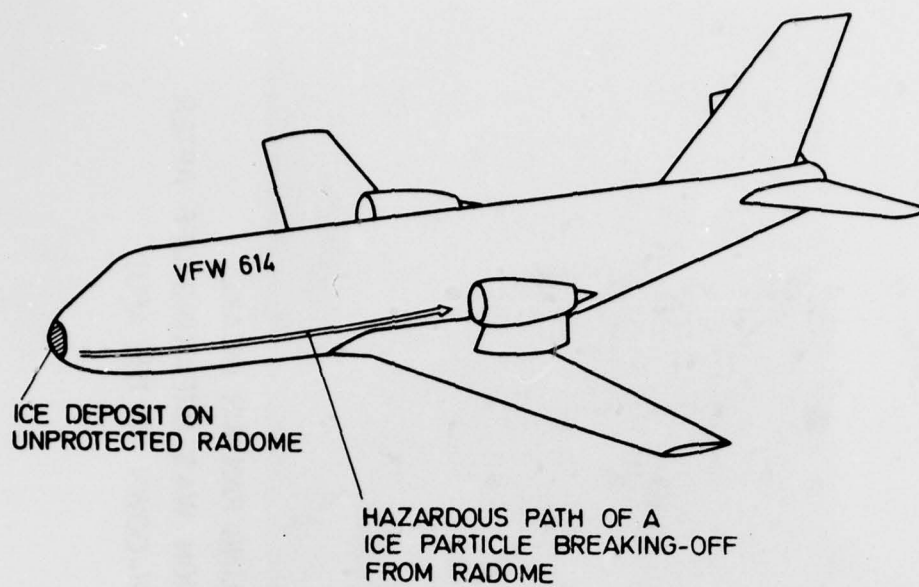Airplane performance penalties associated with icing in terms of landing weight penalties, and when these penalties are assessed, are also discussed. Destination airport temperatures and ice shedding characteristics are shown to be significant in determining the frequency of aerodynamic penalties due to ice.

## NOMENCLATURE

| SYMBOL | UNITS | DESCRIPTION |
|---|---|---|
| $A$ | $Ft^2$ | Ice Cap Cross Sectional Area |
| $C$ | Ft | Airfoil Chord Length |
| $d_m$ | Microns | Drop Diameter |
| $F_m$ | Dimensionless | Total Water Catch Efficiency |
| $I$ | Dimensionless | Cloud Extent Factor |
| $H$ | Feet | Airfoil Projected Height |
| $H_0$ | Feet | Airfoil Projected Height at $0^o$ Angle of Attack |
| $H_\alpha$ | Feet | Airfoil Projected Height at Angle of Attack |
| $I$ | —— | Icing Parameter Defined by Equation 7 |
| $K_0$ | Dimensionless | Modified Inertia Parameter Defined in References 2 and 5 |
| LS | Airfoil | Airfoil Lower Surface |
| ST | —— | Airfoil Stagnation Point |
| $t_0$ | $^o$F | Free Stream Air Temperature |
| US | —— | Airfoil Upper Surface |
| V | Knots | Free Stream Velocity |
| $V_\eta$ | | Air Velocity Perpendicular to the Airfoil Leading Edge |
| $W_\beta$ | $Lb/Hr\text{-}Ft^2$ | Local Water Catch Rate |
| $W_c$ | Lb/Hr-Ft Span | Total Water Catch Rate |
| $\gamma_i$ | $Lb/Ft^3$ | Ice Density |
| $\delta_i$ | Feet | Ice Thickness |
| $\eta$ | —— | Freezing Fraction |
| $\theta$ | Hours or Minutes | Icing Time |
| $\omega$ | Grams/Cubic Meter | Cloud Liquid Water Content |
| $\Lambda$ | Degrees | Airfoil Sweet Angle |
| $\Delta S$ | Feet | Surface Distance Between Upper and Lower Water Drop Impingement Limits |
| $\beta$ | —— | Local Water Collection Efficiency |

## INTRODUCTION

Jet engine aircraft are less susceptible to icing for several reasons. The kinetic temperature rise, due to higher flight speeds, reduces the icing temperature envelope and prevents ice from forming in the higher, liquid water-content clouds occurring just below $32^o$ F. The aerodynamic characteristics of swept airfoils, use of movable horizontal stabilizers from trim, rapid rate of climb and descent of

jet aircraft, all contribute to minimizing exposure to icing conditions and to reducing the effects of ice on airplane performance. In addition, the size of current jet transports and the large power reserve of jet engines reduce the drag effects of airplane icing.

As a result of the greater tolerance to icing of jet aircraft, there arises the question of the need for ice protection on certain areas of the airplane. Inboard wings have not been protected on some piston engine aircraft. Military aircraft such as the B-52 and KC-135 have had tail and wing ice protection systems removed as a result of adverse weather flight test programs.

It is logical, then, to assess the need for airfoil ice protection in terms of airplane handling characteristics and performance. To do this on a consistent basis requires a wind tunnel and flight test program whereby the effects of ice can be simulated since natural icing is not consistent, is difficult and time consuming to obtain, and is subject to shedding before the testing can be completed. This simulation of icing effects has been accomplished on jet transports through the use of artificial ice shapes attached to unheated portions of the wing and tail surfaces. This paper summarizes some of the methods and procedures used to determine these ice shapes and presents a new method of obtaining ice shapes based on recent ice accretion test data correlated with theoretical impingement data.

## ANALYTICAL PREDICTION OF ICE SHAPES

Ice shapes on airfoils are classified as "glaze" or "rime" although many ice shapes will be a mixture of the two. Rime ice is found at combinations of low temperatures and low liquid water contents. The water droplets freeze on impact resulting in a milky-white ice shape, as shown in figure 1, dictated by the airfoil impingement characteristics in terms of water catch, distribution, and impingement limits. The drag and other aerodynamic effects of rime ice are much less severe than glaze ice because of the streamline form, therefore, this type of icing has not been considered in determining the airplane tolerance to icing.



Figure 1—Typical Rime Ice Formation on Swept Airfoil

Glaze ice forms at combinations of high liquid water contents and surface temperatures near freezing. Not all of the water droplets freeze on impact, but some run a short distance before freezing, resulting in a blunt or double horn ice shape as shown in figure 2. This ice is usually clear since there is little or no air entrained in the ice. The upper surface horn acts as a spoiler, increasing drag and reducing lift. This ice shape, because of its "spoiler" action, can affect aerodynamic characteristics in terms of increased drag and decreased maximum lift coefficient. The lower surface horn usually has little effect because of low local air velocities. On highly swept airfoils, glaze ice tends to form as a series of discontinuous cup shapes due to the spanwise velocity component.

The shapes and type of ice is dependent on the surface temperature, which is a complex function of airspeed, liquid water content, ambient air temperature, local flow field around the object, and altitude. A correlation of ice shapes on a small 2-inch diameter unswept cylinder, with these parameters, is shown in figure 3 where $\eta$ is the freezing fraction defined in reference 3 as that part of

the water catch that freezes where it impinges. In general terms, glaze ice is likely to occur at total air temperatures between 25° and 32° F. Between 10° and 25° F, a mixture of rime and glaze ice will occur with glaze predominant in the stagnation area and for high liquid water content conditions.
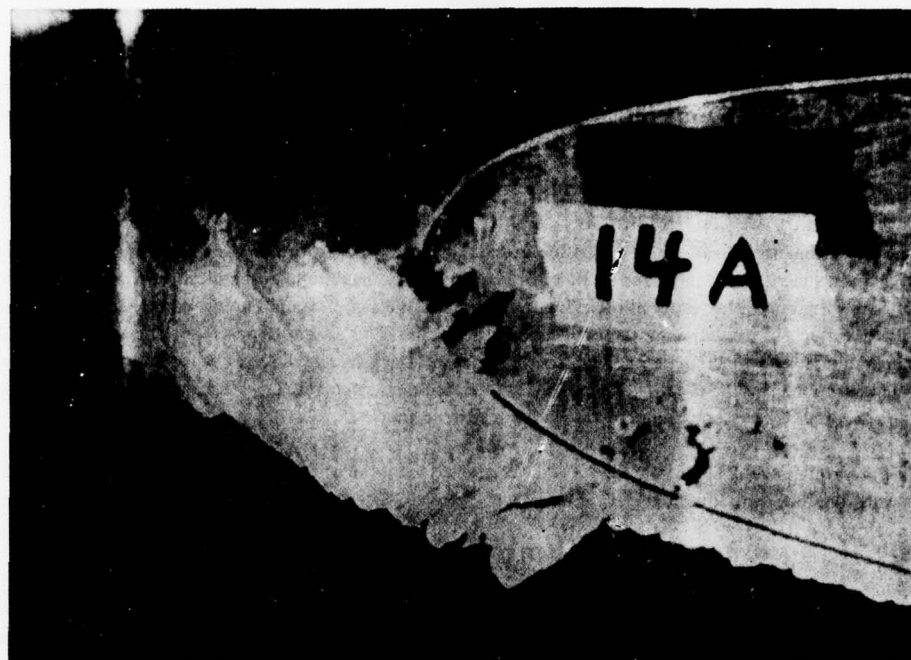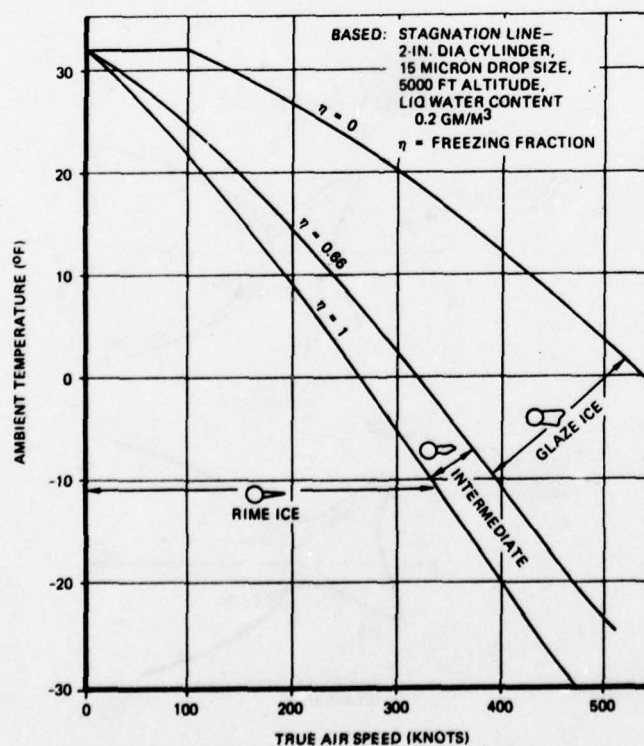


Figure 2—Typical Glaze Ice Shape on Swept Airfoil



Figure 3—Ice Shape Types as a Function of Speed and Ambient Temperature

## CALCULATION PROCEDURES

Procedures previously developed for determining the ice cap size are based on calculating the airfoil water catch and adjusting this water catch or ice thickness into a typical mushroom ice shape. For rime ice, the ice thickness and shape can be calculated directly from the local water catch and ice density since the water freezes immediately on contact with the airfoil. The local ice thickness, $\delta_i$, is related to the local water catch rate, $W_\beta$, by the following equation where $\theta$ is the time in icing and $\gamma_i$ is the ice density.

$$\delta_i = \frac{W_\beta \theta}{\gamma_i} \tag{1}$$

Thus, a theoretical ice shape for rime ice can be estimated by calculating the local water catch rate for various positions in the impingement area. The equation for the local water catch rate is given below where $\beta$ is the local water collection efficiency, V the free stream velocity, $\Lambda$ the airfoil sweep angle and $\omega$ the cloud liquid water content.

$$W_\beta = 0.38\beta \, (V)(COS \, \Lambda) \, (\omega) \tag{2}$$

This procedure, with some modifications, was used for calculating the ice shapes for the Boeing 707 and 727 series airplanes. To account for glaze icing and the effects of ice shape on water impingement, the maximum local collection efficiency, $\beta$ max, was assumed to be 1.0. This means all of the water in the cloud in the path of the airfoil would impinge on the airfoil. This assumption was made to account for the effects of ice shape on water collection efficiencies. This assumption is approximately correct for small airfoils where the maximum local collection efficiency is near 0.8, but becomes overly conservative for larger inboard wings and stabilizers where the collection efficiencies are less than 0.5. The ice thickness calculated using $\beta$ max equal to 1.0 was then adjusted to give a typical mushroom or glaze ice shape using the known impingement limits.

In other procedures, references 2 and 6, the ice shape is determined from the calculated total water catch rate ($W_c$) from bare airfoil impingement data using the following equation:

$$W_c = 0.38 \, V \, (COS \, \Lambda) \, E_m \, (H/C) \, (C) \, \omega \tag{3}$$

In this equation, $E_m$ is the total water collection efficiency based on the airfoil projected height (H), and (C) is the airfoil chord length. This water catch rate is in terms of pounds of ice per hour per foot of span. The cross sectional area of the ice cap is then determined from:

$$A = \frac{144 \, W_c \, \theta}{\gamma_i} \tag{4}$$

A double-peaked glaze ice shape, as shown in figure 4 which contains the calculated theoretical cross sectional area, is then drawn by trial and error.
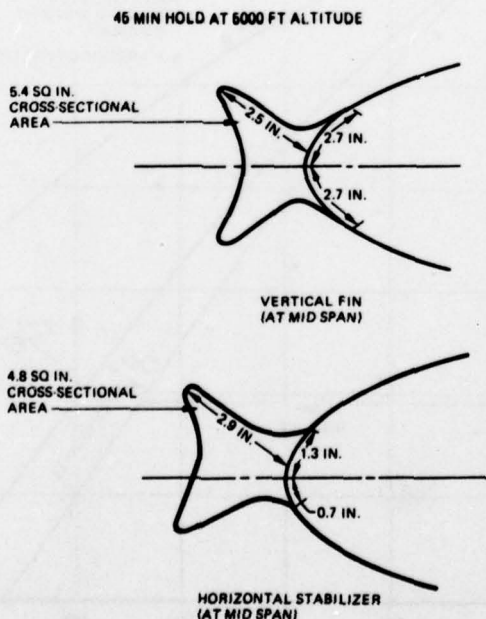


Figure 4—Typical Ice Shapes for Unprotected Tail Surfaces from Ref 2

The above calculation procedures only approximate the actual ice shape since accurate ice accretion data for most airfoils is not available. Also, water drop sizes and resultant collection efficiencies must be checked for the maximum water catch. Figure 5 shows a typical plot of the effect of drop size on collection efficiency and cloud liquid water content. This calculation will generally show that the maximum catch rate will occur with 20 to 25 micron droplets.
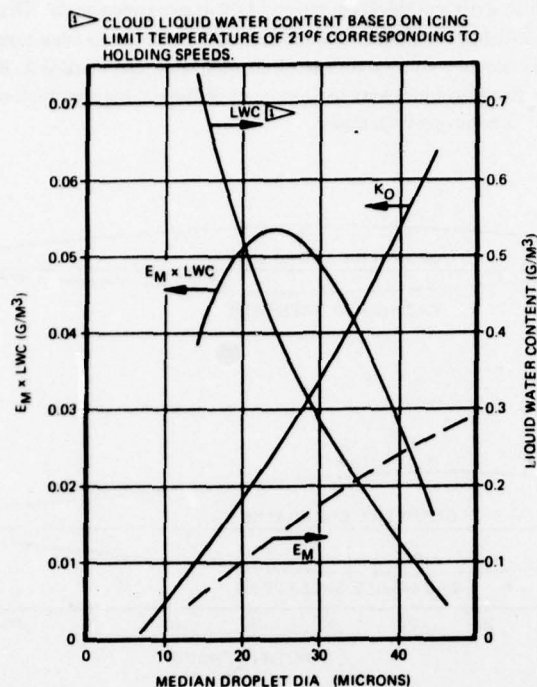


Figure 5—Effect of Drop Size on Water Catch Parameters Holding Flight Speeds

## EXPERIMENTAL DETERMINATION OF ICE SHAPES—NACA ICE SHAPE DATA

A correlation of measured ice shapes from icing tunnel tests with theoretical impingement parameters has been reported in reference 4 (NACA TN 4151) for an unswept symmetrical 4 percent thick airfoil. The data in this report for mushroom ice, plotted in a slightly different manner, is shown in figure 6. It indicates the measured maximum ice height is less than the theoretical height based on the maximum local water catch. This is not surprising since all of the impinging water does not freeze at the point of maximum collection efficiency under these icing conditions. Unfortunately, there are no similar published data for highly cambered swept airfoils. Therefore Boeing initiated a research program to obtain basic ice accretion data on two airfoils representative of the inboard wing and horizontal stabilizer configuration of typical current jet transport aircraft. This program was conducted in the NASA 6-foot by 9-foot icing tunnel at Cleveland, Ohio.
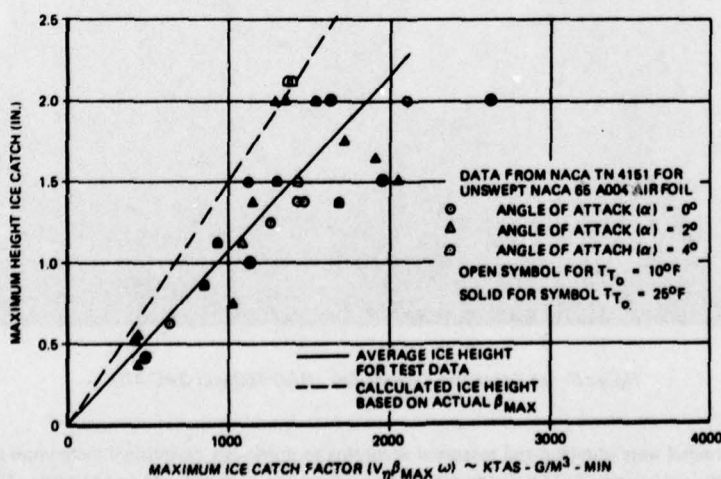


Figure 6—Correlation of Ice Height with Theoretical Impingement Unswept 4% Thick Airfoil

## BOEING ICE ACCRETION TEST SETUP AND PROCEDURE

The models used in this test program were chosen to represent the type of airfoils used on present-day Boeing commercial jet aircraft. Cross sections of these airfoils are shown in figure 7. One model, designated BAC 450, was typical of an inboard wing section with a 12.5 percent thickness ratio and 27.5 degree sweep angle. The other model, designated BAC 470, represented outboard wing and horizontal stabilizer sections with an 8 percent thickness ratio and 40 degree sweep angle. These models, shown in figure 8, have a 6-foot streamwise span and chord length and were mounted vertically in the Lewis icing tunnel at Cleveland, Ohio. Each model was fabricated from aluminum with six thermocouples and three electrical heater pads marked A, B, and C in figure 8, bonded to the inner surface of the leading edge. The thermocouples were used to monitor the leading edge surface temperature during the icing runs and the heater pads were used to assist in removing ice samples.
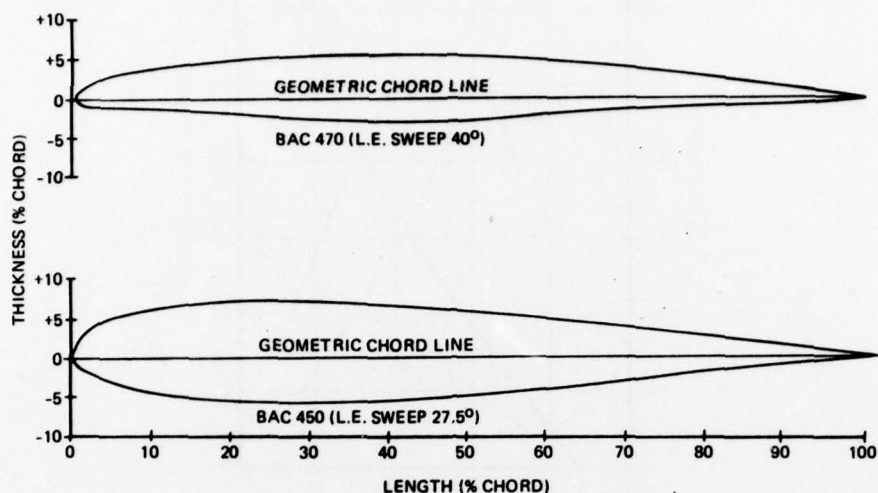


Figure 7—Airfoil Cross Section Streamwise Direction
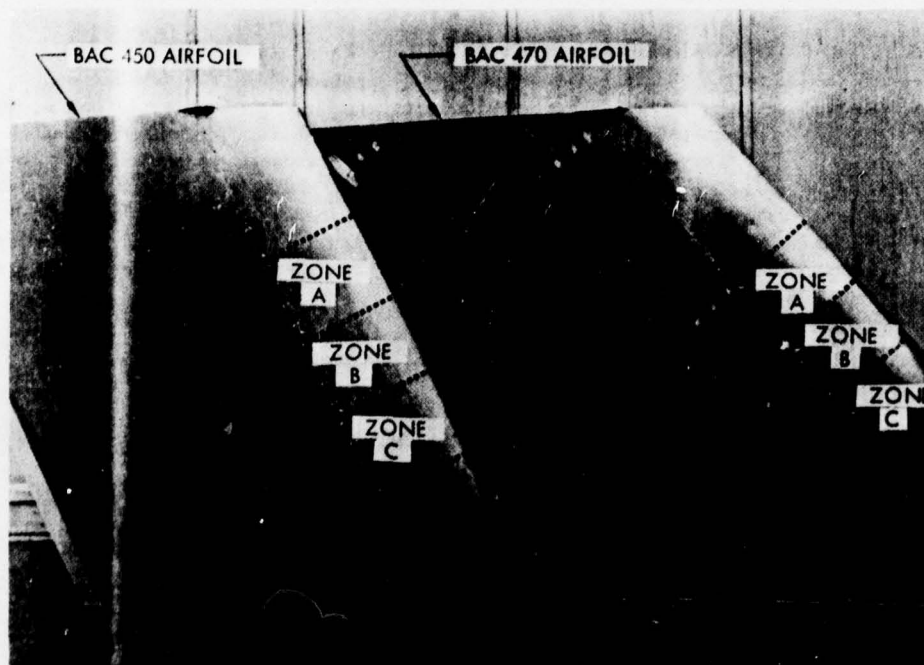


Figure 8—Ice Accretion Test Models   BAC 450 and BAC 470

Icing conditions in the tunnel were obtained and measured according to previously established techniques and calibrations. Icing cloud factors considered in this study were cloud liquid water content, icing time, airspeed, and temperature. Cloud droplet size could not be varied independently due to the limitations in the design of the tunnel spray system. As a result, the cloud droplet sizes increased with increased liquid water content and decreased with an increase in airspeed.

An icing run consisted of a 7.5 or 15 minute exposure of the model to a particular set of icing conditions and airfoil angle of attack. On completion of the prescribed icing time, the tunnel was stopped and measurements taken of the final ice shape. One or more sections of the ice cap, approximately 6 inches in length, were removed using the heater pads and the ice scraper used in reference 4 tests. This scraper is steam heated and has an internal vacuum chamber to assist in drawing off the melted ice so as not to affect the sample weight or shape. The removed sections were then dipped repeatedly in liquid paraffin to create a mold of the ice shape. When the ice in the mold melted, it was poured into a beaker and weighed. The resultant cavity was then refilled with tap water which was then poured into the beaker and weighed to determine the specific gravity of the ice. Representative values of the specific gravity of the ice cap measured in this manner were from 0.75 to 0.91.

A replica of the ice sample was then made by pouring plaster of paris into the mold and later melting the wax in an oven. Photographs of the equipment used to obtain plaster casts of the ice cap are shown in figures 9 and 10. Sample plaster ice cap photographs are shown in figures 11 and 12.



Figure 9—Test Equipment for Weighing and Obtaining Ice Shape Molds
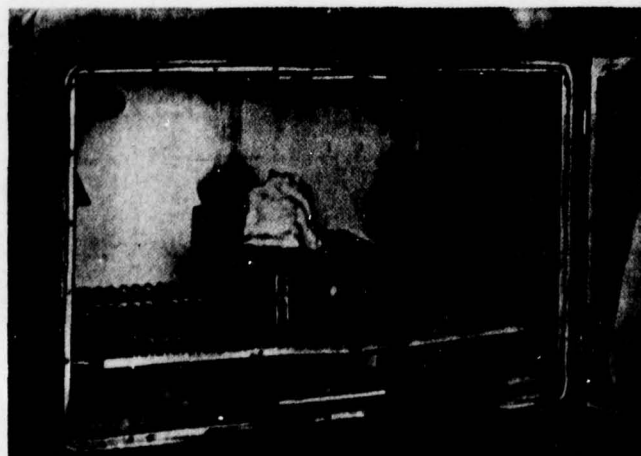


Figure 10—Melting Paraffin From Plaster Ice Cast

5-8



Figure 11—Coating Ice Cap With Melted Paraffin



Figure 12—Sample Plaster Ice Cast

After the ice sample was removed from the mold, the cross section of the ice cap was photographed against a one-quarter inch wire mesh grid held normal to the airfoil leading edge. A typical ice cap cross section is shown in figure 13. Due to the difficulty in discerning the cross sectional outline from the photographs, all ice cap measurements were made from the plaster casts as defined in figure 14.
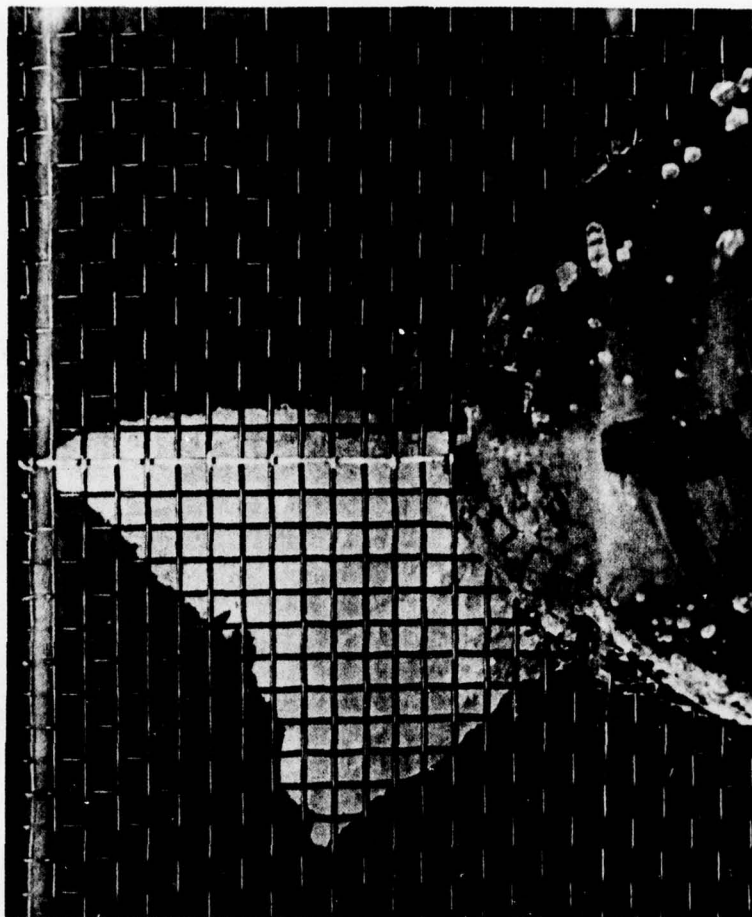
*Figure 13—Installation of Wire Grid Over the Ice Cap*
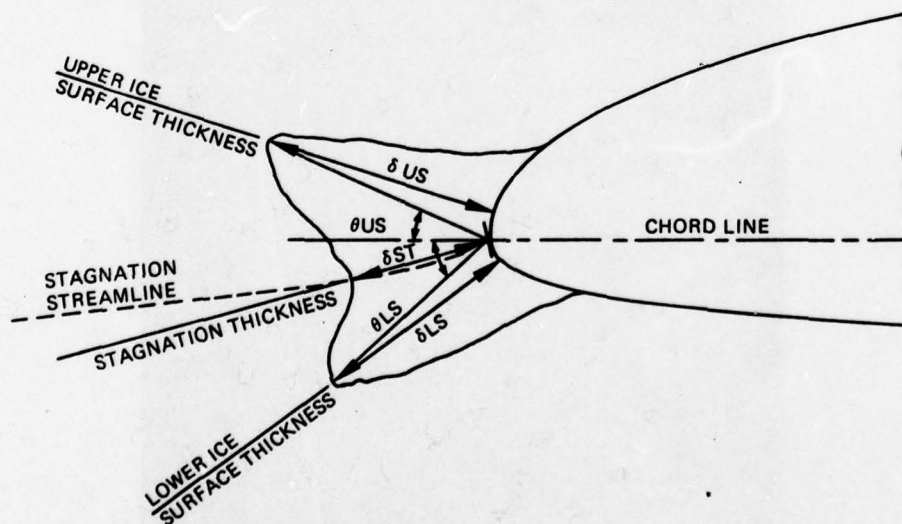


*Figure 14—Ice Shape Dimensions*

The majority of the ice samples were of the glaze type with typical double horn protuberances. A few rime ice samples were obtained and the remainder were mixtures of the two. Figure 15 shows representative ice shapes obtained during this test program. The effect of the wing sweepback was most noticeable in the discontinuous cup shapes formed in the spanwise direction as shown in figures 16 and 17.

6A74214-8

Figure 15—Plaster Ice Cap Replicas



Figure 16—Glaze Ice Shape BAC 470 Airfoil Side View
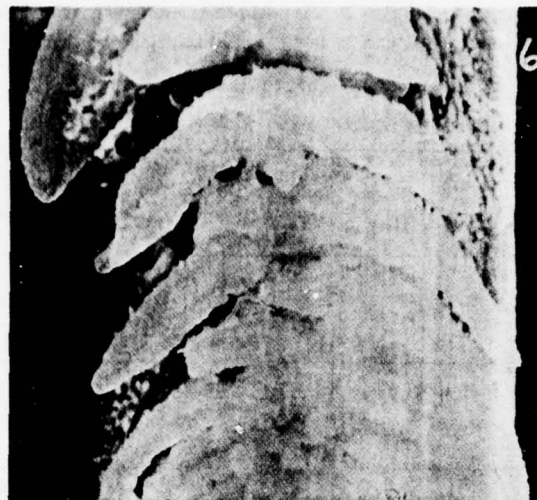
*Figure 17—Glaze Ice Shape BAC 470 Airfoil Frontal View*

The separations were most prominent in the glaze ice formations and became larger as the ice thickness increased. In those samples which tended toward rime ice, the distance between individual cups decreased and in some cases formed a continuous solid ice cap along the span of the airfoil.

The leading edge temperatures for the glaze icing runs varied between 25° and 29° F. Due to the relatively high thermal conductivity of the aluminum leading edge (typical of current aircraft configurations) the chordwise temperature gradient under the ice cap was negligible. Had the leading edge been made of an insulating material, the ice cap could have had a significantly different shape since the impinging water would see a warmer stagnation point surface temperature. This would allow the water to flow further along the surface before freezing. No attempt was made in this study to determine the magnitude of this effect of leading edge material properties on ice shape.

## TEST AIRFOIL IMPINGEMENT CHARACTERISTICS

The theoretical impingement characteristics in terms of water drop collection efficiency and impingement limits are shown in figure 18 for the two angles of attack considered in this study. These data were obtained from a water droplet trajectory computer program and are plotted as a function of a modified inertia parameter $K_O$. This parameter, described and defined in references 2 and 5, allows the impingement data taken for one flight condition to be used for other flight conditions.
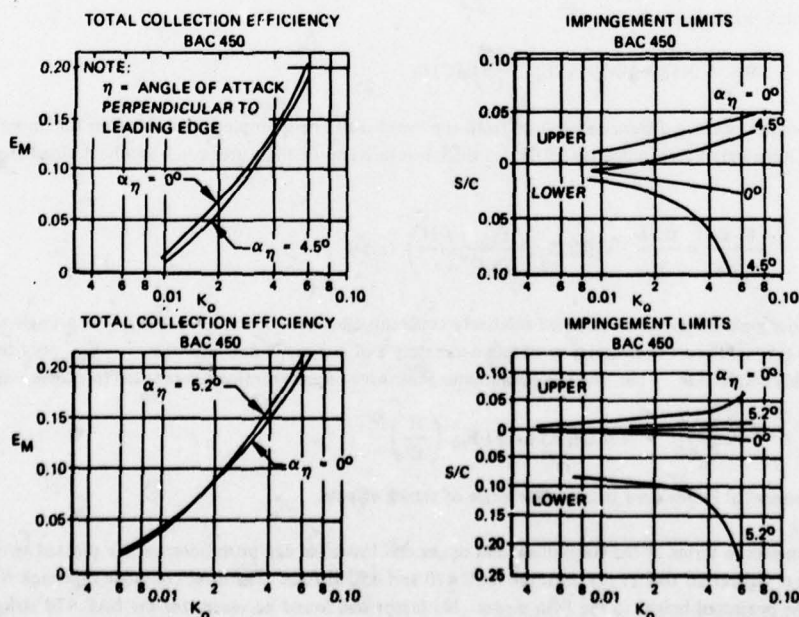


*Figure 18—Test Airfoil Impingement Characteristics*

The projected height of the airfoil as shown in figure 19 was used in this study as the characteristic dimension for overall water drop collection efficiency and in the ice shape correlation parameters. This is in line with the impingement data as presented in reference 2.
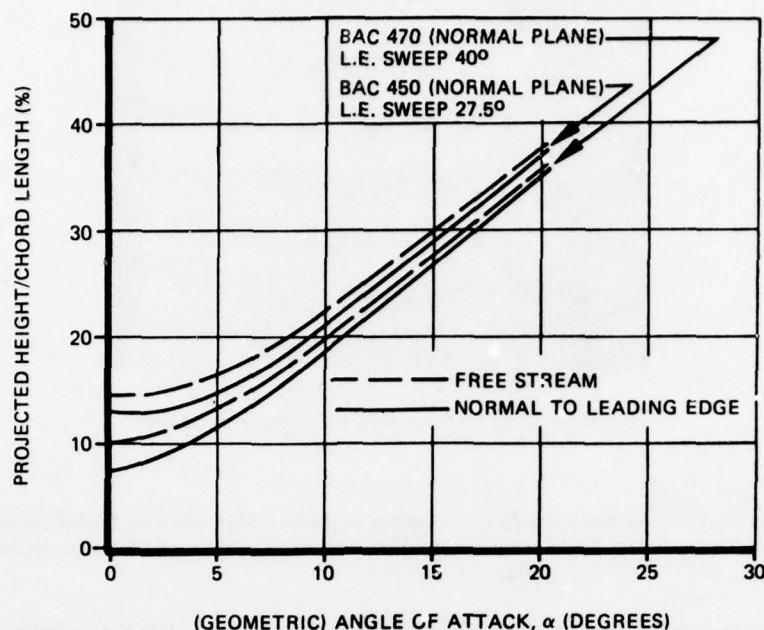


*Figure 19—Airfoil Projected Height BAC 450 and 470*

## ICE SHAPE CORRELATION

Correlation of the measured ice cap dimensions was based on the water catch parameters which are indicative of the ice thickness. Under conditions of glaze icing, the ice thickness is more a function of total water catch or

$$\delta_i = f\left(\frac{W_c \theta}{\gamma_i \Delta S}\right) \tag{5}$$

where the total water catch is calculated from:

$$W_c = 0.38 \, V \, (\cos \Lambda) \, E_m \left(\frac{H}{C}\right) (C) \, \omega \tag{6}$$

And $\Delta S$ is the chordwise surface distance measured from the lower water drop impingement limit to the upper water drop impingement limit. An icing parameter indicative of the ice thickness in terms of the water catch can be defined from the relationship in equation (5) as:

$$\frac{W_c \theta}{\gamma_i \Delta S} = \frac{0.38}{\gamma_i} \, V \, (\cos \Lambda) \frac{E_m}{\Delta S/C} \left(\frac{H}{C}\right) (\omega) \, \theta \tag{7}$$

The ice density under glaze icing can be assumed relatively constant, and further, the term $\frac{E_m/\Delta S}{C}$ is a single valued function for a given $K_O$ value. Since $\Delta S$ is difficult to measure or obtain accurately and is a particular value for $E_m$, only the total collection efficiency was used in this correlation. Thus, the icing parameter indicative of a theroetical average ice thickness reduces to:

$$I = \frac{W_c \theta}{\gamma_i \Delta S} = V \, (\cos \Lambda) \, \omega \, (\theta) \, E_m \left(\frac{H}{C}\right)^X \tag{8}$$

Where X is the exponential factor used to correlate angle of attack effects.

Measured ice thicknesses in terms of the stagnation, and upper and lower ice cap protuberances are plotted against the icing parameter defined by equation (8) in figures 20 and 21 for both the BAC 470 and 450 airfoils. The effect of angle of attack was resolved for the BAC 450 airfoils by raising the projected height to the fifth power. No factor was found necessary for the BAC 470 airfoil since the projected height to chord ratio (H/C) provided sufficient angle of attack correction. These factors are emperical for the range of the test data or from 0 to 4.5 degrees. However, some extrapolation beyond these limits is felt to be valid and within the accuracy of the test data.
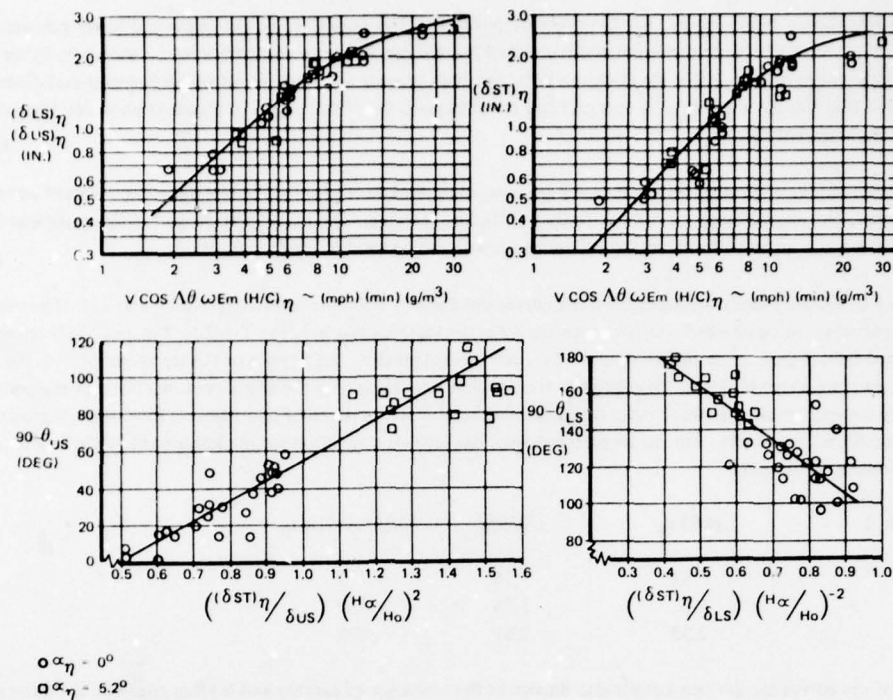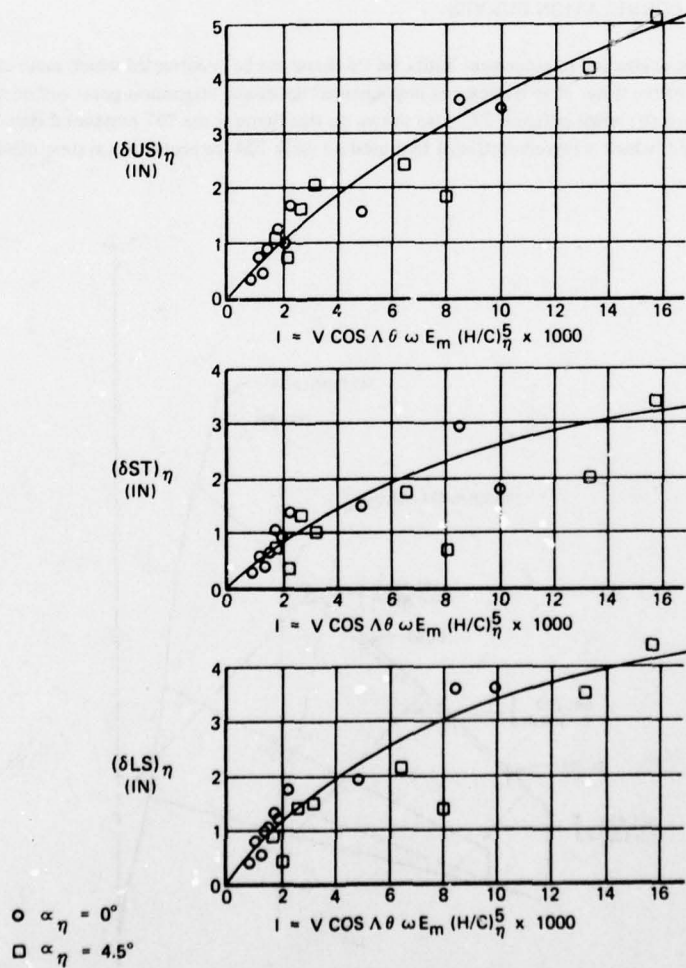
These curves define the ice thickness, but not their relative positions. The angles, which the upper and lower pinnacle dimensions made with the geometric chord line, were measured and correlated in a similar manner. This correlation is shown in figure 20 for the 470 airfoil. These data were not as orderly as the ice thickness data, but they provide a definite trend which is useful in defining the ice shapes. It is not recommended that this ice angle data be extrapolated much beyond the airfoil angles of attack from which the data was obtained without correlating impingement data.

The frontal heights obtained through these ice angles are maximum dimensions since the test data was obtained at or near maximum icing temperatures where the impinging water can run farther aft before freezing. The range of flight and icing conditions during holding or approach are within the test icing conditions, so these dimensions will also be valid for flight conditions.

Some significant trends are readily apparent from the curves obtained by this correlation (figures 20 and 21). The most significant of these is the distinct reduction in slope which occurs once the ice attains a thickness between 1-1/2 to 2 inches. This change in the slope is indicative of a reduced rate of growth for the ice shapes. This can be explained by the physics of the ice accretion. As the ice pinnacles associated with the glaze ice shape builds to these heights, the droplets impinging near the stagnation area become trapped and, assisted by the spanwise velocity component of the swept wing, freeze within the pinnacles instead of contributing to additional growth pinnacles. This is apparent in the more blunt ice shapes. For the larger ice shapes, the ratio of stagnation ice thickness to pinnacle heights approaches unity as shown by the following tabulation:

| Icing Parameter, I | $(\delta ST)_\eta$ | $(\delta US)_\eta$ | $(\delta ST)_\eta/(\delta US)_\eta$ |
|---|---|---|---|
| 3 | .54 | .76 | .710 |
| 8 | 1.5 | 1.75 | .857 |
| 20 | 2.33 | 2.61 | .893 |

A comparison of the curves for the two airfoils also illustrates the influence of camber and leading edge radius on the maximum ice thickness. The BAC 450 airfoil, being blunter, has a larger actual ice accretion area. This resulted in a larger ice cap both in thickness and area over the less blunt, highly cambered BAC 470 airfoil.

## APPLICATION OF ICE SHAPE CORRELATION CURVES

Knowing the ice thicknesses, angles and impingement limits, an ice shape can be constructed which more closely duplicates icing of swept wing aircraft. Knowledge of the water drop trajectories impingement limits and stagnation point will be illustrated for the 747 horizontal stabilizer (BAC 470 airfoil) shown in figure 22. Also shown on this figure is the 707 horizontal stabilizer. The following flight design condition will be used, which is representative of that used on early 707 ice protection system deletion studies:

Figure 22—Comparison of 747 and 707 Horizontal Stabilizer Sizes

**FLIGHT**

$\theta$ = 30 minute hold
ALT = 15,000 feet altitude
V = 377 mph True Airspeed (256 knots indicated airspeed)

**ICING CONDITIONS (FAR PART 25, APPENDIX C)**

$t_o$ = 21°F Icing Limit temperature (ambient air temperature)
$d_m$ = 15 Micron drop diameter ("A" drop distribution)
F = 150 Mile cloud
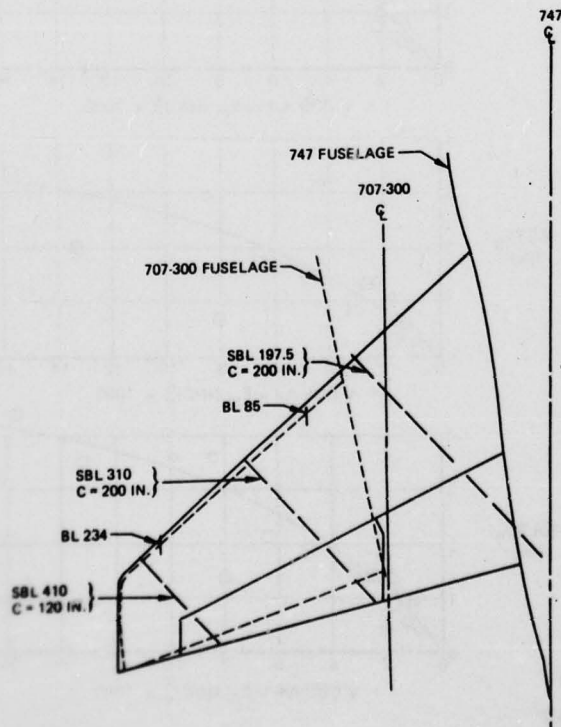$\omega$ = 0.266 g/m³ cloud water content (150 mile cloud)

**AIRFOIL AND IMPINGEMENT DATA**

| Stab. Sta. | Angle of Attack | Sweep Angle | Chord Length | $K_o$ (BAC 470) | (H/C)* (Fig. 19) | (H/C) (Fig. 19) | $E_m$ (Fig. 19) |
|---|---|---|---|---|---|---|---|
| 197.5 | -2.38° | 43° | 280 in. | .005 | .087 | .095 | .020 |
| 410 | -2.38° | 43° | 280 in. | .0109 | .087 | .095 | .051 |

*Projected height for 0 degree angle of attack.

Knowing the impingement and flight conditions, the icing parameter, I, can now be calculated for the horizontal stabilizer station SBL 410 as:

$$I \qquad V (\cos \Lambda) (\theta) (\omega) (E_m) \frac{H}{C}$$

$$= \quad 377 (\cos 43°) (30) (0.266) (.051) (.095)$$

$$I \quad = \quad 10.66$$

From figure 20, the ice pinnacle heights are:

| Stab. Sta. | Icing Par | Ice Thickness (Normal to L.E.) | | | Ice Thickness Streamwise | | |
|---|---|---|---|---|---|---|---|
| | | Upper $(\delta US)_\eta$ | Stag. $(\delta ST)_\eta$ | Lower $(\delta LS)_\eta$ | Upper $(\delta US)_s$ | Stag. $(\delta ST)_s$ | Lower $(\delta LS)_s$ |
| 197.5 | 4.1 | 1.0 | .75 | .99 | 1.37 | 1.025 | 1.36 |
| 410. | 10.66 | 2.03 | 1.84 | 2.10 | 2.78 | 2.52 | 2.78 |

The ice angles can now be calculated from the ratio of ice thicknesses and figure 20.

| Stab. Sta. | Projected Ht. Ratio | Ice Thickness Ratio | | Upper Ice Angle Par. | Upper (1) Ice Angle (Fig. 20) | Lower Ice Angle Par. | Lower (2) Ice Angle (Fig. 20) |
|---|---|---|---|---|---|---|---|
| | $H_\alpha/H_o$ | $\left(\frac{\delta ST}{\delta US}\right)_\eta$ | $\left(\frac{\delta ST}{\delta LS}\right)_\eta$ | $\left(\frac{\delta ST}{\delta US}\right)_\eta \left(\frac{H_\alpha}{H_o}\right)^2$ | | $\left(\frac{\delta ST}{\delta LS}\right)_\eta \left(\frac{H_\alpha}{H_c}\right)^2$ | |
| 197.5 | 1.09 | .75 | .76 | .89 | 46° | .63 | -44° |
| 410 | 1.09 | .908 | .878 | 1.08 | 26° | .74 | -38.5° |

(1) Measured clockwise from geometric chord
(2) Measured counterclockwise from geometric chord.

From the above ice angles and pinnacle heights, the resultant ice shape is drawn as shown in figure 23. The corresponding nominal 3 inch 707 ice shape is also shown for reference based on the previous method whereby all of the impinging water was assumed to collect on the airfoil. Reasonably good agreement between the two methods is shown at the tip.

However, due to the lower collection efficiency at the inboard end of the stabilizer, the latest calculation procedure gives a much smaller ice thickness. This is in line with observations on natural icing flight tests. The difference in the location of the ice caps is due to the higher angle of attack of the less cambered 707 airfoil. This angle of attack is determined from airplane trim requirements.

The method of determining ice shapes developed from the Cleveland test data is applicable to any airfoil. Extrapolation from this data will generally be satisfactory if the airfoils are similar. Consideration should be given to obtaining ice accretion data if the airfoil is considerably different than that tested here, or the surface is considered particularly critical from a flight safety or performance standpoint.

No attempt was made in this test program to obtain ice shapes for extended leading edge devices such as flaps or slats since these are normally retracted during icing conditions. Ice shapes on extended leading edge devices, if required, can be and have been determined from estimated water collection rates.
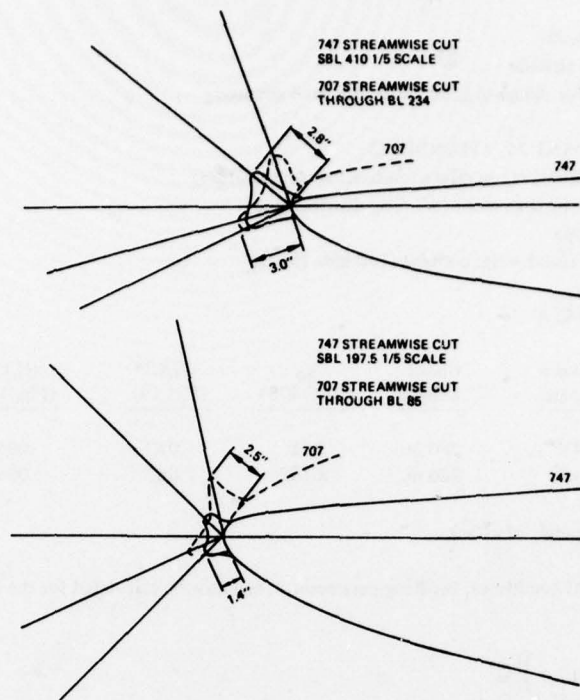
Figure 23—747/707 Horizontal Stabilizer Ice Shapes

## SOME COMMENTS ON FLIGHT TESTING WITH SIMULATED ICE SHAPES

### WIND TUNNEL TESTING

A preliminary evaluation of the effects of ice on airplane performance and stability is usually obtained from wind tunnel testing with ice shapes attached to the unheated airfoil sections. Wind tunnel test results showing the effect on the lift coefficient and pitching moment curves of a typical Boeing jet transport are shown in figure 24. At angles of attack associated with level flight, the ice has little effect other than to increase drag. This effect on airplane drag, with flaps extended, is shown in figure 25. As indicated in this figure, the drag increase due to ice, increases sharply with landing flap settings. It is under these conditions where ice has the most effect on airplane performance.
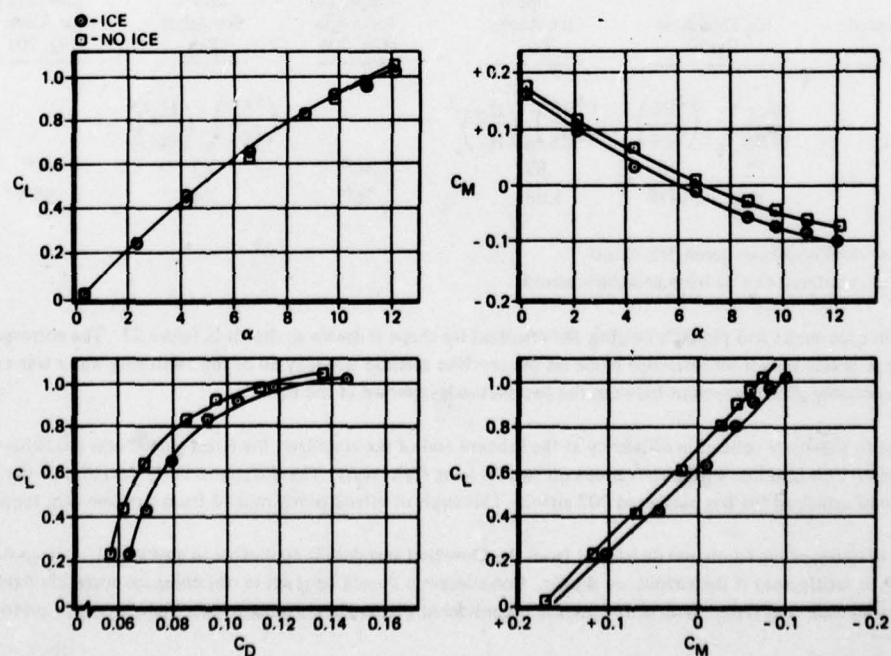


Figure 24—Effect of Ice on Lift Drag and Pitching Moment for a Typical
Jet Transport From Wind Tunnel Data (Flaps Up)
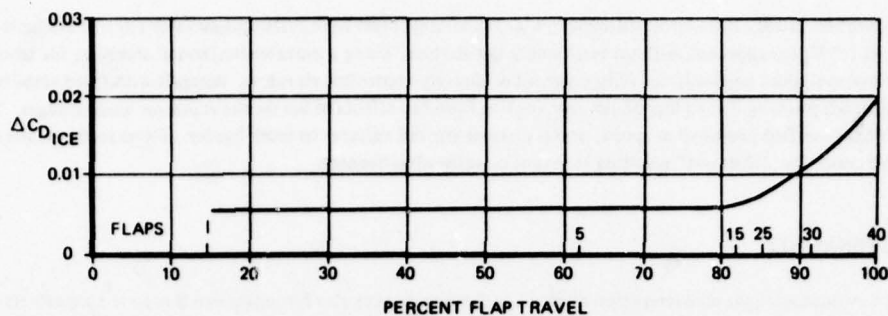
Figure 25—Effect of Ice on Drag for a Typical Jet Transport (Flaps Extended)

## FLIGHT TESTING

The final check of the airplane tolerance to icing is usually obtained through flight testing with simulated ice shapes unless previous data is available or sufficient to determine aerodynamic characteristics or penalties. These simulated ice shapes are made up from a styrofoam core attached to a fiberglass glove which fastens over the airfoil leading edge. Epabond or body putty is applied over the styrofoam ice shape to give a rough outside texture. A typical ice shape used on the 727 horizontal stabilizer is shown in figure 26. Exact simulation of the cup-like protrusions, shown in figure 17, is not considered necessary since the horn or ice pinnacle acts as the spoiler which results in airflow separation. In some conditions, the cup-like protrusions could act like vortex generators and promote reattachment of the airflow to the airfoil. Therefore, only the external ice shape is duplicated, including the sharpness of the ice pinnacles.

The flight test evaluation by FAA pilots includes basic airplane performance data as well as flight characteristics for the following at the most critical center of gravity:

1.  Demonstration of stalls, sideslip, heading changes under engine-out conditions and windup turns.

2.  Demonstration of elevator effectiveness through pushovers starting at 1.4 $V_s$ to flap placard speeds and down to 1.1 $V_s$.

3.  Demonstration of high speed handling characteristics including lateral control evaluation, pushovers, and pullups.

4.  Flap retraction and extension during simulated go-around.

5.  Demonstration of approach and cruise stability through trimming the airplane and stabilizing on airspeed through elevator only.
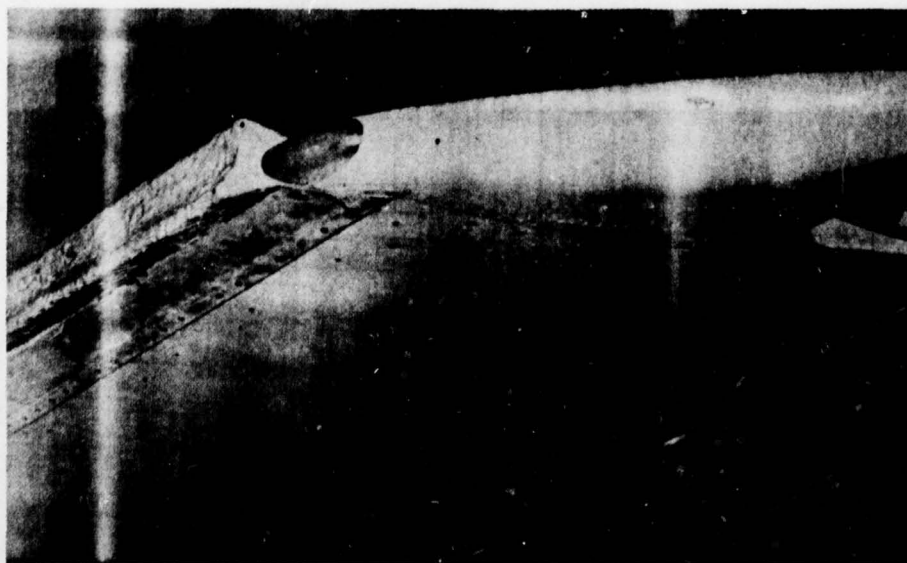


Figure 26—727 Artificial Ice Shape For Horizontal Stabilizer

This latter condition usually is the most difficult in that the aircraft must have sufficient elevator control available to attain speeds between 1.1 $V_s$ and 1.7 $V_s$ for approach without retrimming the aircraft. Using a movable horizontal stabilizer for trim usually means more elevator control available, especially for fully powered or directly controlled elevators. Aircraft with fixed stabilizers have experienced severe nose down pitching due to loss of elevator control from the effects of ice on the stabilizer leading edges. This is usually associated with a change in flap positions or speed, which requires the tail surfaces to work harder. These surfaces, already being at a high lift coefficient condition, "stall out" resulting in loss of elevator effectiveness.

## PERFORMANCE PENALTIES

In addition to evaluating flight characteristics, airplane performance must also be considered due to the ice effects on drag. Figure 27 shows a typical drag polar obtained from flight tests on a Boeing jet transport. These data, along with wind tunnel test data, are used to evaluate the flaps-down approach and landing climb performance as required for use in the flight manual. Figure 28 shows the effect of ice in terms of climb gradient and aircraft gross weight. The increment between the ice-on and ice-off curves must be subtracted from the aircraft maximum allowable landing weight. On short-haul aircraft, where the maximum landing weight is near the takeoff weight, this weight decrease can come out of the payload. This performance penalty has been assessed any time icing conditions en route are anticipated, and the destination airport temperature is below the temperature at which the ice will shed.
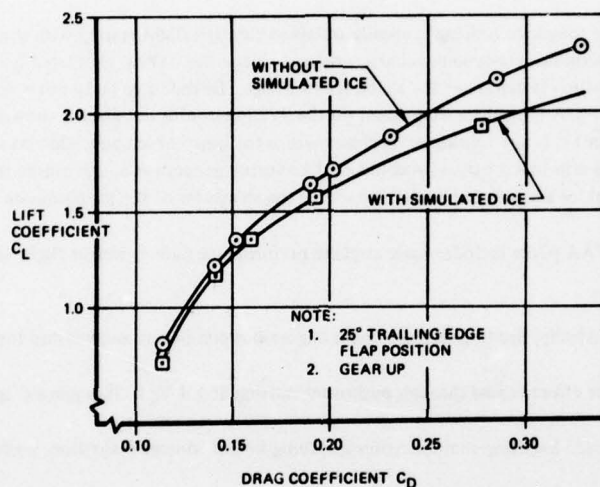


Figure 27—Effect of Ice on Low Speed Drag Polars—25° Flaps—All Engines Operating
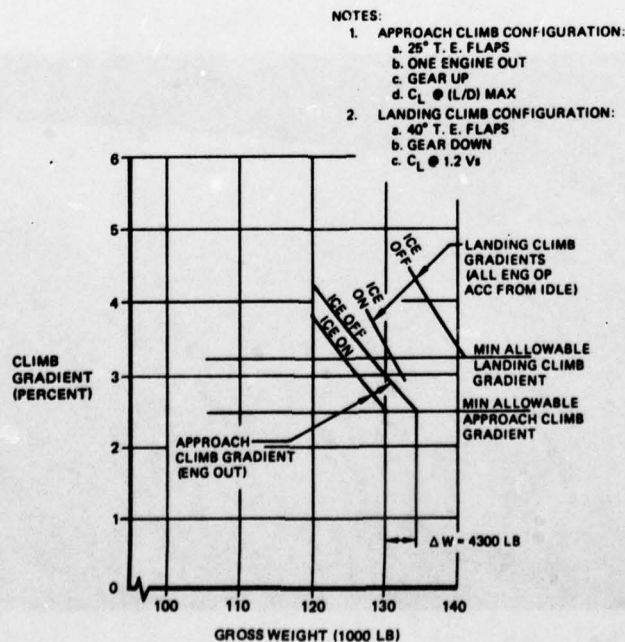


Figure 28 - Effect of Ice on Approach and Landing Climb Gradient-7000 Ft Altitude°

## ICE SHEDDING

Ice shedding characteristics can also be of interest in determining the need for airfoil ice protection since they determine the frequency of application of the airplane performance penalty. This penalty, in terms of the airplane maximum landing weight, is presented in the performance section of the FAA flight manual in terms of destination ambient air temperature. To determine this maximum allowable air temperature requires a knowledge of the airplane descent flight conditions, the resultant airfoil surface temperature under the ice cap and the surface temperature at which the ice sheds.

Typical jet transport time-temperature surface temperature relationships for a descent flight profile are illustrated in figure 29. As the airplane starts the descent phase from cruise conditions, the ambient air temperature starts to increase due to the temperature-altitude lapse rate as shown by the lower line in figure 29. The total temperature, upper line, follows directly as a function of velocity. The surface temperature starts to follow the air temperatures but lags due to the thermal inertia of the ice and airplane leading edge. At some point in the descent, the frictional heating (ram temperature rise) is sufficient to melt the ice-metal bond and the ice sheds. During this time, the surface temperature either remains constant or climbs slowly, due to the latent heat of fusion being supplied to the ice-metal interface. After shedding, there is an abrupt rise in surface temperature as insulation due to the ice is lost and the airfoil is heated by aerodynamic heating effects.
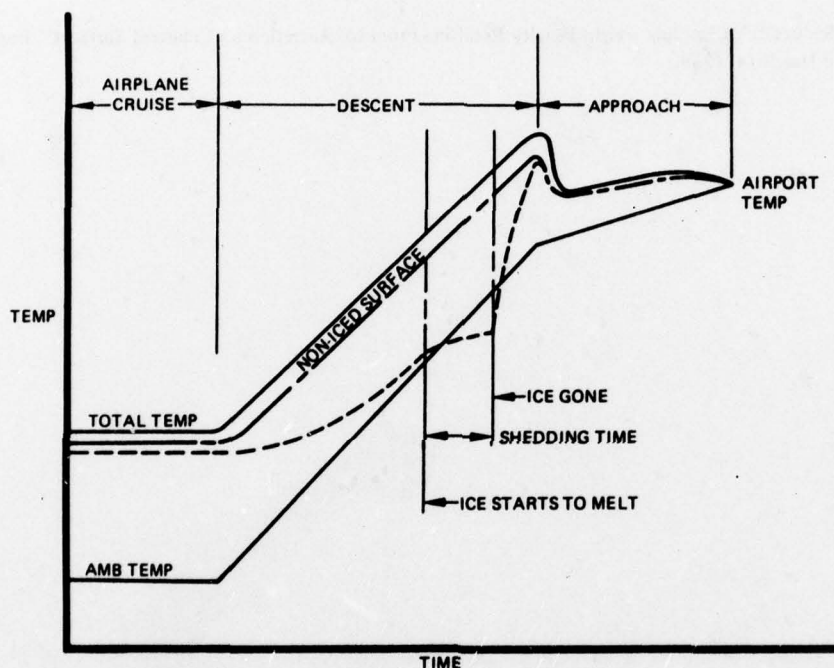


Figure 29—Typical Time-Temperature Profile During Descent

The airfoil surface temperature under the ice cap must be known in order to determine the time at which the ice will shed during a descent. This temperature differs from the total of recovery temperature during descent because of the ice cap thermal capacitance (thermal lag). A method of predicting the time the ice will shed has been developed by Boeing, using laboratory test data in conjunction with a heat transfer analysis. This method, reference 2, has been verified using data from a 737 natural icing flight test.

## CONCLUSIONS

The determination of the need for airfoil ice protection requires the establishment of the effects of large ice accretions on airplane performance. The ice accretion test program conducted by Boeing provides a basis for accurately determining the size and shape of these ice accretions. This has been accomplished by correlating the measured ice cap dimensions with theoretical impingement parameters. Use of this correlation will enable the calculation of artificial ice shapes representative of those which would accrete on the airplane during a severe icing encounter.

**REFERENCES**

1. Airworthiness Standards Transport Category Federal Aviation Regulations, Part 25.

2. Bowden, D. T., Gensemer, A. G., and Sheen, C. A.; Engineering Summary of Airframe Icing Technical Data, FAA Technical Data, FAA Technical Report ADS-4, dated December 1963.

3. Messinger, B. L., "Equilibrium Temperature of an Unheated Surface as a Function of Airspeed", Journal of Aeronautical Sciences, January 1953 (Volume 20, Number 1).

4. Gray, V. H.; "Correlations Among Ice Measurements, Impingement Rates, Icing Conditions and Drag Coefficients for Unswept NACA 65A004 Airfoil", NACA TN 4151, dated February 1958.

5. Sherman, P., Klein, J. S., and Tribus, M.; "Determination of Drop Trajectories by Means of an Extension of Stokes Law", University of Michigan, Engineering Research Institute, Contract AF18(600)-S1, 1952.

6. Stoffel, G. J., "Determination of the Necessity of Tail Ice Protection on Commercial Jetliners", Proceedings of the Fifth Annual National Conference on Environmental Effects on Aircraft and Propulsion Systems, 1965.

7. Brown, F. Z., "Reduction of Landing Weight Penalty Resulting From Ice Accretion on Unheated Surfaces", Boeing Document D6-32244, dated March 14, 1969.

# ICING TEST FACILITIES

# AND TEST TECHNIQUES IN EUROPE

by Marcel PIERRE and Xavier VAUCHERET

*Office National d'Etudes et de Recherches Aérospatiales (ONERA)*
*92320 Châtillon (France)*

♦

# 1. EUROPEAN INQUIRY ON ICING FACILITIES AND TECHNIQUES

The European inquiry was conducted, as suggested by the R.T.D. chairman, by *Marcel Pierre*, previously Director of the Modane Wind Tunnels Department and presently Senior Technical Advisor at ONERA for new facility projects. The inquiry results are presented in tabular form.

## 1.1. Organizations consulted

Table I gives the organizations consulted with their locations plotted on the map, Table II. Among them, some flight test centers and the aircraft and helicopters constructors have not their own icing ground facilities. They use the existing ones, carry out flight tests for the certification of aircraft or helicopters and sometimes develop icing techniques.

It is to be noticed that the atmospheric icing conditions are studied by LDMA at Clermont-Ferrand in France with cloud characteristics measurements in flight.

### Table I — European icing facilities and techniques

| Country | Town | Organization, acronym, sponsor | Facil. n° | Flight test | Techn. |
|---|---|---|---|---|---|
| Austria | Wien | Fahrzeugversuchsanlage - Arsenal (ground vehicles test station) | 1 | | X |
| France | Saint-Cloud | Avions Marcel Dassault - Bréguet Aviation AMD-BA | | X | |
| | Toulouse | Centre d'Essais Aéronautiques de Toulouse - CEAT | 2 | | X |
| | Saclay | Centre d'Essais de Propulseurs-CEPr (engine units test center) | 3 | | X |
| | Brétigny | Centre d'Essais en Vol - CEV (Flight Test Center) | | X | X |
| | Bourges | Etablissement Technique des Armements Terrestres - ETBS | 4 | | |
| | Clermont-Ferrand | Laboratoire de Dynamique et Microphysique de l'Atmosphère - LDMA (dynamic & microphysics of atm. lab.) | | X | X |
| | Modane | Office National d'Etudes et de Recherches Aérospatiales (ONERA) | 5 | | X |
| | Toulouse | Aérospatiale - SNIAS - Aircraft Division | | X | X |
| | Marignanne | " " - Helicopter Division | | X | |
| Germany | Köln | Deutsche Forschungs-und Versuchsanstalt für Luft-und Raumfahrt DFVLR | 6 | | |
| | Bremen | Vereinigte Flugtechnische Werke Fokker - VFW | | | |
| | Wolfsburg | Klima Windkanal Volkswagen (climatic W.T.) | 7 | | |
| Italy | Orbassano | Centro Ricerche Fiat (Fiat test center) | 8 | | |
| Norway | Kjeller | Defence Research Establishment | | X | |
| Sweden | Bromma | Flygtekniska Försöksanstalten-FFA (aeronautical research institute) | 9 | | |
| United Kingdom | Artington Burnley | Lucas Aerospace Ltd | 10 | | X |
| | Boscombe Down | Aeroplane & Armament Experimental Establishment-A & AEE | 11 | | X |
| | Farnborough | National Gasturbine Establishment - NGTE | 12 | | X |
| | Farnborough | Royal Aircraft Establishment - RAE | 13 | | X |
| | Yeovil | Westland Helicopters Ltd | | X | |

**Table II – Locations of European facilities.**
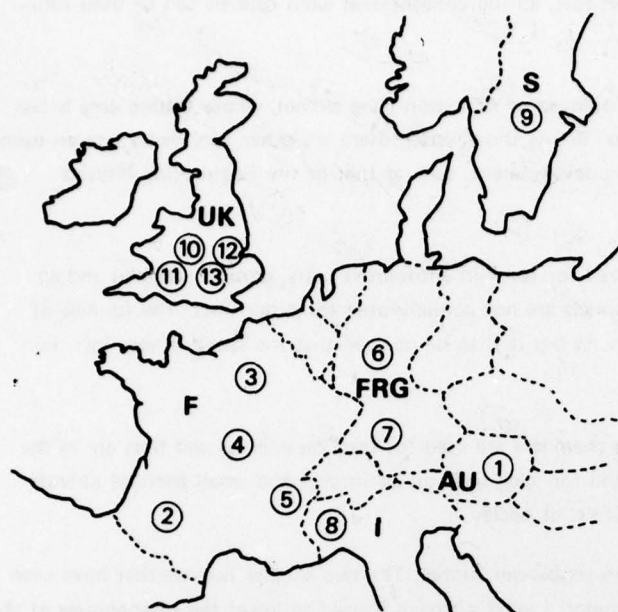


## 1.2. Icing facilities in Europa

Table III lists the European tunnels where icing testing is possible, with some details about these facilities. In fact, these facilities comprise :

— conventional wind tunnels with special equipment for icing testing,

— altitude cells or test chambers, where the flow is induced by the operation of the tested engine itself, or with a free jet, which are in fact open-jet wind tunnels. For example, the cell n°3 west of NGTE has a chamber 7.6 m in diameter equipped with a free jet 2.4 m in diameter.

**Table III – Characteristics of European icing testing facilities.**

| Na tion | Facility | Dim (m) | Max. speed (m/s) | Min. temp. (°C) | Icing MVD (μm) | Cloud LWC (g/m³) | Remarks |
|---|---|---|---|---|---|---|---|
| AU | Ground vehicles test station - Vienna | 4.9 x 4.9 | 32 | −15 | | | Snow & icing tests |
| F | CEAT - Toulouse | Ø 0.25 Ø ⩽ 1 | 250 80 | −40 | 20 → 30 | • | Two test sections • Max. flow rate : 10 g/s |
| | CEPr - Saclay - R2 Cell          R3 Cell | Ø 1.1 Ø 2 | 150 | −60 −60 | 15 → 30 15 → 30 | 0 → 6 0 → 10 | |
| | Etablissement Techn. Bourges | l = 3.75 → 5.5 (acc. to area) H = 3 → 4.1 | 22 → 44 | −40 | — | — | Steam injection |
| | ONERA Modane test center | Ø 8 ** | 150 | −5 to −15 * | 10 → 20 | 0.4 → 10 | * According to ambient cond. ** Icing cloud area : 4 m² saturated test section |
| I | Fiat research center | 3 x 4 | 45 | −45 | — | — | No icing test until now |
| FRG | Volkswagen climatic W.T. | S = 37 m² | 55 | −35 | — | — | No icing test until now |
| U.K. | A & AEE - Boscombe Down Blowertunnel & icing facility | Ø 1.2 Ø 1.8 | 140 110 | −30 −30 | 30 | 3 | LN2 injection |
| | Artington icing tunnel | 0.30 x 0.30 | 100 | −40 | ? | ? | |
| | Burnley altitude test facility | chamber Ø 4 | ? | ? | ? | ? | |
| | NGTE – Cell No 3             Cell No 3 west | chamber Ø 6.1 Ø 7.6 | ? 90* | ? −37 | ? 20 | ? 0.2 → 2.5 | * Free jet Ø 2.4 (1978) |
| S | FFA Bromma wind tunnel | Ø 3.6 | 40 | | | | 2 D : 1 m width No icing test until now |

The FFA wind tunnel at Bromma is not really an icing test tunnel : it is used to study the aerodynamics of profiles including ice accretion simulated by moulding. In fact, all the conventional wind tunnels can be used similarly.

The smallest tunnels, i.e. the tunnels of CEAT at Toulouse or Artington icing tunnel, whose testing area is less than 1 m², are used to test small aeronautical equipments. Beside those listed, there are other very small section tunnels which have limited application, mainly to instrumentation development, such as that of the Engineering Physics Department at RAE Farnborough or at DFVLR.

For information are mentioned the tunnels specialized for tests on automotive, cars, ground vehicles and so forth. Among them, the Fiat and Volkswagen climatic tunnels are not actually used for other tests. The tunnels of Vienna and Bourges offer the possibility to test aircraft parts but it is to be noticed that the speed is very low, i.e. less than 45 m/s.

Some wind tunnels, or rather some cells or altitude chambers are used for tests on engines and thus are in the scope of the PEP. Nevertheless, these facilities are also used for icing tests on air intakes and small parts of aircraft or helicopters ; that is the case for the two cells of the CEPr at Saclay.

The A & AEE tunnel at Boscombe Down is an open jet blower tunnel. The two smaller nozzles that have been recently modified for icing work are 4 ft and 6 ft in diameter. Liquid nitrogen is used to lower the temperature of the airstream. A grid of water spray nozzles provides the icing cloud ; the area in front of the tunnel is large enough to take any size of aircraft.

The Burnley altitude test facility has been used for icing tests since the late 1950 s. Initial anti-icing tests have been carried out on engine intakes for single engines, but for more advanced tests a larger facility is needed.

The NGTE Engine Test Facility has two altitude chambers in which icing tests can be made. The majority of tests simulate wet icing conditions, but some work has been done to investigate icing in mixed conditions, that is an environment containing solid ice particles and supercooled water droplets. Equipment exists in cell 3 for the production of solid ice particles and a similar equipment is under construction for use in cell 3 west and will become available during 1978. Both cells have been used to clear engines for operation in icing conditions. The two cells can also be run in a free jet mode so that icing tests can be made on complete propulsion units (intake and engine) or on full scale air frames, i.e. a complete helicopter fuselage (without rotor) with engine air intakes. To support the icing test programme, NGTE is undertaking work on instrumentation so that the cell test conditions can be more closely defined and controlled. The aim is to provide on-line output of droplet size and size distribution, liquid water content and ice/ water ratio.

The largest European tunnel for icing tests is the S1 Modane tunnel. This wind tunnel offers a test section 8 m in diameter in which the whole range of subsonic velocities can be obtained. Thanks to climatic conditions and cooling by exchange of air with the outside atmosphere, the temperature goes down often in winter below −5, even −10 and sometimes −15°C. It is then possible to create in front of the models an artificial icing cloud corresponding to the standard requirements. To this end, a 4 m² pulverization grid, equipped with 444 compressed air injectors, distributes an homogeneous cloud. The air and water supplies of that grid can be automatically controlled in order to obtain alternate icings, while keeping the droplet diameter constant with periods from 3 to several tens of seconds. The gradual implementation of the facility allowed a number of various icing tests. The first ones concerned actual aircraft elements equipped with de-icers : elements of wings or tails (even complete tails), fuselage radomes. In some cases, and in particular for Concorde, Airbus or for helicopter rotors, tests on reduced scale models were mandatory. By associating the correctly adapted spray grid and the system for testing rotors, icing on a model rotor up to 4 m in diameter is possible. Up to the present, the S1 Modane tunnel can be used for icing tests only during the winter, when adequate temperature levels can be reached. To palliate these drawbacks, ONERA is studying means that would allow artificial cooling of the test section. The realization of such a project would make it possible to reduce the air temperature in the test section by 15°C. This would allow one to do away with local atmospheric conditions for a large number of tests and to carry out the very low temperature tests necessary to qualify some materials, such as de-icing and anti-icing devices, in the whole required range.

## 1.3. Bibliography

Table IV gives the tested models in each facility, the particular techniques developed by each organization and the published bibliography.

**Table IV — Information gathered on icing test techniques in Europe.**

| Facility | Tested models/items | Remarks | Bibliography |
|---|---|---|---|
| GVTS - Vienna (AU) | Full scale : automotive-rallw. cars ground vehicles - Aircraft parts | Very long test section | Booklet : Probleme-Versuche-Forschung |
| A & AEE - Boscombe (UK) Blower tunnel & icing facility | Aircraft wings - Engines & Air intakes - Weapon systems - Helicopters. | Free air tunnel - LN2 injection | Leaflets (A & AEE) : <br> - Canberra WV 787 icing tanker <br> - Environmental test centre <br> - Helicopter icing section <br> - Blower tunnel & icing facility <br> (+ Booklet : .. .. ) |
| Artington icing tunnel (UK) | Small aeronautical equipment | Extension of engine test range under study | Short description (Aug. 77) Aircraft ice protection conference 1962 - D. Napier engineering report DEV/R/1596/942. April 1973 - Lucas. |
| Burnley altitude test facility (UK) | Air intakes - Small helicopter engines - De-icers | | Short description (Aug. 77) |
| NGTE - Cell 3 Farnborough (UK) | Air intakes - Aircraft & Helicopter engines | Icing conditions : wet or mixed (ice + water) | - Short description (Aug. 77) <br> - Rotary wing icing symposium, Edwards AFB. June 1974. |
| FFA - 3.6 m W.T. Bromma (S) | 2 D aerofoils, c ≈ 0.65 m | Simulated ice accretion shapes - Moulding technique | FFA Tech. Notes : AU 816 (1970) - AU 902 (1972) - AU 995 (1974) - AU 1169 (1977) - Memo 90 (1973). |
| CEAT Toulouse (F) | Small aeronautical equipment | Adaptable TS 0.05 to 5 m² | Note Technique CEAT 15/N/77 |
| CEPr Saclay (F) | Full scale : engines - Air intakes Nacelles | Duplication of flight conditions | "Fiches sommaires" on R2 & R6 benches |
| ETBS - Bourges (F) | Large ground veh. & equipment helicopter engines & air intakes | Icing testing possible (not yet performed) | Descr. Note : "Chambre et soufflerie climatique". |
| ONERA Modane (F) S1-MA W.T. | Full scale aircraft parts : flapped wings - Tail surfaces - Radomes - Reduced scale models : half-models (1/6 & 1/12). Helicopter rotors (1/3) | Spray grid in large test section Force meas. Ice accretion - Moulding - Red. scale testing - Min. temp. according to ambient | TP ONERA No 1054 (1972) Réf. 1 to this report. Appendix to this report. |
| LDMA - Aubière (F) | Flight cloud calibration - Icing spray grids ground calib. (ONERA, CEAT, CEPr) | Study of atmospheric icing conditions : droplet diam. spectra & LWC (Knollenberg & Ruskin sensors) | Scientific reports LDMA : No 8 (1974) No 10 (1975), No 11 (1976). Thesis (3d cycle) 1976. |

# 2. PROBLEMS ENCOUNTERED
# IN PERFORMING ARTIFICIAL ICING TESTS IN WIND TUNNELS

In this paragraph, the particulars of the artificial icing tests in wind tunnels are emphasized. The difficulties encountered, easily or hardly solved, and the problems which remain to master are pointed out, relying on examples taken from S1 Modane wind tunnel [1].

## 2.1. Facilities

The *test section dimensions* allow one to carry out tests on real elements, and especially to determine the zones which are to be protected against the ice, and to study the efficiency of de-icing or anti-icing devices. Nevertheless, even with large dimensions, like S1 Modane, one must resort to scaled down models for the helicopter rotors or transport aircraft. For such tests, some particular similarity rules are to be applied (see Section 2.3).

The interest of favourable *climatic conditions* is obvious to reach sufficiently low temperatures : so S1 Modane wind tunnel benefits of alpine conditions at medium altitude. Nevertheless, to extend the season and hours suitable for icing tests and to reach lower temperatures, a supplement of cooling is necessary. Two techniques can be considered : cold fluid mixing or heat exchanger.

The *cold fluid mixing,* with liquid nitrogen or airstream cooled by expansion, does not bring any pressure losses but needs a storage. The disadvantage of this method resides in the ice formation at the cool points, which destroys the droplet supercooling and thus alters the icing phenomena.

This disadvantage disappears with cooling by *exchanger* with liquid ammonia or freon. Exchanger icing must be avoided by dry airstream supply and an open circuit operating layout. The exchangers generate a pressure loss and consequently require extra power. This method is rather expensive in investment cost and needs a cooling fluid storage larger than the liquid nitrogen arrangement.

If the wind tunnel permits conventional tests, the icing tests will take advantage of the existing *instrumentation*. That is the case of the S1 Modane tunnel, used for icing tests but not primarily intended for them. All the test parameters and their variations can be recorded. The photographic motion picture, TV and magnetoscope apparatus are conventional.

Trajectography of shedded ice parts and stroboscopy for rotor tests may be used without difficulties. The particular icing tests method consisting in the duplication of the ice accretion shape by casting (Fig. 1) is easy : this method requires a quick access to the model after icing, to avoid alterations of the ice deposits.

*Fig. 1 — Plaster ice cap replicas (other presentation of fig. 9 of the appendix).*

## 2.2. Artificial icing cloud generation

The generation of the artificial icing cloud must satisfy all the specifications required by the standard regulations for aircraft certification in icing flight conditions. These specifications, established by the official services, define the icing cloud standard characteristics from statistical meteorological data (Fig. 2). The respect of these specifications implies to master separately three parameters :

  — the liquid water content (LWC)
  — the mean volumetric diameter (MVD)
  — the spectral distribution by diameter
     around the MVD.



*Fig. 2 — Icing standard conditions.*

*Compressed air injectors,* with fixed geometry, can be controlled with only two parameters : the water and air flow rates fix the LWC and MVD. To obtain a spectral distribution as close as possible to the standard specification over the whole range, from full scale to 1/12 scale, the injector geometry must be carefully studied. For this purpose, ONERA developed a new type of spray grid and atomizers. Nevertheless, some problems remain critical :

  — small MVD ($\sim$ 10 $\mu$m), associated with large LWC, need high air pressures, then high expansion rates, from which follows a risk to freeze prematurely the droplets. This inconvenience can be overcome by heating the air, sometimes up to 70°C ;
  — small LWC, combined with low wind speed, lead to small water flow rates and eventually a poor pulverization.
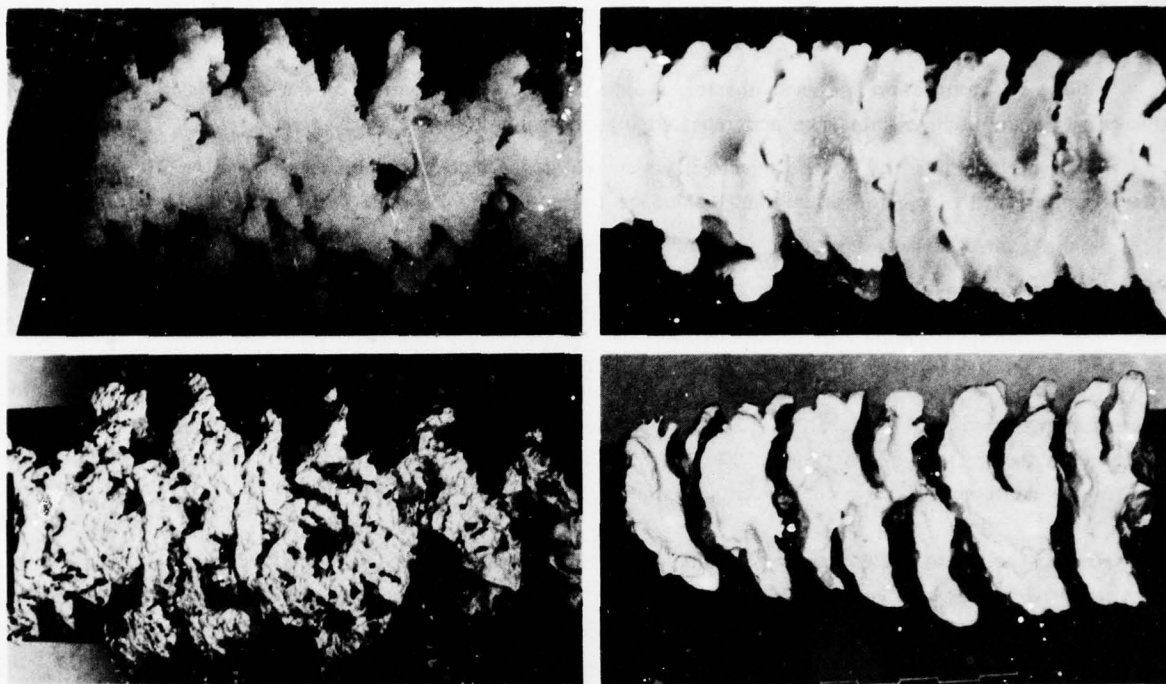
Fig. 1 — Plaster ice cap replicas (other presentation of fig. 9 of the appendix).

## 2.2. Artificial icing cloud generation

The generation of the artificial icing cloud must satisfy all the specifications required by the standard regulations for aircraft certification in icing flight conditions. These specifications, established by the official services, define the icing cloud standard characteristics from statistical meteorological data (Fig. 2). The respect of these specifications implies to master separately three parameters :

- the liquid water content (LWC)
- the mean volumetric diameter (MVD)
- the spectral distribution by diameter
  around the MVD.



Fig. 2 — Icing standard conditions.

*Compressed air injectors,* with fixed geometry, can be controlled with only two parameters : the water and air flow rates fix the LWC and MVD. To obtain a spectral distribution as close as possible to the standard specification over the whole range, from full scale to 1/12 scale, the injector geometry must be carefully studied. For this purpose, ONERA developed a new type of spray grid and atomizers. Nevertheless, some problems remain critical :

— small MVD ($\sim$ 10 $\mu$m), associated with large LWC, need high air pressures, then high expansion rates, from which follows a risk to freeze prematurely the droplets. This inconvenience can be overcome by heating the air, sometimes up to 70°C ;

— small LWC, combined with low wind speed, lead to small water flow rates and eventually a poor pulverization.

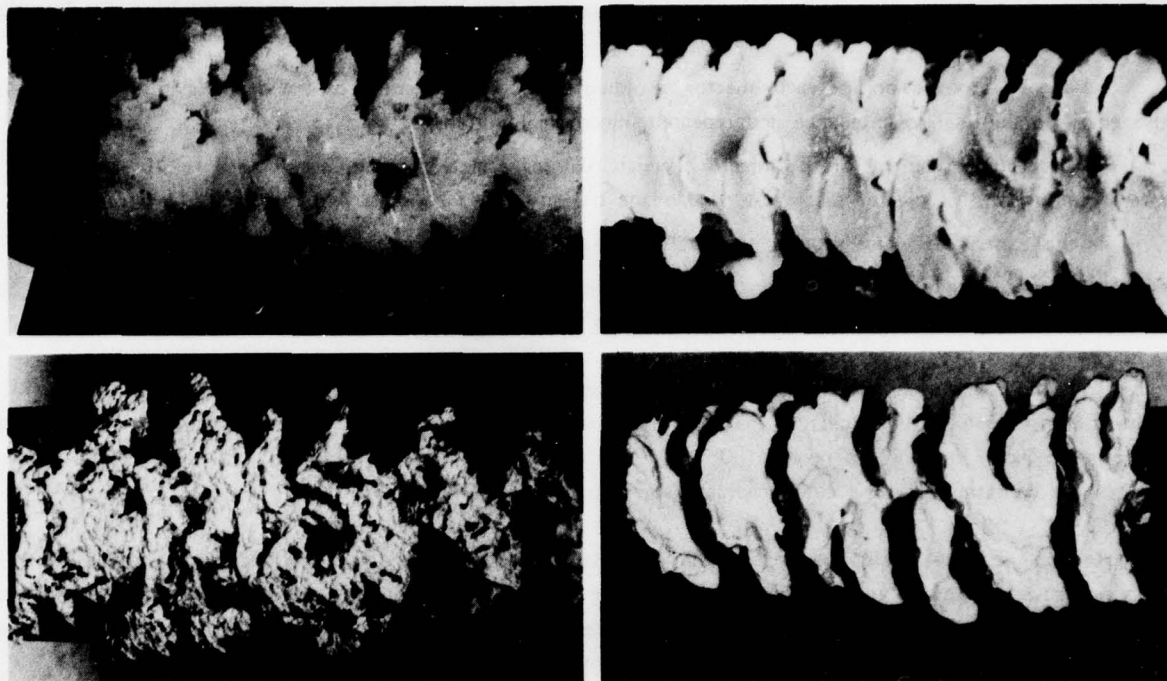A very difficult problem is to get a good *uniformity of the distribution* in the useful icing cloud section. That involves :

— a good atomization for each injector, avoiding the local segregation of the droplets in the injector field ; this entails a thorough maintenance and repeated injector calibrations ;

— an accurate identity of the injectors, which requires a close fabrication tolerance ($\sim 10~\mu m$) and an accurate mounting of the injector pieces (at S1 Modane the spray grid contains 444 injectors) ;

— the control of water supply, separately for each horizontal grid bar ;

— a good design of the grid bar which holds and supplies the injectors from both aerodynamic and mechanical points of view, in order to reduce the grid drag and avoid the bar bending vibrations.

To avoid the *droplet evaporation* between grid and model or along the model, which is mainly due to fine pulverization, an auxiliary installation makes it possible to reach *saturation* in the test section by increasing the hygrometric factor from 60 to nearly 100 %. At S1 Modane, a warm water injection, downstream of the model, ensures the constancy of icing cloud characteristics along the test section.

To cope with the various shapes and locations of the models in the test section, the *spray grid*, when it does not cover the whole test section area, has to be adapted in location and configuration. At Modane, the spray grid can cover a 4 $m^2$ area with various arrangements of the grid bars : figure 4 of appendix shows an example for a half model of Concorde mounted on the test section floor.

Another example (fig. 6 of appendix) shows the spray grid array for rotor models. The aerodynamic field is surveyed by smoke visualizations. The references must be taken behind the grid to take into account the injector air mass flow. Comparative tests, with and without grid, guarantee the validity of the results.

To obtain the *alternance of the continuous and intermittent icing conditions,* between them or with clear sky, specified by certification icing standards, the liquid water content must vary by sharp steps (less than 1 sec), while keeping constant the mean volumetric diameter. This problem has been solved by doubling the whole array of water and compressed air supply, presetting the desired rate values for alternate conditions and switching from one to the other condition and reversely by fully automatic control of quick acting valves, taking into account the response time of the piping.

The *calibration of the icing cloud* is an uneasy problem for all the icing tests, because it should be made "in situ" near the model.

The total water flow rate, divided by the airspeed and the icing cloud area, gives the liquid water content. This assumes that no evaporation, no coalescence, small marginal effects and a good homogeneity are ensured. Local measurements are often less reliable.

The mean volumetric diameter and the droplet spectra are determined by photometric analysis or mechanical catching of samples.

The catching on oiled plate, developed by *Napier*, is a slow, cumbersome and questionable process because of the low sampling rate and the variation of the specimens between sampling and analysis. Moreover, this process underrates the smaller droplets, if no catching factor correction is made.

The catching on the softened surface of a film, along the Bertin method, gives a stable stamp ; the difficult calibration of the stamp/droplet diameter ratio was overcome by an elegant method, using salty solution of known concentration.

During the analysis in situ, it is difficult to avoid alterations of the cloud, due to the probe itself and parasitic condensations. So far, the agreement between simultaneous calibration, by the several known methods, is not quite satisfactory.

### 2.3. Scaled down model tests

As, in some cases, tests on reduced scale models are compulsory, *similarity rules* are then to be applied (see appendix). In fact, one has to call upon a restricted similitude which had been established for those cases, by researchers from Douglas, Lockheed, NAE, and later of BAC and ONERA. This similitude respects the catching rate and the surface heat exchanges through the parameters : LWC, MVD, air speed and icing duration. Moreover, for helicopter rotors, after a certain icing time, the importance of ice deposit stabilizes, due to the ice shedding under the effect of centrifugal force. For tests on reduced scale rotors, it is necessary to simulate correctly this phenomenon, so that the stresses on the ice accretion under the centrifugal force be the same as in flight : this entails the identity of tip speeds, thus of forward speeds [2]. The respect of similitude rules is then obtained by acting on the droplet size, the liquid water content and the rotor r.p.m. During all the time when the rotor is maintained in icing condition, the rotor r.p.m. is kept constant by acting on the driving motors output.

Such a restricted similitude allows the overall study on models for the captation, accretion and ice shedding, and for the determination of the zones which are to be protected against ice. The Reynolds number and sometimes the Mach number are not respected. Nevertheless the similitude ensures reasonably well the thermodynamic exchanges governing the formation of ice deposits, because the flight speeds are rather low and the main phenomena occur around the leading edge where the flow pattern is less affected by viscosity effects. The altitude and the thermodynamics are only approximately respected. For the rotor blades, the aeroelastic characteristics were not simulated until now.
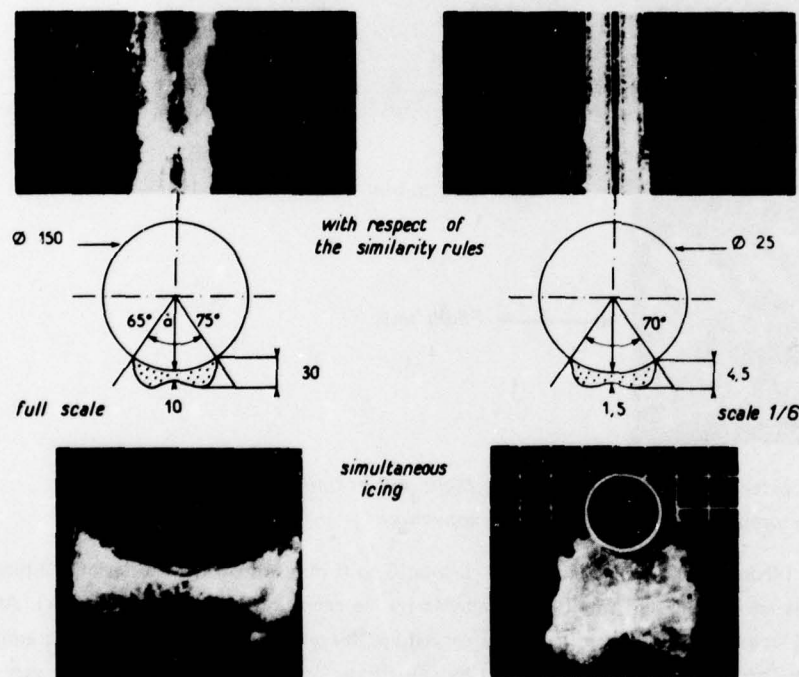


Fig. 3 — Accretion on cylinders at full and 1/6 scale. (Combination of fig. 3 and 12 of the appendix).

According to these considerations, ONERA has assessed the validity of such icing tests on scaled down models with an *experimental control of the similarity rules* by applying it in the wind tunnel to test pieces respectively at full and reduced scales : as an example, figure 3 shows the shapes of accretion obtained on two cylinders at scales 1 and 1/6. The accretions are geometrically quite similar with respect to the similarity rules. Naturally, if the two cylinders are subjected simultaneously to the same icing conditions, for instance full scale conditions, the results obtained on the 1/6 model are quite insignifiant.

The assessment with delta wings with sharp leading edges at incidence, and on conventional profiles, gives good agreement on both the extent and the shape of the accretion.

The *flight/wind tunnel comparisons* offer an essential complement to validate this method. Unfortunately, few flight results can be compared to wind tunnel tests carried out previously (naturally, it would be easier to reproduce in tunnel the flight tests conditions).

According to wind tunnel tests on a 1/6 half model of Concorde at S1 Modane, the deposits on the upper surface were almost non existent, whereas on the leading edge the ice deposits were located at the lower surface with a stratified shape generating natural tear-offs of ice blocks. Such concretions were found again in flight, and the trajectories of the naturally shedded ice parts were similar to those seen in wind tunnel.

Icing tests on a 1/12 model of Airbus led to the determination of the captation zones on the wing and tail leading edges and on the nacelles lips. In both tunnel and flight, the stratified ice deposit shape, so-called "lobster tail" [3],appears figure 4 : it is characteristic of the leading edge icing on a swept back wing.



*Wind tunnel scale 1/12*
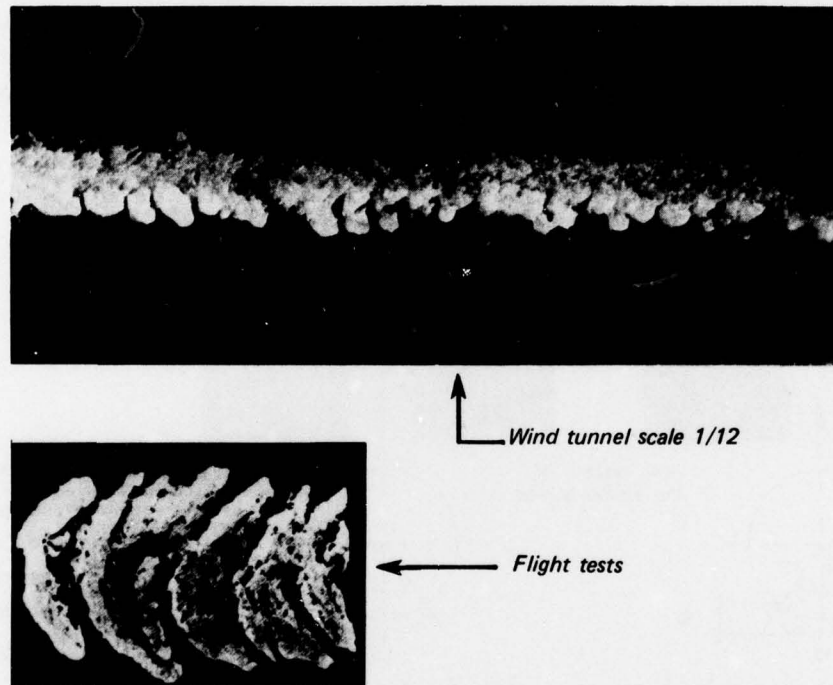
*Flight tests*

Fig. 4 — Lobster tail ice shape of A300 in flight and in tunnel tests.
(other presentation of fig. 20 of the appendix).

In the particular case of rotor blades during an initial period  lasting 5 to 6 minutes on the model of a 3-blade, 1/3 scale rotor, the rotor coefficients are rapidly and significantly altered by ice accretion (fig. 23 of appendix). After that time, the ice starts breaking up locally under the action of the centrifugal force and as an average there is equality between the ice volume deposition by accretion and that evacuated by centrifugation. Rotor coefficients then vary slightly around mean values. The torque increase necessary to maintain the rotation rate constant is of the same order of magnitude as that mentioned by *Lake* and *Bradey* [4] in flight.

As the tunnel test temperature was not very low ($-4°C$), a fraction of water not congealed at impact runs along the blade surface under the effect of centrifugal forces (fig. 22 of appendix). Beyond a relative radius of 0.5, the surfaces are clear of ice, probably due to kinetic heating. These observations agree with those made in flight by *Stallabrass* [5] for temperatures between $-1$ and $-4°C$.

This set of comparisons, though made on non-similar rotors, shows agreements that augur well for the representativity of phenomena studied in the wind tunnel on rotary wings over the whole flight domain.

# REFERENCES

1 CHARPIN F. and FASSO G. — *Essais de givrage dans la grande soufflerie de Modane-Avrieux sur maquettes à échelle grandeur et échelle réduite.* L'Aéronautique et l'Astronautique No 38 (1972-6). also in English, in Proceedings of Ice Protection Conference, published by Lucas Co, London, 1972.

2 ARMAND C. and CHARPIN F. — *Givrage en similitude d'un rotor d'hélicoptère dans la soufflerie S1-MA.* L'Aéronautique et l'Astronautique No 55 (1975-6). English translation US Army, Hanover, NH, n° TL 523 (1976).

3 LASCHKA B. and JESSE R. — *Determination of ice shapes and their effect on the aerodynamic characteristics for the unprotected tail of the A 300 B.* ICAS paper No 74-42 (1974).

4 LAKE H.B. and BRADEY J. — *The problem of certifying helicopters for flight in icing conditions.* Aeronautical Journal, Oct. 1976.

5 STALLABRASS J.R. — *Icing flight trials of a Sikorsky HO4S-2 helicopter.* NAE Laboratory Report LR-219 (1958).

# APPENDIX

## TECHNIQUES AND FACILITIES USED AT THE ONERA MODANE CENTRE FOR ICING TESTS

by Claude ARMAND, François CHARPIN, Guy FASSO and Guy LECLERE

*Office National d'Etudes et de Recherches Aérospatiales (ONERA)*
*92320 Châtillon (France)*

◆

## SUMMARY

Since 1962, the large S1 wind tunnel at Modane has been used to perform icing tests on aircraft parts (wing, tail surfaces, radome ...) at full scale.

During the last years, studies and experimental verifications have been done to promote a technique of icing tests on down-scaled fixed wings. The equations defining the non dimensional ratios, which have to be satisfied to obtain an acceptable similitude of water catching and development of ice accretion, are given.

Lately this down-scaled icing test technique has been extended to rotary wings. The evolutions of the rotor aerodynamic coefficients in icing conditions and the ice distribution on the blades are very similar to those observed in actual flight.

◆

## TECHNIQUES ET MOYENS D'ESSAIS DE GIVRAGE UTILISÉS A L'ONERA (CENTRE DE MODANE)

## RÉSUMÉ

Depuis 1962, l'ONERA utilise la grande soufflerie S1 du Centre de Modane pour réaliser des essais de givrage sur des éléments d'avions à échelles grandeur (ailes, empennages, radômes).

Au cours des dernières années, des études et des vérifications expérimentales ont été réalisées dans le cadre de la mise au point d'une technique de givrage à échelle réduite sur des voilures fixes. Les équations définissant les rapports à respecter pour obtenir une similitude acceptable de la captation et du développement des concrétions de glace sont rappelées.

Dernièrement, cette technique de givrage à échelle réduite a été étendue aux voilures tournantes. Les résultats obtenus dans ce domaine, tant du point de vue des évolutions des coefficients aérodynamiques des rotors en condition givrante que de la répartion de la glace sur les pales, sont très voisins des observations faites en vol réel.

◆

## VEREISUNGSTECHNIK UND – VERSUCHSEINRICHTUNG DER ONERA

## ZUSAMMENFASSUNG

Seit 1962 benutzt die ONERA den grossen Windkanal S1 des Modaner Versuchszentrums zur Durchführung von Vereisungsversuchen an Flugzeugbauteilen wahrer Grösse (Flügel, Leitwerk, Radom).

Im Rahmen der Entwicklung einer Vereisungstechnik im verkleinerten Mass-stab wurden im Verlauf der vergangenen Jahre experimentelle Versuche und Nachprüfungen am Tragflügel durchgeführt.

Es werden die Gleichungen angegeben, welche die zu beachtenden Grössenverhältnisse definieren, um eine annehmbare Ähnlichkeit bei der Entstehung und Ausbildung der Eisanlagerung zu gewährleisten.

In letzter Zeit wurde diese Vereisungstechnik auf Drehflügel erweitert. Die hierbei erzielten Ergebnisse sowohl hinsichtlich des Verlaufs der aerodynamischen Rotorbeiwerte als auch bezüglich der Eisentwicklung entlang der Blätter stimmen mit den im Flug gemachten Beobachtungen gut überein.

# NOTATIONS

$a$     Median volume diameter of droplets ($\mu$m)

$b$     Heat relative factor [3]

$c$     Blade chord

$C_D$     Actual drag coefficient of a droplet

$\overline{C_1}$     Rotor torque coefficient, also rotor power coefficient. If $C_1$ is the torque and $W$ the shaft power :

$$C_1 = 100 \ C_1 / \frac{1}{2} \rho N c R^2 \, U^2 = 100 \ W / \frac{1}{2} \rho N c R^2 \, \omega U^2$$

$k$     Model scale

$LWC$     Liquid water content in clouds (g/m$^3$)

$M_{ab}$     Mach number at advancing blade tip :   $M_{ab} = (V + U) \, / \, sound \ velocity \ in \ the \ test \ section$

$n$     Icing fraction [3]

$N$     Number of blades. Here $N = 3$

$P_a$     Ambient atmospheric pressure (Pa)

$P_o$     Static pressure in the test section (Pa)

$PP_\infty$     Partial water vapour in the atmosphere (Pa)

$R$     Rotor radius (m)

$\overline{R}$     Relative radius (distance to axis, relative to rotor radius)

$R_v$     Reynolds number relative to droplet diameter and droplet velocity

$t_a, \ T_a$     Air static temperature at infinity upstream ($^\circ$C, K)

$U$     Rotor tip velocity. $U = \omega R$ (m/s)

$V$     Rotor forward velocity (m/s)

$V_\infty$     Velocity at infinity upstream (m/s)

$\overline{X}$     Rotor propulsive force coefficient (parallel to wind). If $F$ is the propulsive force : $\overline{X} = 100 \ X / \frac{1}{2} \rho N c R U^2$

$\overline{Z}$     Rotor lift coefficient (vertical). If $Z$ is the lift : $\overline{Z} = 100 \ Z / \frac{1}{2} \rho N c R U^2$

$\alpha_D$     Pitch angle, or inclination of the plane described by the blade tips on the horizontal plane ; positive for pitch up (degrees).

$\alpha_Q$     Inclination of the rotor shaft on the vertical ; positive for pitch up (degrees)

$\theta_c$     Cyclic pitch (degrees)

$\theta_o$     Collective pitch (degrees)

$\Lambda$     Advance ratio. $\Lambda = V/U$

$\rho$     Air density (kg/m$^3$)

$\sigma$     Shear stress in ice (Pa)

$\tau$     Icing time (s)

$\omega$     Rotor angular velocity (rad/s)

## Subscripts

$f$     Actual aircraft or full scale model

$k$     Ratio of the values of a parameter for scale $k$ and full scale (ex. : $P_{a_k} = P_{a_m} / P_{a_f}$).

$m$     Model

# INTRODUCTION

There exist different means for defining the shapes and extents of ice deposits on aircraft frames and on helicopter blades, and for qualifying de-icing and anti-icing devices :

— flight tests in natural icing conditions ;
— flight tests in artificial icing conditions :
. of actual parts mounted on a carrier aircraft, behind a water pulverizing grid,
. of the aircraft itself, flying in an artificial cloud behind a tanker aircraft ;
— ground tests in stationary operation (helicopters) ;
— wind tunnel tests :
. of actual parts or at full scale,
. of full or half models at reduced scale.

The study in artificial cloud implying the creation of clouds of the same nature as those encountered in flight, it is mandatory to know the characteristics of the latter.

Statistical meteorological data enabled the Official Services to define the dimensional characteristics of icing clouds liable to be encountered by aircraft in flight, as well as the technical conditions for granting the icing item its airworthiness certification.

In artificial icing test procedures, among them wind tunnel tests, two cases should be considered : maximum continuous icing, and maximum intermittent icing.

The atmospheric conditions corresponding to maximum icing are defined for water droplets of 20 $\mu$m median volume diameter in the following conditions :

| Atmospheric temperature (°C) | Liquid water content (g/m³) | |
|---|---|---|
| | Continuous | Intermittent |
| 0 | 0.8 | 2.5 |
| — 10 | 0.6 | 2.2 |
| — 20 | 0.3 | 1.7 |
| — 30 | 0.2 | 1.0 |
| — 40 | — | 0.2 |

The temperature and pressure-altitude ranges where these types of cloud may be encountered are defined on figure 1.
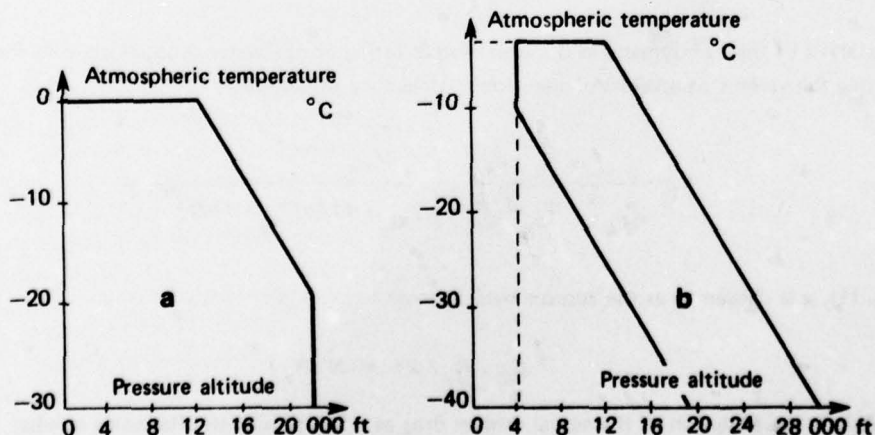


Fig. 1 — Maximum icing conditions. a) Continuous b) Intermittent.

The extent of these types of cloud is considered as unlimited ; however, for demonstration tests it is taken equal to 30 minutes for cruise or stand-by flight configurations, and to the actual flight time for climb or descent flight configurations.

For intermittent icing, the extent of the cloud is supposed to be 5 km ; however, for demonstration tests the corresponding cloud formations are made of 5-km-wide clouds, separated either by clear sky intervals or by clouds of maximum continuous type, defined as above.

# 1 – STUDY OF SIMILITUDE LAWS

The theoretical study of the laws governing icing in similitude conditions requires the analysis of various physical phenomena. The first one is that of the mechanics of water droplet pick-up, which involves the investigation of the trajectories of these droplets in the aerodynamic field of the flow around the icing obstacle. A study of this problem has been made by Langmuir and Blodgett, of General Electric Company [3].

The second of these phenomena is that of the distribution of water, then of ice, on the profiles ; it involves the water content of the cloud, the icing time, and also the convection heat transfer coefficient, defined by *Gelder* and *Lewis* in ref. [ 2].

The third phenomenon, perhaps the most difficult to treat, is that of the thermal balance of a wall in icing conditions. A very detailed study of this problem has been performed by *Messinger,* of Lockheed Aircraft Corp. [3], in which he brings to light the concepts of "heat relative factor, *b*" and of "icing fraction, *n*".

This various studies were put together, with a view to define the relations between the parameters governing wind tunnel similitude tests, by *Mauger, Englar* and *Reaser,* of Douglas Aircraft Comp. [4] and by *Brun*, of Paris University [5].

For industrial tests in similitude conditions, and for similitude icing tests on simple models intended to check the theory, the parameters defining icing clouds have been calculated from the works by *Googan, Jackson* and *Hubbold,* of British Aircraft Corp. [6, 7]. These works made it possible to carry out the transposition from the aircraft flight range to that simulated in the wind tunnel, within the framework of icing restricted similitude. This similitude is restricted, as it is not possible to respect together the Mach and Reynolds number conditions for the aerodynamic flow around the obstacle and the Reynolds number condition for the droplets. But it happens that, in the flight conditions where icing might the dangerous, the aerodynamic field in the ice pick-up zones is little sensitive to these two parameters, as the compressibility and viscosity phenomena in the boundary layer remain inimportant around the leading edges at low or moderate speed.

The analysis of the aerodynamic and inertial forces acting on the water droplets close to the obstacle leads to eq. (1) relating the various parameters of the droplet trajectory similitude :

$$
(1) \qquad k = \frac{a_k^{\,2-x} \; V_{\infty k}^{\,1-x}}{P_{a_k}^{\,x} \; T_{a_k}^{\,\frac{3-5x}{2}} \left[ (T_{a_m} + 117)/(T_{a_f} + 117) \right]^{x-1}} \; .
$$

In eq. (1), $x$ is chosen so as the approximate formula :

$$
C_D \cdot R_V / 24 = K (R_V)^x
$$

represents at best the evolution of the actual droplet drag as a function of the Reynolds number $R_V$ related to its velocity relative to the flow, within the range of values of $R_V$ where this relative velocity intervenes determinantly on the

trajectory deflexion from the streamlines, at full scale and at reduced scale in wind tunnel tests. Figure 2 shows that for a droplet Reynolds number range between 6 and 120, covering both the flight domain and the 1/6 and 1/12 scale domain, the value of $x$ represented by the slope of the straight line passing at best through the points, can be taken as 0.39.
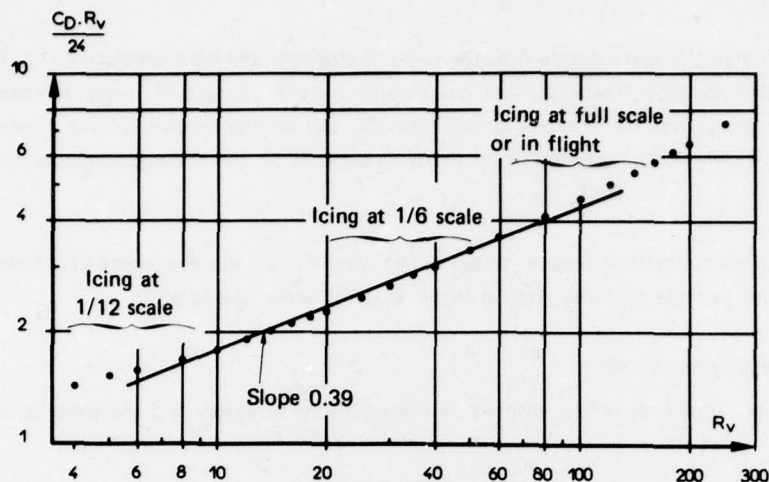


Fig. 2 – Ratio between the actual drag of a droplet and that given by the Stokes law as a function of Reynolds number.

In most cases, the ratio $T_{a_m}/T_{a_f}$ is close to 1, and the practical formula to be used for the calculations becomes :

$$
(2) \qquad k = \frac{a_k^{1.61} \ V_{\infty k}^{0.61}}{P_{a_k}^{0.39}}
$$

The analysis of the various parameters acting on the volume and distribution of ice on the profiles leads to formulas (3) and (4), defining respectively the ratio of liquid water content in the mist and the ratio of icing times :

$$
(3) \qquad LWC_k = \frac{P_{a_k}^{0.8}}{k^{0.2} \ V_{\infty k}^{0.2} \ T_{a_k}^{1.6}}
$$

$$
(4) \qquad \tau_k = \frac{k^{1.2} \ T_{a_k}^{1.6}}{V_{\infty k}^{0.8} \ P_{a_k}^{0.8}}
$$

Equations (3) and (4) are only valid if the parameters relative heat factor $b$ and icing fraction $n$, introduced by *Messinger* [3], are equal in flight and on the model. We then should establish the relation between the variables that ensure the balance between the convective, evaporative and kinetic heat quantities. The formulas obtained in [3] give the equation that relates air temperature, velocity and pressure to the two parameters $b$ and $n$ in the case of an unheated wall :

$$
(5) \qquad \frac{1.06 \cdot 10^6}{P_a} = t_a(1+b) + 1730 \ \frac{PP_\infty}{P_a} + 79.7 \ nb + (3.65 + b) \frac{V_\infty^2}{8370}
$$

The whole set of the above formulas is then applied to the transposition of the actual flight case to its corresponding one in the wind tunnel. The laws are already established in the case of fixed wings, then their field of application is extended to the case of rotary wings.

### 1.1. Icing similitude on aircraft parts

Icing similitude between aircraft and model is ensured if a number of conditions is respected, concerning the aerodynamic field, the thermodynamic exchanges between air, water and ice, the droplet trajectories, the water content in icing clouds and the crossing duration of these clouds.

For an aircraft flying in given conditions, the flight is characterized by the velocity ($V_{\infty f}$), the angle of attack ($\alpha_f$) and the flight altitude ($H_f$). At this altitude corresponds a static pressure ($P_{af}$) and an ambient temperature ($t_{a_f}$). The icing cloud is characterized by its water content ($LWC)_f$, the droplet median volume diameter ($a_f$) and the water vapor partial pressure ($PP_{\infty f}$). The ice deposit on the wing depends on the above parameters and the cloud crossing duration ($\tau_f$).

For a model of this aircraft at scale $k$, tested in the wind tunnel, the equivalent data (subscript $m$) have to be determined in relation to those if the aircraft in flight or at full scale (subscript $f$).

#### 1.1.1. Aerodynamic similitude

The aerodynamic similitude is first ensured by the similitude of shapes and the equality of angles of attack :
$\alpha_m = \alpha_f$.

The flight velocities in icing conditions being usually low, the aerodynamic field does not imply transonic phenomena, and is not modified by a velocity variation. The Reynolds number effect being usually negligible, there is not necessarily an equality between flight and wind tunnel velocities. On the other hand, the aerodynamic coefficients are the same in both cases.

#### 1.1.2. Thermodynamic similitude

The parameters characterizing thermodynamic exchanges between air, water and ice satisfy the relation (5). The four parameters $P_a$, $t_a$, $PP_\infty$ and $V_\infty$ determine the conditions in which thermodynamic exchanges take place, so that eq. (5) is reduced to a homographic relation between $n$ and $b$ :

$$(6) \qquad n = \frac{A_f + B_f\, b}{b}$$

This relation fixes the nature of the thermodynamic exchanges. For the similarity to be ensured, the set of values for parameters $P_a$, $t_a$, $PP_\infty$ and $V_\infty$ should lead to the same relation (6), for the flight and the wind tunnel, so that :

$$(7) \qquad \frac{A_f + B_f\, b}{b} = \frac{A_m + B_m\, b}{b}$$

$$(8) \quad \text{or} \qquad A_m = A_f \qquad B_m = B_f$$

The values of the four parameters are known in flight, so that $A_f$ and $B_f$ are determined. In the wind tunnel, the stagnation pressure and temperature are known, and there exists a relation between $V_{\infty m}$, $t_{a_m}$ and $P_{a_m}$. Lastly, there is a relation between the water vapour partial pressure ($PP_{\infty m}$) and the static temperature ($t_{a_m}$). So there exist four relations between $P_{a_m}$, $t_{a_m}$, $PP_{\infty m}$, and these are all determined if the thermodynamic similitude has to be achieved.

### 1.1.3. Similitude of droplet trajectories

Aircraft and model being geometrically similar, at scale $k$, we must make sure that the droplet trajectories are also similar in flight and in the wind tunnel. The aerodynamic field being the same, the trajectories depend only on the droplet size. The trajectory similitude is ensured if the median volume diameters in flight $(a_f)$ and in the wind tunnel $(a_m)$ satisfy eq. ( 2).

(2')
$$a_k^{1.61} = \frac{k \; P_{a_k}^{0.39}}{V_{\infty k}^{0.61}}$$

In this relation, all the terms on the right hand side are fixed by the previous conditions and, $a_f$ being known, $a_m$ is determined. In fact, the experimenter will choose the parameters so as the similitudes be respected and $a_m$ might be actually obtained with the existing pulverization device.

Equation (2) must be respected for the droplet trajectories to be correct and the ice pick-up on the wing be realistic.

### 1.1.4. Similitude of ice deposits

The importance of the ice deposits depends on the quantity of liquid water in the icing clouds ($LWC$) and the cloud crossing duration ($\tau$). The analysis of the various parameters acting on the volume and distribution of ice on the profiles leads to the relations of similitude defined in eq. (3) and (4).

The set of relations (5), (2), (3) and (4) allows the solution of icing problems at reduced scale on models of fixed wing vehicles.

## 1.2. Icing similitude for rotary wing aircraft

Their laws are defined from these valid for fixed wing aircraft

### 1.2.1. Aerodynamic similitude

It is ensured of the aerodynamic field for each blade section is the same during a revolution in flight and in wind tunnel, on both the full scale and the scaled-down model. To this end, the shaft inclination ($\alpha_Q$), the collective pitch ($\theta_o$) and the cyclic pitch ($\theta_c$) are adjusted so that the disc inclination ($\alpha_D$) be that of the flight and that the geometric incidences be realistic. The rotation speed ($\omega$), tip speed ($U$) and advancing speed ($V$) are adjusted so that the velocity composition be the same in flight and wind tunnel on any point of the disc ; for this, the advance ratio ($\Lambda = V/U$) must be the same. The Mach number of the advancing blade tip ($M_{ab}$) has to be maintained equal only if compressibility phenomena are significant. This was not the case for the tests at S1MA, but as equality of speeds was required for respecting equality of stresses in ice (see section 1.2.4), equality was respected for $V$, $U$, $M_{ab}$ and $\Lambda$. Consequently, the angular velocities were in the inverse ratio of $k$ :

(9)
$$U_m = \omega_m R_m = U_f = \omega_f R_f$$

$$\omega_k = \omega_m / \omega_f = 1/R_k = 1/k.$$

The correct adjustement of these various parameters is verified globally if the lift and torque rotor coefficients are the same in the wind tunnel as in flight.

### 1.2.2. Thermodynamic similitude

Equation (5), valid for fixed wings, applies here in the same way, the parameters, $P_a$, $t_a$, $PP_\infty$, $n$ and $b$ having the same definition, and $V_\infty$ being the instantaneous velocity on the profile section considered, resulting from the composition of the rotating and advancing linear velocities.

Thus, the thermodynamic similitude consists in making to every flight velocity $V_{\infty f}$ correspond a wind tunnel model velocity $V_{\infty m}$ which is a priori different. There is there a contradiction with the aerodynamic similitude, which had been chosen so as to impose equal local velocities in wind tunnel and in flight. Practically, this difficulty was solved by keeping to a velocity calculated to satisfy the aerodynamic similitude. The error resulting in the thermodynamic similitude in the tests at S1-MA is about $0.5^\circ C$, a value of the same order of magnitude as that of the measuring precision of temperature $(t_a)$ during the tests ; for that reason, it has been considered as negligible.

### 1.2.3. Water droplet trajectory similitude

The aerodynamic similitude ensuring the equality of the aerodynamic fields on similar profiles, the trajectory similitude is ensured in the same condition as for fixed wings, and the same eq. (2) applies. The values of velocities $V_\infty$ vary with the profile section and the blade position during a turn ; but the equality of the advance ratio implies that the velocity ratio $V_{\infty k}$ is the same at every point. In the particular case of the S1-MA tests, the velocities being equal, the ratio is 1.

### 1.2.4. Ice deposit similitude

In the same way, the same laws apply as regards liquid water contents and cloud crossing duration. But moreover, in the case of rotary wings account must be taken of the centrifugal forces due to blade revolution, that provokes shedding of ice deposits. For these sheddings to be the same in flight and in the wind tunnel, it is necessary first that shear stresses in ice be the same in both cases. But, all the parameters being fixed, the ratio existing between these stresses is an established fact. Assuming the ice density to be the same in flight and in the wind tunnel :

$$(10) \qquad \sigma = \frac{m\,\omega^2\,R}{s}$$

$$(11) \qquad \sigma_k = m_k\,\omega_k^2\,R_k/s_k = k^3 \cdot k^{-2} \cdot k^{-2} \cdot k = 1.$$

So the shear stresses in ice, in flight and in the wind tunnel and the same in similar sections.

This allows one to hope that natural ice sheddings due to centrifugal forces, as obtained in the wind tunnel, are well representative of those in flight. In fact, the natural sheddings of ice are certainly under the strong influence of the blade flexibility. In the case of the helicopter model used in the tests presented below, the model blades were stiffer than those of the real rotor. The wind tunnel test results are thus pessimistic, as ice will tend to shed more easily in flight.

# 2 — TESTING MEANS AND TECHNIQUES

The specifications of the standards concerning icing conditions in flight required the fabrication of a set-up providing a wall defined icing cloud in test section n° 1 of the S1-MA wind tunnel.

The pulverization grid can comprise 444 air fractioning injectors distributing an homogeneous cloud of droplets whose median volume diameter can be adjusted between 10 and 20 $\mu$m over a 4-m² surface. The liquid water content can be adjusted between 0.4 and 10 g/m³ for velocities reaching 100 m/s.

The air and water supplies to that grid can be automatically controlled so as to ensure alternate icings (conditions of maximum continuous, maximum intermittent and clear sky, according to official specifications) while keeping the droplet diameter practically constant, with periods varying from 3 seconds to several tens of seconds.

Preliminary tests had shown that the droplets evaporated if the air of the main flow was not saturated. This evaporation modified the droplet diameter and the liquid water content of the artificial cloud, which thus caused ice deposits not representative of the set conditions. To palliate this difficulty, the S1-MA wind tunnel was equipped with a saturating device made of 8 pulverization nozzles providing up to 900 dm³/h each, and thus ensuring saturation in the test section by raising the hygrometric degree from 60 to nearly 100%. The permanent monitoring of the hygrometric degree is ensured by an automatic dew-point hygrometer operating by continuous pick-up in the test section (fig. 3).



*Fig. 3 — Icing and saturation devices.*

The pulverization grid can be placed in various points of the test section according to the shape and position of the model (figs. 4, 5, 6).



Fig. 4 — Grid and model installed on the wind tunnel floor.
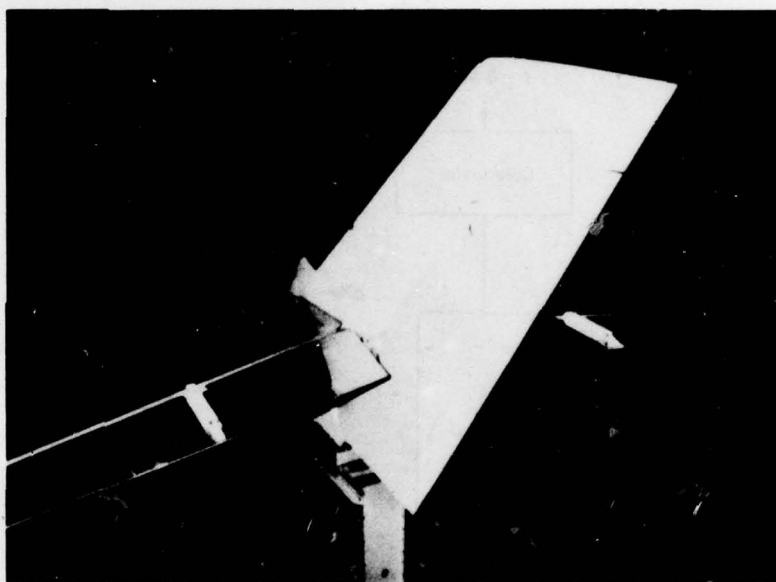


Fig. 5 — Grid and model installed in the centre of the test section.
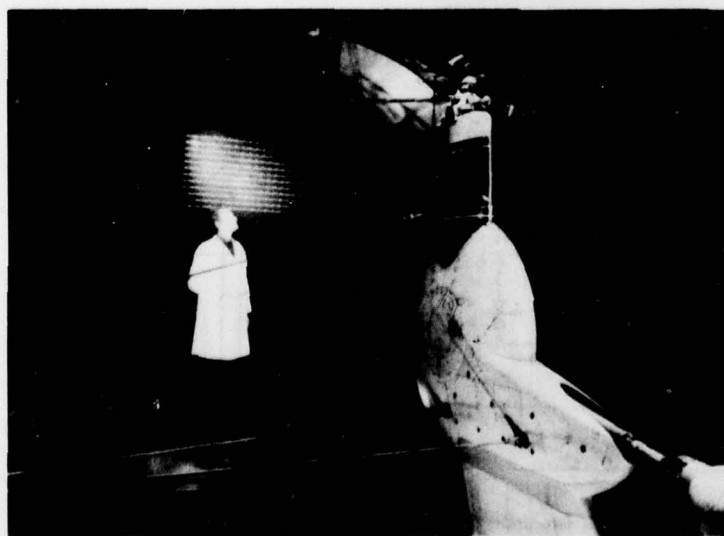


Fig. 6 — Grid and helicopter rotor.

The position of the pulverizing grid relative to the model is determined after a preliminary test, during which the fluid filets surrounding the model are visualized by smoke streaks ; this positioning is later checked with the water droplets.

Tests made it possible to determine the positive or negative pressure drop in the wind tunnel, behind the grid, as a function of air flow, and to take it into account for the determination of the velocity at infinity upstream.

The study of the aerodynamic flow behind the grid was carried out by combing and by comparing wall visualizations, pressure distributions and aerodynamic weighings on the profiles with and without the grid. The perturbating effect of the grid is very low ; an example of this effect is given, in the case of a rotor, on figure 7. The curves on the left present the results obtained, in the same operating conditions, with and without grid in the test section. The curves on the right present another experiment, where the rotor has been weighed behind the grid with and without air injection. The differences are small, of the same order of magnitude as the precision of the measuring instruments used for this experiment. We must then conclude that the presence of the icing grid, in front of the rotor, does not cause any appreciable perturbation in the operation of the latter.
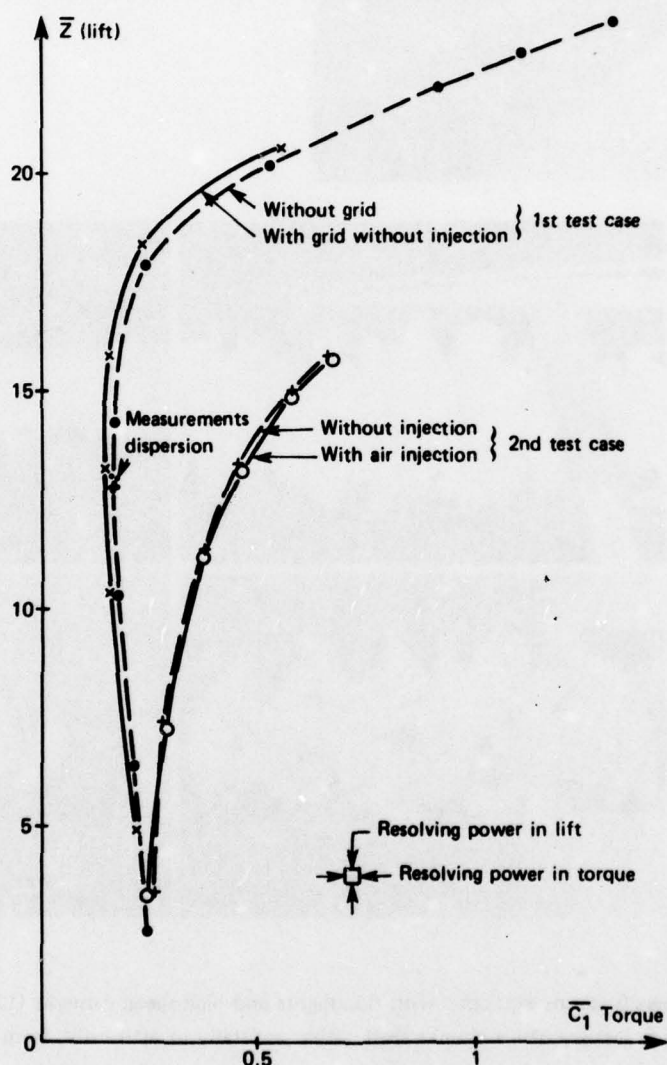


Fig. 7 — Effects of the grid and air injection on rotor coefficients.

The 8-m-dia. S1-MA test section permits the experimentation of large models with a low blockage factor ; these models can easily be reached five minutes after the test, which makes possible the recording of ice deposit extent and shape for photography and by direct measurements. Interpretation of the photographs is made easier by the use of cross-lined patterns or of very precise marks painted on the models, identifying chord percentages or angles (fig. 8). In case of important ice deposits, their castings can be performed (fig. 9). The tunnel floor comprises a balance allowing an angular setting and the measurement of aerodynamic forces on the model before and after icing, as well as a compressed air supply to feed with primary air the ejectors simulating the engine air intakes in some models.
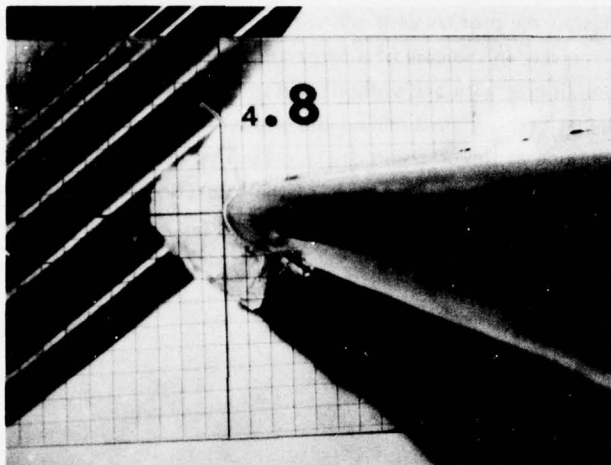


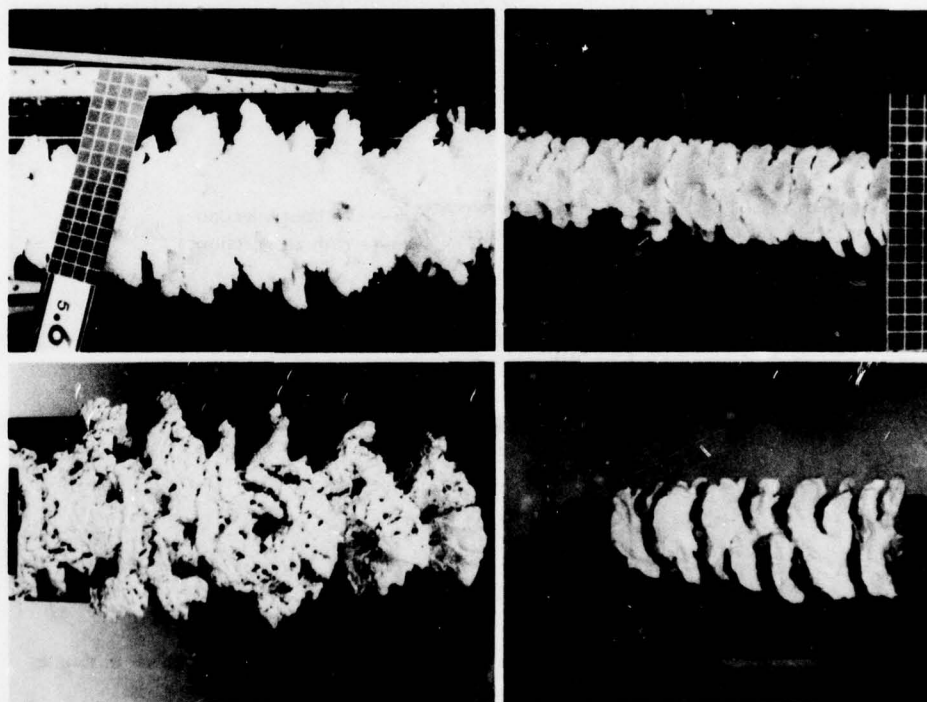Fig. 8 — Profile of an ice deposit measured with a 1 cm-square pattern.



Fig. 9 — Ice samples and their castings.

The test section sidewalls can be equipped with floodlights and high-speed cameras (1200 frames per second) necessary for studying the trajectory of ice chunks shed, either naturally or artifically, from the forward parts of the model.

The particular test rig for helicopter rotors is described in detail in ref. [8, 9, 10]. This set is put into operation under the control of a monitoring system ensuring the safety of personnel and installations. This monitoring and safety system comprises :

— the visualization in two large multitrace screens of the signals provided by strain gages mounted on the blades and the signals from the balance and the torquemeter ; the main parameters are permanently recorded on an analogue magnetic tape ;

— an independent electric supply ensuring the operation of some essential functions (lubrication, pitch control) in case of breakdown of the main electric network ;

— a closed television circuit, with stroboscopic lighting and magnetic recording for the permanent monitoring of the rotor ;

— a particular interphone between the rotor control room and the monitoring room ; order transmission and exchange of essential safety informations are thus ensured without any risk of interference with the routine test communications.

Let us add that the test section and its windows are reinforced and that, before each test, a thorough study of the dynamic characteristics of the test rig and the blades is carried out, this study being liable to lead to modifications of the natural frequencies of parts of the rig.

The acquisition unit allows on-line calculations, for the setting of the test parameters as well as of the results on aerodynamic weighings ; these can be presented on a cathode ray tube as a curve.

The recording on magnetoscope and by photography of the observations made under stroboscopic lighting allows the restitution of ice accretions.

# 3 — VALIDITY OF ICING AT REDUCED SCALE

Having yet no element for comparing icings in flight and at reduced scale in the wind tunnel, it has been considered necessary to check the calculations concerning icing in similitude by comparative wind tunnel tests at full and reduced scale. So ONERA undertook, in parallel with industrial tests, similitude icing tests either on simple shapes such as cylinders or on wing shapes similar to those concerned with industrial tests. These tests were performed first at 1/6 scale, then extended to 1/12 scale. In this case, the calculations are the same as for flight-wind tunnel similitude, but as it is not possible in the wind tunnel to adjust the pressure and temperature, the theoretical thermodynamic icing similitude can not be strictly obtained.

In the cases where the icing similitude laws were not respected, the ice deposits appearing on the models are very dissimilar as regards both extent and shape. Figure 10 presents a set of photographs in which the left hand ones (a) represent icings obtained on models associated with correct clouds, and the right hand ones (b) models associated with clouds not respecting the similitude laws. Icings on cylinders (fig. 10-1-a and b) show very different glaciation angles (80 and 140°). As for ice thicknesses, brought back to the same scale (full scale), they are also widely different : 30 and 180 mm. On delta wings (fig. 10-2-a and b), the icing on the leading edge that appears in normal test is practically non existent on the large model. In the case of icing on segments of thick profiles (fig. 10-3-a and b), the differences are still more dramatic : the correct icing extends up to 2.5% of the chord while on the small model it extends up to 15%, with very different shapes of accretions.
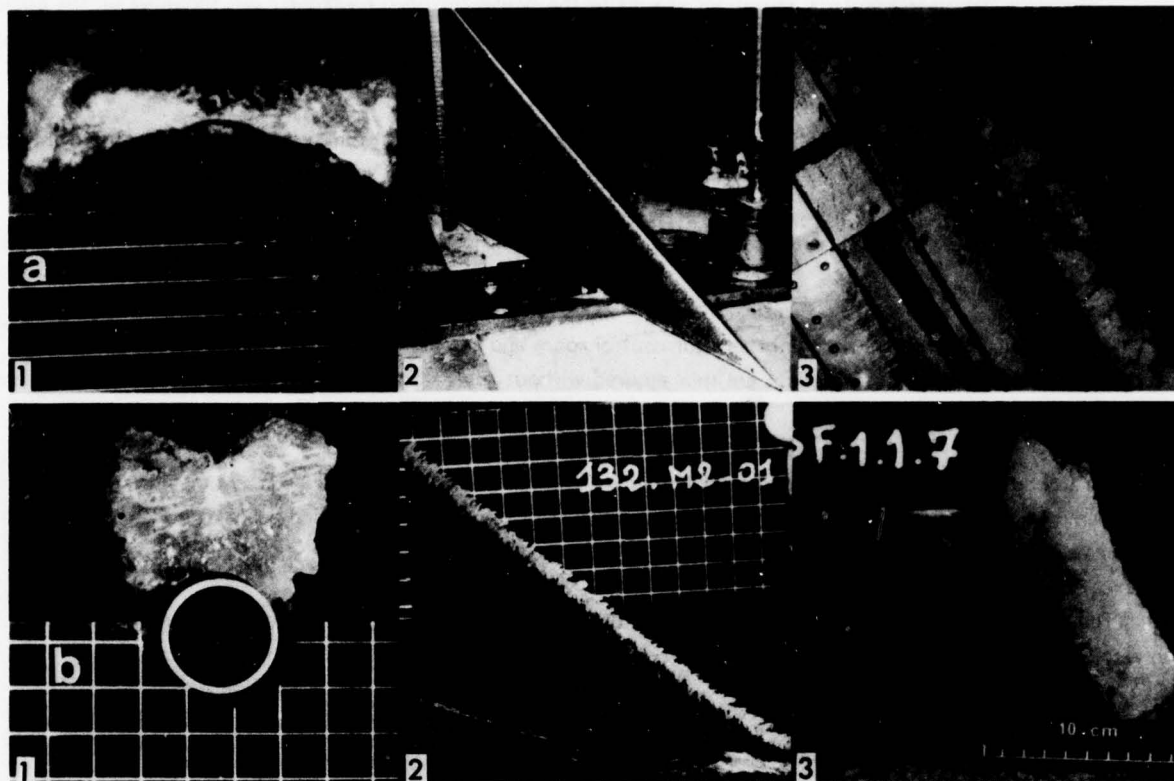
A6-14



Fig. 10 — Scale influence on icing — Tests with the same cloud and models at scales 1 and 1/6.

a) Large model — Similitude respected

b) Small model — Similitude not respected.

1. Cylinder    2. Delta wing    3. Swept leading edge

Figures 11 and 12 show, as photographs and scaled sketches, results of tests on cylindrical models in 1/6 and 1/12 scale similitude. The glaciation angles are very similar, and the thicknesses, brought back to the some scale, are not very different, as shown on Table I :

Table I — Results of similitude tests

| Scale ratio k | Position | $e_f$ (mm) | $e_m$ (mm) | $e_m/k$ (mm) | Relative difference % |
|---|---|---|---|---|---|
| 1/6 | Centre | 10 | 1.5 | 9 | 10 |
| | Sides | 30 | 4.5 | 27 | 10 |
| 1/12 | Centre | 15 | 1 | 12 | 15 |
| | Sides | 40 - 45 | 3 - 3.5 | 36 - 42 | 10 |

Icings at small scale are more regular than those at large scale, when lateral protuberances appear ; on the other hand, the zone localised around the stagnation line of the flow is made of transparent ice in both cases.
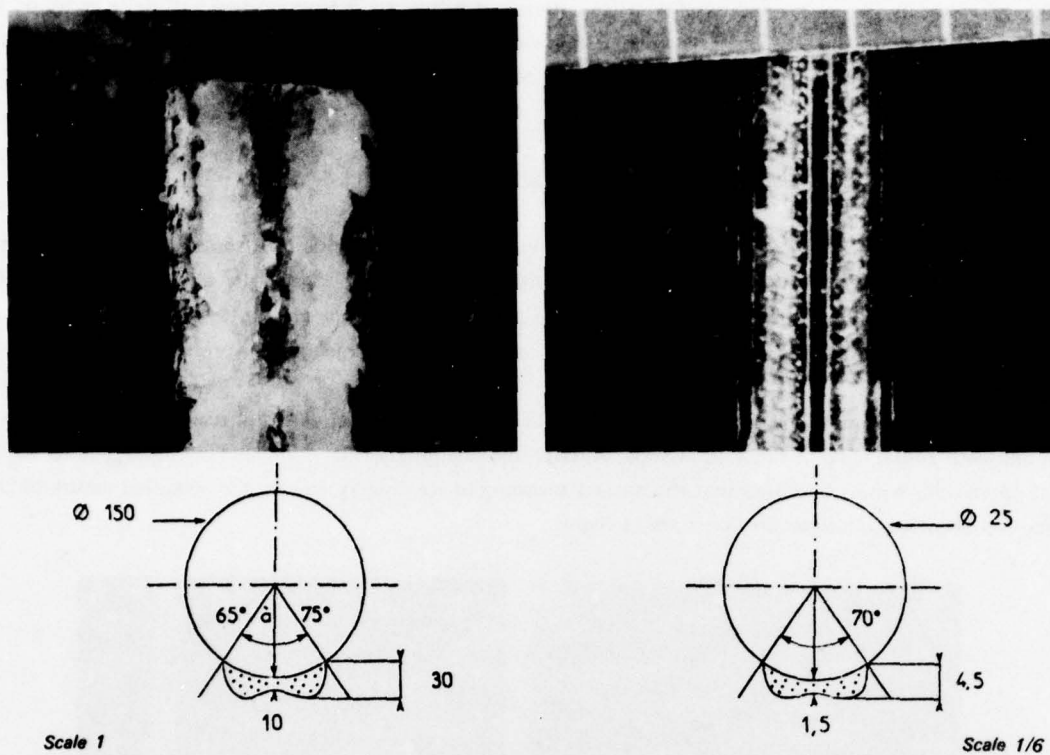
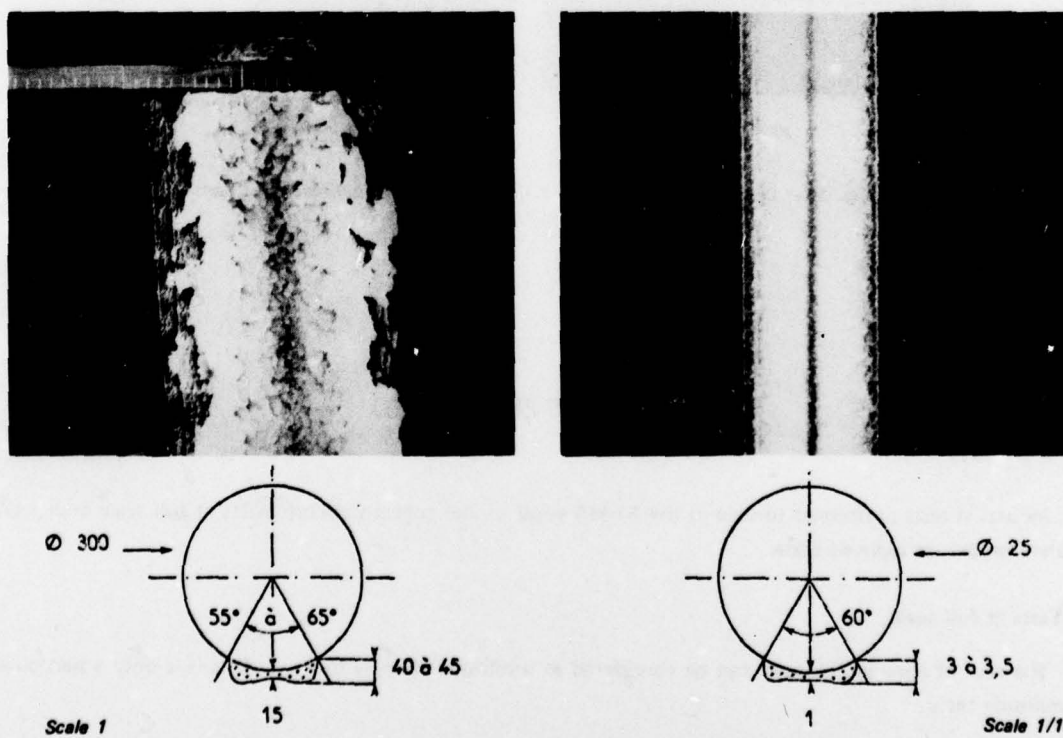Fig. 11 — Comparison of ice deposits on cylinders in similitude conditions.



Fig. 12 — Comparison of ice deposits on cylinders in similitude conditions.

Figure 13 shows the shapes and extents of ice deposits at full and 1/6 scale on two half delta wings of 75° sweep and at 15° angle of attack. On these wings, the ice appears only on the leading edge lower surface, as a corrugated deposit whose section perpendicular to the leading edge has the shape of an isosceles triangle attached by one of its apexes. This shape is observed at both scales.

Other comparisons have been made on thick profiles at incidence [11].

The whole set of experiments made in conditions respecting the similitude laws shows a good agreement as regards both deposit shapes and extents ; however, a slightly smaller deposit is generally observed at small scale, which may be explained by the formation of a small percentage of ice crystals at the grid outlet. This percentage could be higher in tests at small scale, which requires smaller droplets and a higher injection air pressure.

More recently, comparisons between similitude tests in the wind tunnel with full scale tests of an SST air intake, and with actual icing in flight (Concorde, Airbus), provide an essential complement to the validity of the method. Moreover, it must be noted that the natural shedding of ice chunks, due to the stratified nature of the deposits, has been also observed on Concorde in flight.
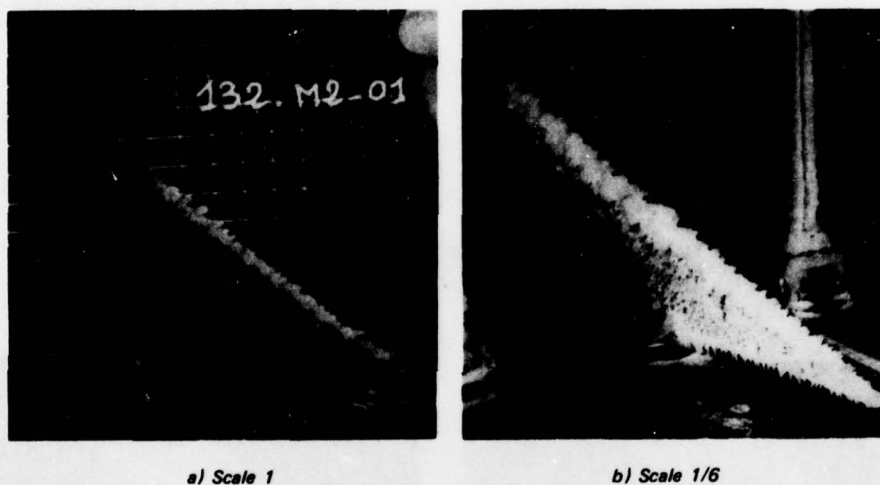


a) Scale 1                                    b) Scale 1/6

Fig. 13 — Comparison of ice deposits on delta wings in similitude conditions.

# 4 — TESTS PERFORMED

Industrial tests performed to-date in the S1-MA wind tunnel concern aircraft parts at full scale and aircraft complete models at reduced scale.

### 4.1. Tests at full scale

The case of icing at full scale can be considered as similitude scale, with $k = 1$. This it is only a particular case of similitude tests.

The tests are usually performed on actual aircraft parts, either to test de-icing devices or to define the zones and shapes of accretions for non de-iced parts.

Figure 14 shows, at the end of a test, the leading edge of an aircraft fin equipped with a pneumatic de-icing device. A non de-iced reference zone carries the ice accumulated during the whole test ; the rest of the leading edge, completely free of ice, demonstrates the efficacy of the de-icing device.

Figure 15 shows the evolution of ice deposition in the central part of non de-iced fins of an aircraft during tests at Mach 0.3 lasting 10, 20 and 30 minutes. During these tests, the drag rise has been measured.

Figure 16 shows the effect of the actuation of the horizontal control surface of a fin after a 30-mn icing test. During the movement, the effort required to break the ice has been measured.

Other tests have been performed with thermal de-icing devices.



Fig. 14 — Icing reference on a pneumatically de-iced leading edge.



Fig. 15 — Evolution of ice deposits on a tail fin during an icing test.

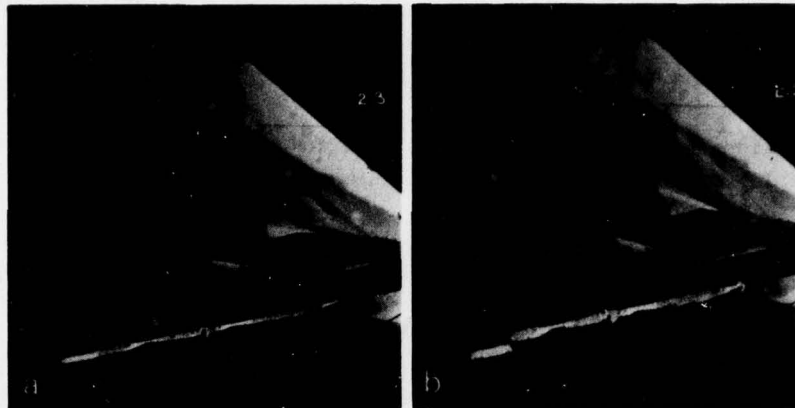a) after 10 mn    b) after 20 mn    c) after 30 mn

Fig. 16 — Actuation of a horizontal fin control surface.

a) before actuation   b) after actuation

## 4.2. Tests at reduced scale

These tests concern wings and fins, as well as rotors.

### 4.2.1. Wing models

The study of icing on Concorde has been performed in cooperation with the British and French Official Services, on a 1/6 scale half model built by the British Aircraft Corporation. These tests aimed at the study of the volume and extent of ice deposits likely to occur on the upper surface and the leading edges of the wing and air intakes during stand-by and approach flights. The tests revealed that upper surface deposits were practically non existent, while the deposits on the wing leading edge were limited to the leading edge lower surface, with a stratified shape promoting natural sheddings by rupture (fig. 17, 18). These very brittle deposits, as well as the natural sheddings whose trajectories had been filmed in the wind tunnel, have been observed during Concorde flight tests. Figure 18 also shows the influence of ice deposits on the longitudinal aerodynamic coefficients.

Similitude icing tests have been performed on a 1/12 scale model of Airbus ; these tests revealed the positions of accretion zones on the wing and fin leading edges and on the engine pod lips (fig. 19). A flight-wind tunnel comparison on the shape of wing leading edge deposits is given on figure 20 : the photograph of the flight tests is taken in the *Laschka* and *Jesse* paper [12]. Both in flight and in the wind tunnel there appears a stratified ice shape, called "lobster tail", that characterizes icing on a swept leading edge.



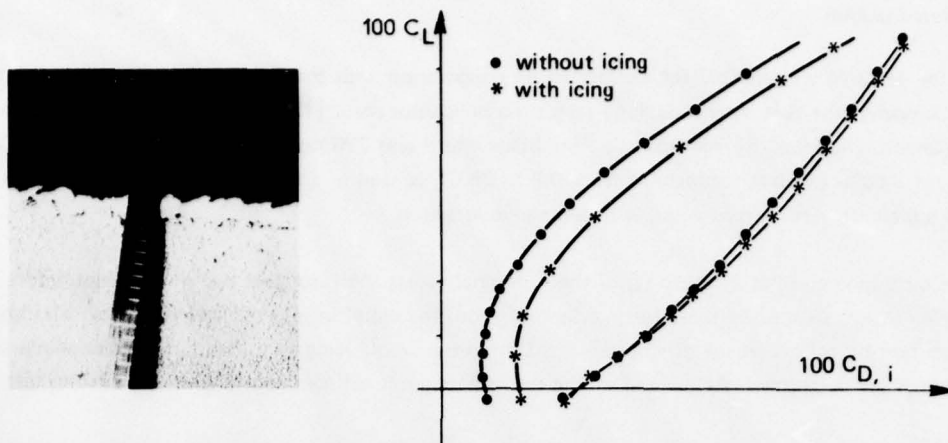Fig. 17 — Ice deposit on a 1/6 scale half model of Concorde.

Fig. 18 — Influence of icing on the 1/6 scale half model of Concorde.



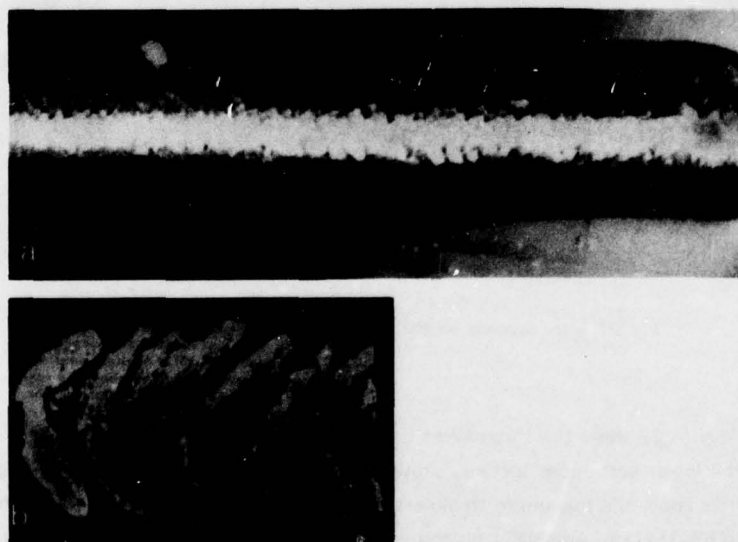Fig. 19 — Similitude icing on a 1/12 scale model of Airbus.



Fig. 20 — Airbus : flight-wind tunnel comparison.

a) wind tunnel test - 1/12 model

b) flight test, from [12] - Casting

### 4.2.2. Rotor models

During the 1973-74 winter, ONERA performed, in cooperation with the French official services and the Aérospatiale Company, the first similitude icing tests on a helicopter rotor [13]. These tests were performed on a 4-m-dia. 3-blade rotor, supplied by Aérospatiale ; the blade chord was 210 mm and the root profile a NACA 0012. The hub allowed a collective pitch adjustable from 0.9 to 26.5°, as well as a cyclic pitch setting. The rotor blades were made of a glass fiber reinforced resin, with a metallic longeron.

The test technique consists in adjusting to their nominal values the rotor and the wind tunnel before icing injection of icing cloud. As soon as these settings are obtained, the cloud in injected and the rotor rotation speed is maintained constant by action on the driving motors. During the whole icing test, aerodynamic weighings and magnetoscope recordings are performed. At the end of the test, photographs of ice deposits are taken in the test section.

An example of these photographs is presented on figure 21. The four parallel white lines are located at 5, 10, 20 and 30% of the chord respectively. The two white lines numbered 3 and 5 are respectively at 0.3 and 0.5 R. The photographs of figure 21 show that ice deposits appear in the central zone of the rotor, close to the hub, and that the blades are free of ice for any relative radius above 0.5 R. This absence of ice may be explained by the increase in kinetic heating along the span, due to that of the local aerodynamic velocity $(\vec{V} + \vec{U}\,\overline{R})$, and/or by the increase of centrifugal force along the span.
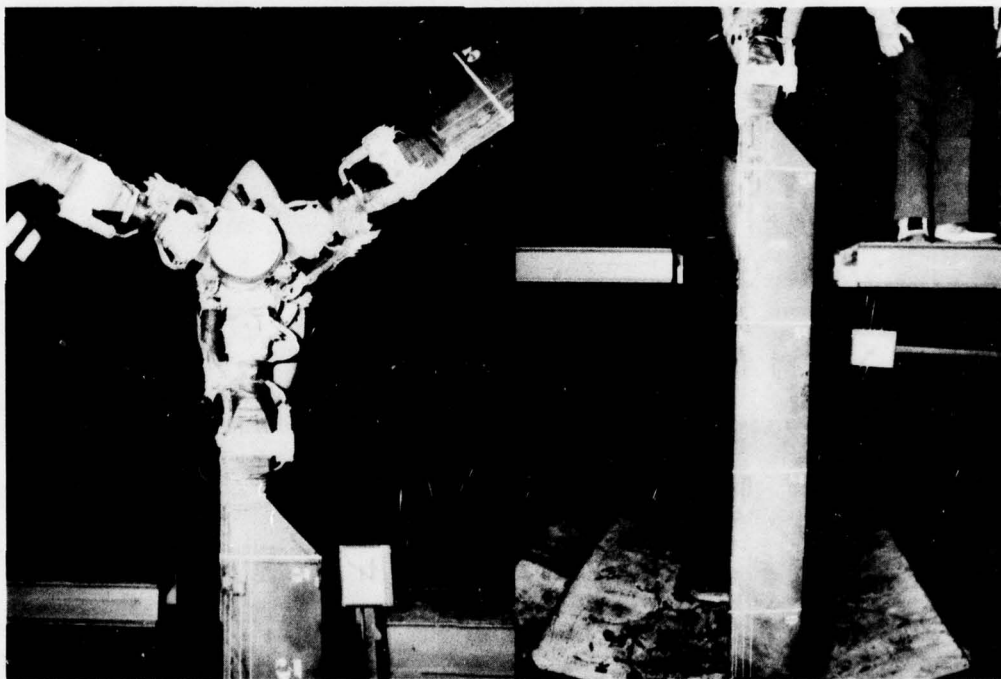


*Fig. 21 — Ice deposits on the hub and blade upper surface.*

The photographs of figure 22 show the three views defining the extents of ice deposits near the root of one of the blades. The views of the lower and upper surfaces show that the ice deposit on the leading edge is localized in the first 5% of the chord. In this zone, the maximum thickness is about 5 mm, corresponding to 8.5 mm at the full scale of a 6.7-m-dia. rotor ($k = 0.6$). There is, especially on the upper surface, a rather thin deposit of transparent ice provoked by the residue of water picked up at the leading edge, not transformed into ice at impact and flowing under the effect of aerodynamic and centrifugal forces ("run-back" phenomenon). The test temperature was not very low ($-4°C$), and the fraction of water transformed into ice at impact is relatively small, so there is an important percentage of water able to run along the surfaces.

The leading edge deposit is not very smooth ; there appear on the photographs of figure 22 some dents (marked by arrows) corresponding to ice sheddings that occurred during actual icing. Visual stroboscopic observations, as well as restitutions from the magnetoscope, revealed that after an icing duration of some five minutes during which ice settles regularly on the blade leading edge, cycles take place during which ice settles, grows and is torn off. The period of such cycles is difficult to determine, but is somewhere between 10 and 20 seconds, corresponding to 20 and 40 seconds at full scale. The icing test could last a very long time without the cumulated amount of ice becoming more important than during a single cycle ; as an average, there is as much ice deposited as evacuated by centrifugation.
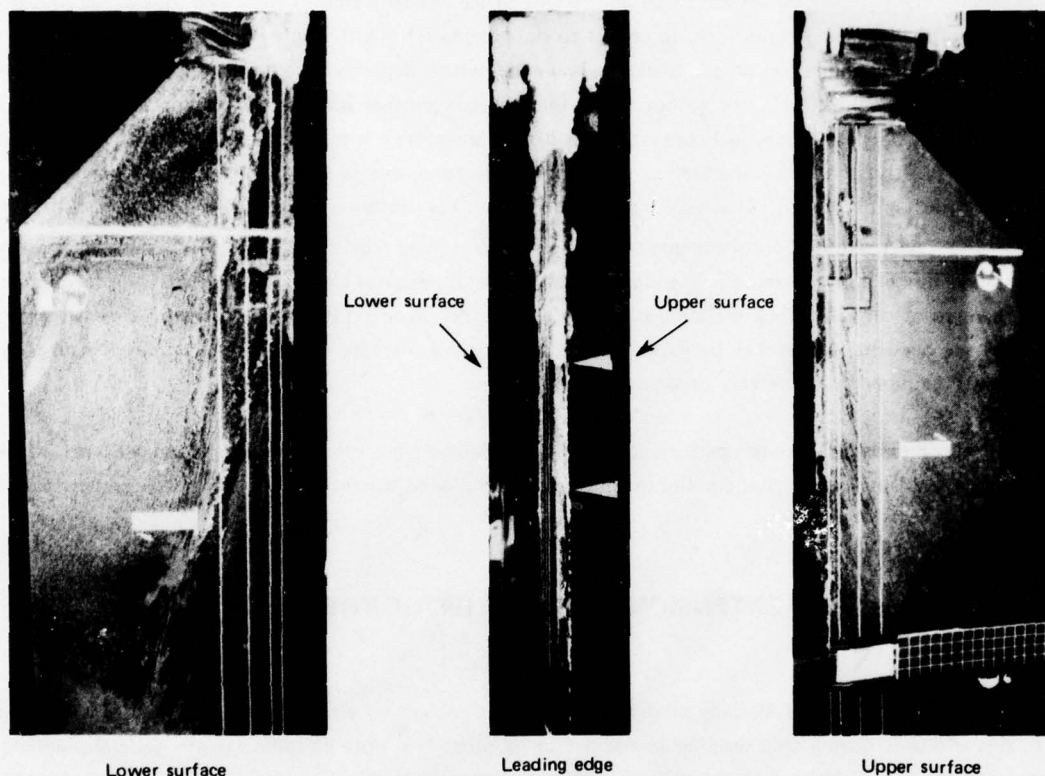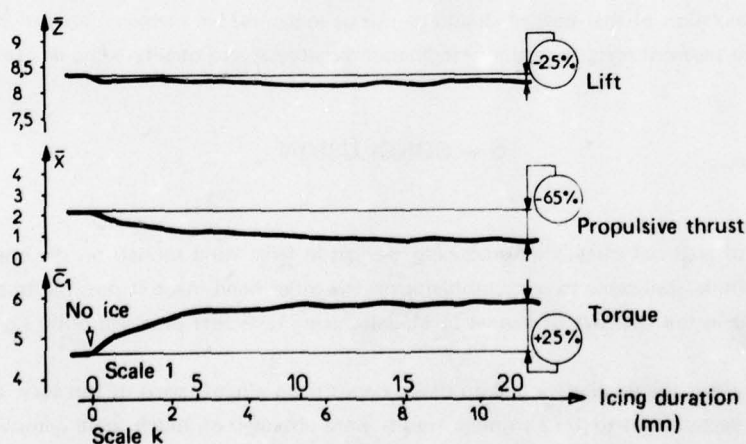


Fig. 22 — Ice deposits on a rotor blade.



Fig. 23 — Variations in time of rotor coefficients.

The cycle phenomenon appears, as regards aerodynamic weighings of the rotor, as constant values after 5 to 6 minutes of icing (see fig. 23) : on the three main parameters, i.e. lift, propulsive thrust and torque, there is a rather

rapid evolution from the icing onset, then a tendency to stabilize, when the above cycling phenomenon takes place. This stabilization is obtained, in the test case mentioned here, with a lift drop of 2.5%, a rise in the torque required from the constant speed motor of 25%, and a decrease in propulsive thrust of 65%. During the whole icing duration, the monitoring of the strain gages, and also of the dynamic values of the signals provided by the dynamometric unit, did not show any significant increase as regards vibrations.

No flight test results are yet available that are strictly comparable to these performed in the wind tunnel, but it is possible, as regards the comparison on the shape and extent of ice deposits and on the evolutions of aerodynamic parameters during flight in icing conditions, to confer to documents ref [14 through 19]. In [14], *Stallabrass* shows that there is a limit to ice extension on the blade leading edge, which depends on external static temperature and is due to kinetic heating. Still in [14], the author shows that there is another limit of ice thickness, due to centrifugal shedding of ice chunks. These theoretical considerations on the spanwise limitations are confirmed by some flight tests presented in [15 through 18]. Icing behind the leading edge zone, due to the "run-back" phenomenon (see fig. 22), is also found in flight [14, 15]. The results obtained in flight, as described in ref. [14, 15, 17, 19], show increases in the torque and power required from the engine during flights in icing conditions quite comparable to those measured in the wind tunnel (30% increase in torque), as well as the appearance of a stabilization of the torque when the cyclic phenomenon of centrifugal ice shedding is reached. *Lake* and *Bradey* [19] mention the great sensitivity of the rotors to small ice deposits, which may be explained by the very fast increase of the torque required from the driving motor in the wind tunnel from the very onset of icing conditions.

This set of comparisons, though performed on rotors different from that tested in the wind tunnel, show such similarities that there is no doubt that similitude icing tests in the wind tunnel give a very close representation of tests in actual flight.

## 5 — EXTENSION POSSIBILITIES OF THE TESTS

The large S1 wind tunnel of Modane used for icing tests is cooled by air exchange with the atmosphere, and can be used to this end only during cold weather in the winter months. This time limitation in the general planning of the wind tunnel operation is thus complemented by a random limitation due to meteorology. To palliate these difficulties, ONERA is studying means for artificially cooling the test section. A project combining a low temperature exchanger and expansion of air at high pressure should provide the frigories necessary to reduce the air temperature in the wind tunnel by 15°C. The realization of that project should permit us to ignore, for a large number of tests, the local atmospheric conditions, and to perform tests at very low temperature necessary to qualify some devices such as de-icing and anti-icing systems.

## 6 — CONCLUSION

The development of artificial icing-cloud-producing devices in large wind tunnels on the one hand, and that of theoretical laws of similitude applicable to icing problems on the other hand made it possible to perform in wind tunnels, and in particular in the ONERA S1 tunnel of Modane, icing tests that provided quite significant results.

These results concerned the qualitative pile-up of ice deposits on aircraft parts at full scale and of complete aircraft models at reduced scale, down to 1/12 ; similar results were obtained on much more complicated structures such as helicopter rotors. Measurements taken during these tests provided quantitative results quite comparable to those obtained in flight.

It is thus possible to use in a practical way the wind tunnel to predict the performance of new fixed or rotary wing aircraft from wind tunnel tests. Future technological developments should increase the yearly amount of such tests.

# REFERENCES

1   LANGMUIR I. and BLODGETT K.B. -- *A mathematical investigation of water droplet trajectories.* AAF Technical Report 5418, February 1946.

2   GELDER T.F. and LEWIS J.P. — *Comparison of heat transfer from airfoil in natural and simulated icing conditions.* NACA T.N. 2480, September 1951.

3   MESSINGER B.L. — *Equilibrium temperature of an unheated icing surface as a function of airspeed.* IAS Preprint No 342. Presented at Annual Summer Meeting, June 1951.

4   HAUGER H.H., ENGLAR K.G. and REASER W.W. — *Analysis of model testing in an icing wind tunnel.* Douglas Aircraft Company Inc., Report No SM 14993, May 1954.

5   BRUN E.A. — *Icing problems and recommended solutions.* AGARDograph No 16, November 1957.

6   GOOGAN R. and JACKSON E.T. — *The use of scale models in an icing tunnel to determine the ice catch on a prototype aircraft, with particular reference to the Concorde.* B.A.C. (Operating) Ltd, Filton Division, Aircraft Engineering Dept. SST/B75T/RMMoK/ 242. Issue 1, 24th July 1967.

7   GOOGAN R. and HUBBOLD J.A. — *Icing tests on a 1/6th scale model (G14) at Modane.* Preliminary B.A.C. test programme SST/B72T - 51/5027 - Issue 1, 7th August 1968.

8   SCHWEISCH A. — *Installation d'essais de rotors d'hélicoptères dans la grande soufflerie de Modane-Avrieux.* in Fluid dynamics of rotor and fan supported aircraft at subsonic speeds, AGARD Conf. Proc. No 22 (1968).

9   PIERRE M. — *Caractéristiques et possibilités de la grande soufflerie sonique de Modane-Avrieux.* Note Technique ONERA No 134, (1968).

10  LECARME M. et ARMAND C. — *Essais de rotor d'hélicoptère dans la Grande Soufflerie de Modane.* L'Aéronautique et l'Astronautique No 24, (1970-8).

11  CHARPIN F. et FASSO G. — *Essais de givrage dans la grande soufflerie de Modane-Avrieux sur maquettes à échelle grandeur et échelle réduite.* L'Aéronautique et l'Astronautique No 38 (1972-6). English version published by Lucas Aerospace, Ltd, London, 1972 in the Proc. of Ice Protection Conference.

12  LASCHKA B., and JESSE R.E. — *Determination of ice shapes and their effect on the aerodynamic characteristics for the unprotected tail of the A.300B.* ICAS Proc. 1974, Proceedings of the 9th Congress of the International Council of the Aeronautical Sciences. Haifa, Israël, 25-30/8/74. Edited by R.R. Descter, J. Singer. Weizmann Science Press of Israël, 1974, Jerusalem.

13  ARMAND C. et CHARPIN F. — *Givrage en similitude d'un rotor d'hélicoptère dans la soufflerie S1MA.* L'Aéronautique et l'Astronautique No 55 (1975-6).

14  STALLABRASS J.R. — *Some aspects of helicopter icing.* Canadian Aeronautical Journal, Vol. 3, No 8, October 1957, p. 273-283.

15  STALLABRASS J.R. — *Icing flight trials of a Sikorsky HO4S-2 helicopter.* NAE Canada, Laboratory Report LR-219, April 1958.

16  BRYSON L.B., HEENAN F.E. and JOHNSON C.A. — *Helicopters in the Royal Navy.* Aeronautical Journal, August 1972.

17  Mc KENZIE K.T. — *The all weather helicopter.* Proceedings of the Ice Protection Conference, published by Lucas Aerospace Ltd, London, 1972.

18  MAURICE E. — *Le givrage sur hélicoptères.* Etat Major de l'Armée de l'Air. Bulletin de sécurité du vol No 118, Sept. 1974, p. 23-26.

19  LAKE H.B. and BRADEY J. — *The problem of certifying helicopters for flight in icing conditions.* Aeronautical Journal, October 1976.

# ICING TEST FACILITIES IN CANADA

by
T. R. Ringer
Section Head, Low Temperature Laboratory
Division of Mechanical Engineering
National Research Council of Canada
Ottawa, Canada
K1A OR6

## SUMMARY

The icing simulation facilities for research, development and testing at the National Research Council of Canada are described. The major facilities include a low speed icing wind tunnel, a high speed variable density tunnel, a refrigerated jet engine test cell and a helicopter icing spray rig. An Appendix is included that lists reports and papers published on icing since 1935.

## INTRODUCTION

Icing research and test facilities were in use in Canada during the early 40s, although at that time most of the work was conducted during flight testing and only limited ground test facilities were available. The construction of an open circuit, naturally refrigerated, icing wind tunnel to be powered by an aircraft engine and propeller was carried out between 1942 and 1945, although it was never placed in service. Ultimately the building containing this open circuit tunnel became the nucleus of a much larger building designed for icing and cold weather research.

The NRC Low Temperature Laboratory of the Mechanical Engineering Division was opened in 1948[1]. The physical plant of this laboratory consisted of a large refrigeration system in addition to three cold chambers and an icing wind tunnel. The facility that subsequently has become known as the Low Speed Icing Wind Tunnel was originally placed in operation in 1950. In the early 60s a high speed icing tunnel was installed in an extension to the Low Temperature Laboratory building.

In the late 40s the Engine Laboratory of the NRC Mechanical Engineering Division operated a field station at Churchill, Manitoba, in which jet engines could be tested under natural low temperature conditions. Icing of jet engines was first carried out at the Fort Churchill location. Ultimately icing tests were transferred to Ottawa in one or more of the engine test cells at the Engine Laboratory.

In the early 50s following work on propeller and wing protection for fixed wing aircraft, the Low Temperature Laboratory undertook construction of an icing research facility in which a helicopter could be hovered. While the original design was not satisfactory the redesigned helicopter spray rig has now been operated for over twenty years on two sites.

In addition to the icing facilities of the Low Temperature Laboratory and the Engine Laboratory, the Fuels and Lubricants Laboratory has conducted tests on aircraft engine carburetor icing with a specialized facility[2][3]. Outside of the National Research Council there exists one other icing wind tunnel in Canada at the University of Alberta that has been used primarily for non-aeronautical icing investigations[4].

## LOW SPEED ICING WIND TUNNEL

This is a closed return circuit tunnel vented to atmosphere at the working section[5][6]. The layout of the tunnel with a number of representative cross sections is shown in Figure 1. The tunnel shell is of steel plate reinforced with steel ribs and supported on concrete piers. The fan section is the only fixed portion while the remainder of the tunnel slides on the supports to allow for expansion and contraction. Figure 2 shows the tunnel shell construction.

A 1000 HP synchronous speed electric motor driving through a variable speed electro-magnetic coupling provides power to an eight-blade fan. The drive assembly is shown in Figure 3.

The air stream is cooled by direct evaporation of ammonia in the bank of cooling coils located in the lowest velocity zone of the tunnel. The refrigeration system is a three-stage ammonia compression plant of 1000 HP capacity. At maximum air speed and under summer condensing temperatures, a minimum temperature of $-20\,°C$ can be obtained. At lower speeds temperatures of $-40\,°C$ can be obtained.

Air-atomizing water sprays located upstream of the working section produce the cloud water droplets. A liquid water content up to $3\ gm/m^3$ can be obtained. Median droplet diameters down to 15 microns can be obtained. Tap water is used to supply the sprays of this tunnel. The cloud liquid water content is controlled by the supply of water to the nozzles which is monitored by visual indicating flowmeters.

The Low Speed Icing Tunnel was designed with a number of features to allow for icing that reduce the aerodynamic effectiveness and result in a low energy ratio. Between the diffuser and the fan a large low velocity settling chamber was provided so that icing of the fan would not result. The divergent section between the fan and the cooling coil section has a greater angle than desirable because of space limitations.

This tunnel has been used for a wide variety of icing research and test programs for the past quarter century[7]. In the early 50s the research and test work on the electro-thermal de-icing system for the wings and empennage of the CF 100 was conducted. The icing of engine inlets of various types has been investigated as is indicated by Figure 4. The icing of swept wings and delta wing shapes was investigated.

The performance of hot gas leading edge protection has been investigated in this tunnel since auxiliary compressed air is available at the test section from sources in other laboratories.

Non-aeronautical icing research on electrical transmission lines, communications equipment and ship components has been carried out. Provision has been made to simulate freezing rain in the working section of the tunnel for some of the non-aeronautical icing work.

## HIGH SPEED ICING WIND TUNNEL

This wind tunnel is a closed circuit variable density icing tunnel. The vertical cross-section of the tunnel is shown in Figure 5. It is powered by a 600 HP D.C. motor driving a two-stage compressor through a speed increaser. The original design provided maximum velocities up to Mach 0.9 in a 1-ft. square by 18-in. long working section. Recently a semi-permanent insert ahead of the working section has been installed that limits speeds to approximately 300 knots while improving the low speed icing simulation.

The tunnel shell is a sealed and reinforced steel structure, thus permitting a variation in the static pressure at the working section from sea level to the equivalent of 30,000 ft. altitude by application of a 150 cfm vacuum pump. This tunnel is refrigerated by the same three-stage ammonia plant as the low speed tunnel, thus simultaneous operation of the two tunnels is not possible. The high speed tunnel is cooled using a secondary refrigerant, trichloroethylene, pumped through a finned tube heat exchanger. Temperatures as low as -40°C can be attained in the tunnel with temperature control in the range of ±0.5°C.

Icing is produced in the working section by pneumatic atomized water droplets introduced into the air stream by nozzles upstream of the working section. The icing simulation can be varied over concentrations up to 2 $gm/m^3$ with a droplet size of 20 microns.

Due to the small size of the working section of this tunnel, it has been employed primarily for icing instrumentation research, calibration and development tests. It has been used to test high speed aircraft components subject to icing only to a limited extent.

## HELICOPTER ICING SPRAY RIG

In 1953 interest in helicopter icing arose as a result of a request from the Canadian naval services. A prototype spray rig described in detail in NRC publication 4530[8] was operated in the 1953-54 winter. A second spray rig was designed and constructed during 1954 that subsequently has been modified and moved to a second test site[9]. This spray rig has been operated since the winter of 1954-55 with a somewhat variable utilization each winter.

The test site of this icing facility is at the northwest extremity of Uplands International Airport in Ottawa. As shown in Figure 6, it has access to one runway and thus some fixed wing aircraft have been able to taxi onto the test site for icing tests, although the road was provided to tow out unserviceable helicopters.

The spray rig provides a cloud 75 feet wide by 15 feet deep from a nozzle array of 161 steam atomizing water nozzles mounted on a steel frame. The steel frame can be positioned either at the bottom of the supporting mast or in the uppermost position so that the cloud is approximately 50 feet above ground level. A wind velocity of approximately 10 mph is required to move the cloud away from the array and provide an adequate streaming cloud for a helicopter to hover in and have good coverage of the main and tail rotor.

The maximum L.W.C. that can be obtained in the spray rig is approximately 0.8 $gm/m^3$. The droplet size is normally 30 microns median volume diameter. The ambient temperatures available in Ottawa permit testing to -25°C, although lower temperatures are usually experienced. The icing season in Ottawa is restricted to the time interval between 15 November and 15 March.

Details on the helicopter spray rig are given in NRC report LR-186A[9]. Although this publication describes the spray rig as installed on its initial site, the major change that resulted was an increase in the area of the test site and greater safety for both the flight crews and the rig operators.

## ENGINE ICING TEST CELL

Since the late 40s the Engine Laboratory of the National Research Council has been engaged in jet engine icing research, development and testing to assist manufacturers and operators. Originally an icing test facility was built at Fort Churchill, Manitoba. It consisted of a single straight-through test cell of 15 x 15-foot cross-section. The facility was operated during the winter months utilizing the natural refrigeration available at this location. For icing, a mobile water spray rig was positioned in front of the engine inlet.

In the early 50s the icing test work was transferred to the main Engine Laboratory in Ottawa. Currently, number 4 test cell is equipped for icing tests of turbopropeller and turbojet engines[10]. The test cell has a 25-foot diameter working section and will accept engines up to 500 lbm/s airflow and 50,000 lbf thrust. This test cell has an air-trichloroethylene heat exchanger to cool the inlet air. The refrigeration capacity is such that a 15°F depression can be obtained with a mass flow of 100 lbm/s. This cell is operated from approximately 1 December to 31 March when temperatures are suitable.

A 36-nozzle spray rig, located in the intake duct, simulates the icing cloud. To simulate ice crystals, two banks of stacked circular saw blades cut ice in blocks into particles that are blown into the intake duct by centrifugal fans.

An Appendix is included listing the unclassified reports and papers on icing prepared by four labor-

atories of the NRC Mechanical Engineering Division during the past four decades.

## REFERENCES

1. Orr, J. L. and Henshaw, D. G., A New Canadian Laboratory for Arctic Testing, NRC No. 2038, Refrigerating Engineering, Vol. 57, No. 9, Sept. 1949, pp. 878-882.

2. Gardner, L., Aircraft Carburetor Icing, National Research Council of Canada, IME Newsletter, Vol. 2, No. 1, April 1973.

3. Gardner, L. and Moon, G., National Research Council of Canada, Aircraft Carburettor Icing Studies, July 1970, NRC Aeronautical Report LR-536.

4. Lock, G.S.H., Some Aspects of Ice Formation with Special Reference to the Marine Environment, Trans. North East Coast Inst. of Eng. and Shipbuilding, Vol. 88, No. 6, July 1972, pp. 175-184.

5. Rush, C. K. and Wardlaw, R. L., National Research Council of Canada, Wind Tunnel Simulation of Atmospheric Icing Conditions, presented to Advisory Group AGARD, Fifth General Assembly, Ottawa, Canada, June 1955.

6. Rush, C. K., National Research Council of Canada, The NRC Icing Wind Tunnels and Some of Their Problems, 19 April 1955, NRC Laboratory Report LR-133.

7. Low Temperature Laboratory Staff, Ice, Icing and Ice Breaking, National Research Council of Canada, IME Newsletter, Transportation Series, Vol. 9, No. 4, July 1977.

8. Stallabrass, J. R., Some Aspects of Helicopter Icing, NRC No. 4530, Canadian Aeronautical Journal, Vol. 3, No. 8, Oct. 1957, pp. 273-283.

9. Bailey, D. L., National Research Council of Canada, Description of the Spray Rig Used to Study Icing on Helicopters in Flight, Sept. 1960, NRC Aeronautical Report LR-186A.

10. Chappell, M. S. and Grabe, W., Aircraft Engine Anti-icing, National Research Council of Canada, IME Newsletter, Standards Series, Vol. 1, No. 4, March 1972.
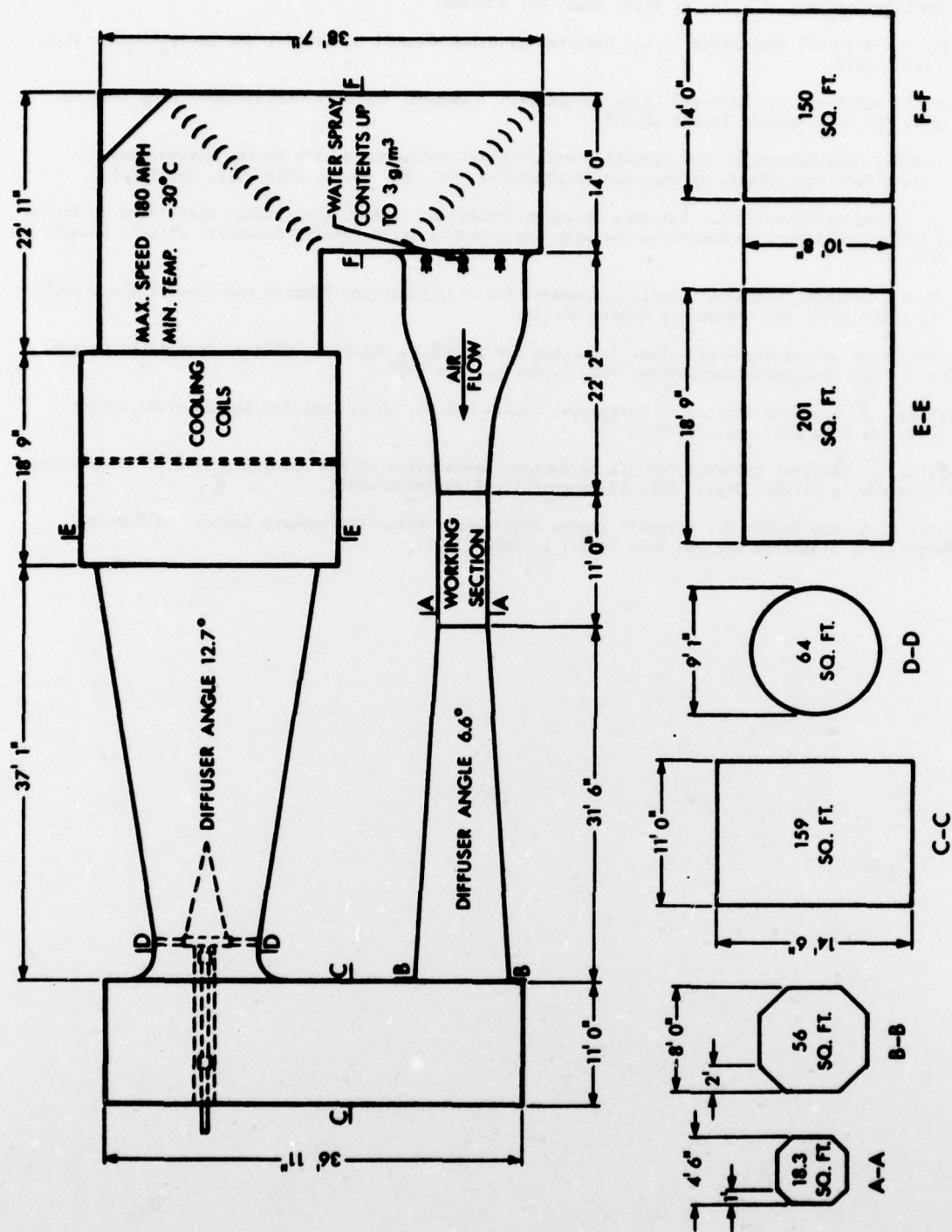
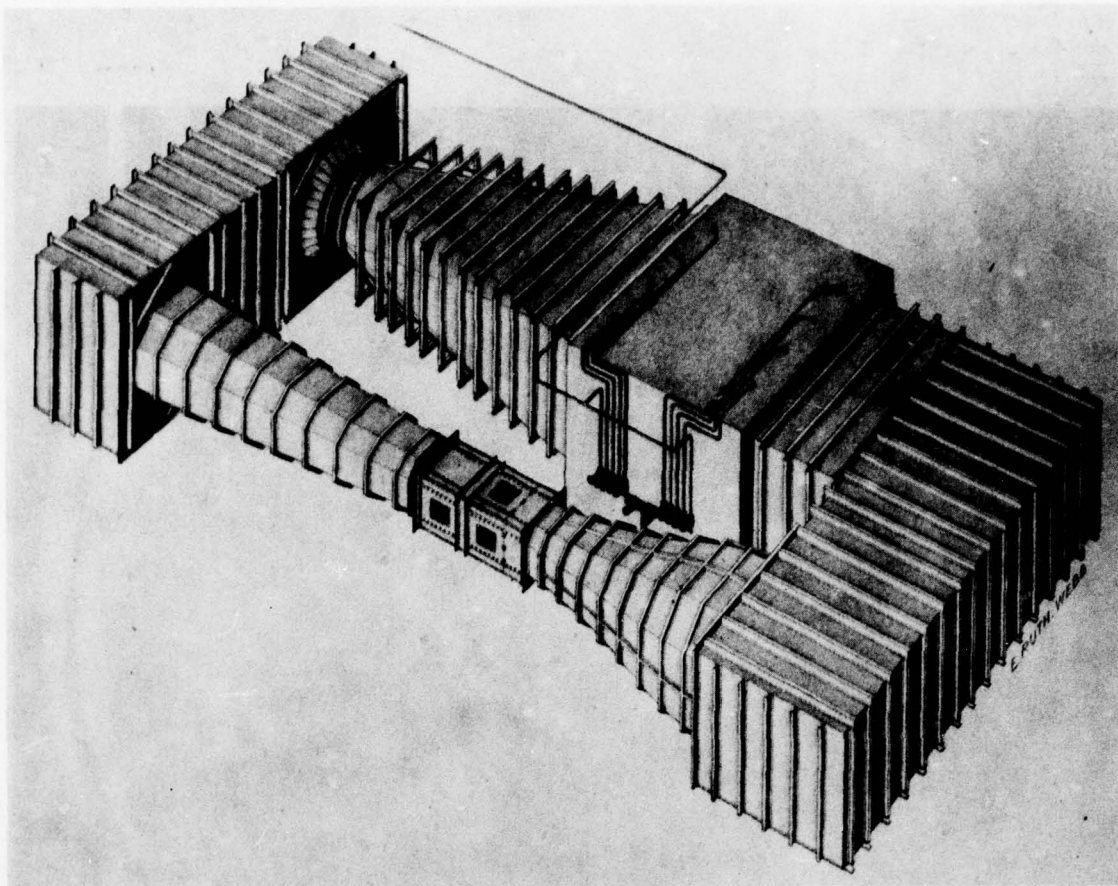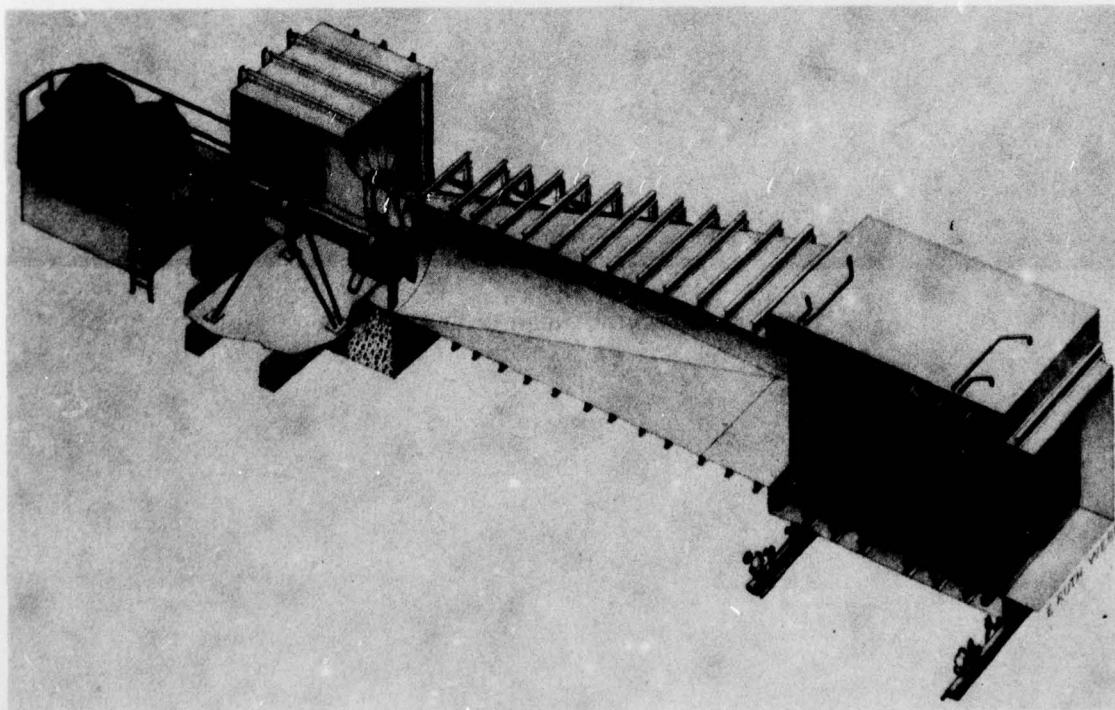FIG. 1: N.R.C. LOW SPEED ICING WIND TUNNEL

**FIG. 2:  TUNNEL SHELL**



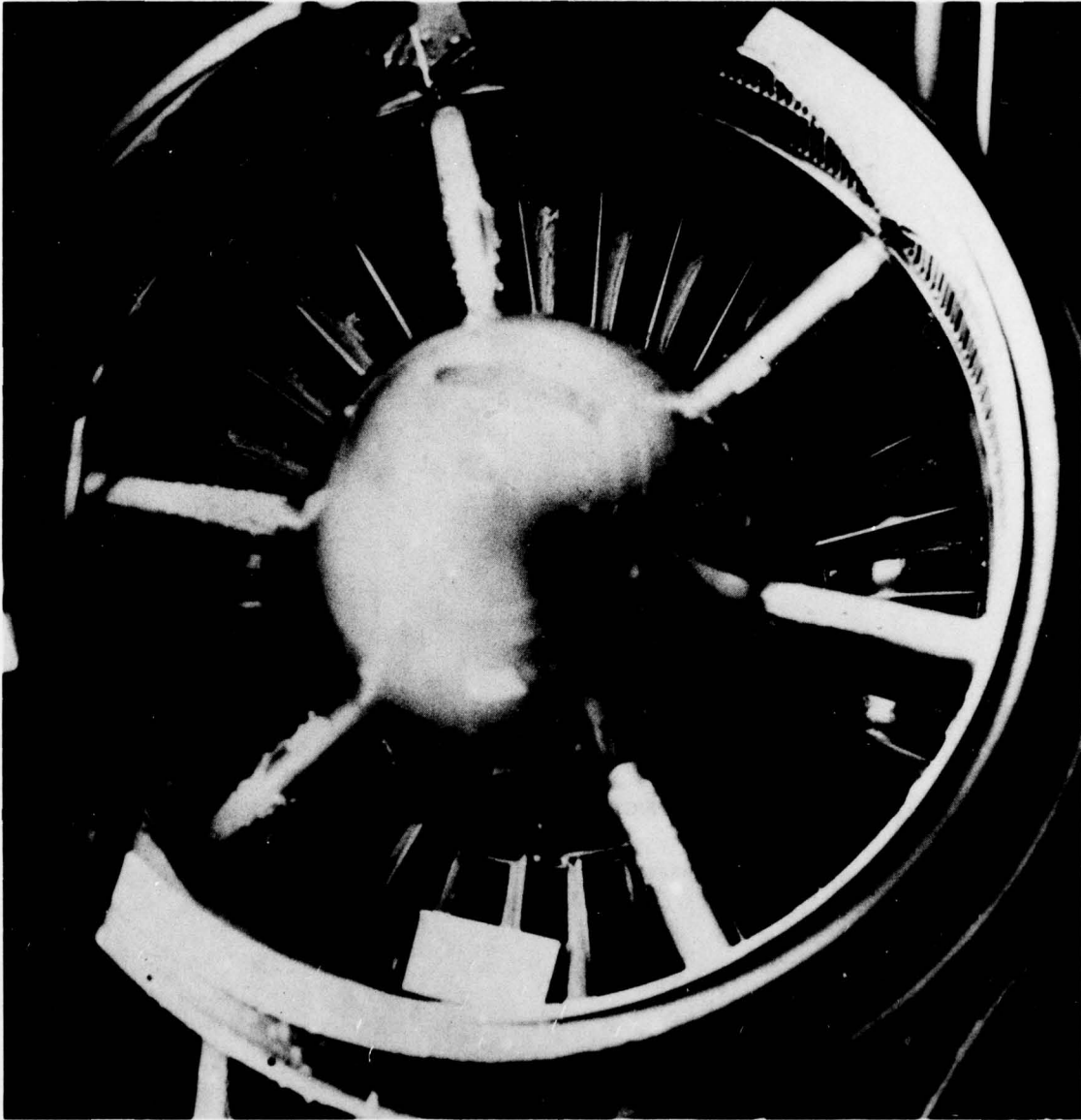**FIG. 3:  DRIVE, FAN AND COOLING COILS**

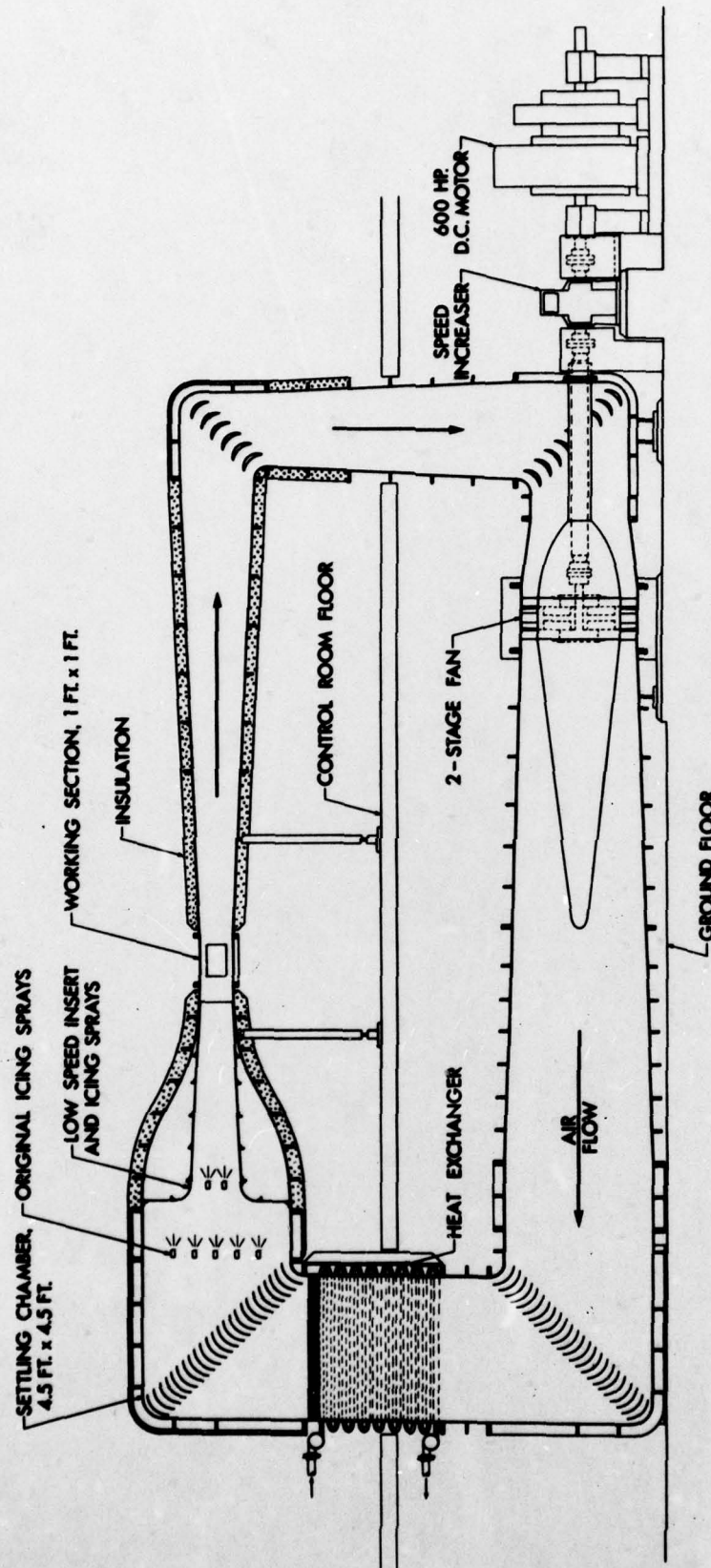FIG. 4: EXPERIMENTAL ENGINE INLET WITH ICING

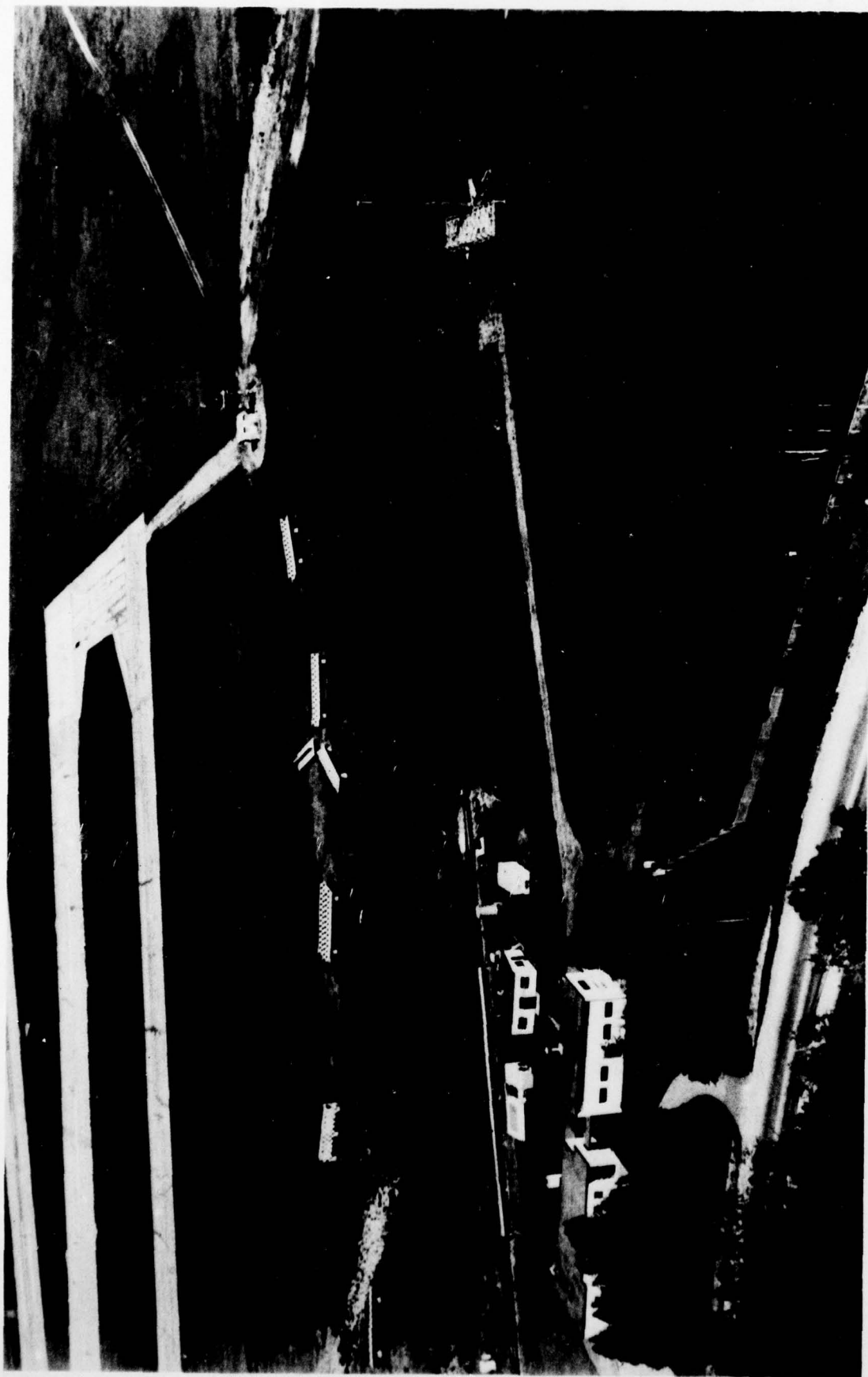FIG. 5: HIGH SPEED ICING WIND TUNNEL

FIG. 6: HELICOPTER ICING TEST FACILITY

# APPENDIX A

## NATIONAL RESEARCH COUNCIL OF CANADA

### ICING REPORTS AND PAPERS

1. **LOW TEMPERATURE LABORATORY**

   **Reports:**

   MET-491   The Effect of Icing During Helicopter Ground Run-up.
   J. R. Stallabrass and R. D. Price. April 1967.

   MET-513   Engine Snow Ingestion in the Bell 206A Jet Ranger Helicopter.
   J. R. Stallabrass. January 1971.

   LR-3   Orifice-Type Ice Detector - Preliminary Icing Tunnel Tests of Functioning as Ice
   Detector, Rate-of-Icing Meter, and Icing-Severity Meter.
   D. Fraser. July 1951.

   LR-32   Thermodynamic Limitations of Ice Accretion Instruments.
   D. Fraser, C. K. Rush and D. C. Baxter. 22 August 1952.

   LR-43   Electrically Heated Aircraft Windscreens.
   J. H. Milsum. 18 December 1952.

   LR-49   Meteorological Design Requirements for Icing Protection Systems.
   D. Fraser. March 1953.

   LR-50   Note on the Flight Testing and Assessment of Icing Protection Systems.
   D. Fraser. March 1953.

   LR-70   Electro-Thermal De-icing Systems: Their Design and Control.
   J. L. Orr, J. H. Milsum and C. K. Rush. March 1953.

   LR-71   The Characteristics of an Orifice-Type Icing Detector Probe.
   D. Fraser. 9 June 1953.

   LR-72A   Some Thermal Aspects of the Design of Heated Probes for Measuring Cloud Water Content.
   D. C. Baxter. August 1958.

   LR-95   An Approximate Method for Estimating the Transient Heat Flow Distribution in a De-icing Pad.
   R. L. Wardlaw. 21 January 1954.

   LR-129   Reference Pressure Probes for an Orifice-Type Icing Detector.
   D. Fraser and D. C. Baxter. 6 April 1955.

   LR-133   The N.R.C. Icing Wind Tunnels and Some of Their Problems.
   C. K. Rush. 19 April 1955.

   LR-186A   Description of the Spray Rig Used to Study Icing on Helicopters in Flight.
   D. L. Bailey. September 1960.

   LR-206   Icing Measurements with a Single Rotating Cylinder.
   C. K. Rush and R. L. Wardlaw. September 1957.

   LR-263   Flight Tests of an Experimental Helicopter Rotor Blade Electrical De-icer.
   J. R. Stallabrass. November 1959.

   LR-270   A Comparison Between the Spanwise and Chordwise Shedding Methods of Helicopter Rotor
   Blade De-icing.
   J. R. Stallabrass and G. A. Gibbard. January 1960.

   LR-334   Review of Icing Detection for Helicopters.
   J. R. Stallabrass. March 1962.

   LR-350   On the Adhesion of Ice to Various Materials.
   J. R. Stallabrass and R. D. Price. July 1962.

   LR-364   Ice Shedding Tests on a 10-Foot Sharp-Edged Delta Wing at Low Angles of Attack.
   C. K. Rush. December 1962.

   MD-30   A Theoretical and Experimental Investigation of the Effects of Kinetic Heating on Ice
   Formation on Aircraft Propeller Blades.
   C. D. Brown and J. L. Orr. December 1946.

   MD-40   A Review of Radiation Scattering Methods for Measuring Cloud Droplet Size.
   D. C. Baxter. April 1954.

   MD-50   The Icing of Cylinders in Conditions of Simulated Freezing Sea Spray.
   J. R. Stallabrass and P. F. Hearty. July 1967.

MD-51          Methods for the Alleviation of Ship Icing.
                  J. R. Stallabrass. August 1970.

LTR-LT-24      Experimental Determination of the Degree of Cooling of Spray Droplets.
                  Staff of Low Temperature Laboratory. October 1970.

LTR-LT-34      The De-icing Characteristics of a Reinforced Elastomer Diaphragm on a Two-Foot
               Dish Antenna.
                  J. R. Stallabrass. February 1972.

LTR-LT-42      Preliminary Measurements of Snow Concentration.
                  J. R. Stallabrass. September 1972.

LTR-LT-69      Supercooled Fog and Rime Icing Conditions at Ottawa on 25 and 26 February 1976.
                  J. R. Stallabrass. August 1976.

TR-32          Comparative Tests of Two Icing Detectors.
                  D. Fraser. June 1952.

## Papers and Lectures:

The Characteristics of Supercooled Clouds During Canadian Icing Experiments 1950-1953.
K. G. Pettit. Published in the Proceedings of the Toronto Meteorological Conference, 1953, pp.269-275.

Criteria for the Design, Assessment and Control of Icing Protection Systems. D. Fraser, K. G. Pettit
and E. H. Bowler. Published in Aeronautical Engineering Review, Vol. 11, No. 7, July 1952.

Note on the Flight Testing and Assessment of Icing Protection Systems. D. Fraser. Presented at the
Airplane Icing Information Course, University of Michigan, Ann Arbor, 30 Mar.- 3 Apr. 1953.

The Design of Electro-thermal De-icing Systems. J. L. Orr. Presented at the Airplane Icing Informa-
tion Symposium - Engineering Research Institute, Univ. of Michigan, Ann Arbor, April 1, 1953.

Aircraft De-icing by Thermal Methods. J. L. Orr, D. Fraser, J. H. Milsum. Presented at Fourth
Anglo-American Aeronautical Conference, London, England, August 1953.

Aircraft Gas Turbine Ice Prevention - The Design and Development of Hot Air Surface Heated Systems.
D. Quan and C. K. Rush. Presented at the Canadian Aeronautical Institute Annual General Meeting,
28 May 1957.

Some Aspects of Helicopter Icing. J. R. Stallabrass. Reprinted from the Canadian Aeronautical
Journal, Vol. 3, No. 8, Oct. 1957. Presented at the C.A.I. Annual General Meeting, 28 May 1957.

Canadian Research in the Field of Helicopter Icing. J. R. Stallabrass. Presented to the Helicopter
Association of Great Britain, May 9, 1958. Published in Journal of the Helicopter Association of
Great Britain, Vol. 12, No. 4, August 1958.

Icing Problems of High Speed Aircraft. C. K. Rush. Presented at the Napier Aircraft Ice Protection
Conference, May 1960.

On the Adhesion of Ice to Various Materials. J. R. Stallabrass and R. D. Price. Published in the
Canadian Aeronautics and Space Institute Journal, September 1963.

Icing and the Rescue Helicopter. T. R. Ringer, J. R. Stallabrass and R. D. Price. Presented at the
AGARD Helicopter Symposium, Paris, France, 22-24 May 1967.

Icing and the Helicopter Powerplant. J. R. Stallabrass and R. D. Price. Presented at the Propulsion
and Energetics Panel, 31st Meeting, Ottawa, June 1968.

The Characteristics and Effects of Helicopter Icing. J. R. Stallabrass. Presented to the Department
of Transport, Aircraft Accident Investigation Seminar, Ottawa, 13 April 1970.

Icing Induced Structural Problems. J. R. Stallabrass and R. D. Price. Presented at the Joint AHS-
AIAA-UTA Symposium on Environmental Effects on VTOL Designs, Univ. of Texas, Arlington, Texas,
17 November 1970.

General Review of Helicopter Icing. J. R. Stallabrass. Presented at the International Helicopter
Icing Conference, Ottawa, 23-25 May 1972.

Thermal Aspects of De-icer Design. J. R. Stallabrass. Presented at the International Helicopter
Icing Conference, Ottawa, 23-25 May 1972.

Icing Instrumentation - The Ice Detection Problem. J. R. Stallabrass and P. F. Hearty. Presented at
the Gas Turbine Operations and Maintenance Symposium, Edmonton, 21-23 October 1974.

The Development of Electro-Thermal Propeller De-icing. J. L. Orr. NRC DME-NAE Quarterly Bulletin
article, 1947(4), Oct.-Dec. 1947.

Learning More About Aircraft Icing. D. Fraser. NRC DME-NAE Quarterly Bulletin 1951(3), July-Sept.
1951.

On the Measurement of the Properties of Supercooled Clouds. K. G. Pettit. NRC DME-NAE Quarterly Bulletin 1954(2), Apr.-June 1954.

Helicopter Icing Research. J. R. Stallabrass. NRC DME-NAE Quarterly Bulletin 1957(2), Apr.-June 1957.

The Airborne Concentration of Falling Snow. J. R. Stallabrass. NRC DME-NAE Quarterly Bulletin 1976(3), July-Sept. 1976.

Measurements of the Concentration of Falling Snow. J. R. Stallabrass. Presented to the Eleventh Annual Congress of the Canadian Meteorological Society, June 1, 2 & 3, 1977, Winnipeg, Man.

## 2. ENGINE LABORATORY

### Reports:

**PAE-19**
**(also MD-1)**
Investigation of the Possibility of Preventing Ice Formation on Wings and Propellers of Aircraft by the Utilization of Exhaust Gas.
M. S. Kuhring. May 1935.

**PAE-27**
Further Investigation of the Possibility of Preventing Ice Formation on the Propellers of Aircraft by Utilization of Exhaust Heat.
M. S. Kuhring. June 1938.

**ME-159**
First Interim Report on Icing Investigation of Turbo-Jet Engines.
J. J. Samolewicz and G. A. Macaulay. Sept. 1947.

**ME-186**
Spray Nozzles for the Simulation of Cloud Conditions in Icing Tests of Jet Engines.
N. Galitzine, C. R. Sharp and L. G. Badham. August 1950.

**LR-60**
A Method for Calculating the Evaporation from Water Sprays in an Icing Tunnel.
E. L. Smith and O. R. Ballard. May 1953.

**LR-124**
Assessment of a Proposed Jet Engine Icing Test Bed for Simulating High Speed Flight.
D.A.J. Millar. February 1955.

**LR-305**
A Resume of Simulation Techniques and Icing Activities at the Engine Laboratory of the National Research Council (Canada).
M. S. Chappell. May 1961.

**LTR-ENG-17**
Some Icing Tests on Selected Screen Samples.
M. S. Chappell and W. Grabe. December 1972.

**LTR-ENG-30**
Stationary Gas Turbine Icing: Some Design Guidelines for Blowing Snow Environments.
W. Grabe and M. S. Chappell. October 1974.

### Papers:
Icing Tests on the JT15D Turbofan Engine. W. Grabe and G. K. Vanslyke[*].
Presented at the 10th National Conference on Environmental Effects on Aircraft and Propulsion Systems, Trenton, N. J., 18-20 May 1971.

Icing Tests on a Small Gas Turbine with Inertial Separation Anti-Icing System. W. Grabe and D. Tedstone[*]. Presented at the PEP 51st (A) Specialists' Meeting on Icing Testing for Aircraft Engines, Westminster, London, England.

Aircraft Engine Anti-Icing. M. S. Chappell and W. Grabe. NRC DME Newsletter, Vol. 1, No. 4, Mar. 1972.

Stationary Gas Turbine Icing Problems: The Icing Environment. M. S. Chappell. NRC DME/NAE Quarterly Bulletin No. 1972(4).

Icing Problems on Stationary Gas Turbine Powerplants. M. S. Chappell and W. Grabe. Presented at the 11th National Conference on Environmental Effects on Aircraft and Propulsion Systems, Trenton, N. J., 21-24 May 1974.

* Pratt and Whitney Aircraft of Canada Limited.

## 3. FUELS AND LUBRICANTS LABORATORY

### Reports:
**LR-536**
Aircraft Carburettor Icing Studies.
L. Gardner and G. Moon. July 1970.

### Papers:
Aircraft Carburetor Icing Studies. L. Gardner, G. Moon and R. B. Whyte. SAE Paper 710371.

Aircraft Carburetor Icing. L. Gardner. NRC DME Newsletter, Standards Series, Vol. 2, No. 1, April 1973.

## 4. GAS DYNAMICS LABORATORY

Reports:

MT-3      The Use of Alcohol for Ice Prevention and its Effect on the Performance of Axial Flow - Gas Turbines.
D. G. Samaras and A. J. Bachmeier.  April 1948.

MT-7      Performance of an Axial Flow Turbo-Jet with Alcohol Deicing.
D. G. Samaras and A. J. Bachmeier.  May 1948.

# REPORT DOCUMENTATION PAGE

| 1. Recipient's Reference | 2. Originator's Reference | 3. Further Reference | 4. Security Classification of Document |
|---|---|---|---|
| | AGARD-AR-127 | ISBN 92-835-1302-9 | UNCLASSIFIED |

| 5. Originator | Advisory Group for Aerospace Research and Development<br>North Atlantic Treaty Organization<br>7 rue Ancelle, 92200 Neuilly sur Seine, France |
|---|---|

| 6. Title | AIRCRAFT ICING |
|---|---|

| 7. Presented at | an AGARD Fluid Dynamics Panel Round-table Discussion on Aircraft Icing held at the Government Conference Center, Ottawa, Canada on 30 September 1977. |
|---|---|

| 8. Author(s) | 9. Date |
|---|---|
| Various | November 1978 |

| 10. Author's Address | 11. Pages |
|---|---|
| Various | 140 |

| 12. Distribution Statement | This document is distributed in accordance with AGARD policies and regulations, which are outlined on the Outside Back Covers of all AGARD publications. |
|---|---|

| 13. Keywords/Descriptors | | |
|---|---|---|
| Aircraft | De-icing | |
| Ice prevention | Anti-icing additives | |
| Ice formation | Defrosting | |

14. Abstract

Icing of unprotected aircraft components is a major problem engineers are faced with during the development phase of an aircraft programme. Ice accretions as well as their shape have to be predicted in order to investigate their effect on aerodynamic flight safety and performance and to decide on the need for anti-or de-icing systems. The Fluid Dynamics Panel of AGARD sponsored a round-table discussion on the subject of Aircraft Icing, on 30 September 1977, in Ottawa, Canada, in conjunction with an FDP Symposium on Unsteady Aerodynamics. The seven papers presented, covering a broad spectrum of topics, are presented in this Advisory Report.

AGARD Advisory Report No.127
Advisory Group for Aerospace Research and Development, NATO
AIRCRAFT ICING
Published November 1978
140 pages

Icing of unprotected aircraft components is a major problem engineers are faced with during the development phase of an aircraft programme. Ice accretions as well as their shape have to be predicted in order to investigate their effect on aerodynamic flight safety and performance and to decide on the need for anti-or de-icing systems. The Fluid Dynamics Panel of AGARD sponsored a round-table discussion on the subject of Aircraft Icing on 30 September 1977, in Ottawa,

P.T.O.

---

AGARD-AR-127

Aircraft
Ice prevention
Ice formation
De-icing
Anti-icing additives
Defrosting

---

AGARD Advisory Report No.127
Advisory Group for Aerospace Research and Development, NATO
AIRCRAFT ICING
Published November 1978
140 pages

Icing of unprotected aircraft components is a major problem engineers are faced with during the development phase of an aircraft programme. Ice accretions as well as their shape have to be predicted in order to investigate their effect on aerodynamic flight safety and performance and to decide on the need for anti-or de-icing systems. The Fluid Dynamics Panel of AGARD sponsored a round-table discussion on the subject of Aircraft Icing on 30 September 1977, in Ottawa,

P.T.O.

---

AGARD-AR-127

Aircraft
Ice prevention
Ice formation
De-icing
Anti-icing additives
Defrosting

---

AGARD Advisory Report No.127
Advisory Group for Aerospace Research and Development, NATO
AIRCRAFT ICING
Published November 1978
140 pages

Icing of unprotected aircraft components is a major problem engineers are faced with during the development phase of an aircraft programme. Ice accretions as well as their shape have to be predicted in order to investigate their effect on aerodynamic flight safety and performance and to decide on the need for anti-or de-icing systems. The Fluid Dynamics Panel of AGARD sponsored a round-table discussion on the subject of Aircraft Icing on 30 September 1977, in Ottawa,

P.T.O.

---

AGARD-AR-127

Aircraft
Ice prevention
Ice formation
De-icing
Anti-icing additives
Defrosting

---

AGARD Advisory Report No.127
Advisory Group for Aerospace Research and Development, NATO
AIRCRAFT ICING
Published November 1978
140 pages

Icing of unprotected aircraft components is a major problem engineers are faced with during the development phase of an aircraft programme. Ice accretions as well as their shape have to be predicted in order to investigate their effect on aerodynamic flight safety and performance and to decide on the need for anti-or de-icing systems. The Fluid Dynamics Panel of AGARD sponsored a round-table discussion on the subject of Aircraft Icing on 30 September 1977, in Ottawa,

P.T.O.

---

AGARD-AR-127

Aircraft
Ice prevention
Ice formation
De-icing
Anti-icing additives
Defrosting

| | |
|---|---|
| Canada, in conjunction with an FDP Symposium on Unsteady Aerodynamics. The seven papers presented, covering a broad spectrum of topics, are presented in this Advisory Report.<br><br>Papers presented at an AGARD Fluid Dynamics Panel Round-table Discussion on Aircraft Icing held at the Government Conference Center, Ottawa, Canada, on 30 September 1977.<br><br>ISBN 92-835-1302-9 | Canada, in conjunction with an FDP Symposium on Unsteady Aerodynamics. The seven papers presented, covering a broad spectrum of topics, are presented in this Advisory Report.<br><br>Papers presented at an AGARD Fluid Dynamics Panel Round-table Discussion on Aircraft Icing held at the Government Conference Center, Ottawa, Canada, on 30 September 1977.<br><br>ISBN 92-835-1302-9 |
| Canada, in conjunction with an FDP Symposium on Unsteady Aerodynamics. The seven papers presented, covering a broad spectrum of topics, are presented in this Advisory Report.<br><br>Papers presented at an AGARD Fluid Dynamics Panel Round-table Discussion on Aircraft Icing held at the Government Conference Center, Ottawa, Canada, on 30 September 1977.<br><br>ISBN 92-835-1302-9 | Canada, in conjunction with an FDP Symposium on Unsteady Aerodynamics. The seven papers presented, covering a broad spectrum of topics, are presented in this Advisory Report.<br><br>Papers presented at an AGARD Fluid Dynamics Panel Round-table Discussion on Aircraft Icing held at the Government Conference Center, Ottawa, Canada, on 30 September 1977.<br><br>ISBN 92-835-1302-9 |

# AGARD

## NATO ⊕ OTAN

### 7 RUE ANCELLE · 92200 NEUILLY-SUR-SEINE
### FRANCE

Telephone 745.08.10 · Telex 610176

**DISTRIBUTION OF UNCLASSIFIED**
**AGARD PUBLICATIONS**

AGARD does NOT hold stocks of AGARD publications at the above address for general distribution. Initial distribution of AGARD publications is made to AGARD Member Nations through the following National Distribution Centres. Further copies are sometimes available from these Centres, but if not may be purchased in Microfiche or Photocopy form from the Purchase Agencies listed below.

## NATIONAL DISTRIBUTION CENTRES

**BELGIUM**
Coordonnateur AGARD – VSL
Etat-Major de la Force Aérienne
Quartier Reine Elisabeth
Rue d'Evere, 1140 Bruxelles

**CANADA**
Defence Scientific Information Service
Department of National Defence
Ottawa, Ontario K1A OZ2

**DENMARK**
Danish Defence Research Board
Østerbrogades Kaserne
Copenhagen Ø

**FRANCE**
O.N.E.R.A. (Direction)
29 Avenue de la Division Leclerc
92 Châtillon sous Bagneux

**GERMANY**
Zentralstelle für Luft- und Raumfahrt-
dokumentation und -information
c/o Fachinformationszentrum Energie,
Physik, Mathematik GmbH
Kernforschungszentrum
7514 Eggenstein-Leopoldshafen 2

**GREECE**
Hellenic Air Force General Staff
Research and Development Directorate
Holargos, Athens, Greece

**ICELAND**
Director of Aviation
c/o Flugrad
Reykjavik

**ITALY**
Aeronautica Militare
Ufficio del Delegato Nazionale all'AGARD
3, Piazzale Adenauer
Roma/EUR

**LUXEMBOURG**
*See* Belgium

**NETHERLANDS**
Netherlands Delegation to AGARD
National Aerospace Laboratory, NLR
P.O. Box 126
Delft

**NORWAY**
Norwegian Defence Research Establishment
Main Library
P.O. Box 25
N-2007 Kjeller

**PORTUGAL**
Direcção do Serviço de Material
da Força Aerea
Rua da Escola Politecnica 42
Lisboa
Attn: AGARD National Delegate

**TURKEY**
Department of Research and Development (ARGE)
Ministry of National Defence, Ankara

**UNITED KINGDOM**
Defence Research Information Centre
Station Square House
St. Mary Cray
Orpington, Kent BR5 3RE

**UNITED STATES**
National Aeronautics and Space Administration (NASA)
Langley Field, Virginia 23365
Attn: Report Distribution and Storage Unit

THE UNITED STATES NATIONAL DISTRIBUTION CENTRE (NASA) DOES NOT HOLD
STOCKS OF AGARD PUBLICATIONS, AND APPLICATIONS FOR COPIES SHOULD BE MADE
DIRECT TO THE NATIONAL TECHNICAL INFORMATION SERVICE (NTIS) AT THE ADDRESS BELOW.

## PURCHASE AGENCIES

*Microfiche or Photocopy*
National Technical
Information Service (NTIS)
5285 Port Royal Road
Springfield
Virginia 22161, USA

*Microfiche*
Space Documentation Service
European Space Agency
10, rue Mario Nikis
75015 Paris, France

*Microfiche*
Technology Reports
Centre (DTI)
Station Square House
St. Mary Cray
Orpington, Kent BR5 3RF
England

Requests for microfiche or photocopies of AGARD documents should include the AGARD serial number, title, author or editor, and publication date. Requests to NTIS should include the NASA accession report number. Full bibliographical references and abstracts of AGARD publications are given in the following journals:

Scientific and Technical Aerospace Reports (STAR)
published by NASA Scientific and Technical
Information Facility
Post Office Box 8757
Baltimore/Washington International Airport
Maryland 21240, USA

Government Reports Announcements (GRA)
published by the National Technical
Information Services, Springfield
Virginia 22161, USA